بسم الله الرحمن الرحيم

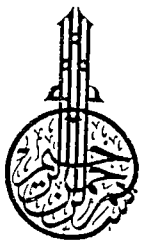

THE UNIVERSITY OF HULL

THE PERFORMANCE OF ULTRA-HARD CUTTING TOOL MATERIALS IN MACHINING AEROSPACE ALLOY TA48

being a thesis submitted for degree of
DOCTOR OF PHILOSOPHY

in the University of Hull

by

FARHAD NABHANI
M.Sc (Warwick), ASM, AMIM, C.ENG

January 1991

dedication

to my beloved parents

ABSTRACT

A study has been made of the respective performance of cubic boron nitride (CBN) and polycrystalline diamond (PCD) cutting tool materials and compared to various coated and uncoated tungsten carbide grades when cutting titanium alloy workpieces. Two important experimental techniques were employed during the course of this work, firstly a quasi-static contact method was employed to establish the workpiece/tool interfacial temperature above which strongly adherent layers may be formed. This technique revealed that the critical temperatures which marked adhesion and welding, were 740, 820 and 800 °C for coated and uncoated carbides, and 760 and 900 °C for PCD and CBN tools respectively. Furthermore, the technique has been used to study the integrity of the bulk tool material, and/or individual coatings on their substrates, when welded junctions formed between the tool and workpiece are separated. With regard to the latter it was observed that in all cases fracture was initiated in the bulk of the harder tool material rather than in the workpiece or at the welded junction interface. Secondly, a quick-stop technique was used to study chip formation and tool wear when cutting with carbides, CBN and PCD tools under nominally the same conditions.

The predominant wear mechanisms for each of the tool materials was found to be based on a diffusion/dissolution process. The wear process is discussed in detail for each of the tool materials and reasons advanced for observed differences in performance when removing material from a titanium alloy workpiece. The wear resistance and quality of the machined surface was found to be superior when cutting with the ultra-hard materials than with the carbide grades and in particular the PCD tool was found to produce exceptionally good surface finish. In the case of coated carbide tool grades rapid removal of the coated layers occurred leaving the substrate vulnerable to reaction with the workpiece material and this is

considered to explain the seeming absence of beneficial effects when cutting with these grades.

ACKNOWLEDGEMENTS

I would like to express my sincere appreciation and thanks to Professor Chris. A. Brookes for all the help and inspiration he has given me in supervising the course of my research. A dedicated and enthusiastic educator, Chris has been a pleasure to work with.

This work had benefited greatly from the insight and broad experience of Dr. R. D. James. His constructive criticism and suggestions throughout the work have had a great influence on the direction of the work.

Thanks are also due to friends and colleagues, particularly Mrs J. Brookes and Drs A. Parry, M. Lewus, P. Radcliffe and P. Kerry.

Over the past three years, a tremendous number of people have made contributions to the project either directly or indirectly, although it is not possible to mention everyone, I would like to single out Drs R. Caveney and P. Heath of debeer's for providing the tool tips and Mr G. Lee of British Aerospace (Brough) for providing the workpiece material.

The author's grateful thanks should go to the following colleagues and technicians: Messrs G. Robinson, B. Dibhah, J. Hebden, M. Trought, M. Bielby and Miss C. Clive of the EDM department for their assistance in machining experiments, work on SEM and processing the films.

The author is most grateful to Miss X. Hu and Mrs W. Taylor for typing this thesis from the original manuscript.

Special thanks are due to De Beer's company for having the confidence to sponsor this work. It is hoped that future developments, based on our new understanding, will justify this trust.

TABLE OF CONTENTS

CHAPTER 3

CHAPTER 4

CHAPTER 5

LIST OF FIGURES

LIST OF TABLES

CHAPTER 1

INTRODUCTION

1.0 INTRODUCTION

Metal Cutting is the process of removing a thin layer of work material from the surface of metal by driving a harder wedge shaped tool symmetrically into the workpiece material. The thin metal layer removed, known as a chip or swarf, is deformed throughout its volume and impinges upon the rake-face of the tool, moving over it in a direction away from the direction of motion of the workpiece. Despite the fact that there are many different industrial metal cutting processes, such as drilling, milling, turning, shaping, and so on, the above mentioned features are common to all of these.

The process of cutting involves the use of a hard, sharp edge of a small cutting area which is greater than it can support over the area to which it is applied. The edge must therefore be harder than the metal to be cut and Tabor's study of single point scratching suggests that if the tool is less than 1.2 times harder than the metal it will cease to cut a chip from a flat surface (1).

Today metal-cutting is a very important aspect of manufacturing industries. The automotive industry, electrical engineering, railways, ship-building, aircraft manufacture, production of domestic appliances and the machine tool industry itself all rely heavily on metal cutting and have large machine shops with many thousands of employees (2). In 1981 in the UK there were over 1 million machine tools, 85% of which were metal cutting machines (3). It has been estimated that more than a million people are directly engaged in machining and other related activities, and the cost of metal cutting in the UK in 1981 was calculated at approximately £20 million (4).

It is generally accepted that modern machining technology began with the industrial revolution, since it is from this era that cutting tools have played a major role in manufacturing processes which make a substantial contribution to the wealth

upon which our society thrives. Due to the resulting importance of, and heavy demands on, the cutting tool industry, developments have had to be made towards producing stronger tool materials and new machine tools. As a result, development and production of high speed steel (HSS), coated carbide, alumina ceramic, sintered diamond, sintered cubic boron nitride, and silicon nitride tools was initiated. The aim of these developments was to increase productivity and achieve greater precision in the metal cutting industry.

As with coated cemented carbide and the more conventional ceramic tool materials, the range of polycrystalline compacts based on diamond and cubic boron nitride (CBN) has increased dramatically since their commercial introduction in the early 1970's. Polycrystalline tooling has a cosmopolitan air with products from major manufacturers in the USA, Japan, South Africa and the USSR. Both synthetic and natural aggregates are used, with a number of manufacturers offering an infrastructure of blank/insert shapes and sizes, with various grades being based on grain size.

Like natural diamond, the synthetic diamond compact is susceptible to temperature degradation, and it is this feature which to a large extent limits the field of application to non-ferrous and non-metallic materials. In contrast, CBN and coated carbide tools offer the capability to operate with tool interface temperatures of up to 1200 $^{\circ}$C with minimal oxidation effects (5). The retention of high strength at high temperature is a particular requisite for the machining of aerospace titanium alloys, and it is in this area that PCD, CBN and coated carbide have major application.

The successful synthesis of diamond is one of the important scientific achievements of the latter half of the twentieth century. It has not only enabled the economic manufacture of diamonds for industrial use, but also has made it possible to tailor grain size, strength, and friability by controlling the pressure, temperature and processing time during synthesis. The direct production of diamonds of a given

size eliminates the need for crushing, which can weaken the product by resulting in cracking. Grains of different friability are required for different applications. In addition, diamond synthesis has opened up a new and exciting field of high pressure, high temperature technology capable of producing new stable phases of other materials and cubic boron nitride (CBN) is a typical example. The commercial availability of different types of synthetic diamonds and CBN, both in loose form and as sintered compacts, has opened new vistas for the production engineer and much research remains to be done before it is possible to take full advantage of these ultra hard materials. However, there would appear to be considerable scope for the use of these materials when machining titanium aerospace alloys.

Titanium alloys are attractive materials to aerospace designers due to their inherent combination of strength, lightness, and resistance to corrosion. However, they pose considerable problems in manufacturing because of its poor machinability. Traditionally, high speed steel and solid carbide monolithic cutting tools have been employed and a relatively short lifetime or the need for frequent cutter re-grinding has been accepted. More recently there has been a move towards the adoption of insert tooling based upon coated carbide systems. With the evolution of a number of new cutting tool materials there is evidence to suggest that the use of some of the ultrahard materials, such as those based on polycrystalline diamond or cubic boron nitride, may be advantageous in machining of titanium alloys. However, the cost of both the workpiece material and the tool is not trivial in these cases and, therefore, there is a need to develop experimental techniques for evaluating new materials for cutting that are simpler, quicker and less expensive than machining trials.

Most tool materials wear rapidly during the machining of titanium alloys, even at moderate cutting speeds. Current machining practice limits the cutting speed to less than 7 m/s in order to minimise tool wear. In addition, tool vibrations are induced by the grossly inhomogeneous plastic deformation in the primary shear zone

producing distinct chip segmentation. Such vibrations may be accentuated by inadequate stiffness of the component parts of the machine tool structure. Together, these factors limit the machining productivity of these materials. Unfortunately, very little is known about the detailed mechanism of chip formation or temperatures generated when machining these alloys. In this investigation, specific attention is paid to the role of the interface between the workpiece and the rakeface of the tool, on the mechanism of wear.

Two experimental techniques are employed. In the first, the effect of temperature on the adhesion of workpiece to tool material is investigated in order to determine the critical temperature above which there is immediate seizure on contact. The structural and chemical nature of the interface is studied and the nature of subsequent failure of the adhesive couple (ie at the interface; within the workpiece; within the tool) identified. In the second technique, the 'Quick-Stop' device is used to investigate, in a similar way, the structure of the chip and its interface with the rakeface, during single point cutting. The principal objective is to establish the mechanism of wear rather than the wear rate, under controlled conditions.

CHAPTER 2

LITERATURE REVIEW

2.0 LITERATURE REVIEW

2.1 HISTORICAL BACKGROUND

Over the last 30 years or so, extensive literature has accumulated on the machining of titanium. Firstly, titanium was employed in lockhead tests which revealed that wear was slightly high, and finish was coarse (6).

The Massachusetts Institute of Technology (MIT) carried out low speed turning of titanium and its alloys from 1954 to 1957. The tests were mainly concerned with steel, for comparison, and to gain a theoretical knowledge of the process cutting of titanium (7). The final report in 1957 (8) showed the feed force component to cross the power force component before the point of complete failure was reached. The outcome of these experiments was a recommendation of K25 grade carbide. This recommendation was based upon results associated with the tool life equation, cutting fluid tests and flank wear.

Siekmann carried out a number of tests in 1956 to obtain precise grades of carbide with varying conditions when machining titanium alloys. In turning tests at a feed of 0.28 mm/rev, a cast iron grade (883) was superior to a steel grade at all speeds. However, premature failure of tools was attributed to chipping and increasing the feed was found to reduce tool life (9).

In 1957 Loo of North American Aviation noted that, the mixture of sulphurized oil gave longer tool life when using carbide cutters. Dripping oil was sprayed on the cutter with compressed air to carry away the swarf and to cool the cutter.

Michigan University produced a series of reports on high speed milling in 1961 (10). Experiments were carried out to determine whether it was possible to increase rate of removal by milling at relatively high cutting speeds. At all high

speeds up to 660 m/min, the carbide cutter tool failed immediately and surface finish was poor.

In 1962, the US Airforce produced a comprehensive account of the machining of heat-resistant alloys. Their recommendations were similar to those made by the industrial concerns in the late 1950s (11) in recommending tungsten carbide cutter (C-2 grade) for face milling.

A detailed investigation of milling conditions for titanium alloys was made by Vaughn (12), who published his results in 1966. His experiments include varying cutting speed, feed rate, tool material, tool geometry, machine tool set-up and cutting fluid. His report indicated that climb milling gave greater tool life than conventional milling, and suggested that the optimum feed rate for a given cutting speed/cut geometry is essential when machining titanium alloys.

Two papers were presented at a conference on Machinability in 1965, and subsequently published in 1967. One of the papers (13) deals with the metallurgical factors affecting the machinability of titanium, and the other paper (14) promotes a practical approach to the machining of titanium. The first of the two papers (13) explains that the difficulties associated with machining titanium alloys cannot be attributed to work hardening, and that the thin chip resulting from the high shear angle, and the absence of a built-up edge to dissipate heat, combined with the very low thermal conductivity of titanium alloys leads to a much higher surface heating of the tool, resulting in contamination of the titanium. It was also suggested that the higher pressure produced by the thin chip, coupled with the excessive heat generated led to pressure welding of the chip to the tool.

The second paper (14) makes the statement that titanium is not difficult to machine and that rigid machine tools with adequate power, speed and feed will solve the problems with machining titanium. Surface treatments employing solid lubricants

such as Sulfiniz, molybdenum disulphide, graphite, etc, have not provided much improvement, as they appear to be removed rapidly from the tool surface and are carried away on the first few chips. Phosphates gave the best results of the chemically active cutting fluids tried, and showed great promise as a cutting medium, but suitable corrosion inhibitors were not found before improvements in tool materials rendered further work on these fluids "unnecessary". Chlorinated cutting fluids were found to be effective, but were banned because of their toxicity.

The recent interest in achieving higher metal removal rates in the machining of titanium alloys has led General Electric to conduct extensive research in this field. In the 1980 Annual Technical Report of GE's Advanced Machining Research Programme, papers were presented on chip formation (15, 16), alternative tool designs (17) and pulse laser experiments (18), and also on high-speed machining of titanium with various tool materials in both laboratory (19) and production (20) environments.

Komanduri performed experiments with Laser-Assisted Machining (LAM) of a preheated billet of Ti 6A1-4V and had found that it is possible to modify the usual periodic, catastrophic, shear-failed chip to a more continuous chip by heating the work material ahead of the shear zone to a high temperature (16). He believes that this facilitates an alpha (α) to beta (β) allotropic transformation of the titanium. Cutting forces were reduced by approximately 50% with LAM, and the continuous chip reduced chatter. The problem of handling the preheated workpiece is difficult enough to render this method unfeasible in production. The success of the LAM approach depends largely on the ability to heat the work material directly ahead of the shear zone without heating the material near to the tool tip. The high temperature near the tool tip may cause rapid plastic deformation and accelerated wear of the tool.

All of the above mentioned research aimed to achieve higher metal removal rates in the machining of titanium, particularly in turning. It is clear that either

temperatures have to be reduced through a new method of cooling and/or a cutting material must be found which can withstand the thermal and mechanical shocks, and chemical attacks that are associated with titanium machining.

It is possible that lubricants can be found which reduce friction and subsequently the temperature at the tool-chip interface, but lubricants will not be effective at higher cutting speeds.

Grumman Aircraft performed cutting tests on titanium alloys with direct nozzle application of both liquid nitrogen and liquid carbon dioxide. An increase in tool life and cutting speed were reported, but only an abstract for this work is available for review at this time (21).

It is known that the Technical University of Aachen in West Germany is conducting research in the use of liquid nitrogen cooling for machining titanium. A request for further information (22) indicated that significant increases in tool life were obtained, but that the added cost of providing liquid nitrogen was greater than the savings made due to increased tool life. Only limited information is available, since details of the research are confidential.

Joshi (23) experimented with liquid nitrogen as a cryogenic coolant for the profile milling of titanium alloys. He has found that a combination of liquid N_2 and soluble oil reduces tool wear possibly by providing a solid lubricant action and/or improving the rate of heat transfer. But since his tests were conducted with HSS, cutting speeds were limited to 16 m/min.

If solid lubricants are to be applied, the process will have to be a continuous one, as in Cook (24) or Veharas (25) metallizing approach. At higher cutting speeds on titanium, however, the effect of the coating may be reduced by the forcing of the coating from the interface. These processes emphasize the need to develop a new

cutting tool material to achieve higher metal removal rates in machining titanium alloys, and which maintains its mechanical integrity at high cutting speeds.

Within the past decades there have been significant developments in tool materials used for cutting steel and cast-iron, namely the introduction of coated carbides and aluminia-based ceramics containing stabilized zirconia. However, tools used for machining titanium alloys have not received any specific attention. Although extensive work has been carried out in the last thirty years in an effort to find the limits of application of HSS and cemented WC tools for this purpose, very little work has been done with alternative tool materials. Despite the fact that machining titanium alloy is a major production problem, and it is very attractive to the Aerospace industry. The most recent research in high speed machining of titanium alloys was conducted at General Electric (26). Two ballistic test facilities were used to test a variety of work materials. Tests were planned on titanium alloys and cutting was achieved with cutting speed limited to 60 m/min. Attempts to raise the cutting speed resulted in rapid cratering and/or plastic deformation of the cutting edge. These failure modes are attributed to the generation of high tool temperatures.

The ability to sustain high cutting temperatures is dependent upon the properties of the tool material used. Only a limited number of potential tool materials are available in solid form that have the thermal-mechanical properties that are necessary for high speed metal cutting. These materials are carbide tools (coated and uncoated), polycrystalline diamond, and polycrystalline CBN. In the present study, polycrystaline diamond (PCD), cubic boron nitride (CBN) and coated cemented carbide (CVD) tools have been used in machining of titanium alloys. At the present time only a few detailed studies of the wear mechanisms of these tool materials have been reported (27). A substantial research programme was undertaken in an effort to determine which of these tool materials might be the most wear-resistant and what material properties are critical in determining the wear resistance.

Because of the relative simplicity of the geometry of the process and the continuous nature of the cut, the turning process was chosen. Two novel techniques; quasi-static and quick stop, were selected as the appropriate tests to determine the basic wear properties of the various tool materials.

2.2 TERMINOLOGY USED IN MACHINING

Several methods of indicating the geometry employed in metal cutting are used at present, and although standard terminology is sought by many people, this has not been universally achieved. The following is a list of terms used in turning on a lathe with a single point cutting tool.

Three perpendicular motions are provided by the lathe in order to generate the finished surface on the bar. Two of these motions are given to the tool while the third is provided by the rotation of the workpiece. The workpiece is held in the head stock of the lathe and rotated about an axis parallel to the lathe bed. The depth of cut taken by the tool is measured perpendicular to the axis of rotation of the workpiece and is its decrease in radius.

The tool is moved at right angles to the depth of cut to provide the feed or undeformed chip thickness. The velocity with which the workpiece passes the cutting edge is referred to simply as the cutting speed. The depth of cut is measured in millimetres, the feed in millimetres per revolution (mm/rev) and the speed in surface metres per minute (Figs 2.1).

As machining proceeds, the chip passes over the tool and is discarded. The face over which the chip passes is called the 'rake' face of the tool. This face may be inclined to the axis of rotation of the workpiece so that the chip is deflected through an angle less than a right angle. This tool is then said to have a positive rake angle, which is measured from the axis of rotation. A negative rake angle turns the chip through an angle greater than a right angle, causing the chip to flow back against the rotation of the workpiece.

In order to prevent rubbing of the workpiece against the tool, clearance angles are provided at the cutting edges of the tool. Two faces meet at every cutting edge, one of these being the rake face. If the second face is the flank face, the cutting edge

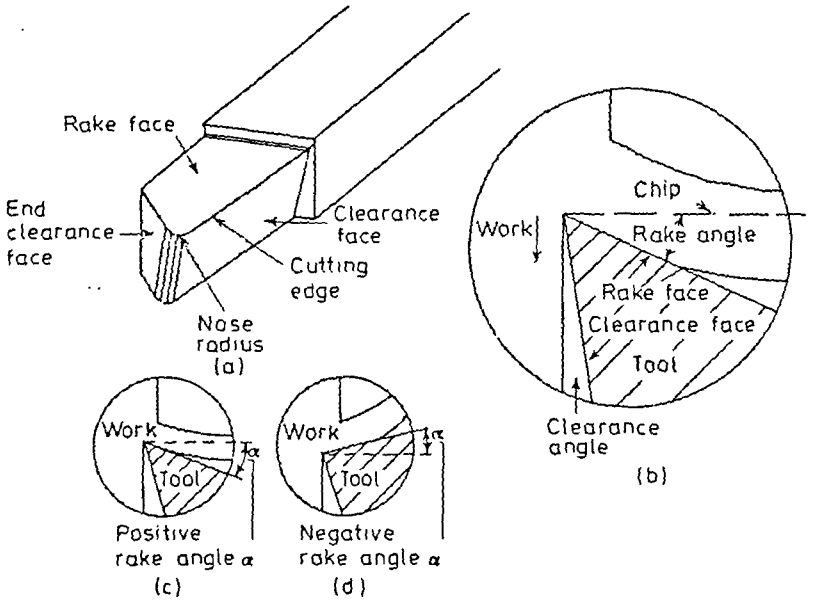

Fig 2.1 Cutting tool terminology (2).

is known as the primary cutting edge. If the second face is the end clearance face, the cutting edge is the secondary cutting edge. In order to strengthen the point where two cutting edges meet, a nose radius is sometimes provided. A further clearance angle, known as the trail angle is provided for the secondary cutting edge and this is the angle between the axis of rotation of the workpiece and the secondary cutting edge.

In order to produce a chip, shear takes place in two zones. The first is the primary shear zone (or plane) and this is the boundary between the unsheared work material and the body of the chip. The second is at the interface between the tool and the chip on the rake face. This is known as the secondary shear or flow zone of the chip. A third feature, which is often seen as a built-up edge (BUE), is a stagnant zone of metal on the tool, and this replaces the cutting edge.

Turning may be divided into three major categories; orthogonal, semi-orthogonal and non-orthogonal. In the first case, only the primary cutting edge is used and this is typified by turning on the end of a tube. The speed, feed and primary cutting edge are all at right angles to the workpiece. In semi-orthogonal cutting the nose radius and secondary cutting edges are also used and this is typified by turning on the outside of a bar. The primary cutting edge speed and feed are again mutually perpendicular to the bar. For non-orthogonal cutting any or all variables above may be altered, but the most typical is that of using an approach angle on the primary cutting edge which means that this edge is inclined to the axis of rotation.

2.2.1 SURFACE FINISH

In metal cutting the machined surfaces are formed by fracture under shear stress. The new surface probably rarely originates precisely at the cutting edge of the tool (2).

Wallbank (16) has shown that a flow zone is developed. The work material wraps itself around a sharp cutting edge and the new surface is formed where the work material breaks contact with the tool flank a short distance below the cutting edge. The contact between the flank face and the new workpiece surface is responsible for the surface roughness. Damage to the cutting edge results in a replication of this on the newly formed surface but the effect can be modified by further contact with the unworn flank face of the tool. The size, shape and distribution of micro-irregularities on the newly formed surface depends on the workpiece material as well as the flank face roughness of the tool.

The finish is dependent on the feed and nose radius of the inserts. Excessive nose radii can give rise to vibration, which will result in a rougher finish. Cutting edge build up which forms at certain temperatures, may also cause a rougher finish. Each nose radius has a corresponding maximum feed which will produce the best possible surface finish. The appropriate values are readily available from tables. The theoretical value (53) of surface finish can easily be calculated from the following equation .

$$H_{Theor} = S^2/8r \text{ mm}$$

where: s = feed in mm/rev

r = nose radius in mm.

2.2.1.1 MEASUREMENT OF SURFACE FINISH

In order to study surface finish and its effect on the performance of the product in operation, a number of quality control instruments have been developed. These enable a check on tolerances to be made easily and the necessity of experience to be minimised. Some of these instruments may be used by unskilled and

semi-skilled operators but those of a more complex nature should be used by qualified operators.

There are many methods used for the measurement of surface finish. These include; the use of a mechanical stylus, microscope, reflectivity measurements, and even some manual methods, such as visual inspection or the use of a finger nail to trace across the surface. The latter is only acceptable in industries where the surface finish is thought to be of secondary importance.

The Taylor-Hobson Talysurf is a typical stylus instrument which provides a selection of roughness and waviness parameters, together with profile graphs. The measurement data are obtained via the movement of a stylus, at constant velocity, across the surface of the specimen. This movement is amplified electronically and the data automatically analysed. The parameter values are then selectable at will from the stored information.

Several different indices are used in measuring surface finish and the most common are described here. Also, some terminology which is invariably encountered is also defined.

a) Centre Line Average (Ra)

The Ra value is the standard adopted in Great Britain, and since 1955, in the USA. It is defined as the average height from a mean line of all ordinates of the surface, regardless of sign.

If an irregular surface is divided by its centre line then a number of areas are produced which can be measured by Planimeter. Dividing the sum of these areas by the length of the sampling line gives a centre line average of the profile height, Fig 2.2

$$Ra = (A_1 + A_2 + A_3 + ... + A_n)/L$$

$$Ra = (\Sigma A)/L$$

Where ΣA = sum of areas above and below the mean line in mm^2

L = length of trace in mm.

b) Root mean square (RMS) value

This measure was standard until 1955 in the USA after which the standard was changed to Ra value. It is defined as the square root of the mean of the squares of the ordinates of the surface measured from a mean line, Fig 2.3.

If equally spaced ordinates are erected at 1, 2, 3, 4 ... n, whose heights are $h_1, h_2, h_3 \ldots h_n$, then

$$Rq = \frac{\sqrt{h_1^2+h_2^2+h_3^2+\ldots+h_n^2}}{n}$$

or $$Rq = \frac{1}{L}\int_0^L h^2 \, dL^{1/2}$$

where h is an ordinate form the centre line and L is the sampling length.

c) Roughness, Waviness and Error of form

Often some characteristics of surface geometry are not classified within the roughness category. Two classes of these arise. "Errors of form" are generally associated with deflection of the workpiece whereas "Waviness" is often associated with an incorrectly set up workpiece or irregularities in the feed mechanism "Roughness" is generally associated with chatter (Periodic tool-workpiece deflection), feed marks (produced by impression of the nose radius of the tool on each revolution) and fine scale surface damage to these feed marks. Most modern surface finish measuring instruments can discriminate between these by use of a

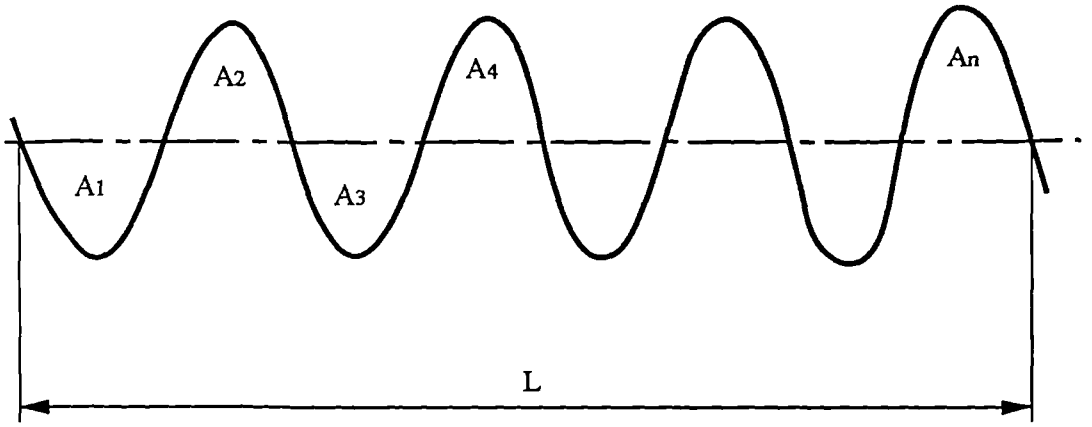

Figure 2.2 Graphical representation of C.L.A.

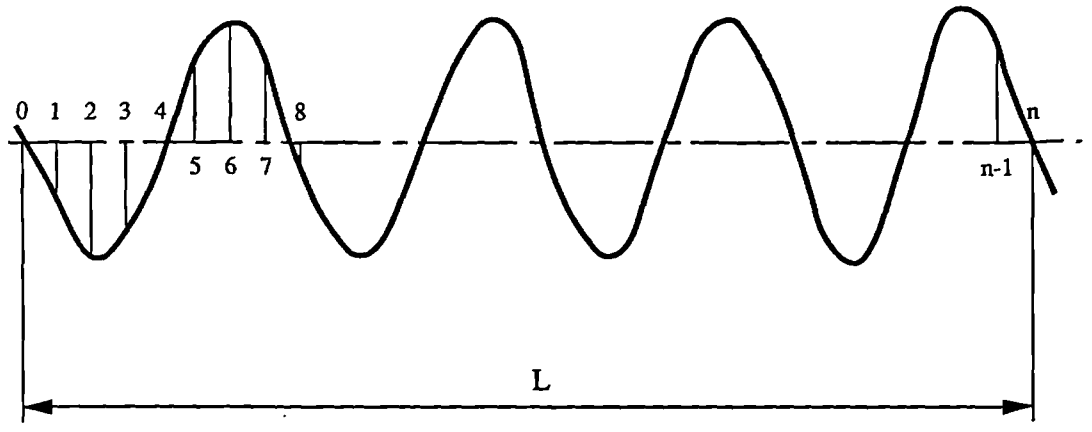

Figure 2.3 Graphical representation of R.M.S.

wavelength filter which attenuates wavelengths longer than, say, 0.8 mm in the roughness calculations.

The information obtained from the Talysurf has the widest application in quality control in industry. The most common parameters used are the RMS and CLA values of the surface and these have been found to correlate well with a number of performance criteria. It must be noted that these are not the only way of characterising surfaces and that others may prove more advantageous, for specific applications.

2.3 THEORIES OF MACHINING

In most metal forming processes, the shape of the product is entirely defined by exterior constraints, such as rolls or dies. In the case of machining, swarf is produced which is only constrained by the tools and the chip is able to take up any thickness it desires. From the definition of the shear plane angle, it can be seen that this angle would define the thickness of the chip (Figure 2.4) if it could be measured or calculated. The first attempt to define the shear plane angle for a continuous chip, with respect to the forces on the tool and the rake angle of the tool, was made by Ernest & Merchant (29). To do this they assumed that conditions of friction acted between the tool and the bottom of the chip which did not vary within the contact area. The cutting force and drag force were measured and the coefficient of friction, hence the angles of friction (δ) were calculated. They next assumed that the shear plane angle would be such that the energy expenditure would be a minimum and this led them to derive a formula:

$$\phi = \pi/4 + \alpha/2 - \delta/2 \qquad (1)$$

They noticed that as the machining speed increased, the shear plane angle (ϕ) was also increased; to account for this it must be assumed that the angle of friction decreases with speed. In a later paper, Merchant (30) shows that the formula is at fault and that it gives answers for the shear plane angle that are too high. He also gives several formulae based on geometrical considerations which can be used to calculate the shear plane angle and the shear stress (τ) on the primary shear plane. If the chip thickness (t_2) is known. The most useful of these formulae are reproduced below:

$$\tan \phi = (t_1/t_2) \cos \alpha / [1 - (t_1/t_2) \sin \alpha] \qquad (2)$$

$$\tau = \cot \phi + \tan (\phi - \alpha) \qquad (3)$$

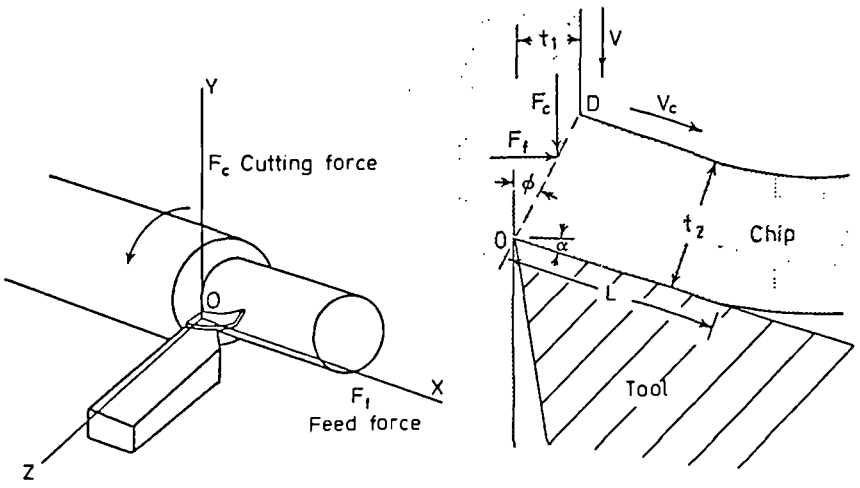

Fig 2.4 Forces acting on cutting tool (2).

The force on the shear plane (F_s) can also be easily calculated.

$$F_s = F_c \cos \phi - F_f \sin \phi \qquad (4)$$

These formulae all assume that there is no chip spread perpendicular to the direction of chip flow and parallel to the rake face; that the primary shear occurs on a plane; and that the chip produced is rectangular in cross-section. In practice the assumptions are found not to be true. However, the formulae are useful because a set of data can be quickly worked through for comparison. Merchant (31) next published a modified version of the earlier formula:

$$\phi = C/2 + \alpha/2 - \delta/2 \qquad (5)$$

Here C was referred to as the machining constant, a constant related to the rate of change of shear strength with compressive strength. For this equation to agree with the earlier one, C would have to be 90°; Experiments by Chang and Hegginbotham (32) found C to have the value of $67^\circ \pm 5\%$. The reason for the disagreement from the ideal value of 90° was accounted for by the fact that the primary shear took place over a three dimensional zone rather than a two dimensional plane, a viewpoint held by other workers (31-33). Hill (34) questioned the validity of Merchant's argument for the variation of C from the expected theoretical value of 90°. He stated that the variation of shear strength with compressive stress would have to be excessively large to account for such a difference and questioned the validity of the minimum energy criterion. Hill agreed with Merchant's geometric formula and suggested a formula defining the shear plane angle from plasticity theory:

$$\phi = \pi/4 + \alpha - \delta \qquad (6)$$

but continued to say that it would be invalid for high values of negative rake angle and that the angle found for the shear plane angle would tend to be low. In a later

paper, Hill (35) propounded the opinion that, even for one particular geometry, a range of shear angle values were possible and were dependent upon different initial conditions. The assumption is still made that the coefficient of friction is constant over the whole of the contact area (Fig 2.5). Permissible values of ø were plotted on a graph of against (δ - α) one of the boundaries, where $\delta >> \alpha$ was shown to be equation 6. Another notable point was that the whole of the permissible region falls below Ernest & Merchant's formula.

Lee & Schaffer (24) by assuming plane strain in an ideally plastic material, produced a simple triangular slip line field for machining. Two of the sides of the triangle were taken to be the primary shear plane and the contact length between the chip and the tool. The net was constructed from straight lines, hence variations of friction within the contact was still ignored. The formula derived was the same as equation 6. Variation of the coefficient of friction, with varying machining conditions, was accepted and they presumed that when the friction stress exceeded the shear stress of the chip material, adjacent to the rake face of the tool, shear would occur within the chip along the rake face. Shaw et al (25) reasoned that the accepted laws of friction were not valid for the tool-chip interface in machining. They noticed that the derived value for the coefficient of friction varied as the rake angle varied, and therefore could not agree with the classical laws of friction. This variation was thought to be due to the result of work hardening on the primary shear plane, and hence the coefficient of friction was affected by the shear plane angle. They also suggested that the shear plane was not necessarily on the line of maximum shear stress, due to the interaction of the friction stress. The slip line field approach was extended by Palmer and Oxley (21) to account for a shear zone rather than a primary shear plane; the field produced was found to be admissible except at the cutting edge where infinite accelerations would have been needed. Their expansion of the field at the cutting tip also leaves room for improvement, in that it necessitates a gap to be present between the cutting edge and the chip, similar to a crack going on ahead of

the tool. The detailed development of the slip line field approach is beyond the scope of the present work, but the work of Kudo (26) would appear to be the culmination of this approach. As in all slip line field models, the assumptions are made that the metal is rigid, plastic and does not work harden. The proposed models account for straight chips, where the friction is constant across the contact area, and for curly chips where the friction varies. The models are obtained by constructing fields using curved lines. The varying angles at which these lines meet the rake face of the tool demonstrate the changing conditions of friction at the chip-tool interface. The models also allow for a curved shear plane, and are developed to include a shear zone. Kudo's explanation that the variation of friction stress across the contact area causes curly chips has been confirmed by the work of Childs & Richings (27), but other explanations (24, 28) were that the chip curl was caused by residual stress and thermal stress gradients. It is quite probable that all of these mechanisms play some part in the final amount of curl or lack of curl in the chip. Despite the considerable amount of effort put into the development of a slip line field to explain machining, complete agreement with practice has never been achieved.

The failure of the slip line field approach to give a simple explanation of machining encouraged Rowe & Spick (28) to look again at the consumed energy approach. The object of the theory was to predict the shear plane angle. The shear zone approaches a plane as the cutting speed increases, for a continuous, non-hardening chip with simple shear at the shear plane. The approach was that the shear plane angle would be such that the total energy expended at the primary shear plane, and in the region of the tool, would be at a minimum. Assuming plane strain conditions and no work hardening, the following equation was derived from considering the energy requlred to remove a unit volume of metal:

$$\cos\alpha * \cos(2\phi-\alpha) - \beta * x * \sin^2\phi = 0 \qquad (7)$$

Where x was the ratio of the tool-chip contact length to the feed projected onto the rake face ($t1/\cos\alpha$), and β was the ratio of the shear strength of the chip-tool interface to the shear strength of the metal being machined. ß can vary from 0 to 1 representing the range from full sliding to full sticking at the interface. A family of curves of cutting energy against shear plane angle was plotted for different values of contact length (Fig 2.5). It was shown that due to the greater expenditure of energy on the rake face of the tool, as the contact length increased, the shear plane angle decreased. The effect of work hardening was suggested to be that of expanding the shear plane to a fan shaped zone, hence increasing the chip thickness. Experimental work by Williams et al (29) proved to be in agreement with the Rowe &Spick theory (28), but the energies found in practice were higher than those predicted. It was assumed that this discrepancy was the result of the formation of a collar when machining. The collar formed when machining is in the form of a radial collar existing on the bar being cut, and is formed by work material being displaced ahead of the tool. The size of the collar increases to an equilibrium value depending upon the work material and the cutting speed. In general the size of the collar decreases as the cutting speed, and brittleness of the work material, increases. A technique which utilised two tools was employed to show that substantially less energy was absorbed when no collar was allowed to form.

As in the case of the slip line field theories, the minimum energy criterion theories also fell short of accurately describing the machining process. Neither of the approaches accounted for the behaviour of real metals - probably because the assumption of ideal plasticity is unrealistic.

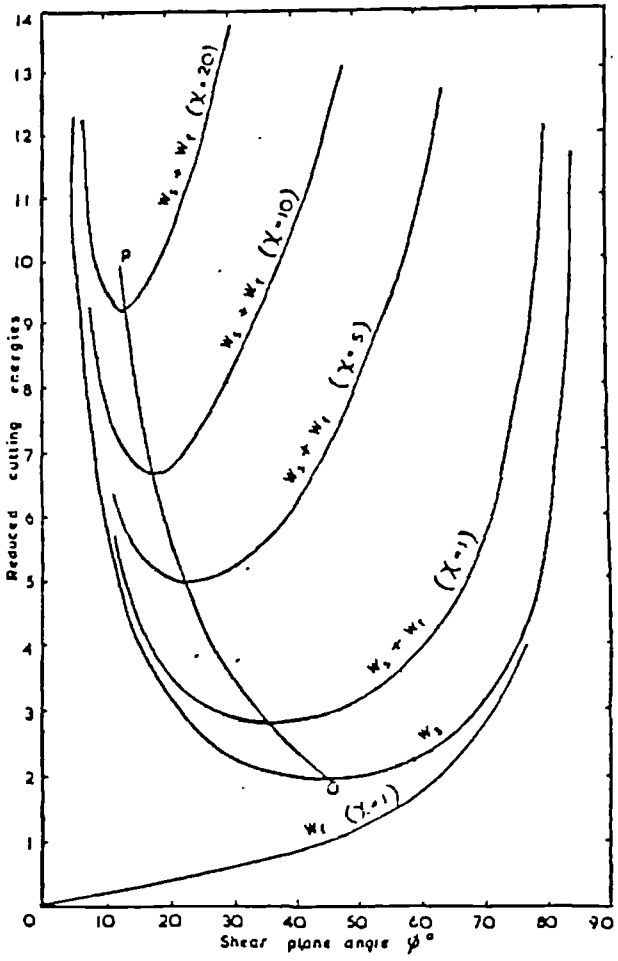

The variation with shear plane angle of the shear plane energy W_s, and the energy expended at the tool face W_f for various values of the length of chip-tool contact, together with the total energy expenditure $W_s + W_f$.

Fig 2.5 Graphical representation of the Rowe-Spick theory (40).

2.4 FORCES IN METAL CUTTING

The forces acting on the tool are an important aspect of machining. For those concerned with the manufacture of machine tools, a knowledge of the forces is needed for estimation of power requirements and for design of structures adequately rigid and free from vibration. The cutting forces vary with the tool angles, and accurate measurement of forces is helpful in optimizing tool design. Scientific analysis of metal cutting also requires knowledge of the forces, and in the last eighty years, many dynamometers have been developed capable of measuring tool forces with considerable accuracy (42).

For a semi-orthogonal cutting operation in lathe turning the force components can be measured in three directions, (Fig 2.4), and the force relationships are relatively simple. The component of the force acting on the rake face of the tool normal to the cutting edge, in the direction OY is called here the "cutting force", F_c. This force, which tries to bend the tool, is usually the largest of the three force components, and acts in the direction of the cutting velocity. The force component acting on the tool in the direction OX, which opposes the feed, is referred to as the "feed force", F_f. The third component, acting in the direction OZ, which tries to press the tool backwards, is called the "radial force", F_r. This is the smallest of the force components in semi-orthogonal cutting and, for purposes of analysis of cutting forces in simple turning, it is usually ignored and often not even measured.

The magnitude of these forces depends primarily on the feed and the cutting rake angle. In addition, the cutting force varies with the material, the depth of cut and also, to a limited extent, the cutting speed.

Work by Heath et al indicates that there is a significant difference in radial force, during the cutting of super alloy material while using chamfered and unchamfered edges of square Amborite tools (Fig 2.6). Furthermore, the principal

cutting forces acting on the workpiece can be reduced considerably by using Amborite in place of ceramic (Fig 2.6c) (43).

For conditions where a continuous chip is formed with no built up edge, the work is sheared in a zone close to the shear plane (OD in Fig 2.4) and, for the purpose of this simple analysis, it is assumed that shear takes place on this plane to form the chip. The force acting on the shear plane, F_s, is calculated from the measured forces and the shear plane angle:

$$F_s = F_c * \cos\phi - F_f * \sin\phi$$

The shear stress K_s, required to form the chip, is:

$$K_s = F_s / A_s$$

where A_s = area of shear plane

ϕ = shear plane angle.

The area of the shear plane is very variable and it is this area which exerts the dominant influence on the cutting force often more than outweighing the effect of the change in shear strength with speed of the metal being cut (1). In orthogonal cutting the area of the shear plane is geometrically related to the undeformed chip thickness *t*, (ie the feed), to the chip width *w* (depth of cut), and to the shear plane angle, ϕ.

$$A_s = t_1 * w / \sin\phi$$

The forces increase in direct proportion to increments in the feed and the depth of cut, which are two of the major variables under the control of the machinist. The shear plane angle, however, is not directly under the control of the machinist, and in practice, it is found to vary greatly under different conditions of cutting.

An increase in rake angle gives rise to a decrease in both the cutting and the feed forces. Excessive increase in the rake angle will weaken the tool edge which may well lead to its premature failure. The strongest tool edge is achieved by a negative rake, and this is frequently used for harder grades of tool materials which lack toughness. Considerable research, (44-48) has been devoted to the hypothesis that cutting forces, or some related variable, could be used to sense tool wear during the operation. In addition, several adaptive control machining systems have been developed which monitor force-related variables, such as spindle deflection. Examples of these are the Machotech and Cincinnati Milacron systems. However, the objective of using spindle deflection as the measured variable is not to sense tool wear. Instead, the purpose of the controller is to adjust speed and/or feed in order to maintain spindle deflection at a certain level which is consistent with efficient operation of the machine tool. Such a control strategy, however, also serves the function of protecting the tool against breakage due to high peak loads.

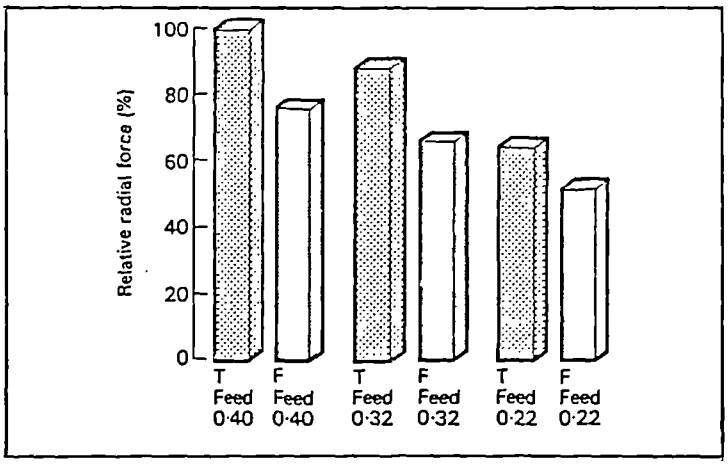

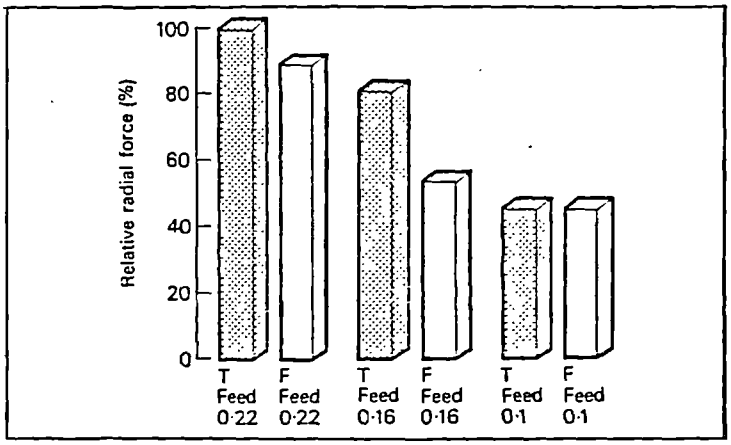

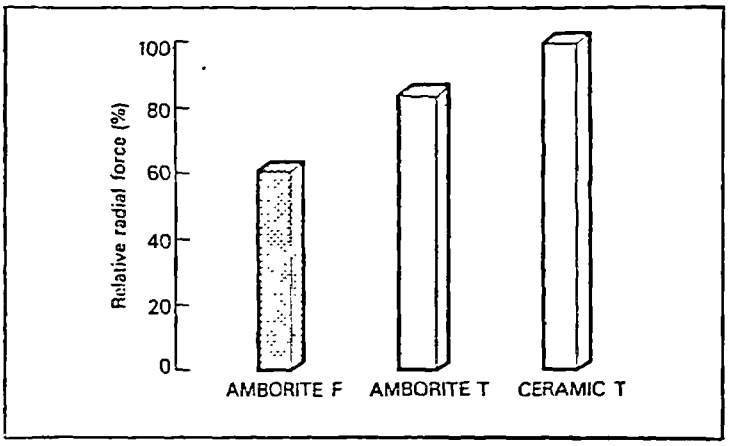

T -- champher
F -- unchampher

Fig 2.6 a) Relative radial forces for round Amborite inserts

b) Relative radial forces for square Amborite inserts

c) Relative radial forces for ceramic and Amborite (43).

2.5 HEAT IN METAL CUTTING

The power consumed in metal cutting is largely converted into heat near the cutting edge of the tool and many of the economic and technical problems of machining are caused directly or indirectly by this heating action (49). The cost of machining is very much dependent on the rate of metal removal, and may be reduced by increasing the cutting speed and/or the feed rate. However, there are limits to the speed and feed above which the life of the tool is shortened excessively, since increasing these factors means increasing heat which is a major factor in limiting tool life.

A large amount of heat is generated in all machining work. Some of the heat is absorbed by the workpiece and some by the tool, but the greatest part of the heat is retained by the chips which remove about 75% of the total (Fig 2.7). However, the tool temperature is much higher than that of the chips, and is generally assumed to be about twice as high.

Childs and Rowe (50) concluded that under normal cutting conditions, the largest part of work is done in forming the chip at the shear area. They have also developed an equation for temperature increase in the body of the chips. A reasonable estimate of the temperature increase can be made using this model. Heat at tool/work interface is a very important factor in relation to metal removal rates. This heat which is the most important source of temperature rise in the tool is generated in the flow zone.

Braiden (51) investigated the three major zones where heat is generated in metal cutting. These zones are the primary shear zone, the secondary shear zone and the flank face of the tool. The energy involved in plastic deformation to form the chip is converted into heat, which is generated in the primary and secondary shear zones.

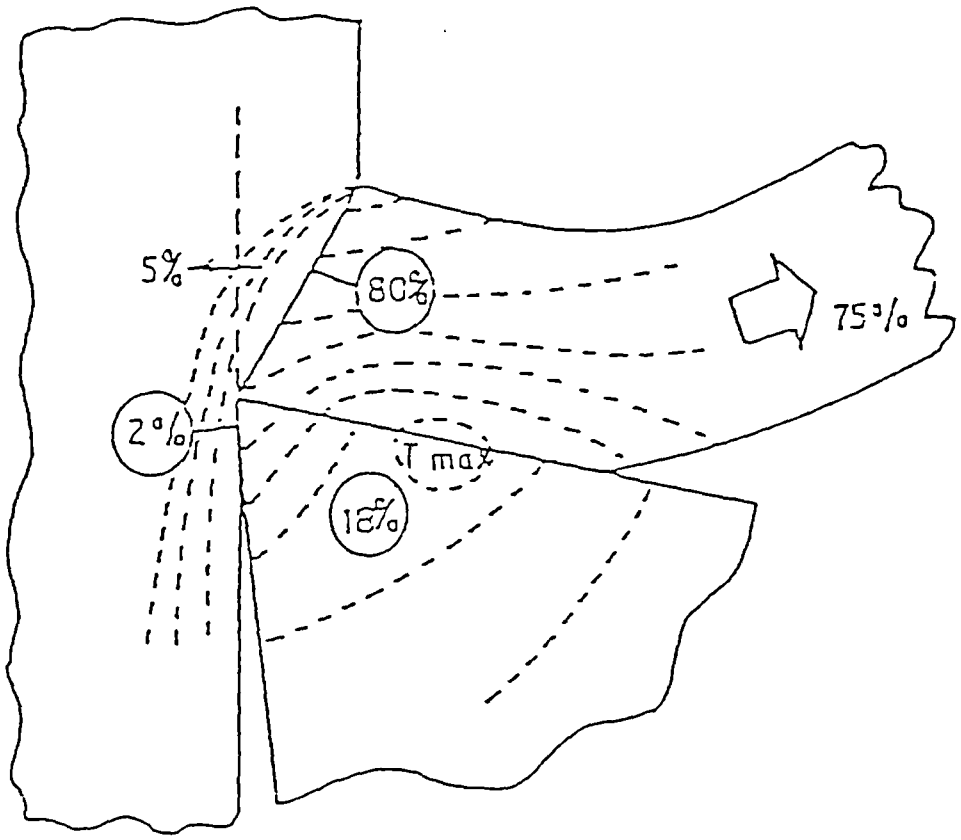

Fig 2.7 Representation of the generation and dissipation of heat in metal cutting (52).

Figures 2.8 and 2.9 illustrate how the heat generated is distributed in the tool, work material and the chip (52, 53). The illustrations show that most of the heat resulting from the work done on the shear plane, to form the chip remains in the chip and is carried away with it, while only a small amount is conducted into the tool and work material. The heat generated at the tool/chip interface is transferred to the tool and the chip. The heat generated at the tool flank/workpiece interface is the result of the rubbing of the freshly generated surface and the flank face of the tool. If the tool is perfectly sharp and the clearance angle is sufficiently large, the flank face will not be in contact with the work material and therefore no heat will be generated. However, the tool gets dull during the cutting process, and if the clearance angle is small, the contact area between the flank face and the workpiece could be large enough to cause frictional heat. This could also be referred to as the heat due to shear-strain developed at the seizure region.

The temperature of the chip remains almost constant until it is separated from the rake face of the tool. This is so for the following reasons. First, the transfer of heat from the chip by way of convection or radiation is minimal because of the short exposure involved when the chip traverses from the shear plane to the rake face. Secondly heat is not dissipated from the chip to the tool, since it is believed that the temperature of the tool (at the rake face) is higher than that of the chip due to heat generation in the flow zone. Heat transfer from the flow zone to the chip is also minimal because of the short contact interval between segments of the chip and the tool.

The above explanation is used to show that the heat carried away by the chip does not contribute to the heating up of the tool. An increase in metal removal rate leads to a proportional increase in temperatures which have a direct influence on tool wear rate and tool life. Consequently the measurement of temperature distributions in

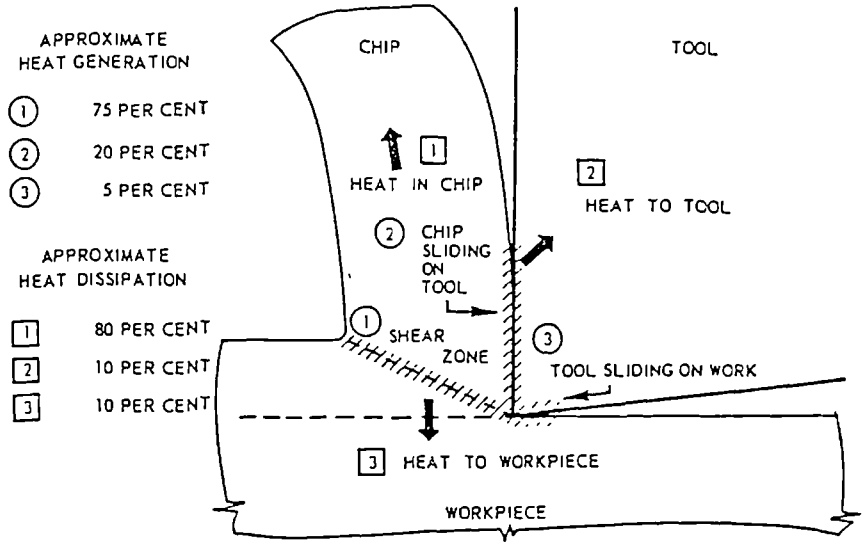

Fig 2.8 Energy partition (heat generation and heat dissipation) in the machining of steel (223).

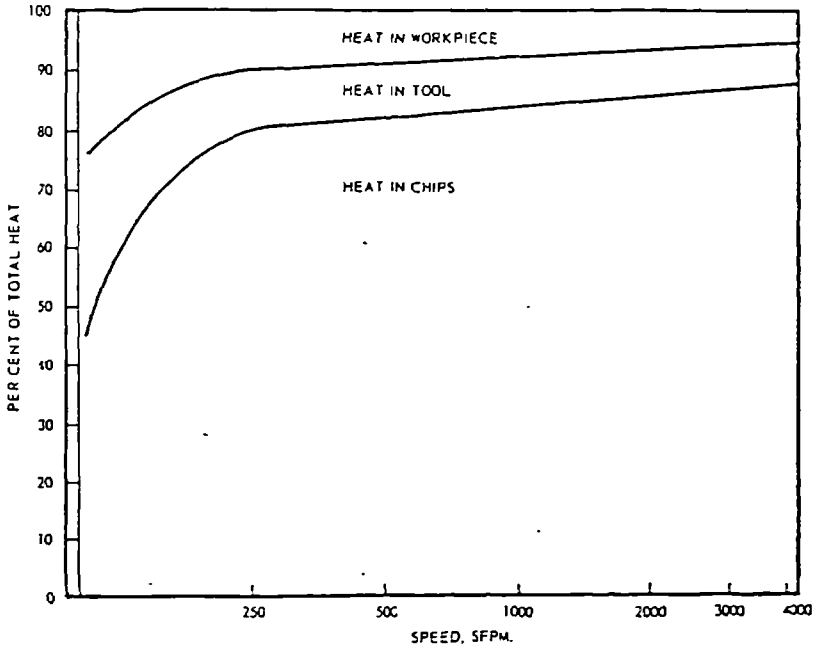

Fig 2.9 Variation in the relative amount of heat in the chip, tool and workpiece with respect to the cutting speed (223).

chip, tool and workpiece and how these temperatures originate is an important area of research despite the practical difficulties involved.

2.5.1 MEASUREMENT OF METAL CUTTING TEMPERATURES

The aim of investigating the metal cutting temperature is to be able to predict conditions prevailing at the tool/chip interface. A lot of experimental techniques have been employed to determine temperatures in the tool. The techniques employed are difficult and complicated, mainly due to the inaccessibility of the tool region which is engaged in the cutting process, and because of the very limited geometrical area of the tool on which tests are carried out. All the experimental techniques developed for investigating tool temperatures are based on estimation of temperatures by drawing analogies from other forms of measurable entities.

In an attempt to measure the temperature generated at the rake and flank faces of a cutting tool, the embedded thermocouple technique has been used by many workers (54-57). A drawback with such a technique is that it does not give a temperature distribution and instead an average value of the chip temperature is recorded.

In order to explore the temperature contours outside the areas of contact, Koch and Trent (58) made use of thermal paints and natural oxidation colours respectively. These independent investigations reported temperatures above 500 ^{o}C in roughing cuts.

A good means of determining temperatures developed in high-speed cutting tools was devised by Trent and Wright (59, 60). The method relies on temperatures in excess of 600 ^{o}C being developed at the chip/tool interface causing a series of recognisable overtempered structures to be generated within the tool. The technique

has had wide application and has given useful temperature data for cutting a wide variety of ferrous (59, 61, 60) and non-ferrous (59, 62, 63) metals.

The temperatures generated when cutting with WC-Co and Wc-(Ti,Ta,W)C-Co tools are not so easy to assess since structural changes visible on an optical scale do not arise. Naerheim (64) estimated tool temperature, by measuring the "quenched in" tungsten content of the cobalt binder regions lying close to the chip/tool interface, by using an Electron Microscope Microprobe Analyser (EMMA). On calibrating the dissolved tungsten content in these regions with temperature, this worker demonstrated that the temperature of a WC-6% Co tool was often as high as 1050 $^{\circ}$C $\pm$ 40 $^{\circ}$C, within 5μm of the chip/tool interface. Although this method works, it is too cumbersome to be employed as a regular research tool since it requires lengthy and tedious preparation of thin foils carefully extracted from "quick-stop" tool specimens.

Dearnley (65) has developed a technique which allows the construction of cutting tool temperature maps representative of the distribution and magnitude of temperature endured by cemented carbide inserts during metal cutting. The technique uses a series of iron and non-silicon bonded carbides; each binder type transforms to austenite at a characteristic temperature during metal cutting, subsequently forming a transformation product which appears as a heat affected zone when metallographic sections are etched in nital and viewed between crossed polarizers or under dark-field illumination.

More direct methods of assessing tool temperatures have been tried. One method, described by Boothroyd (66), relies on measuring the emf generated between the tool and workpiece, but has the disadvantage of only giving a mean temperature value and is incapable of resolving the steep temperature gradients described earlier. Kusters (67) attempted to measure these gradients by inserting the hot junction of a thermocouple into a spark eroded cavity lying just beneath the tool

rake face contact zone. This procedure was repeated for a series of tools each having a couple placed in a slightly different part of the chip/tool contact length. Hence, by using an identical set of cutting conditions for each tool, it became possible to construct isotherms from the resulting data. Although this method is fairly accurate the tedious nature of the whole method makes it rather impracticable.

Temperatures arising at the tool flank face have been assessed by Chao et al (68) who used a lead sulphide photoconducting infra red detector concealed within a slotted tubular workpiece. This allows the periodic exposure of the flank face of the tool to the detector. Although this method is reasonable, it is limited to facing operations and the quantity of emitted radiation is likely to be affected by an adherent work material on the flank face thereby creating some error.

2.5.2 TEMPERATURE AT THE INTERFACE

From metallographic evidence, Trent (69) concluded that on the rake face of the tool, the temperature increased away from the cutting edge and could possibly reach 1300 $^{\circ}$C. Calculations by other workers (70-72) showed that this was indeed likely. However, Chao and Trigger thought that 1300 $^{\circ}$C was perhaps too high. They (72) also reasoned that crater wear had little effect on the rake face temperature, but rake temperature increased appreciably with progressive flank wear. The distribution of temperature along the rake face was thought to be such that the temperature increased from the cutting edge to a maximum just before the termination of the chip-tool contact length. According to several workers (70, 73 and 74) the change of thermal conductivity of a tool has little effect on the temperature generated at the interface. Chao and Trigger (74) qualified this, and stated that although the average rake face interface temperature remained the same, the distribution varied. The variation was such that the temperatures towards the end of the chip-tool contact

length were higher for tools of lower conductivity. Chao and Trigger (72) calculated the temperature distribution along the flank face of the tool, and showed that the hottest point was some distance below the cutting edge or worn flank face/workpiece contact region. This was later proved correct experimentally by Chao et al (73) who continued to show flank face temperatures increased with speed and artificially reducing the contact length. Special tools were prepared with the rake face ground such that the tool-chip interface was less than that which would naturally occur. The peak temperature was found, by measuring the infra-red radiation, to be 100 $^{\circ}$C lower for the reduced contact length tools, but the temperature at the cutting edge was found to be higher. They also gave results to show that as machining speeds were increased, the maximum temperature approached closer to the back of the chip-tool contact length.

The partition of heat produced during machining is also important. At the present time, no quantitative explanation has been given, but qualitative suggestions have been put forward. Weiner (71) demonstrated that heat evolved at the primary shear plane would flow into the body of the workpiece as well as into the chip. The fraction of heat passing into the workpiece tended to unity as the shear plane angle approached zero. Reichenbach (75) calculated that when machining copper, only 1.1% of the heat produced at the tool-chip interface would flow into the tool, but suggested when machining titanium alloys, a lot higher percentage of the heat produced would flow into the tool; this was due to the thermal conductivity of titanium being less than that of copper. Rapier (70) also stated that most of the heat produced at the tool-chip interface remained in the chip, not only because the thermal conductivity of the chip was usually higher than that of the tool, but was also due to the temperature gradient in the chip, perpendicular to the rake face, being steeper than that in the tool. Boothroyd (76) showed by infra red photography, that the temperature gradients in the chip were indeed greater than those present in the tool.

Work carried out by Trent and Smart (77) using the technique developed by Wright and Trent (78) has shown that the temperatures existing within the tool are not solely dependent upon the forces, feed and speed with which the machining is carried out. They found that when they machined Nimonic 115 alloy, the temperatures produced led to failure of the tool at a much lower cutting speed than when machining a titaniuun of similar room temperature strength. Also, the forces measured when cutting the nimonic were not much different from those encountered when cutting the titanium at a similar speed. Upon sectioning the nimonic chips and preparing for the metallographic examination, it was seen that the secondary shear zone of the nimonic chips was much thinner than that of the titanium chip. Therefore, it was concluded that whilst the same amount of energy had been expended in secondary shear in each material, the volume of the metal sheared in the case of the nimonic was much less; hence, its temperature had been raised much more than that of the titanium.

It is essential when considering temperatures produced in machining, to account for the material properties, and perhaps even the chemical properties of the tool and work material, as well as their thermal properties and the mechanical aspects of the process. As yet, little work has been performed to include these parameters in the study of heat evolution in metal cutting. However, recent trends seem to indicate that their importance is being accepted since comprehensive research has been devoted to understanding the mechanism of wear chip formation.

2.6 CHIP AND BUILT UP EDGE FORMATION

The mode of chip formation is perhaps the most important aspect of any metal cutting operation. This is by virtue of its effect on the nature of chip/tool and, under certain circumstances, tool/workpiece contact. Chip formation also influences tool forces and temperatures, tool wear, and workpiece surface finish (79). It has been indicated by Trent (2) that the formation of all types of chip involves shearing of the workpiece material in the region of a plane (the shear plane) extending from the tool cutting edge to a position where the upper surface of the chip joins the workpiece surface. Three basic chip types have been identified (80); A continuous chip, a continuous chip associated with the presence of a BUE, and a discontinuous chip. Whilst continuous chips are produced by steady plastic deformation and the latter by unsteady plastic deformation accompanied by periodic fracture, the BUE has been described as a wedge of workpiece material between the chip and tool (79).

The built up edge, or built up nose, exists as a cap of work material attached to the rake face of the tool over which the chip passes during machining. The BUE is not always present, its existence depending upon the machining conditions employed and the work material being cut. Ernst and Merchant (81) thought that the built up edge was formed due to high friction on the rake face causing shearing to produce a triangular wedge adhering to the rake face. Shaw (82) proposed a different mechanism, which has been accepted more generally. The assumption that Shaw made was that as the chip passed along the rake face it would shear parallel to the rake face along the weakest plane, not necessarily at the interface if welding between the bottom of the chip and the tool occurred.

The BUE is therefore built up in layers; if the weakest plane is slightly above the rake face of the tool then a stationary layer will exist adhering to the tool; if shear then becomes more favourable on another plane slightly further away from the rake face a second layer will become attached to the first; eventually the BUE is formed.

The BUE is not a perfectly stable structure and exists in various forms. These shapes were described by Trent (83), and Hegginbotham and Gogia (84), and it was decided that they were defined by four (Fig 2.10) basic shapes:

i) the positive wedge

ii) the rectangular wedge

iii) the negative wedge

and iv) the layer type wedge.

It was also concluded by these researchers, that the BUE only existed under certain conditions. It was decided that this was due to the temperature in the region of the built up edge. As the temperature increased, due to increased rate of metal removal, the form of the BUE changed, decreasing in size, from type (i) to type (iv) and then the BUE disappeared completely. The writers also commented on the effect of the BUE on surface finish; when a BUE was present the surface deteriorated; as the size of the BUE decreased the surface finish improved. This was due to the BUE not being a stable structure; hence, particles which broke from the BUE became attached to the surface of the workpiece. The presence of a BUE when machining can easily be detected by the rough appearance of the back of the swarf. Opitz and Gappisch (85) agreed with Shaw (82) that the mode of formation of the BUE was due to the change in strength of steels at different temperatures, and concurred with the aforementioned researchers that the BUE disappeared at high temperature. They suggested that the BUE could only exist at cutting speeds where the temperature at the bottom of the chip was below the recrystallisation temperature of the work material. Another theory concerning the formation of the BUE is proffered by Opitz and Konig (86). They have suggested that the BUE occurs in steels due to the phenomenon known as blue-brittleness. This is due to the increase in strength of a steel over a range of temperature between 250 $^{\circ}$C and 400 $^{\circ}$C, the exact range

depending on the steel in question. The blue-brittleness approach has accounted for the existence of the BUE only occurring within certain limits whilst machining. According to theory, these conditions are such that the temperature resulting within the region of the BUE only develops when more than one phase is present in the workpiece; also that they exist in other materials besides steels. It was found that less than 1% of a second phase may be all that is necessary to produce a BUE; hence many commercially pure metals may be classed as two phase with respect to their ability to cut with a built up edge.

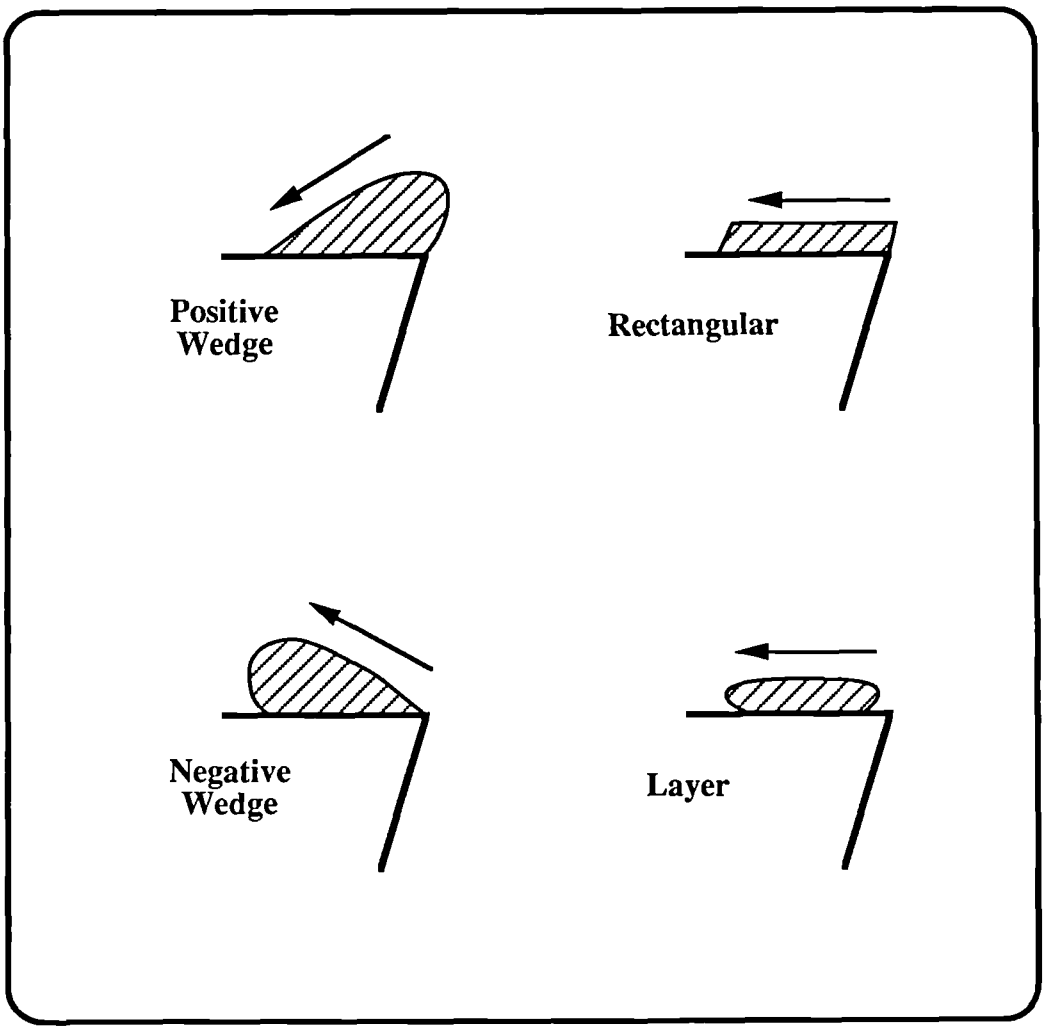

Fig 2.10 **The four different shapes that Built up edge can adopt.**

2.7 THE FLOW (OR SHEAR) ZONE

Shear zones are formed when a chip moves over the cutting tool under conditions of seizure between the underside of the chip and the tool. Seizure occurs where the tool and workpiece surfaces are interlocked or bonded (2). In order to produce a chip, shear takes place in two zones viz: the primary and secondary shear zones. The boundary between the unsheared work material and the body of the chip is known as the primary shear zone. The secondary shear zone is at the interface between the tool and the chip on the rake face. The secondary layer is a portion of the chip which has been rendered unusually plastic as a result of high temperatures. The work materials do not rub together as in standard friction theories but seizure occurs at the interface and shearing of the chip material takes place in a region close to the rake face.

Extensive study of the flow zone has been carried out by Trent (87), Opitz (85) and others (88-90). Zorev (88) initially proposed that there is insufficient time for recrystallisation of the metal in the secondary shear zone even at temperatures of about 1000 ^{o}C. Other workers (2, 89 and 90), however, believe that chip softening and recrystallisation is possible.

When cutting mild steel at high speeds the flow zone is only 25 μm thick (50). Intense deformation occurs in this zone. Ruthermore, Opitz discovered the important role played by certain oxides, present in steel as a result of particular deoxidation practices, in the formation of the secondary shear zone. Oxides lower the softening point of the chip material adjacent to the tool face thereby providing a protective stationary secondary shear zone at lower cutting speeds. Manganese sulphide can also have a similar influence on the secondary shear zone (91). Trent has also shown that there is no distinct boundary separating the flow zone from the body of the chip but rather a gradual merging of the two.

2.8 STRESS IN METAL CUTTING (STRESSES ON THE TOOL)

In machining of metals, work pieces are found to undergo local deformation in the vicinity of tool edge. The features of chip deformation encountered are different depending on the deformation and fracture characteristics of the work piece material. However, it is difficult to illustrate the relation between these characteristics and the chip deformation involved in machining.

A large part of the cutting force required in machining is transmitted to the work material through the tool rake face, giving rise to local plastic deformation of work piece. To date, a large number of the useful investigations of cutting force have been reported, but it is not yet clear what kind of stress distribution exists in the tool-chip contact region. It is most important to know the stress distribution acting along the tool rake face in machining in order to understand the mechanisms of chip deformation and the relation between chip deformation and characteristics of the workpiece.

According to Zorev (92), the normal stress distribution in tool chip contact region may be closely represented by a power function. Alternatively, Palmer and Oxley (93) suggested that the chip does not come in contact with tool near the edge point, ie normal stress does not exist there.

The study of Chandrasekaran et al (94) gave the actual change in stress distribution due to changes in tool rake angle under photoelastic experimental conditions. Other distribution curves have been shown (95, 96). In the work by Kato et al (97), the stress distribution was measured directly with a split tool whilst actually machining various metals. The method of measuring of stress distribution (98) was based on the use of a composite tool divided into two parts parallel to a cutting edge in order to measure separately the force acting on one section of tool (Fig 2.11). As the forces acting on the rake face 1 of the edge part T2 are transmitted

independently to the measuring parts, the experimental determination of the forces acting separately in that region is possible.

The extensive work of Trent (2) in a simple turning operation, indicates that two stresses of major importance act on the tool.

i) The cutting force (F_c) acting on a tool with a small rake angle imposes a stress on the rake face which is largely compressive in character (Fig 2.4). The mean value of this stress is determined by dividing the cutting force, F_c by the contact area but, since the contact area is usually not known accurately, there is considerable error in its estimation.

ii) The feed force (F_f) imposes a shearing stress on the tool over the area of contact on the rake face. The shear stress is smaller than the compressive stress acting on the same area (since the $F_f < F_c$). Frequently the mean shear stress is between 30% and 60% of the value of the mean compressive stress (2).

When a worn surface is generated on the clearance face of a tool (flank wear) both compressive and shear stresses act on this surface. Although the contact area on the flank is sometimes clearly defined, it is very difficult to arrive at values for the forces acting on it, and there are no reliable estimates for the stress on the worn flank surface (2).

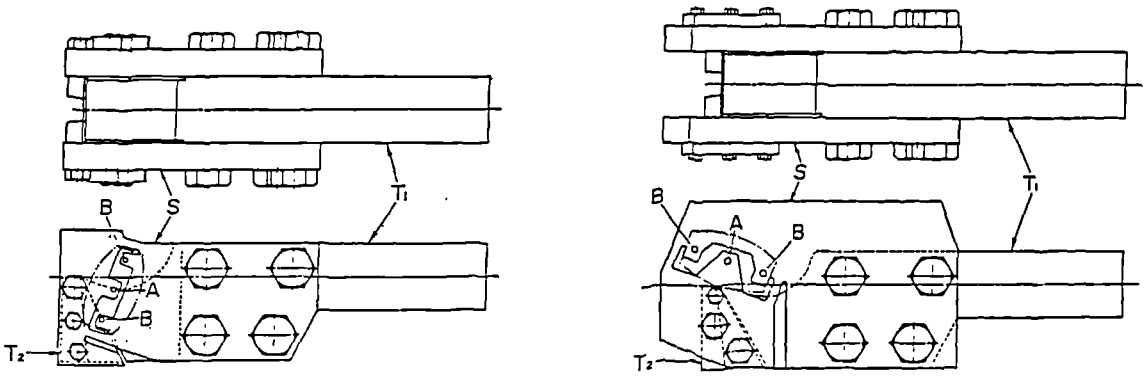

(a) Tool for normal force measurement

(b) Tool for frictional force measurement

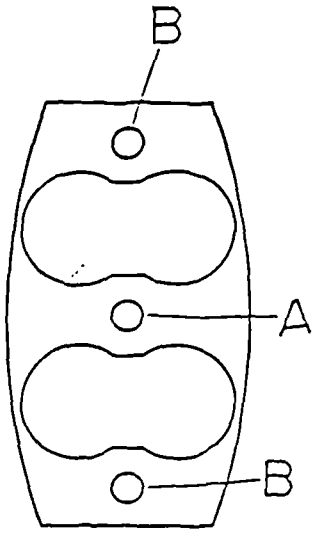

(c) Measuring piece

Fig 2.11 The above devices were developed in order to facilitate the measurements of each force. Thedetail of their construction is shown here. The forces N and F are measured by means of the devices (a) and (b), respectively. The changes in the force acting on the edge part give rise to a small movement of the edge side relative to the shank side. The displacement of point A proportional to the applied force is detected electrically by the measuring pieces bolted to both the side of the shank. Resistance strain gauges are located on the inner sides of the four thinner portions of the measuring pieces (c) and connected to each other as a wheatstone bridge (98).

2.9 CUTTING TOOL MATERIALS

The development of tool materials for cutting applications has been evolutionary and accomplished very largely by practical means. A very large number of tool materials has been tried, and the successful novel tool materials which have been proved by extensive trials, are the products of the persistent effort of thousands of craftsmen, inventors, technologists, scientists, blacksmiths, engineers, metallurgists and chemists. The tool materials which have survived and are commercially available today, are those which have proved best able to satisfy the demands put upon them in terms of the life of the tool, the rate of metal removal, the surface finish produced, the ability to give satisfactory performance in a variety of applications, and the cost of tools made from them. In general,the following points must be considered when selecting a tool:

i) Adequate strength and retention of its properties at elevated temperatures,

ii) Sufficient toughness to withstand impact,

iii) Thermal shock resistance,

iv) Chemical Stability.

Trent (2) states that the agents of this "natural selection" are the machinist, foreman, toolroom craftsmen, tooling specialists, cost and buyers, who effectively decide which of all potential tool materials shall survive.

The main groups of the present day cutting tool materials can be divided into the following categories:

i) plain carbon steel

ii) high speed steel

iii) cemented carbide

iv) ceramic

v) diamond

vi) cubic boron nitride

2.9.1 PLAIN CARBON STEELS

Plain carbon steel, generally called carbon steel, was the earliest material used as a cutting tool (Figs 2.12 and 2.13) and, by 1870, it had become the chief cutting tool material. Metallurgically, these materials are alloys of iron and carbon ranging from 0.85-1.5 percent. Their hardness ranges from 55-64 Rockwell C, but the materials begin to soften at about 150 $^{\circ}$C. At about 200 $^{\circ}$C the materials lose their hardness and become too soft to be effective.

There are many types of carbon tools steels used for many purposes, eg. for the manufacture of punches and dies and as hand tools such as chisels, wrenches and hammers. The use of carbon tool steels for cutting tools is, in these days, rather limited, mainly on account of the loss of hardness beyond 150 $^{\circ}$C. However, carbon steels have the advantage that tools made from them are easy to fabricate and acquire a keen cutting edge. Owing to these two properties, this material is used in the manufacture of farm tools which, because of their large line of contact with the work, are operated at low speeds.

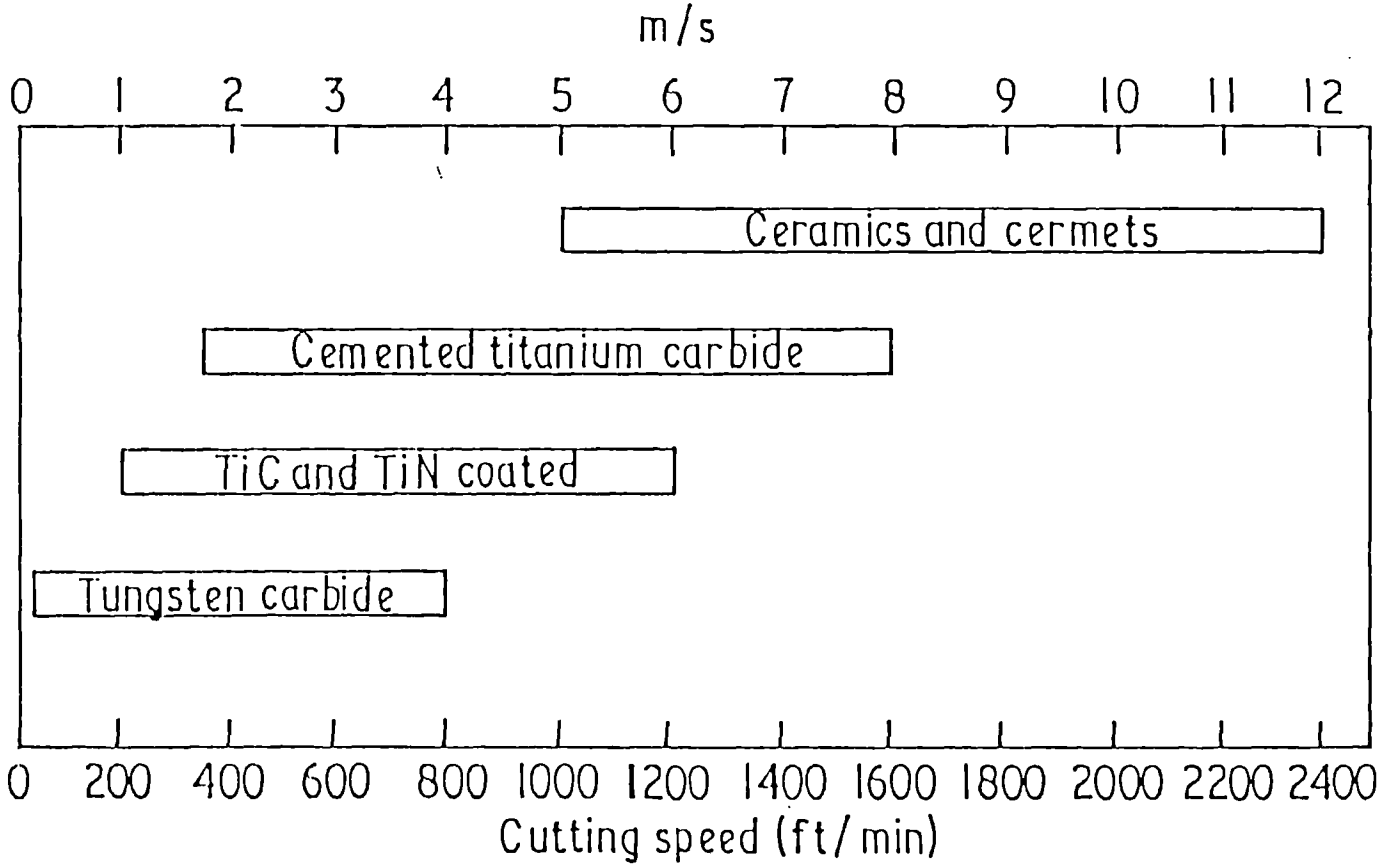

Fig 2.12 Cutting speed vs. tool material.

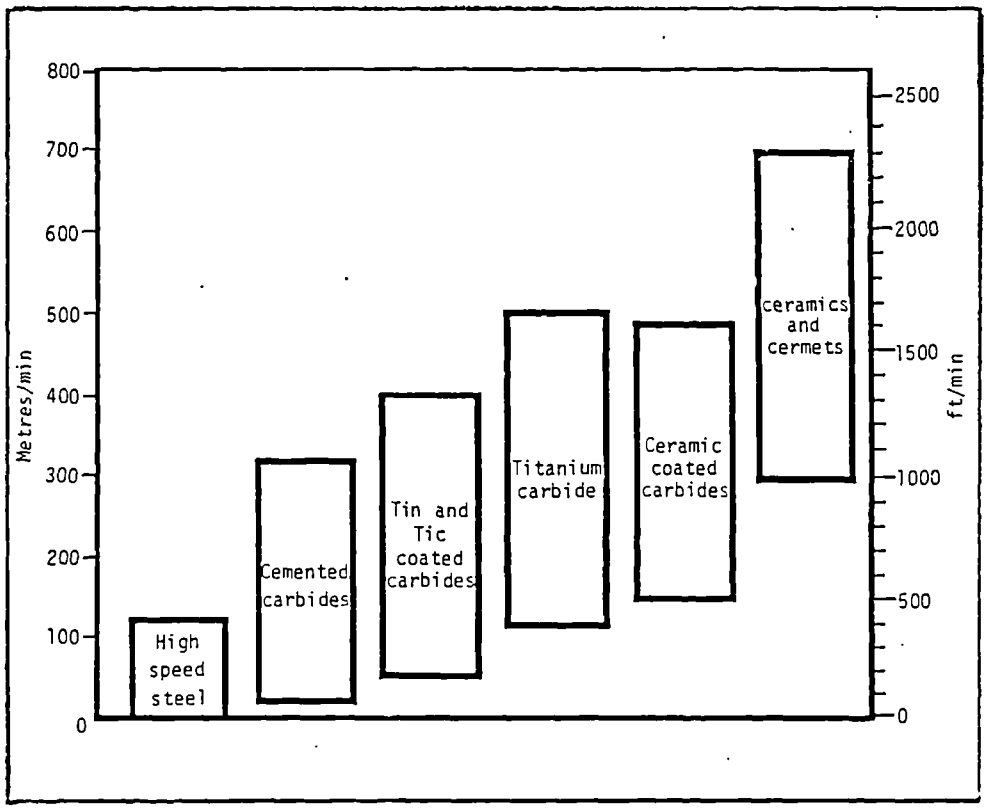

Fig 2.13 Graphical representation of approx speed ranges for turning carbide.

2.9.2 HIGH SPEED STEEL TOOLS

Present day high speed steels fall into two main categories, those containing tungsten and those containing molybdenum. Early high speed steels depended entirely upon tungsten for the formation of the MgC carbides present in the matrix. However, immediately prior to the Second World War and during it, due to shortages of tungsten, molybdenum was added to replace part or all of the tungsten. Only 1% of molybdenum was needed to replace 1.5 to 2% of tungsten. In general, tool steels based on tungsten have better hot hardness than those based on molybdenum, but those containing molybdenum have better wear resistance (99). The carbon content of these steels is typically 0.75 to 1.4%, the carbon being essential for the formation of the various carbides which promote wear resistance in the high speed steels. Other alloying additions include vanadium, cobalt and chromium. Vanadium is added to form V_4C_3 which increases wear resistance; cobalt increases the hot hardness of the steel and chromium improves the hardenability as well as the hot hardness (99-100). When producing these highly alloyed steels there is a marked tendency for banding to occur, which is caused by carbide segregation in the original steel ingot. To lessen the likelihood of this happening, metals are inoculated and forging and billet rolling is carefully planned (100). Recently, high speed steels have been produced using powder metallurgy techniques; specimens have been examined by Dulis and Neumeyer (101). They found that the carbide distribution within this steel was much more even and consistent than in a similar steel produced by conventional methods. The austenitising response time was faster than conventionally produced steels, hence decarburisation during heat treatment was less of a problem. Also, tool-life tests showed that the tools produced from powders had longer lives under the test conditions chosen; the tool-life increased as the powder from which the tools had been pressed decreased in size. Dimensional changes occurring during the heat treatment of the powder metallurgy tools was only a third of those encountered when heat treating conventional high speed steels. The

heat treatment of high speed steels, for optimum properties during machining, consists of austenitising, then quenching to produce martensite. This is followed by a single or double tempering procedure to ensure that no austenite is retained, the martensite matrix is toughened, and most importantly, that secondary hardening has occurred. The secondary hardening is necessary to endow the high speed steel with good high temperature properties.

Opitz and Konig (86) found that the wear rate of high speed steel tools increased with speed in most cases. However, when a BUE was present it protected the rake face, and the rake face wear rate decreased. However, the flank face wear rate was increased, due to the abrasive effect of the particles of the BUE which repeatedly broke away. The speed at which the tool failed was also shown to decrease as the feed increased. Hence, the wear rate was seen to increase as the rate of metal removal increased. Bownsword et al (102) concluded that at low speeds adhesion and abrasion wear accounted for the wear of high speed steel tools, but at high speeds (high rates of metal removal) plastic deformation of the tool preceded its collapse. They found that the chip was adhering to the tool in all the cases that they examined, and decided that at high machining speeds wear was due to the fall in the flow stress of the steel tools, and that this was caused by the temperatures which existed at the rake face. These high temperatures existed due to shear with the bottom of the chip. Wright (103) agreed that wear of high speed steel tools, at high cutting speeds, was due to plastic deformation of the tempered martensite matrix along the rake face. He also found that deformation could be detected when machining at low speeds if metals were being machined which possessed high strength at high temperatures. The nose of the tool was deformed by being pushed down below the level of the rake face, which increased the contact at the flank face and increased the heat produced at this source. This soon led to plastic flow of the tool edge which rapidly caused tool failure. In brief, it was possible for failure by plastic flow of the tool material to be instigated by heat generated at the flank face though, usually, heat

generated at the rake face was found to be the cause of tool deformation. Low speed wear of high speed steels mostly occurred as flank wear, rake face cratering only commencing as speed increased (86) with plastic flow then predominating. At high cutting speeds the temperatures which existed at the rake face were sufficient to soften the tool steel to the extent that it could be deformed by the chip material. The zone at the bottom of the chip was able to do this due to the increase in the flow stress of the chip material caused by the strain rate effect (102). This overcame the decrease in flow stress of the chip caused by the high temperature in this region. Wright (103) also showed that hard particles in the chip material ploughed along the tool and formed grooves in the rake face.

Due to their toughness high speed steel tools are frequently used when intermittent cutting is employed, for example when milling. Although the toughness of high speed steels is good, hot strength properties are inferior to those of cemented carbides; hence, they are not able to be used for machining at such high speeds as are cemented carbides. There is still plenty of scope for the use of high speed steels in machining, and a wide range of steels of different compositions is available for use in varying applications, depending on the toughness or the hot hardness required.

2.9.2.1 COATED HIGH SPEED STEEL

A development which could have important repercussions on the application of HSS cutting tools is the coating deposition method so successfully applied to carbides. The most commonly used technique, chemical vapour deposition, involves temperatures above those used in the heat treatment of HSS and therefore creates difficulties and requires careful subsequent heat treatment procedures to restore hardness and toughness. Nevertheless it can be used, and TiC and TiN treated tips can be obtained commercially.

Cutting trials conducted in the UK on TiN coated tools by Cutanit Ltd indicate improvements in the order of two to three times the tool life in operations such as form turning, facing and parting-off. Because of the inherent toughness of HSS (103), these coated tools should be well suited to interrupted cuts in operations such as milling. It has been found that some regrinding, on the clearance face is possible, without performance deterioration.

2.9.3 CEMENTED CARBIDES

Cemented carbides (sometimes also called less appropriately sintered carbides) are a group of sintered materials, the outstanding properties of which are high hardness and wear resistance. The success of cemented carbides in practical applications is closely related to their method of manufacture. Refractory carbides of the transition metals (such as WC, TiC, TaC, Cr_3C_2 or Mo_2C) are combined with a tough binder metal (most often cobalt, but in some cases nickel or other metals from the iron group).

Typical microstructures of commercial alloys are shown in Figure 2.14. In these combinations the positive properties of the components are superimposed; the main component (carbide phase) confers hardness and wear resistance, whilst the ductile binder contributes the toughness necessary for most applications.

'Tailor-made' composite materials in which the advantageous properties of the components are combined have been a concept to which extensive technical and scientific efforts have been devoted during the last decade. However, most attempts in this direction have not lived up to expectations, owing to the fact that the negative properties of the components are usually retained as well. Optimized properties as in the case of cemented carbides are seldom achieved (104).

The history of cemented carbides began in Germany during the first World War with successful attempts to produce drawing dies from tungsten carbide. The decisive breakthrough was achieved by Schroter in the early 1920s. Powders of tungsten carbide and cobalt were mixed and dense parts prepared by compacting the mixture and by heating the compacts above the melting point of the binder phase. Today, it is practically impossible to say whether this discovery was derived from a theoretical concept, or was essentially a result of good luck. The first patent in the field of sintered cemented carbides was issued in 1923 followed by numerous others (105-108).

From the beginning, cemented carbide technology was backed up by considerable research activity. Reviews on the achievements of basic research in the field of hard metals were published recently (107-108). The rapid development of WC co-alloys was expanded to other combinations. With multiple carbide alloys based on mixtures of WC-TiC with additions of (Ta, Nb)C, high speed machining of steel became possible. A large part of these later developments took place in the USA, Austria and Sweden, and more recently, in Japan, although most of the key inventions had been made in Germany. During the Second World War, because of a shortage of tungsten, the discovery and large scale production of tungsten carbide-free hard metals with titanium carbide as the main components was also started in Germany. From this group, titanium carbide-nickel alloys with additions of molybdenum carbide are still used for the shaping of materials which wear tools rapidly (109).

As shown in Figure 2.15, the historical development of cemented carbides follows three lines:

i) Improvements of tungsten carbide-based alloys achieved by addition of further carbides and alloying the binder phase, by the development of submicron tungsten carbides alloy, by hot isostatic recompaction after

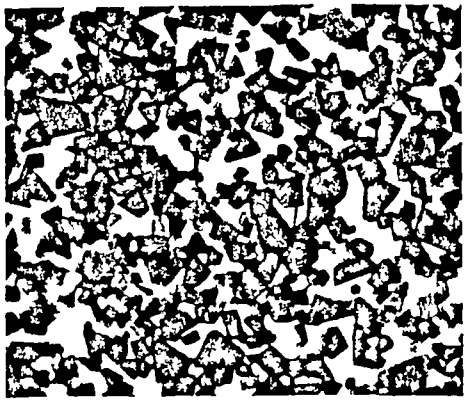

a) WC-10 wt-%Co alloy Formvar replica, electrolytic etch, x3000,

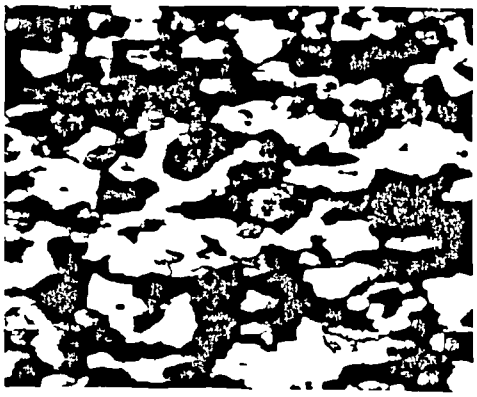

b) TiC-WC-TaC-Co alloy electron emission photograph (Balzers Methioscope) x3200

Fig 2 14 Microstructure of technical grades of cemented carbides (109)

Year(s)	WC-base sintered alloys	Year(s)	TiC- (and TaC)-base sintered alloys	Year(s)
1922–25	WC+Co (Widia*)	1929–31	TiC–Mo_2C+Ni, Cr, Mo (Titanit*)	1909
1927	Graphite-free WC+Co			1914
1928–29	WC with stellite binder	1930–31	TaC+Ni, Co (Ramet*)	1917
1931	WC–TiC+Co (Widia X*)	1931	TiC–TaC+Co	
1931	WC–TaC+Co (Carboloy*)	1931	TiC+Cr, Mo, W, Ni, Co (Böhlerit*)	1922
1932	WC–TiC–(Ta, Nb) +Co (Firthite*)	1938	TiC–VC+Ni, Fe	1930–31
1938	WC–Cr_3C_2+Co	1944	TiC–NbC+Ni, Co	
1951	Acid-resistant WC–Ni	1948–50	TiC–(Mo_2C, TaC) +Ni, Co(Cr)	1950–51
1956	WC–TiC–Ta(Nb)C–Cr_3C_2+Co	1949	TiC–VC–NbC–Mo_2C +Ni	1952–61
1959	WC–TiC–HfC+Co	1965–70	(TiC–Mo_2C)-mixtures +Ni, Mo	1953–55
1965	Hot isostatic compaction	1968–70	Solid-solution and precipitation-hardened alloys (Ti, Mo)C+Ni, Mo	1955–60
1967–70	Submicrometre WC+Co			1955–73
1967–70	WC–Fe, Ni, Co			
1968	WC–TiC–TaC–NbC +Co			1961–70
				1970
				1970 to present

*These names are trade names of products

Fig 2.15 Development of hard metals cutting tool materials (109).

liquid-phase sintering to reduce the number of flaws and porosity and by other refined production techniques.

ii) Tungsten-free alloys are finding increased technical interest owing to their advantages for special applications and to concern over supplies of raw material;

iii) Important discoveries closely related to cemented carbide technology either resulting in competitive (eg. ceramic cutting tools) or expanding and/or improving the classic cemented carbides (eg. carbonitride and boride hard metals or surface-treated WC-Co alloys) (109).

2.9.3.1 COATED CARBIDES

A constant problem in carbide manufacture has been to combine the crater resistance of high titanium grades with the toughness of grades containing higher cobalt and little or no TiC. The usual answer has been a compromise, the production of hard metals with intermediate amounts of TiC or WC/TiC/Ta(Nb)C grades with good toughness and reasonably high resistance to cratering.

An interesting development pushed to probably its limit of usefulness by Wickman Wimet, was the 'Laminated' tip. In this a core of cobalt-bonded tungsten carbide was given a sintered-on layer of a high titanium grade. Metallurgical bonding in this class of product is good, but different expansion between the core and surface layer sets up thermal stresses under cutting conditions where considerable heat is generated and spalling may occur. Nevertheless, more progress with this approach might have been made had it not been for the advent of pure TiC coatings.

Carbide and other coatings are without doubt the most important single development in the hard metal industry in recent years. Like most technological

achievements, it is difficult to pin them down to one particular inventor or organisation, but much of the original work certainly seems to have come from the Swiss Watch Research Institute (Laboratories Suisse de Recherches Horlogeres), where vapour-deposited TiC was first intended as a wear-resistant coating on watch cases and components. It was subsequently seized upon and developed by a number of progressive carbide manufactures, as the answer to the perennial steel-cutting problem.

Pure titanium carbide coatings are usually produced by reactive deposition from the gaseous phase, whereby for example, titanium tetrachloride vapour is converted to extremely finer-grained titanium carbide crystals. These are 'grown' from a substrate of conventional sintered carbide, as a coating only a few micrometres thick. Although the bond between substrate and coating was originally thought to be stress-free, even at this scale thermal effects were found to exist, and spalling could not be completely eliminated.

2.9.3.2 PERFORMANCE OF COATED CARBIDES

T. E. Hale and D. E. Graham (110) in a paper published on the influence of coating thicknesses and compositions upon metal cutting performance indicate that the popularity of multi layered carbides stems from their superior combination of wear resistance and breakage resistance, relative to uncoated carbides. Figure 2.16 shows a 5 micron TiC coated carbide used for this comparison. It showed a bend strength reduction of about 25% which increases the wear resistance by a factor of 2.5 to 4.0.

Figure 2.17 shows crater wear rate vs Al_2O_3 coating thickness. It can be seen that the crater wear rate increased after the coating was penetrated. Up to 5 micron relatively low rates were obtained and then their rates increased rapidly. Even when

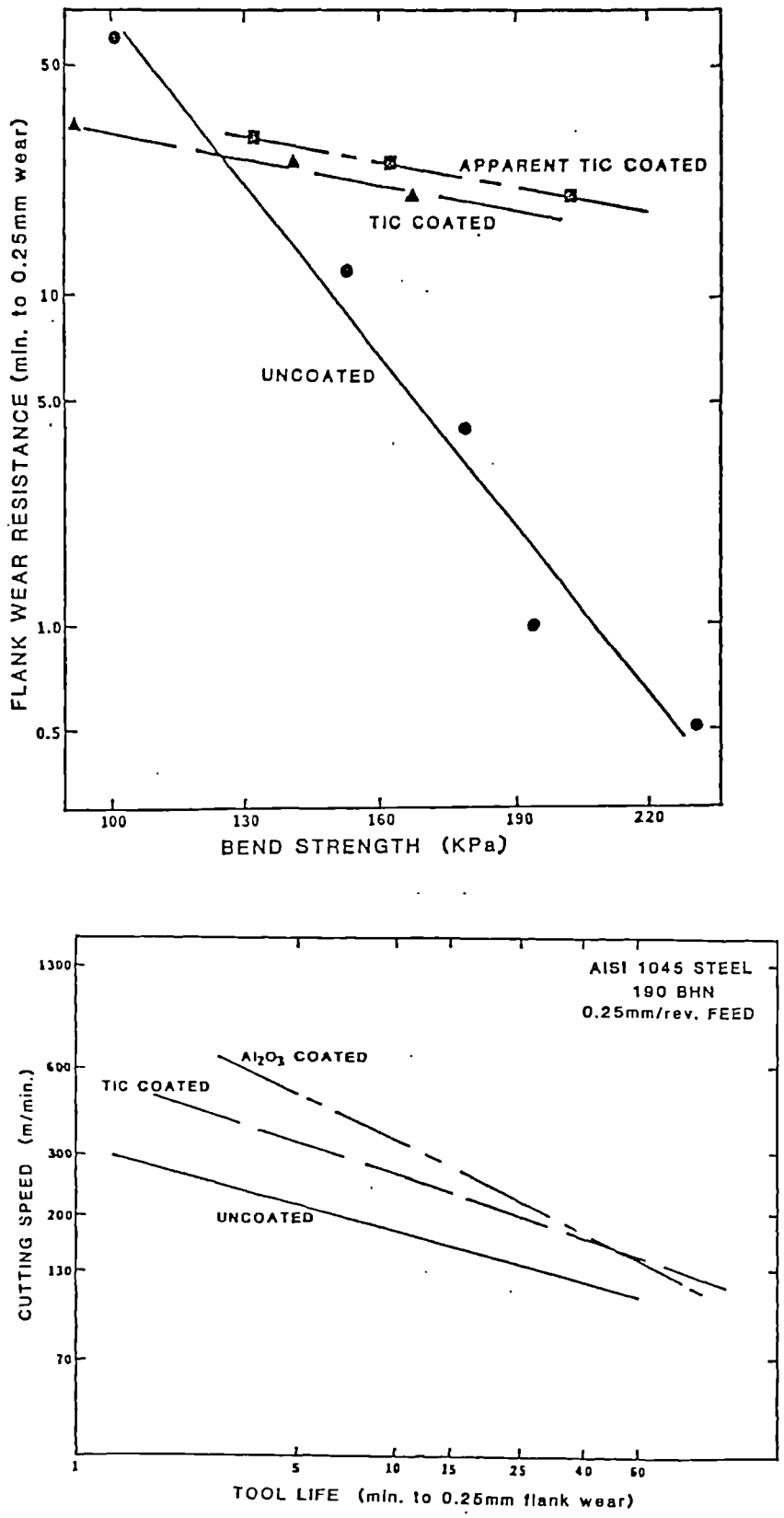

Fig 2.16 a) Flank wear resistance versus bend strength

b) Cutting speed versus tool life (110).

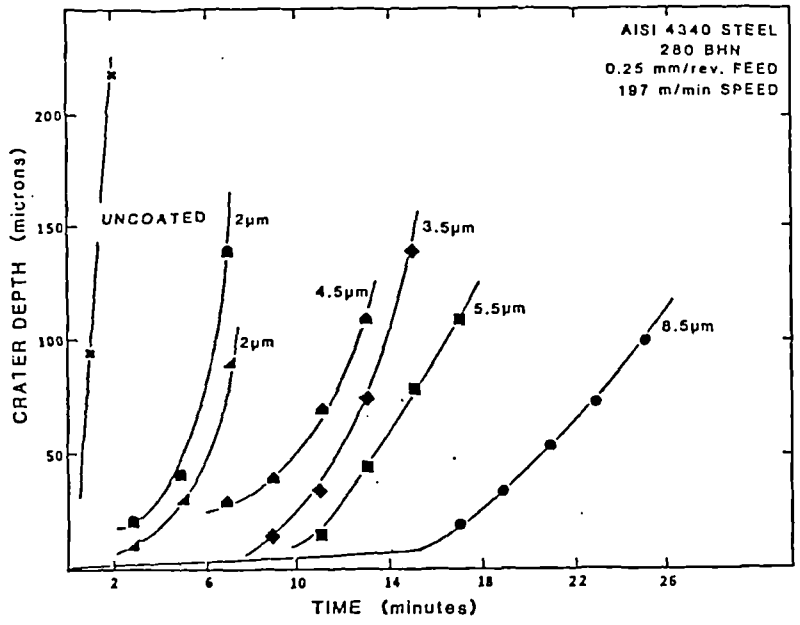

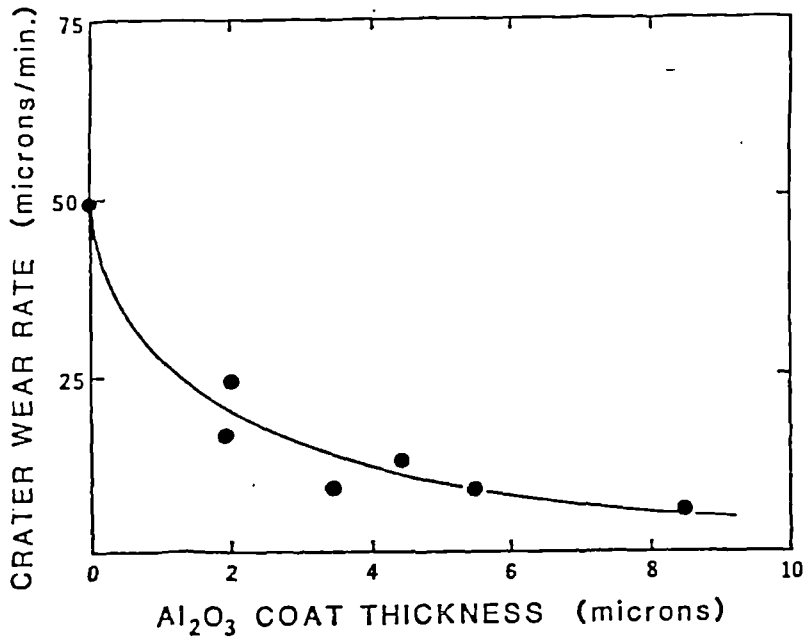

Fig 2.17 a) Crater wear versus Al_2O_3 coat thickness

b) Crater wear rate after coat penetration versus coat thickness (110).

the coating was penetrated, the coating at the edge of the crater retards the crater growth at a rate dependent upon coating thickness. The inherent crater wear resistance of Al_2O_3 coating, which is provided by a chemical/diffusion reaction barrier at the chip contact zone, is more than twice that of TiC or TiN coating (110).

Figure 2.18 was obtained from the results of machining AISI 1045 steel at 300 m/min with 5 inserts of the same material but one with no coating, one fully coated and three partially coated inserts. This indicates the critical region for flank wear appears to be a narrow zone at the bottom of the flank wear scar. Coatings thus improve the flank wear resistance.

Figure 2.19 shows the influence of coating thickness on flank wear for Al_2O_3 and TiC coatings. This proves that flank wear resistance is insensitive to coating thickness beyond a minimum value of 5-9 microns. As cutting-speeds increase the chemical wear increasingly dominates. Thus more abrasion resistant coatings, such as TiC, work better at lower speeds, whilst more chemically stable coatings, such as Al_2O_3 resist wear better at high speeds.

Schintlmeister (111) investigated the effect of the geometrical parameters of TiC and TiN coatings on their transverse rupture strength (TRS). Thick coatings (above 5-6 microns) and the presence of the Eta phase reduces the TRS. An equiaxed grain structure of the coated layer provides a greater TRS than a columnar or an amorphous structure. Schintlmeister and Pacher (112) observed that the composite coatings of TiC and Ti(C,N) performed better than a single coating of TiC or TiN.

Sadahiro (113) developed a Ti(N,C,O) type coated tool to achieve better chemical stability and wear resistance than TiC and TiN coated tools. Under suitable conditions and sufficiently high speeds the tool had a longer life than TiC and TiC + Al_2O_3 coated tools. Krapantek (114) carried out wear tests of coated tools and

conventional uncoated carbide tools and observed that tools of the TiC/$A1_2O_3$ and TiN/Ti (C,N)/TiN types were greatly superior to tools coated with Tic/Ti (C,N)/TiN.

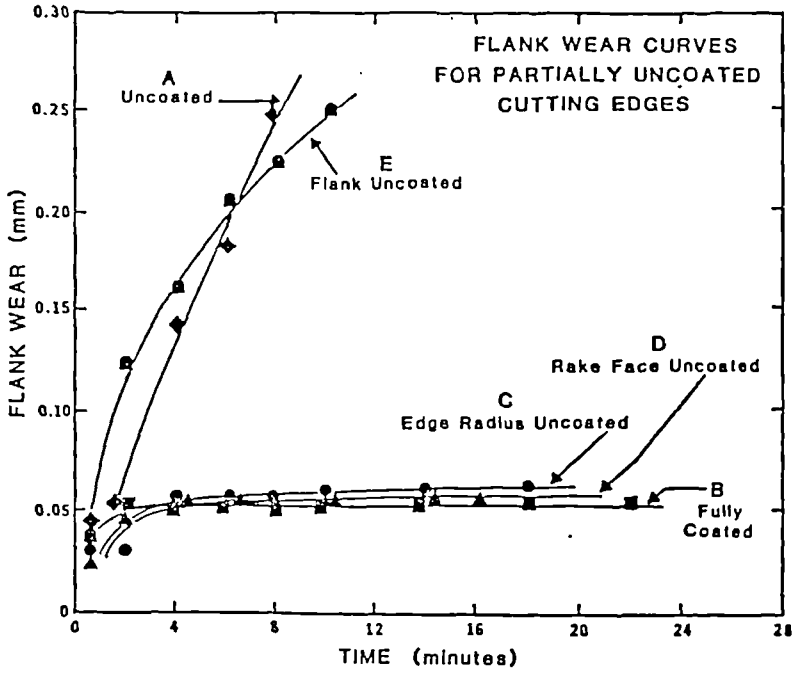

Fig 2.18 Crater wear resistance as a function of thickness for Al_2O_3 (110).

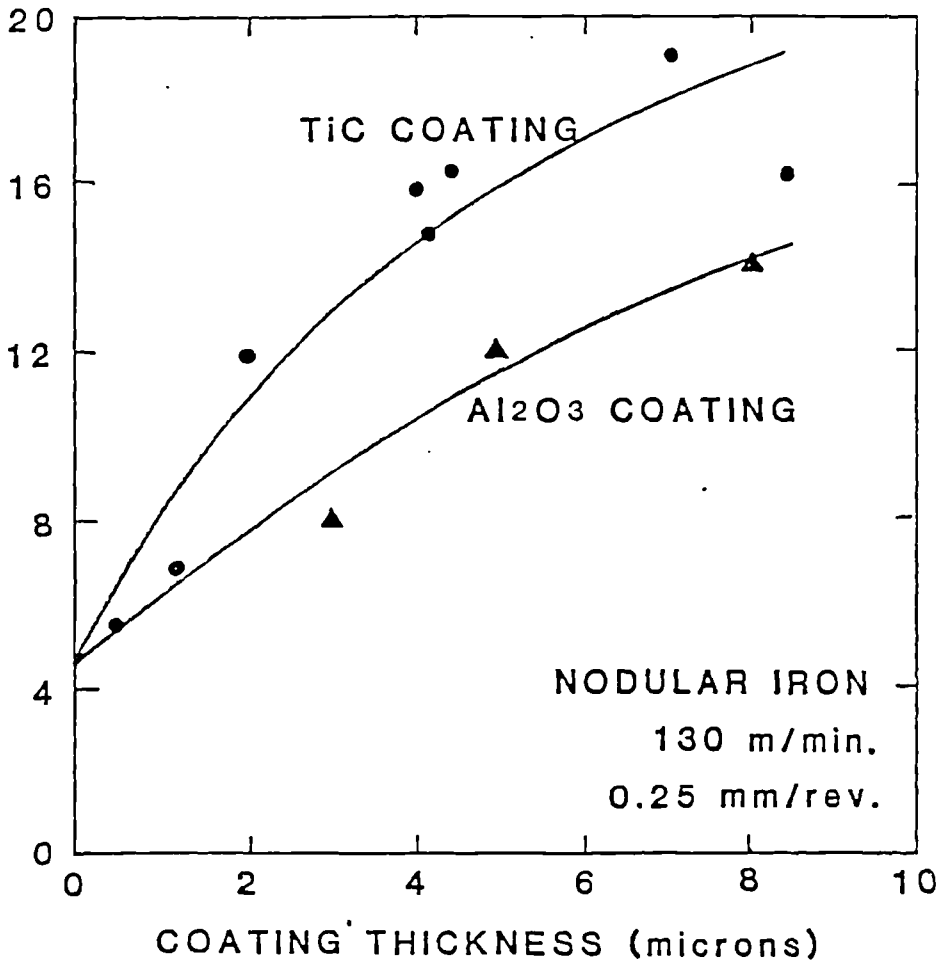

Fig 2.19 Time to 0.25 mm flank wear as a function of coating thickness for TiC and Al_2O_3 coating (110).

2.9.4 CERAMIC

More than 20 years ago, aluminium oxide ceramic cutting tool materials were under active development in the UK and elsewhere, but difficulties associated with lack of strength and toughness at the cutting edge led to the disappearance of many of the earlier materials. More recently there has been a revival of interest, mostly in the USA and Germany, following improvements in the properties of ceramic tools. Improved processing techniques, include hot pressing, control of microstructure with high purity materials and selected additives, and the use of substantial mixtures of 15 to 30% titanium carbide. These modified ceramic materials are termed cermets and have enough strength for machining at feeds of say 0.4 mm/rev and for face milling cast iron and perhaps even steel. Strength, thermal shock resistance and impact resistance are still the limiting factors in the performance of ceramic tools and they are not usually recommended for interrupted cutting (2).

Ceramic cutting tool material, made by way of sintering, offers great resistance to wear and little tendency towards diffusion. However, low bending fatigue strength and vulnerability to impact, as well as thermal shock leads to fracture which often ends tool life prematurely. Sufficient rigidity of the machine, workpiece, and tool, together with high machine power and a suitable arrangement of the cut-in and cut-out conditions are all preconditions for an economic use of these tools.

Basically, ceramics fall into three categories:

a) Alumina based pure oxides with more than 90% purity, less than 2% porosity and a fine grain size (6.5 microns) but with poor thermal and mechanical shock resistance and unpredictability at certain speeds.

b) Cermets - which fall into the "carboxide" category and are formed by mixing up to 15% of TiC in a matrix of Al_2O_3 and having a very fine grain size (2

microns). These have similar properties to alumina but with improved thermal and mechanical shock resistance.

c) Sialons (Si-Al-O-N) are silicon nitride based materials with aluminium and oxygen additions. Silicon nitride (Si_3N_4) has useful properties, including high hardness (2000 Hv), bend strength better than that of alumina (900 MPa) and a low coefficient of thermal expansion ($3.2 * 10^{-6}$), leading to good thermal shock resistance. It has been tried as a cutting tool material, but has not been used industrially, because the production of high density accurately shaped tools requires costly hot pressing processes.

2.9.5 DIAMOND

Diamond-tipped tools have been used for fine finish machining for many years. Because diamond reacts chemically with ferrous metals at higher cutting speeds, diamond tools have no practical use in the machining of steels or cast iron. However, they are suitable for machining very abrasive, non-metallic materials such as ceramics, plastics, rubber and fibre glass. They are also useful for machining aluminium and its alloys, including the highly abrasive silicon-aluminium alloys used in some internal combustion engine parts. A whole range of non-ferrous metals such as brass, bronze, copper and their alloys are also machinable with diamond tools (2).

The first reference to the use of manufactured polycrystalline diamond for metal cutting was made by Semko et al (115) in 1970 following its use for cutting glass reinforced plastics, which was reported by Semko et al (116) in the previous year. He found that, in turning an aluminium alloy containing 11-13% silicon (a typical piston alloy), ballas tools had a life 100 times greater than that of the most suitable grade of sintered carbide tool. He also observed a difference in the cutting

forces obtained with the two types of tool in that the forces for the ballas tool were 1.5 to 3 times lower than those for carbide.

Towards the end of 1972, the General Electric Co USA (117) announced that it had successfully manufactured synthetic polycrystalline diamond suitable for use as a cutting tool. The material was different from the other types so far reported in that it consisted of a layer of diamond powder, sintered to a thicker substrate of sintered tungsten carbide.

Various reports of successful applications of this material (called compax diamond) and "megadiamond" appeared in technical journals during 1973 and 1974, such as American Machinist (118). In this report, both materials were cited as having been successful in cutting a variety of workpiece materials - including aluminium alloys with high silicon contents. In most cases, higher cutting speeds were being used than with sintered carbides and an increased tool life was observed.

In 1976, Bex and Wilson (119) described a new polycrystalline diamond tool material manufactured by De Beers Industrial Diamond Division. The material, called Syndite, was very similar in appearance to compax diamond, in that it consisted of a synthetic diamond layer on a sintered tungsten carbide substrate. Bex reported that in cutting aluminium/silicon alloy containing 18% silicon, Syndite had a similar economic cutting speed to single crystal diamond and thus it could be used as a direct substitute. Furthermore, single-crystal diamond lacks impact resistance and may crack or chip easily under impact and, being a product of nature, it varies in properties. Thus, its level of performance as a cutting tool is not predictable. Finally, the wear resistance of single-crystal natural diamond is anisotropic and thus, for minimum tool wear, the diamond must be carefully orientated. Many of these difficulties have been overcome with the development of polycrystalline diamond tool blanks in which small individual crystals of diamond are compacted in random orientation, and bonded to a tungsten carbide base.

In 1977, De Beers described machining tests on Ti-6AL-4V which compared the performance of a Syndite tool, made from a 90° segment brazed on to a steel shank, to that of a multi-coated carbide tool in turning a 65 mm square by 145 mm long billet to a diameter of 64 mm (120-122). At a cutting speed of 56 m/min the carbide tool was badly worn after a single pass over a length of 70 mm, representing a total stock removal of 0.07 cm^3 . The Syndite tool, under the same intermittent cutting conditions, was able to remove 132 cm^3 of material before showing signs of comparable wear. Excellent surface finish was obtained with the Syndite tool, which was tested at depths of cut up to 3 mm with good results. The coated carbide tool is not necessarily a good basis for comparison, but the results from the Syndite tool were impressive in their own right.

De Beers published a series of reports on Syndite in 1979 that dealt with tests of the material in various machining applications, as well as wire drawing, grinding wheel dressing and rock drilling applications. Turning tests were performed on Ti-6A1-4V and Syndite was shown (122) to give twice the stock removal rate of a tungsten carbide tool in this application (under their equivalent chip thickness criterion).

The present work showed that carbide tools lasted for a maximum of 2 minutes at high speed machining (200 m/min), while syndite tools were used for 24 minutes and were still capable of further use.

Haltemprice Timber (Humberside factory) recently changed from HSS to PCD tipped cutters largely because of the excessive downtime experienced due to frequent changing of HSS cuttters. Actual machining costs are about the same but with HSS cutters the machine was out of action for at least one hour every eight shifts. Following the introduction of Syndite, tool changing takes place every fortnight, after some 4000 door panels have been machined. The HSS cutters needed

replacing after machining only 50 panels and HT estimates that production rates have increased by around 14%.

The idea of using diamond for machining titanium is not new in that diamond turning tools have been used to achieve high surface finishes on space vehicle components since as early as 1976. In an article by Milbrandt in Industrial Diamond Review in that year, diamond turning tools were reported to give not only better surface finish, but also to have performed operations on thin walled parts which were difficult to perform without distortion of the part when using carbides (121). The diamond lathe tools showed excellent life and could be used at four times the cutting speed of carbides for the same operations.

2.9.5.1 POLYCRYSTALLINE DIAMOND (PCD)

Polycrystalline diamond tools are aggregates of randomly oriented particles, which behave as an isotropic material in many applications. Natural diamonds have only one large crystal unlike PCD which has thousands of randomly placed crystals joined together. It is because of this random orientation that the problem of cleavage or fracture is not severe. The overall performance of the tool will not be affected when one or two crystals fracture as there are thousands of crystals which are correctly aligned. The basic structure of the tool is a laminated one with a dense layer of synthetic PCD bonded to a tungsten-carbide (WC) substrate with the aid of an intermediate refractory metallic bonding layer. The WC layer provides adequate toughness and resilience particularly during shock loading. Better performance of the tool is ensured by the polycrystalline layer. This layer also absorbs any stresses which may result, for instance, from the differing thermal properties of the PCD zone and the carbide substrate. This structure can out perform natural diamond in terms of its abrasion resistance.

2.9.5.2 PROPERTIES OF PCD

1. High Hardness

PCD has a very high hardness approaching that of single crystal diamond. The hardness of both single crystal diamond and PCD decreases as the temperature increases as with other tool materials. Brookes and Lamber (123) have shown that the high temperature hardness of diamond is much higher than that of other tool materials, Figure 2.20.

2. Thermal Conductivity

PCD has a comparatively high thermal conductivity of about 560 w/m $^{\circ}$C. This is slightly lower than that of natural diamond (665 w/m $^{\circ}$C).

3. Abrasion Resistance

PCD tooling has higher abrasion resistance than natural diamond. The high abrasion resistance of PCD coupled with its high resistance to loading enables it to be used for effective machining of non-ferrous materials.

The main advantages of sintered polycrystalline tools over natural single crystal tools are better control over amounts of inclusions and imperfections, higher quality, greater toughness and wear resistance resulting from the random orientation of diamond grains and the corresponding lack of simple cleavage planes. Also, sintered tools can be manufactured to meet strategic needs since nature or some artificial control does not dictate their availability.

2.9.5.3 MANUFACTURING PROCESS OF PCD

Polycrystalline diamond is produced by sintering together carefully selected fine diamond particles at very high temperatures and ultra-high pressure, a process

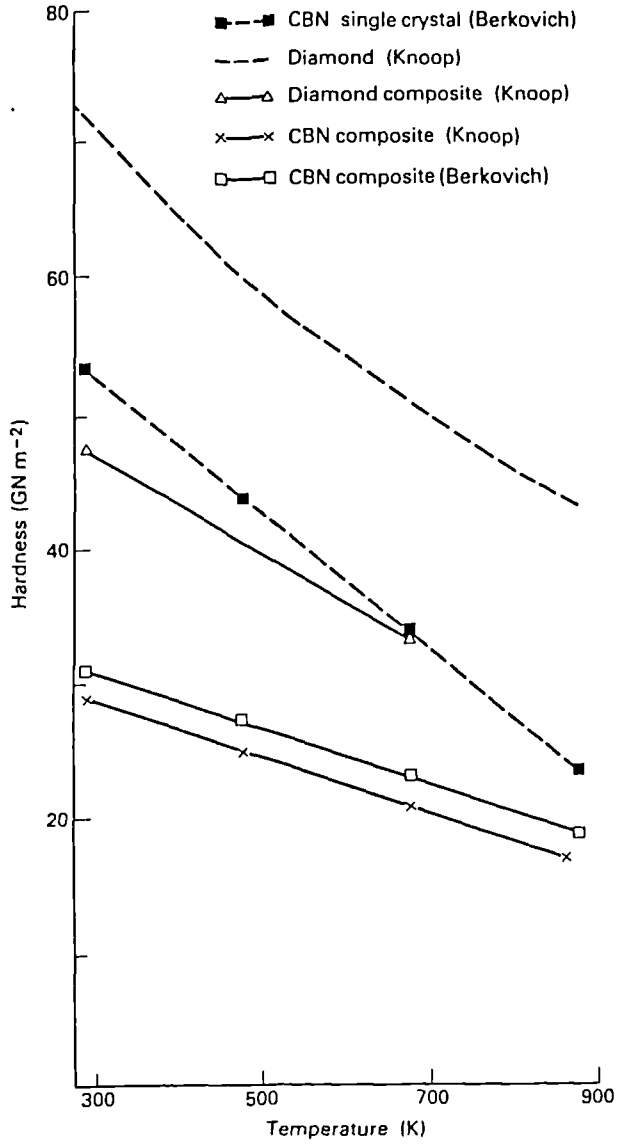

Fig 2.20 The effect of temperature on the hardness of ultrahard material (GNm^{-2} = GPa) (123).

first developed in the 1950s. There are two stages involved in the production of PCD. The first stage involves the production of the diamond grit, which is widely used as an abrasive for grinding non-ferrous and ferrous materials. This is followed by a stage in which the grit is compacted into the required shape (124). The same ultra-high pressure technology is employed in both processes. The sintering process is rigidly controlled within the diamond stable region. Diamond is the metastable cubic form of carbon while graphite (an extremely soft material) is carbon in a stable hexagonal form. Diamond is produced from graphite by transforming the crystal structure of carbon from hexagonal to cubic form under the appropriate conditions of pressure and temperature, and with the aid of a suitable catalyst solvent.

Initial attempts at diamond synthesis were carried out by Bridgman (125) who was able to maintain temperatures near 3000 K at a pressure of about 29 Kbar for short periods of time. The time duration was too short to enable the conversion of graphite directly to diamond. Later investigation by researchers at the General Electric Company discovered that the presence of certain catalysts increased the rate of conversion of graphite to diamond to a practical level at relatively low temperatures and pressures (126, 127). Subsequently, Bundy (128) discovered that the direct conversion of graphite to diamond without catalysts is possible, but only at extremely high pressure (above 125 Kbar) and temperature (about 3000 $^{\circ}$C). The graphite collapses spontaneously into PCD under these conditions.

There are a number of elements used as catalysts in diamond synthesis. These include chromium (Cr), manganese (Mn), tantalum (Ta), as well as all the elements of group VIII of the periodic table (129). Carbides and compounds of these elements that decompose at or below diamond synthesis conditions may also be used. The catalytic elements play a dual role during diamond synthesis; as a catalyst and as a good solvent for graphite, but poor solvent for diamond. The graphite first dissolves into the catalyst and is then converted into diamond at the appropriate conditions of

pressure and temperature within the diamond stable region. The diamond precipitates since it is relatively insoluble in the molten catalyst. This phenomenon allows more of the non-diamond form of carbon to go into the solution. Since the catalytic element must be in the molten state, this establishes a lower temperature limit for a given catalyst. Each catalyst has a different pressure-temperature region of effectiveness. Nickel is the most commonly used catalyst in diamond synthesis at pressures of 75 to 95 Kbar and temperatures of about 2000 $^{\circ}$C. The effectiveness of nickel could be due to the fact that its unit cell is the same size as that of diamond.

The rate of diamond formation is dependent on the sintering pressure. Higher pressure, above the equilibrium line at a given temperature increases the rate of diamond nucleation and growth. Diamonds formed at pressures substantially above the equilibrium line develop from many nuclei and have a skeletal structure. This type of diamond is very friable and mainly used in resin or vitrified grinding wheels. Large and more perfect single crystals of diamond are formed by subjecting the reaction mixture to pressures and temperatures closer to the equilibrium for a longer time, to develop fewer nucleation sites. A twinned structure is frequently obtained when the growth rates (pressure) are very high. Temperature also has a major influence on the crystal habit and colour of diamonds produced.

The PCD inserts are made up of a thin layer (0.5 to 1.55 mm) of fine grain size diamond particles sintered together and metallurgically bonded to a cemented carbide substrate. The firm bonding ensures extreme hardness and toughness, excellent abrasion resistance as well as high thermal conductivity. The tool tip formed is usually about 3 mm thick. The production process involves the initial packing of fine diamond powder (1 to 30 μm) on a support base layer which has a dual function; as a support and toughening agent as well as providing stability in both handling and fabrication (130).

The retention of diamond particles in a metal bonded tool can be improved by holding the particles mechanically and bonding them chemically to the binding metal. This is achieved by coating the particles with titanium which forms a carbide with diamond and alloys with the metal used in the matrix (131). The advantage of increased particle retention and titanized coating is the decrease in surface graphitization at high temperatures which results in a reduction of weight loss and increased retention. Sintered diamond tools are finished to shape, size and accuracy by laser cutting and grinding.

The high cost of sintered PCD in comparison to cemented carbide or ceramic tools, is mainly due to the very expensive processing technique. This involves high temperature and high pressure sintering and finishing methods for diamond tools. However PCD tooling is used in many applications despite its high costs because the increased productivity, and prolonged tool life are economical on an overall cost per part basis.

The successful synthesis of diamond has not only enabled the economic manufacture of diamonds for industrial use but also has made it possible to tailor grain size, strength and friability by controlling the pressure, temperature and processing time during synthesis. The manufacture of diamond with the required size has eliminated the need for crushing which weakens the product by leaving behind cracks of uncontrolled size.

2.9.5.4 AVAILABILITY AND USES OF PCD

The use of PCD in commercial quantities started in the early 1970s. PCD tools commercially available as Compax tools were produced by the General Electric Company, USA, and Syndite produced by De Beers. Composite tools can be clamped or brazed to shanks, ground, lapped and polished. Worn composite tools can be reground, the grinding taking longer than for carbide tools.

PCD tools are suitable for fine machining cuts on non-ferrous and very abrasive nonmetallic materials such as graphite, plastics, glass reinforced plastics, ceramics, rubber, chip board and fibre board plastics etc (Table 2.1). They are also used for machining abrasive wheel dresser wear parts, wire drawing dies, rotary drill bits, presintered (green) and sintered tungsten carbide as well as gold, silver and titanium alloys (132).

Wood materials, such as chipboard, MDF, hardboard and hard natural woods, have always proved difficult to machine using conventional HSS or carbide cutting tools. The toughness and enhanced wear resistance of PCD makes it the ideal tool material for machining these types of wood materials. Not only is tool life far greater, which in itself often justifies the high initial outlay, but savings can also be made in reduced downtime for tool changing. This is particularly true of mass production systems where CNC machinery is employed.

A negative rake (-5°) PCD tool with suitable edge preparation is required for effective machining of pressed and sintered tungsten carbide because PCD tools are very brittle. However, high positive rake ($+15^{\circ}$) geometry is recommended when machining softer materials like aluminium-silicon alloys, super-finishing of aluminium or copper front surface mirrors and motor commutators. Positive rake PCD tools are commonly used.

Nonferrous metals	Abrasive nonmetallics
Silicon-aluminium alloy	Carbon
Brass Alloys	Ceramics, unfired
Bronze alloys	Epoxy resins
Copper & Copper alloys	Fibreglass composites
Lead alloys	Graphite
Manganese alloys	Phenolics
Precious metals	Plastics
Tungsten carbide	
Pre-sintered	Rubber
	Wood by-product
	Wood

Table 2.1 Materials suitable for machining with PCD tools.

2.9.6 CUBIC BORON NITRIDE

Cubic boron nitride can no longer be described as a new cutting tool material. It was developed in the 1960s and has been available in the USA and UK, at least in small quantities, for trial purposes since the early 1970s. Polycrystalline cubic boron nitride is manufactured by a high pressure technology similar to that required for polycrystalline diamond and is similarly available bonded to a carbide substrate in relatively small tips. Cubic boron nitride is said to be (apart from diamond) the hardest and most abrasion resistant material known to man, but unlike diamond it is impervious to chemical attack by ferrous metals and to oxidation at high machining temperatures.

The possibility of polycrystalline boron nitride being used for single point cutting tools was first discussed by Verschagin et al (133) in 1971. In 1972, a series of reports emanated from the USSR about the use of this type of tool material, mainly for cutting high strength steels. Martirosov et al (134) however, also referred to its effective use for machining high strength irons. The form of the tool, according to the information given by Martirosov, appeared to be similar to the carbon diamond tools also manufactured in the USSR.

In 1972, a brief report (117) referred to the manufacture by The General Electric Co of a cubic boron nitride tool material similar in form to their compax diamond. In 1973 Hanneman and Hibbs (135) reported on "Borazon Compact Cutting Tools". These were made by General Electric Co, USA, and the report compared the properties of the new tool material with those of its competitors, diamond and sintered carbide, and described the manufacturing process in some detail. Its usefulness in cutting some difficult-to-machine nickel and cobalt based superalloys was highlighted but some mention was also made of its application to the machining of chill cast iron.

Bakul et al (136) described the use of Ismit cutting tools (polycrystalline cubic boron nitride) for machining cast iron (Table 2.2). It was concluded that the use of Ismit instead of an MOZ grade sintered carbide provided an improved surface finish in addition to a 40%-60% increase in material removal rate, and six to eight times longer tool life.

Later in 1975 Herzog (137) reported on the use of Borazon CBN tools for machining a variety of workpiece materials. Rough turning parameters were listed for twenty one different materials including various steels, irons and supperalloys; some guidelines for turning were also given in which it was suggested that the tool would perform best at metal removal rates an order of magnitude higher than with conventional tools.

2.9.6.1 PROPERTIES OF CBN

CBN is made up of two interpenetrating face centred cubic lattices, one of boron atoms and the other of nitrogen atoms. The structure of CBN is very rigid, although not all the bonds between neighbouring atoms are covalent. Twenty five per cent of the bonding is ionic (123). This composition therefore produces CBN which is the next hardest substance to diamond. The hardness of CBN decreases with increments in temperature. However, the hardness value is higher than other tool materials at any temperature. Polycrystalline CBN has a very high hot hardness. The hardness of CBN at 750 ^{o}C is approximately equal to that of oxide ceramics and tungsten carbide at room temperature.

CBN tools can withstand edge temperatures up to 1300 ^{o}C. This is because the lattice structure of CBN does not revert to the hexagonal form at temperatures belwo 1200 ^{o}C under atmospheric pressure (145). Polycrystalline CBN consists of a randomly oriented intergrown mass of CBN crystals of micron size. The

Alloy steel (Hardened)	Cobalt base alloys
4140 - Chrome-moly	Golmony
52100 - Chromium	Stellite
8720 - Nickel-chrome-moly Wallex	
Chilled iron	Ni Hard (cast)
Flame-sprayed alloys	Stainless steel, 420
Meehanite iron	Tempered stainless steel,440 (tempered)

Nickel base alloys	Tool steels
Inconel	A-2 air hardening cold work
Incoloy	D-2 high carbon high chronium
K-monel (Age hardened)	M-2 may high speed
Rene 77	O-1 oil-hardening cold work
Waspalloy	S-5 shock-resisting

Table 2.2 Materials suitable for machining with CBN tools

anisotropic behaviour of single crystals, which easily cleave along certain lattice directions does not occur in the polycrystalline material, which is isotropic and does not have cleavage planes.

CBN tools have high thermal stability. The tool has no practical oxidation below 100 °C (138). This gives the insert the hardness of boron nitride combined with the toughness of cemented carbide. Polycrystalline CBN has higher thermal conductivity (100 to 135 w/m °C) than tungsten carbide tools. A major advantage of CBN when compared with diamond is its greater stability at higher temperatures in air or in contact with iron and other metals. CBN is stable in air for long periods at temperatures over 1000 °C and its behaviour as a cutting tool suggests that it does not react rapidly with steel at considerably higher temperatures (2). It has high chemical resistance to most work materials at high machining temperatures. CBN has a lower coefficient of thermal expansion than the carbides.

2.9.6.2 MANUFACTURING PROCESS OF CBN

Hexagonal boron nitride is the starting material for producing CBN. The crystal structures of hexagonal boron nitride and graphite are very similar. CBN has a finer crystal structure than diamond (131). The similarities in the crystal structure of diamond and hexagonal boron nitride prompted Wentorf to investigate the possibility of a high temperature, high pressure, stable, cubic form of boron nitride, similar to diamond. Initial attempts to produce CBN using the same process as that of diamond synthesis proved unsuccessful until Wentorf (139) devised a means of producing CBN using entirely different catalyst solvents. These catalyst solvents were found to be the alkali metals, the alkaline earth metals, their nitrides, antimony, tin and lead or a combination of these. They are added during production to lower the combined pressure/temperature transition ceiling. The catalysts (or additives) govern the exact

transition during production and are therefore a commercial necessity. Some of the catalysts are effective only at high pressures and temperatures. Later investigations revealed the possibility of transforming hexagonal boron nitride directly to denser forms without a catalyst (140). The size of the resultant crystal formed with the later method is small (1 μm or less).

The larger grain size of commercial CBN crystals could only be produced in the presence of a catalyst (preferably magnesium (129)). The higher the atomic weight of the cataltyst, the higher the pressure necessary to effect the transformation. The most effective catalysts were found to be nitrides of magnesium, calcium or lithium. The presence of a small quantity of water or boric oxide (B203) greatly reduces the efficiency of any catalyst.

The exact mechanism of transformation of the hexagonal boron nitride to cubic form is not yet known. However, it is assumed that the catalyst metal first converts to its nitride at the operating conditions. The nitride then reacts with some of the boron nitride to form a loose complex compound which acts as a molten solvent, dissolving the remaining boron nitride. Some of the boron nitride is subsequently precipitated as CBN. The reaction conditions should be kept between 3 to 5 minutes since the size of the CBN particles increases with time. Impurities in the CBN can be in the form of nitrides of catallytic elements, free boron and boric oxide.

Different processes are presently being used for the production of CBN composite materials. The products can be either polycrystalline CBN bonded onto cemented tungsten carbide or polycrystalline CBN composite material without any metal support. A small amount of metal is blended with the boron nitride to achieve full density. Conventional sintered CBN contains a cobalt alloy as a bonding material. Titanium nitride and titanium carbide are used as a bonding material for the new type of CBN developed known as Sumiboron and Borazon respectively. The properties and cutting performance of CBN are determined by the rigid

polycrystalline boron nitride. The small addition of a metal plays only a minor role. it may affect the tool properties through its action during sintering which must influence the structure of the product. Tabuchi et al (141) have reported another method of producing CBN tools with a special ceramic as the binder instead of metal. The tools produced by this method have similar properties and performance characteristics as the ones produced with a metal binder.

Substantial plastic deformation of the CBN particles occur at the areas of contact between the CBN crystals during the extremely high pressure synthesis process. The high pressure concentrates only at the contact areas between the CBN crystals. It does not extend to crystal surfaces at points away from the contact areas (voids). These surfaces not reached by the high pressure are quickly converted to hexagonal boron nitride because of the very high temperature at this point where CBN is unstable. Catalyst material is brought into the voids in the compact to reconvert any hexagonal boron nitride to CBN, thereby completing the orientation process between the existing crystals.

2.9.6.3 AVAILABILITY AND RECOMMENDED USE OF CBN

CBN is commercially available as Borazon and Amborite marketed by the General Electric Company and De Beers respectively. They are produced as unbacked inserts which are used on both sides. CBN inserts are available, chamfered and unchamfered in round, square, triangular and rhombus shapes. They are usually used with negative rake with chamfers on the edge similar to those on ceramic tools. This geometry enables them to be used for interrupted cutting of hardened steels such as the turning of bars with slots or holes or in use as milling cutters despite their brittleness.

The initial application of CBN was in the tool and cutter grinding of high speed steel where there were problems with conventional abrasive tools (131). CBN replaced synthetic and natural diamonds which are not thermally stable and readily react with iron at high temperature. CBN has a combination of mechanical and thermal properties which have enabled it to be used for the machining of difficult to cut materials such as hardened steels and die steels. Martensitic cast iron (Nihard), Chill cast iron, white iron, grey cast iron (Meehanite), superalloys excluding titanium-based metals, etc. In short CBN tooling could be used for effective machining of materials having a hardness greater than 55 RC (approximately 620 HV) with the exception of superalloys (130).

CBN inserts can be used for wet machining of metals which have a hardness of above 45 RC (approximately 480 HV). An abundance of coolant is required in these cases. The use of coolants has no effect on the tool life of polycrystalline CBN tools during turning operations. The coolant boils before reaching the actual cutting zone. Catastrophic tool wear due to chipping occurs when coolants are used for milling operations. Coolants can be used to avoid thermal expansion of the workpiece and tool holder. Direct contact of the coolant with the milling tool should be strictly avoided in this case.

The machining of softer ferrous alloys (medium carbon and free machining steels) is technically feasible with CBN tooling but it is uneconomical. CBN tools are successfully used for the milling of hard ferrous materials with very high metal removal rates when compared with grinding. Round chamfered CBN tools are employed for milling operations because of their high geometric strength.

2.9.6.4 REQUIREMENTS

Small negative lands and honed (small radius) cutting edges are recommended for CBN tools used for heavy interrupted cutting and milling. A

negatively raked geometry (-5°) is normally used due to the inherent brittleness of CBN tools. CBN tools, like diamonds are thermally unstable at elevated temperatures. Unbacked polycrystalline CBN tools are specially recommended for roughing cuts since the inserts are solidly clamped into normal tool holders which allow only a few microns of thermal expansion. Care must be taken to ensure that the tool is properly supported and clamped during use to prevent premature failure. Shear stresses are developed at the interface between the polycrystalline CBN and the tungsten carbide substrate at high cutting temperatures due to the difference in thermal expansion coefficients between the two components. This problem can be minimised by the application of coolant to protect the zone. However with the use of greater depths of cut and high cutting speeds, the coolant cannot cool the tool sufficiently. This results in tool failure due to the separation of the local substrate layer. This type of failure does not occur in solid polycrystalline CBN clamped into tool holders. The tools have adequate toughness which allows them to be used for the continuous and interrupted cutting of ferrous materials as well as in milling operations.

2.9.7 CONCLUSION

Polycrystalline tooling offers a very cost effective method of machining abrasive or difficult-to-machine materials. Furthermore, its ability to maintain a keen cutting-edge makes it very desirable for machining materials where good surface finish is an important requirement. In fact, different grades of polycrystalline diamond are offered to cover highly abrasive materials or materials requiring excellent finishes.

Another benefit of polycrystalline tooling is the possibility of eliminating potentially costly grinding operations with high hardness ferrous materials. CBN tooling is capable of maintaining part size and stringent surface finish requirements for extended production runs. A large cost saving may be achieved by eliminating grinding and using hard turning for a wide range of high hardness materials.

The most significant benefit of polycrystalline tooling is realised in sustained production during long production runs with abrasive or difficult-to-machine materials. Poor tool selection, lack of rigidity, lack of proper tool care, or any variable not controlled properly, are all detrimental to the economics of polycrystalline tooling, because of the higher initial cost. An effective re-lap program combined with proper tool care may extend polycrystalline tool life many times, depending on tool and applications.

2.10 WEAR MECHANISMS AND ASSOCIATED PROBLEMS IN MACHINING

2.10.1 TOOL WEAR

Tools continue to cut efficiently only as long as the shape of the edge remains precise. Failure of the tool by plastic deformation of the edge and by fracture have been investigated. The precise shape of the tool edge may also be changed more slowly by one or more wear mechanisms by which very small changes in shape occur progressively. If tools are properly used, tool life is determined by one or more of these progressive wear mechanisms. Wear on cutting tools occurs at a number of positions (Fig 2.21).

2.10.1.1 TOOL WEAR MEASUREMENTS

Wear occurs at a number of locations on a cutting tool:

1. On the flank of the tool below the cutting edge. The wear which occurs on this surface is called the "flank wear" and results from the rubbing contact with the work surface which has been newly created by the cutting edge of the tool (Fig 2.21).

2. On the top or rake face of the tool. This is called "crater wear" and results from the action of the newly created chip against the rake face. The crater is a dished section of the tool face, which forms where we would normally expect most wear due to the high contact stresses and high interface temperatures. At low speed the crater curvature corresponds to the chip radius of curvature. In general, as the crater grows, it will eventually intersect the wear land. Thus, as wear progresses, the general tool geometry can vary considerably.

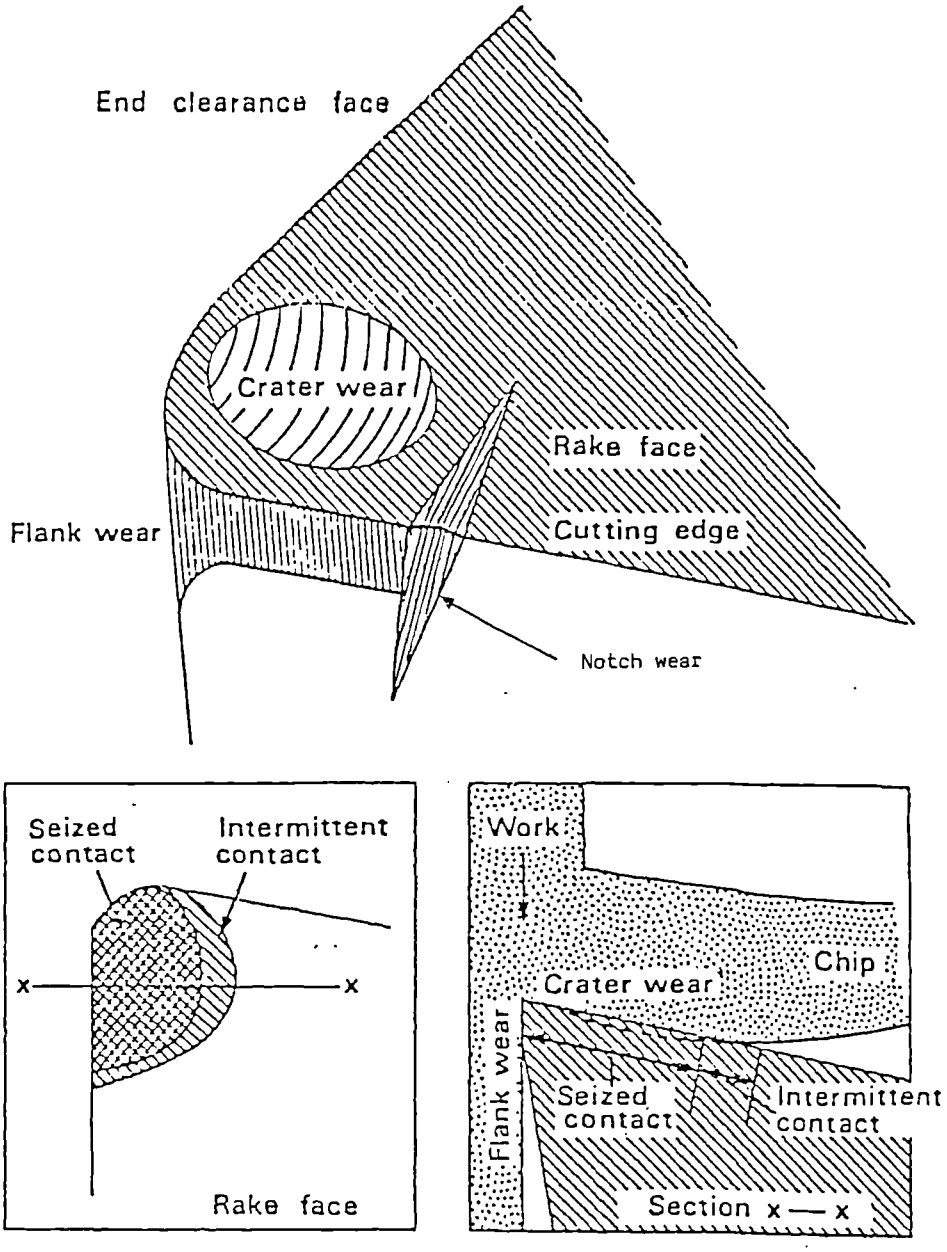

Fig 2.21 The schematic diagram of wear regions (60).

3. Nose radius wear forms at the nose radius and near the end relief face. The wear here is partially a continuation of the wear land around the nose radius, and partially a series of grooves that often develop as shown. The grooves are spaced a distance (the feed) apart (Fig 2.22), and contribute to the increased roughness of the finished part as wear progresses.

4. A groove often forms at the outer diameter of the workpiece and can become quite large compared to the other wear zones. Because it is generally not associated with the finished surface of the workpiece, this groove is not particularly harmful, except that it may affect regrinding time of monolitic tools.

The two zones that are most readily documented and which seem to give an overall indication of the wear process, are the wear land length (KB) and the crater depth (KT) (Fig 2.22).

These forms of wear will vary somewhat depending on the type of machining operation (turning, milling, drilling etc). In some operations crater wear will be the more important and lead to eventual failure of the tool. In other situations, flank wear will be the predominant form of wear.

The conventional method of determining the wear status of a cutting tool is to stop the machining operation, remove the tool, and examine the cutting edge under a microscope. Unfortunately, it is time-consuming and expensive to periodically interrupt the cutting process, take out the tool, and measure the dimensions of flank wear or crater wear. In attempting to devise an on-line wear measuring technique, a visual inspection of the cutting-edge during operation is clearly not feasible because the workpiece and chip obstruct the view. To circumvent this difficulty, an indirect method of measuring tool wear is required, in which some intermediate variable that is directly related to wear, is measured. Almost all of the research directed at on-line tool wear monitoring has utilized this indirect measuring approach. Such a measuring

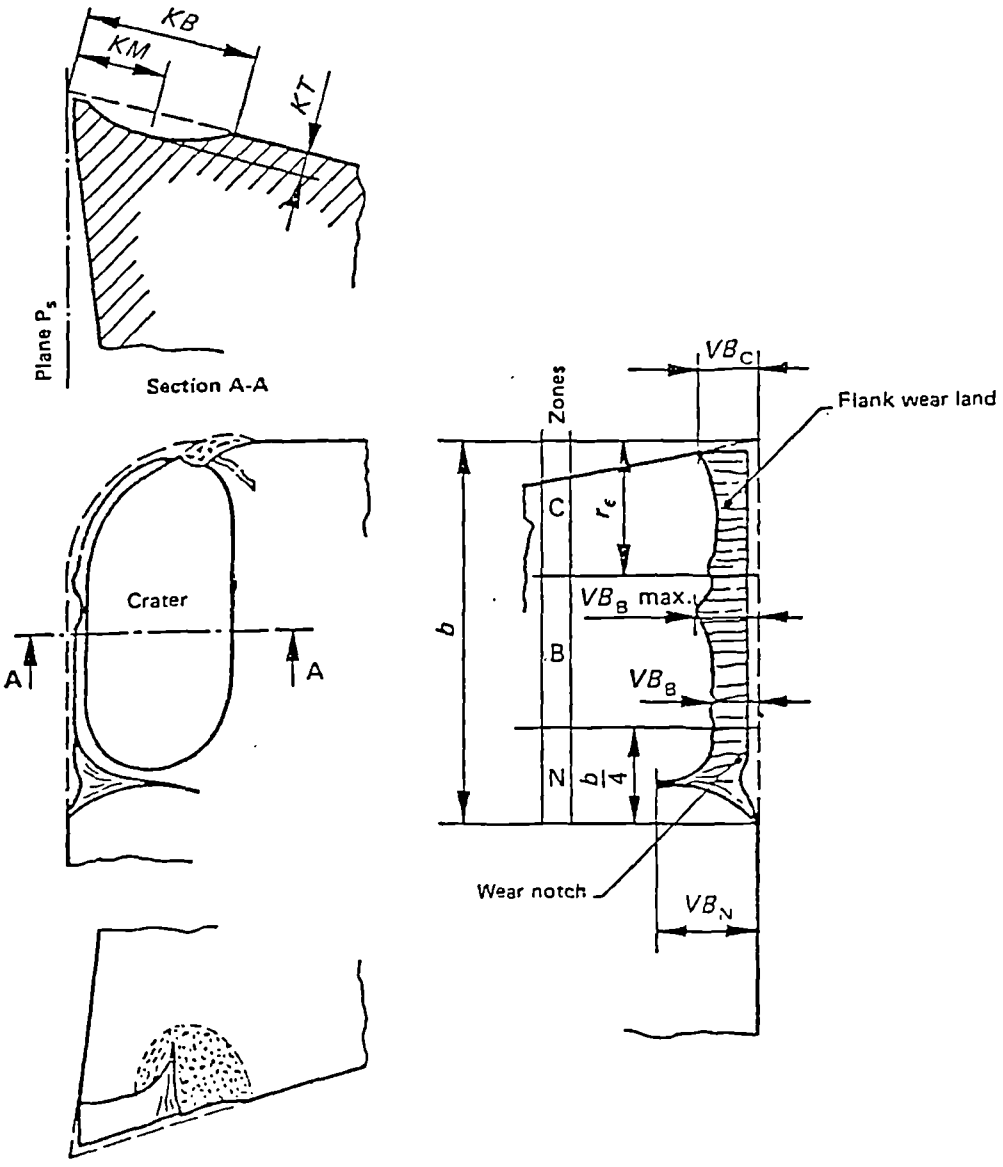

KB = crater width
KM = crater centre distance
KT = crater depth

Fig 2.22 Types of wear on turning tools after BS 5623 (1979).

technique suffers from a sort of double jeopardy. First, whatever the measured variable related to tool wear, there are possible errors involved in its direct measurement. No measurement is free from sources of error. Second, there are potential errors in establishing the relationship between the measured variable and tool wear. This would commonly be referred to as the calibration for most measurement processes. In spite of these obvious difficulties with the indirect approach, it is a common way of dealing with measurement problems (perhaps more common than indirect measurement). Most researchers seem to consider it the only feasible way in which tool wear can be sensed during the machining process.

2.10.2 MECHANISM OF WEAR

All cutting tools, in order to satisfy their functional requirements, possess relatively good mechanical, physical, and chemical properties. These normally include, high hardness, toughness, compressive, tensile and shear strength, chemical stability under high temperature, and thermal shock resistance. It is not, as yet, possible to achieve all these properties in a single tool. However good the tool may be, in terms of wear resistance, it still does wear during operation by a number of different wear mechanisms.

It is, therefore, necessary for extensive study and research to be carried out in this field, to exploit full benefits of different tool materials and improve their resistance to different wear mechanisms.

The most common wear mechanisms encountered in metal cutting are described below.

2.10.2.1 ABRASIVE WEAR

The wear is often considered synonymous with abrasion, but this is not true for cutting tool wear. Abrasion is a process by which material is removed from a softer surface by harder projections or particles which remove small amounts of material by ploughing. With cutting tools this is less likely to be a major mechanism of wear than in other situations, because the tools are always harder than the work material. There are machining operations in which the work material contains particles (Table 2.3), such as non-metallic inclusions, which are harder than the tool and these may cause abrasive wear. But, in most cases, it is unlikely that the removal of material from the tool by the mechanical action of hard particles is a major cause of wear. There are, however, exceptions: eg. when the surface of a casting contains large amounts of embedded mould material, it may cause rapid wear, particularly when using high speed steel tools. The hardness of the tool is probably, in most cases, a good measure of its resistance to abrasive wear.

2.10.2.2 ATTRITION WEAR

Attrition describes a wear process in which the tool shape is changed by the periodic removal of distinct small fragments of the tool material. These fragments are usually a few microns in size, or possibly just less than a micron. To understand this process in metal cutting, it is necessary to consider the condition at the interface between the tool and work material. The high contact stresses and the high temperatures generated at this interface have already been emphasized (142) and these conditions alone would make it difficult to prevent seizure between tool and work materials at the interface. The relative speed between tool and work material and the contact stresses are often much more severe than those used in friction welding. In addition, the tool is cutting continuously into clean metal, so it is not surprising that

observation shows the two surfaces are often completely bonded together during the cutting operation over large parts of the interface (142).

In many operations, conditions are such that the two surfaces are not completely bonded together for the whole cutting time, but are periodically separated over part of the interface. This is particularly true if the tool is plunging in and out of the work material, if a built-up edge is formed on the tool and is periodically broken away, or if the machine tool lacks rigidity so that vibration occurs. Under these conditions, small fragments are frequently removed from the tool surface as work material bonded to it is pulled away or flows unevenly across the tool. This is most likely to occur at relatively low speeds and it subjects very small local areas of the tool to tensile stresses. High speed steel tools are found to resist attrition wear better than cemented carbides in many conditions (142). The very high hardness of cemented carbide tools does not give them superior resistance to attrition wear, and there are many cases where the life of high speed steel tools is greater than that of cemented carbides under the same conditions of cutting. This is particularly true at relatively low cutting speeds (142). For example, cemented carbides are rarely used for drills for this reason, and a continued market for high speed steel tools is likely to exist for operations where attrition is the principal wear mechanism. If, however, cemented carbides are used under conditions of attrition wear the carbides with a grain of 1 micron or less have been shown to be much superior to coarse grained carbide (142).

2.10.2.3 DIFFUSION WEAR

When cutting steel, cast iron and other high melting point materials at high speed high temperatures are generated at the interface between tool and work material (1). When cutting steel with high speed steel tools at 30-50 m/min the interface

temperature at the hottest part often exceeds 800 °C. At higher speed using cemented carbides,temperatures over 800 °C at the interface were recorded by Trent et al (143-144). At such temperatures, diffusion rates are relatively high and it has been demonstrated that the tool and work material are normally in metallic contact on large parts of the contact area so that there are no barriers for diffusion between the two. A variety of interactions between tool and work materials is possible under these conditions. A major cause of wear in tools used to cut high melting point metals at high speed is diffusion of metals and carbon atoms from the tool into the stream of work material flowing over the tool surface, thus, dissolving the tool into the work material just as a block of salt dissolved by a stream of water running over its surface.

The rate of diffusion wear depends on temperature and also on the rate of solution of the tool in work material. This is particularly important for cemented carbides tools. Tungsten carbide (WC) is dissolved easily in hot steel and for this reason WC-Co alloy tools fail as a result of rapid crater wear when cutting steel at high speeds. TiC and TaC are much less readily dissolved and the rate of crater wear of cemented carbides based on these two materials is much lower (142). TiC or TaC bonded with nickel or cobalt are however much less tough than WC-Co alloys and a compromise has been adopted.

While diffusion wear is most clearly demonstrated in relation to cratering at the hottest part of the tool it is probably also a major factor in flank wear during the high speed cutting of cast iron and steel. As the cutting speed is raised, the rate of flank wear increases and the rate of flank wear also can be reduced by addition of TiC and TaC to WC-Co alloy tools. Where tool life depends on diffusion wear, the chemical composition of the tool material is of more importance in relation to wear resistance than mechanical properties such as hardness. But the rate of wear by diffusion depends both on the tool and the work materials.

Loladze (145) has obtained an equation for predicting theoretical tool life under conditions of diffusion wear when machining steels and other alloys with cemented carbide tools. He assumed that all the material removed from the tool in the contact zone resulted from diffusion, dissolution, and material transfer into the work material flowing over its surface. Satisfactory agreement with his practical data was demonstrated.

Other authors (146-148) have suggested that diffusion and chemical reaction between tool and work material results in structural changes in the tool weakening it and allowing fragments of the tool to be mechanically removed from the tool surface by the moving chip. Hartung and Kramer (146) have studied tool wear when machining titanium alloys. Their conclusion is that tool materials with the greatest potential, either dissolve in or chemically react with titanium alloys during machining. When a chemical reaction occurs, a layer forms with a thickness which is determined by the balance between the rate of diffusion of tool material through the layer and the rate of solution of the reaction layer in the workpiece.

2.10.2.4 ADHESIVE WEAR

When surfaces rub together, particularly in the absence of lubricant films, some adhesion occurs at the points of rubbing contact. The friction is primarily the force required to shear the junctions so formed. There is no basic mystery about inter-facial adhesion; if the surfaces touch so that they support a normal force, the atoms must be in contact and interatomic forces will become appreciable. The extreme case is when clean surfaces of similar metals make contact to form a solid junction. Although this junction may be full of imperfections, its strength may be comparable with that of the bulk material This process occurs even at room temperature (cold welding) but it will be more marked at higher temperatures where

interfacial diffusion will be accelerated (149). Since high temperatures may be generated at the surface by the sliding process itself, the interfacial interaction may be even more marked. The friction force breaks these interfacial junctions and often is responsible for the plucking of a piece of material out of one or both of the surfaces (149).

Adhesive wear in machining operations is a relatively straightforward concept. The tool is invariably chosen to be harder than the work and if a junction is formed at the metal/work interface, the tool will generally pluck out a fragment from the work. The process of plucking-out will leave the fragment in a very work-hardened condition and it may well be hard enough to score or groove the work. The accumulation of transferred material from the work to the tip of the tool is, of course, the origin of the BUE. This nose acts as an extension of the tools, and to some extent protects the tool from wear. However the built-up edge may occasionally break-away with a small portion of the tool itself. This is particularly likely if the tool is heterogeneous in structure so that local regions may be appreciably weaker in tension or shear than the overall strength.

Adhesive wear of the tool is therefore likely to be most marked if the tool is of non-uniform strength. Another factor is the effect of the rate of deformation on the relative strength properties of tool and work. High cutting rates will have two opposing effects; frictional heating will tend to soften both the work and the tool, making them more ductile, but, on the other hand, high rates of strain will tend to make them more brittle. If the rate at which adhesion junctions are broken is such that the tool material ceases to be ductile, a relatively large fragment may be removed from the tool by fracture. One example of this is the interaction between a soft metal like copper and a hard brittle material like sapphire (149). Buckley (1967) (150) has shown that under conditions of strong adhesion the copper can pluck pieces of sapphire out of the harder surface.

The best way of minimizing adhesive wear is by reducing the amount of adhesion. The most common method to reduce adhesive wear is by using a lubricant. However, it is not clear whether the lubricant acts mainly as a coolant or as a means of reducing friction and adhesion. If it acts as a true lubricant it is highly desirable to know how the lubricant gets into the work/tool interface and how quickly it can interact to be effective. Another approach is to make the work relatively brittle so that the removed chip easily fragments and breaks away from the tool face.

2.10.2.5 PLASTIC DEFORMATION

Plastic deformation is classified as a permanent change in shape or size of a solid body without fracture. This process is a direct result of the application of sustained stress beyond the elastic limit. It differs from tool wear in that no tool material is actually removed. Plastic deformation occurs when there is a high concentration of compressive stress at the tool rake face (close to the cutting edge) making the tool edge deform downwards causing an acceleration of various wear processes which ultimately reduce the life of the tool.

Many workers agree that, during cutting, the compressive stress acting on the rake face of tool is a maximum at, or close to, the cutting edge. When the stress is too high it may cause the tool to deform downwards. When cutting materials like steels, the cutting edge stays relatively cool and may not be permanently deformed by high compressive stresses. However machining of titanium based alloys generate high temperatures and hence tools are more likely to be damaged by deformation.

Loladze (151) states that, if the hardness of the tool material at the melting point of the work material is greater than six times the shear stress in the shear plane then the cutting tool will under no practical condition experience plastic failure.

According to Trent, deformation could be detected at an early stage in laboratory tool tests by polishing the clearance face of the tool optically flat before conducting the tests, and observing the face after the cutting test using optical interferometry. Any deformation in the form of a bulge on the clearance face could be observed and measured as a contour map formed by the interference pattern.

2.10.2.6 WEAR DUE TO CHEMICAL INSTABILITY

In contrast to the wear processes controlled by the mechanical behaviour of materials, cutting tools can wear by the chemical dissociation of hard materials and the chemical dissolution of the dissociated materials in the workpiece. This process has been investigated extensively at MIT by Suh and his associates. (152-157).

In the early phase of the MIT work the chemical stability hypothesis was supported by a variety of experimental results, the most convincing being the correlation between the wear rates of various tool materials and the free energy of formation (see Fig 2.23 for free energies of formation). According to this hypothesis it was reasoned that oxides and nitrides are, in general, superior to carbides as cutting tool materials owing to their low free energy of formation, although there are exceptions due to exceptional solubility of a particular tool material in the workpiece. Among the group IVb and Vb carbides, hafnium carbide is the most chemically stable material. It also has the highest melting point of all known solids, ie 7050 ^{o}F (3885 ^{o}C), which indicates that its hot hardness must also be superior to that of many other substances.

Recently, Kramer (155) showed that the wear of various group IVb and Vb carbides could not be explained in terms of the diffusion of elements from the cutting tool into the chip since the diffusion rate is of orders of magnitude smaller than the observed wear rate. Therefore a hypothesis was made that once tool materials are

dissociated in the chip, they are transported by "convective" mass transfer due to the velocity component perpendicular to the tool surface. This velocity component must be present in order to satisfy the mass continuity relation because of the slowing of the chip as it traverses the tool face. The solubility of the tool materials was then computed analytically from equilibrium thermodynamic considerations. This analysis accurately predicted the experimentally observed wear rates of group IVb and Vb carbides.

For the tool material to dissolve in the workpiece the tool material must first dissociate - which is supported by the strong correlation between the experimentally observed wear rates and the free energy of formation. Then at equilibrium

$$G_{ij} = G^{m}_{i} + G_{j}^{m} \qquad (1)$$

where G_{ij} is the free energy of formation of the tool material, G_{i}^{m} the relative partial molar free energy of solution of component i and G_{j}^{m} the relative partial molar free energy of solution of component j. The relative partial molar free energy of solution of component i of the solute is related to the concentration C_i of the component by

$$G_{i}^{m} = G_{i}^{xs} + RTlnc_{i} \qquad (2)$$

The excess free energy G_{i}^{xs} is a measure of the departure of the solution of component i in the workpiece from ideality (R is the universal gas constant and T is the absolute temperature). Once the excess free energies are known the concentrations of the elements in the tool can be computed from eqns (1) and (2). Table 2.3 shows the estimated equilibrium concentrations computed by Kramer (155). The wear rates are then computed relative to the wear rate of hafnium carbide. These predictions are shown in Table 2.4. The agreement between the experimental

Potential tool material	Free energy of formation (cal mol $^{-1}$)	Estimated equilibrium concentration (solubility)	Experimental results extrapolated to 1600 K
ZrO_2	-190300	$3.60*10^{-8}$	
Al_2O_3	-278300	$5.55*10^{-7}$	
Ti_2O_3	-260800	$8.22*10^{-7}$	
TiO_2	-156300	$1.52*10^{-6}$	
TiO	-90020	$1.40*10^{-5}$	
HfN	-52604	$1.53*10^{-4}$	
HfC	-49122	$1.97*10^{-4}$	
ZrN	-51356	$2.93*10^{-4}$	
$TiC_{0.75}O_{0.25}$	-52395	$5.42*10^{-4}$	
ZrC	-42714	$8.42*10^{-4}$	
TiN	-45150	$1.04*10^{-3}$	
TaC	-34604	$1.41*10^{-3}$	$2.1*10^{-3}$
TiC (iron)	-39520	$1.86*10^{-3}$	$6.1*10^{-3}$
NbC	-32236	$2.01*10^{-3}$	$6.8*10^{-3}$
BN (graphitic)	-26100	$9.65*10^{-3}$	
WC	-8144	-	$2.6*10^{-2}$
VC	-23416	-	$3.2*10^{-2}$
TiC (nickel)	-39520	$2.24*10^{-2}$	$6.3*10^{-2}$
Diamond	-	$9.30*10^{-2}$	
Si_3N_4	-51850	$9.50*10^{-2}$	
B-SiC	-14548	$4.30*10^{-1}$	

Data from Ref 155.

Table 2.3 Estimated and reported solubilities of potential tool materials in alpha-iron at 1600 K.

Carbide	Relative wear rate				
	1600 K	1500 K	1400 K	1300 K	Test results
HfC	1	1	1	1	1
TiC	7.65	8.82	10.6	12.8	2.75
$TiC_{0.75}O_{0.25}$	2.26	2.41	2.61	2.86	-
ZrC	4.44	4.87	5.47	6.20	5.51
TaC *	6.33 (9.43)	7.19 (10.7)	8.39 (12.5)	9.98 (14.9)	10.6
NbC *	9.13 (31.0)	10.6 (36.0)	12.7 (43.1)	15.6 (52.8)	23.7
WC	(107.0)	(153.0)	(215.0)	(332.0)	237.0

Data from Ref 155.

* Terms without parentheses are calculated on the basis of the solubility estimated from thermodynamic properties. Terms in parentheses are calculated using the reported solubilities (see Table 2.3).

Table 2.4 Comparison of theoretical predictions with test results: predicted relative wear rates at various temperatures (V_{wear}(HfC) = 1)

results was obtained using coated cemented carbide tools which were prepared by a chemical vapour deposition technique (158-159).

The only exception to the generally good agreement is the wear rate of TiC which is lower than that predicted. It appears that this is caused by the formation of the oxycarbides TiC_xO_y as a result of the diffusion of oxygen into the TiC lattice as is indicated by the good agreement between the wear rate predicted for $TiC_{0.75}O_{0.25}$ and TiC-coated tools. This finding is consistent with the earlier work of Carson et al (156). They created titanium oxycarbides from powders of TiO and TiC so as to lower the free energy of formation without significantly affecting the hardness of the carbide. As shown in Fig 2.23b the lattice parameter of the TiO-TiC solid solution does not vary linearly with the volume fraction of TiC which indicates that the solid solution is not ideal. The hardness variation is shown in Fig 2.23c. Cemented carbide tools were sputter coated for wear tests using the $TiC_{0.5}O_{0.5}$ and $TiO_{0.25}C_{0.75}$ samples prepared in this manner. It was found that the oxycarbide-coated tools wore at about the same rate as the TiC-coated tools. At the time the work was done it was speculated that the loss of oxygen during sputtering might also have contributed to the observation of a wear resistance which was less than expected. Since then experimental evidence (160) has indicated that stoichiometric oxycarbides do improve wear resistance. These facts reinforce the view that oxycarbides can increase the chemical resistance and that even TiC can be transformed into oxycarbides during cutting provided that there is sufficient oxygen dissolved in the workpiece.

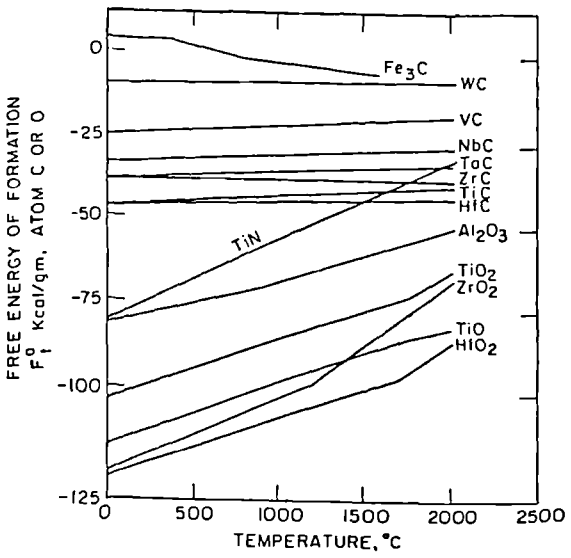

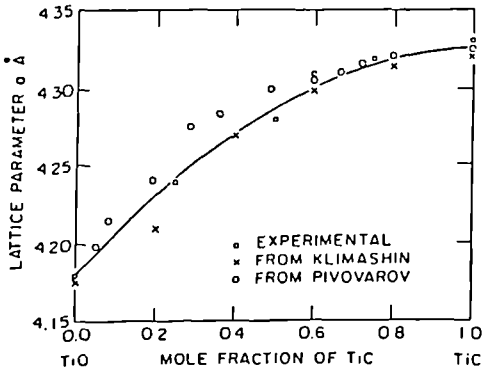

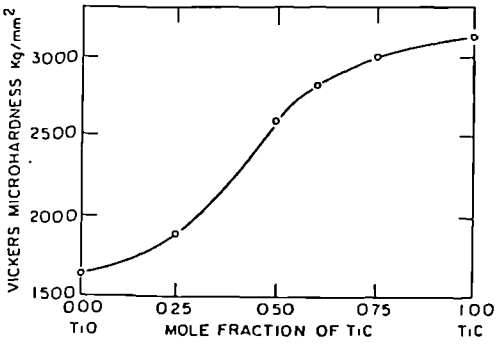

Fig 2.23 a) Free energies of formation of some tool-related carbides and oxides as a function of temperature

b) Lattice parameter of titanium oxycarbide as a function of carbon and oxygen content

c) Vickers microhardness on single grains of titanium oxycarbides as a function of carbon and oxygen content (154).

2.11 MACHINING OF TITANIUM AEROSPACE ALLOYS

Many papers were written on the machining of titanium in the early 1950s. Before this time, titanium was not commercially available and little was known about its machining characteristics. These early papers dealt mostly with what were the best machining speeds, feeds, tool geometries and coolants to use when producing titanium components, and were generally based on experience in the production of actual components (Table 2.5 and 2.6). Some recommended negative rake angles (161) whilst others claimed that positive rake angles improved machinability (162-163). It was found that heavy feeds would give longer tool lives than fine feeds (164-165) if flank wear was the controlling factor (ie. at lower speeds). Also, it was generally agreed that carbide tools were superior to high speed steel tools unless chipping was likely to determine tool life.

Boston (166) observed that the chips produced when machining titanium were thin and that the contact area between the chip and tool was small; therefore, high stresses would exist at the rake face. He also stated that there was no evidence for a BUE being present, and that the temperatures produced in the tool were higher than those found when machining stainless steels or low carbon steels. The thin chips produced when machining titanium were found to be typical, with the shear plane angle usually approaching 45°. Distortion within the titanium chips was seen to occur along distinct planes, the regions between these planes being relatively undistorted (166-167).

Despite the low cutting forces when cutting titanium and its alloys, compared with steels of similar strengths the tool life is less than with steel. This apparent anomaly can be explained when the stress on the tool is considered. The contact areas existing between titanium chips and the tools are much smaller than those existing between the steel chips and the tools. Therefore, the energy expended, per unit area, is often greater when machining titanium and temperatures are higher, as a

Code	Tool material	Hardness, VPN	Typical composition	ISO rating, where applicable	Application
SS1	HSS	835	0.75%C-18%W		Drills, reamers, milling cutters, broaches
SS2	Super HSS	850 min.	1.5%C-12.5%W, 5%Co-5%V-5%Cr		Milling cutters, parting tools
SS3	Super HSS	900 min.	1.3%C-9.5%W 10%Co-3.5%V 4%Mo-4.5%Cr		Milling cutters
SS4	Cobalt HSS	835	0.8%C-18%W 4%Cr-1%V 5%Co		Milling cutters
1	Tungsten carbide	-	-	P40	Heavy rough turning
2	Tungsten carbide	-	-	K05	Form tools
3	Tungsten carbide	-	-	K10 K20	General turning,milling, and automatics

Table 2.5 Various tool materials used for turning Aerospace alloys.

Code	Type	Application
A	Chlorinated neat oil	Automatics
TM1	Heavy duty EP soluble oil, 20-35:1	General turning and milling
TM2	Synthetic soluble fluid, 40:1	Finish, turning and milling
BL	Chlorinated and Sulpho-chlorinated neat oils	Drilling, reaming broaching, and tapping
G1	Translucent soluble oil, 50:1 Nitrite-amine rust inhibitor, 40-60:1 dilution	Grinding with aluminium oxide wheels
G2	Heavily chlorinated neat oil light viscosity	Grinding with silicon carbide wheels

Table 2.6 Various cutting fluids used for turning Aerospace alloys

consequence (166-169). Another reason for temperatures being high in tools used to cut titanium has been advanced; the low thermal conductivity and low thermal capacity of titanium leads to a greater proportion of heat flowing into the tool than with most other metals. This also causes higher temperatures to be produced at the base of the titanium chip (161, 168-170).

When using cemented carbides to machine titanium, it was found better to cut with those grades containing tungsten carbide with a cobalt binder. Tools containing additions of titanium carbide had a shorter life (168). Loladze (171) has suggested that this was due to the titanium carbide in the tool dissolving in the titanium chip, where as Hollis (163) considered that the lower thermal conductivity of tools containing titanium carbide led to higher interface temperatures and hence faster tool wear.

Fersing & Smith (172) found that the feed load for tools containing no titanium carbide was less than that measured for tools containing a percentage of titanium carbide. They also noticed that a set of chips produced using tools containing titanium carbide were discoloured whereas chips produced under the same conditions using wholly tungsten carbide tools were bright - implying that the first set of chips was hotter than the second set. Merchant et al (168) found that, if they heated blocks of titanium and cemented carbides together, a brittle layer formed at the interface when titanium carbide was present in the cemented carbide block, but the interface was strongly joined when the block consisted only if tungsten carbide with cobalt as the binder.

Early workers often assumed that difficulties arose when machining titanium due to its supposedly high rate of work hardening (161), which caused hardened surface layers to be formed. Holt and Purcell (162) accounted for hardness variations at the surface of titanium castings being due to absorbed oxygen and nitrogen. They stated that titanium forgings had appreciable work hardening rates and concluded that

both of these phenomena combined to create problems when machining. Boston (166) and later workers (169) have shown that the work hardening rates of titanium and its alloys are less than those of steels and nickel, hence the earlier assumption for the lack of machinability of titanium is invalid. Child and Dalton (169) considered the problem, and concluded that short tool lives occurred when machining titanium due to interstitially absorbed oxygen and nitrogen hardening the surface of components. This hardened surface is often found after forging and is removed abrasively and/or by pickling before machining is carried out (165, 168).

When titanium or its alloys are machined commercially the tool geometry is arranged such that, for a given depth of cut and feed, the metal is removed over a lengthened cutting edge. For turning tools, this usually entails employing an approach angle of 45° a large nose radius, and a small positive rake angle. The machining of titanium is not difficult, providing rigid machines are used, and speeds are kept low with respect to those used for machining steels. Active extreme pressure lubricants have been found to be the most effective when machining titanium, but care must be taken to protect machine tools from their corrosive effects (165-172). The high initial cost of the metal, combined with the low cutting speeds for optimum machining, ensures that titanium components are expensive and limited to special applications.

Work by Kreiss (173) on the machining of a titanium alloy, showed several interesting effects when the cutting forces were measured such that their variation with respect to time could be recorded. It was found that the vertical cutting force on the tool varied periodically, as may be expected from the saw tooth form of the chips produced, but the horizontal force remained almost constant. This he explained by assuming that the friction between the chip and tool was constant and the chip moved continuously across the contact area of the tool. Metallographic evidence suggested that a layer of work material formed on the tool over which the chip slid at cutting

speeds below 80 m/min. The reason put forward for the absence of this layer above 80 m/min depended upon the effect of temperature on the bond strength between the work material and tool material. He suggested that the bond between the work material and the tool was stronger than the cohesion of the work material at low temperatures However, weakening of the tool/work material bond occurred when high cutting speeds generated high temperatures thus enabling the layer to be removed by the chip. Tool wear was considered to be due to friction, combined with temperature and pressure, with the force variations also inducing wear by fatigue. High speed steels were shown to be plastically deformed due to the temperatures and pressures acting on the tools. Kreiss pointed out that, despite the layer, tool wear still occurred due to the temperature and pressure variations experienced by the tool acting through the work material layer. He also suggested that the variation of stress levels in tools could be caused by temperature, the levels of stress in a tool increasing as its thermal conductivity decreases.

CHAPTER 3

EXPERIMENTAL PROCEDURES

3.0 EXPERIMENTAL PROCEDURES

3.1 INTRODUCTION

The cutting of titanium alloys remains a problem despite many recent developments in cutting tool materials. In the current work, specific attention is paid to the role of the interface, between the workpiece and the rake face of the tool, on the mechanism of wear. Two experimental techniques are employed. First, the effect of temperature on the adhesion of workpiece to tool material is investigated in order to determine the critical temperature above which there is immediate seizure on contact. The structural and chemical nature of the interface is studied and the nature of subsequent failure of the adhesive couple (ie at the interface within the workpiece or within the tool) identified. In the second, the 'quick stop' technique is used to investigate in a similar way the structure of the chip and its interface with the rake face during single point cutting.

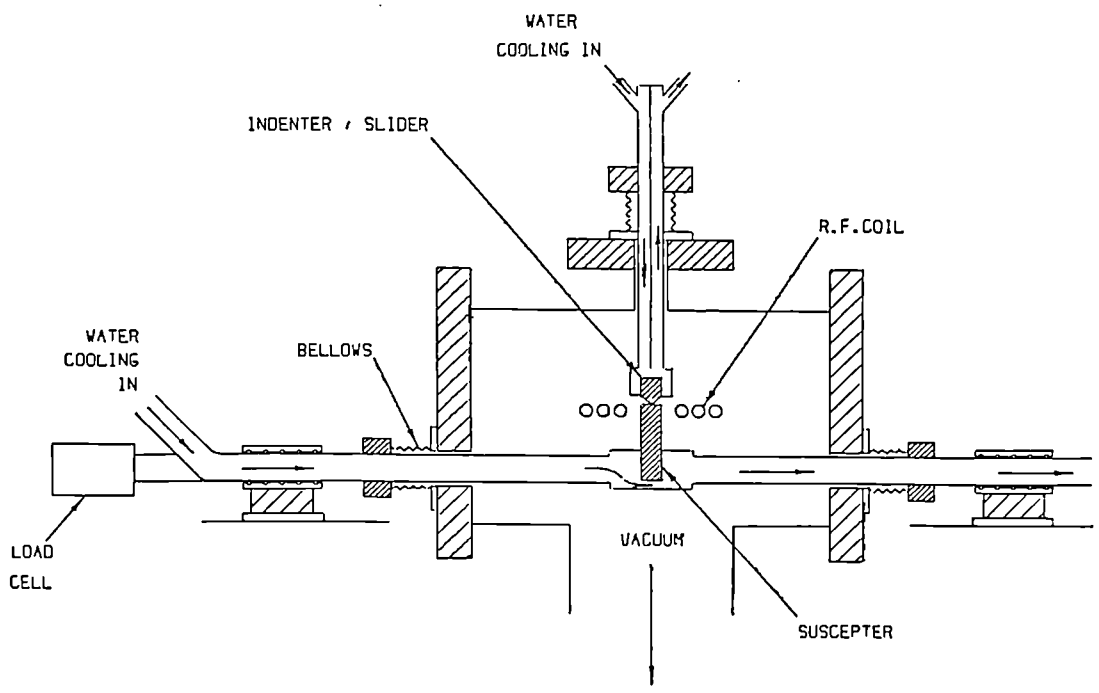

Fig 3.1 Schematic cross section of high temperature apparatus.

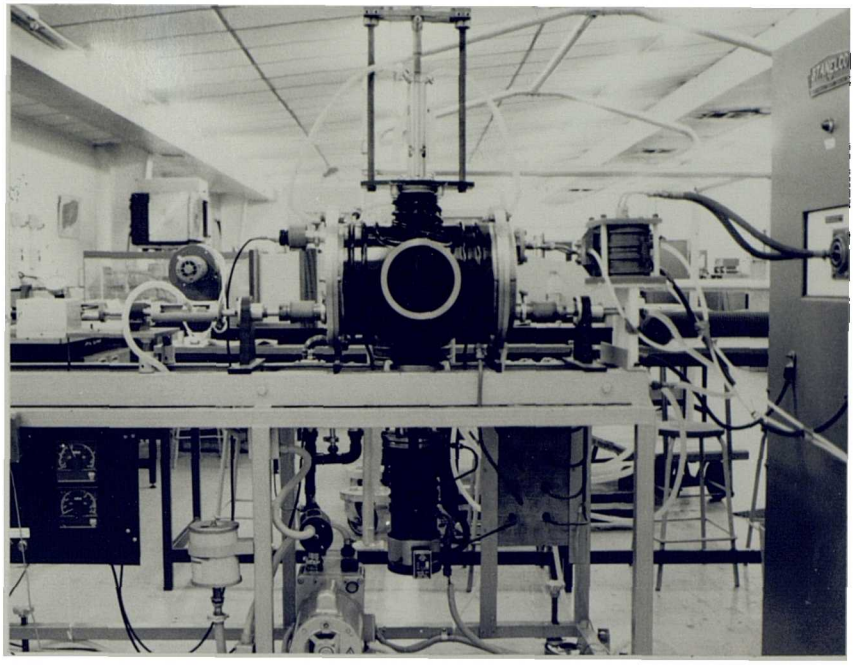

Fig 3.2 Apparatus used for adhesion tests at elevated temperatures.

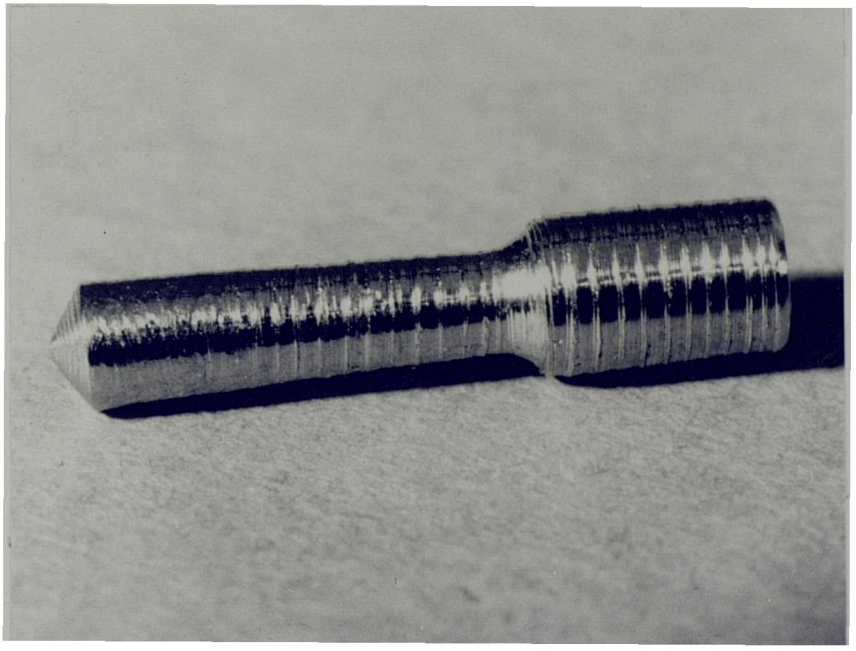

Fig 3.3 Titanium Alloy (TA48) cone used in Quasi-static Adhesion tests.

3.3 CUTTING TOOLS

Selection from a large number of commercially-available indexable inserts is rarely done on a scientifically correct basis and assessment of the widely different grades of uncoated and coated cutting tools is a difficult task. However, the carbide cutting tools used during this work were based on those grades which are currently being used in the aerospace industry.

Although there are several large manufacturers of uncoated and coated tungsten carbide indexable inserts, and a wide variation in their grades, machining optimization is unlikely to be attainable by selection between products from different manufacturing companies. This is due to the fact that, every manufacturer produces a range of insert grades which can be utilized for particular cutting operations. Consequently, it seems more logical to concentrate on a number of options offered by one manufacturer.

There are many considerations in optimising the selection of a cutting tool material for a particular workpiece material, but here we shall concentrate on the ultra-hard materials.

3.3.1 TOOL MATERIALS

The metal cutting tests were carried out on Kennametal grades KC850, KC910 and K68 and De Beers PCD and CBN (polycrystalline diamond, cubic boron nitride). The K68 is uncoated tungsten carbide and the other two Kennametal grades were tungsten carbide substrates coated with double and triple layers of different coatings deposited by chemical vapour deposition (CVD) processes, the KC850 is triple coated layers (TiC-TiC/N-TiN) the outer layer TiN, middle Ti (C,N) and inner

TiC, with the coating thickness of 4, 3, 3 micron respectively. The KC910 had a TiC coating 6 micron thick with an outer layer of Al_2O_3 to a thickness of 3 micron.

The uncoated tools and substrates of the coated tools were fabricated from tungsten carbide as the main constituent, and a small amount of cobalt as binder, with variable but small additions of titanium carbide, tantalum carbide and niobium carbide.

The aggregate of cubic boron nitride (Amborite), consists of particles of about 1.2 micron in size with a filler or matrix phase comprising aluminium compounds (boride and nitride) with a HK1 hardness of approximately 3100 Kg/mm^2 (30.1 GPa). Amborite is produced by De Beers from cubic boron nitride by sintering together carefully selected particles. The tools are cut from the basic sintered discs and diamond ground to the final ISO standard in the form of an indexable square insert.

Polycrystalline diamond (PCD) tools manufactured by De Beers were also used. This proprietary range of tool materials is known as Syndite. Syndite is produced by hot pressing high quality synthetic diamond powder, with a typical grain size of 10 micron, in the presence of a metallic phase at temperatures above 1400 $^{\circ}C$ and at pressure of the order of 60 bar. The hot pressing process is rigidly controlled and results in a final product that is an intergrown mass of randomly orientated diamonds in a metal matrix. The diamond is not merely bonded in the metal, but also considerable intergrowth has taken place between the diamond particles.

The hot-pressed diamond composite is then brazed onto a tungsten carbide substrate at temperatures in the region of 700-750 $^{\circ}C$ for one minute. The brazing materials are based on silver and copper and consequently the process is known as silver brazing or silver alloy brazing.

The configuration of the coatings and designations of the experimental tools are given in Table 3.1.

3.3.2 WORK MATERIAL

The workpiece material used throughout all these experiments was an as rolled and annealed titanium alloy with a nominal composition specification (in weight percentage) given as Al 5; Mo 4; Sn 2-2.5; Si 6-7; Fe 2.0 max; H 0.015; O 0.25; N 0.05; Ti remainder. It had a Knoop hardness (2 kg load) of 440 kg/mm^2 (4.31 Gpa) and the microstructure consisted of an elongated alpha phase in a fine, dark etching, beta matrix.

At room temperature the structure of titanium is closed packed hexagonal with a c/a ratio of 1.587; this structure is known as the alpha phase and exists up to 882 $^{\circ}$C, above which there is a phase transformation to a body centred cubic structure known as the beta phase. This phase is more easily worked than the alpha phase. Oxygen, nitrogen and carbon dissolve interstitially in titanium, stabilising the alpha phase and increasing the strength appreciably.

3.3.3 TOOL GEOMETRY

All the inserts used were of square shape, 3 mm thick, with 9 mm cutting edge length and a 0.8 mm nose radius.

The inserts were classified according to the international standards organization (ISO) system and designated by the producer's own numbering system in conjunction with the ISO grading number (Table 3.1).

To reduce plastic deformation of the cutting edge at high cutting speed, and to optimize the number of available cutting edges per tool, square negative rake inserts of cubic boron nitride (Amborite) were chosen for the tests.

Tool Materials	Commercial grades	ISO	Tool holders
Polycrystalline diamond	Syndite	R123-90/010	CRDNN 2525 M09
Cubic boron nitride	Amborite	SNMN 090308F	CSDNN 2525 M09
Coated carbide (TiC/Ti(C,N)/TiN)	KC850	SPGN 090308	CSDNN 2525 M12-1D
Coated carbide (TiC/Al_2O_3)	KC910	SPGN 090308	CSDNN 2525 M12-1D
Uncoated carbide	K68	SPGN 090308	CSDNN 2525 M12-1D

Table 3.1 Cutting tool materials used for machining TA48

3.4 MACHINING PROCEDURE

3.4.1 CNC LATHE

A series of single point turning tests were conducted using a Churchill 'Computurn' 290 CNC lathe, with all tool materials, at a surface speed of 100 m/min, a feed rate of 0.25 mm/rev; a depth of cut of 1.0 mm and without a lubricant. These conditions were chosen to maximize rake face temperature and to conserve the limited workpiece material. In addition to the principal surface speed of 100 m/min, several different speeds ranging from 25 to 200 m/min (in 25 m/min steps) were used after a series of preliminary tests. The CNC lathe was the main machine tool used for the major part of the experimental turning work.

The machine spindle was driven by a 16 kw d.c motor via a separate gearbox and had an operating speed range of 20-5000 rev/min. The carriage and cross slide were located in front of the spindle with the carriage above the cross-slide. The lathe was equipped with a hydraulically indexing tool post with double tool holding fixtures, and each unit accommodated eight tools. The spindle speed was displayed on a speed indicator and the control panel was mounted on a fixed external attachment where the computer programme was displayed and controlled according to the operator's instruction.

3.4.2 QUICK STOP

In order to observe the chip formation process during machining, it is necessary to 'freeze' the cutting action by means of a suitable quick stopping technique.

At present, the most successful quick stopping devices depend on the rapid acceleration of the tool away from the work by means of an explosive charge. A quick stopping device based on a design reported by Williams et al (41) has been constructed and is shown in Figure 3.4. The principle of operation depends on a tool holder, pivoted about its end with a tool tip retained at the correct lathe centre height by a shear pin below and retaining spring above. Some modification on the tool holder and lathe were made in order to achieve the optimum performance.

The Quick-stop (QS) device, as shown in Figure 3.4 consists of a humane killer gun positioned above the tool holder which is supported by a notched shear pin of heat treated silver steel or brass. The gun consists of a solid captive bolt which is projected at a high speed when the gun is fired. The captive bolt strikes against the tool holder breaking the shear pin and the tool accelerates rapidly away from the cutting position. The tool holder allows the tool to clear the workpiece at an angle of 8° as it moves downwards. This avoids any contact between the tool and the workpiece once the pin is broken. The hollow cavity of the quick-stop block is packed with plasticine so that it traps the broken shear pin pieces and the tool holder when the gun is fired. This also prevents the tool holder from rebounding back into the workpiece.

The type of quick-stop device used has been analysed by Williams et al (41) who showed the mean acceleration of the tool from the chip bottom to be $32.5 * 10^7$ mm/sec. Hence for a feed of 0.2 mm/rev and cutting speed of test, the removal of the tool no longer affects the chip flow after a distance of 0.375 mm from the chip root.

3.4.3 FORCE MEASURING SYSTEM

The accurate measurement of the forces acting on a cutting tool is one of the difficulties experienced in metal cutting research that remained unsolved for a long time until the development of suitable force and torque dynamometers. The advent of

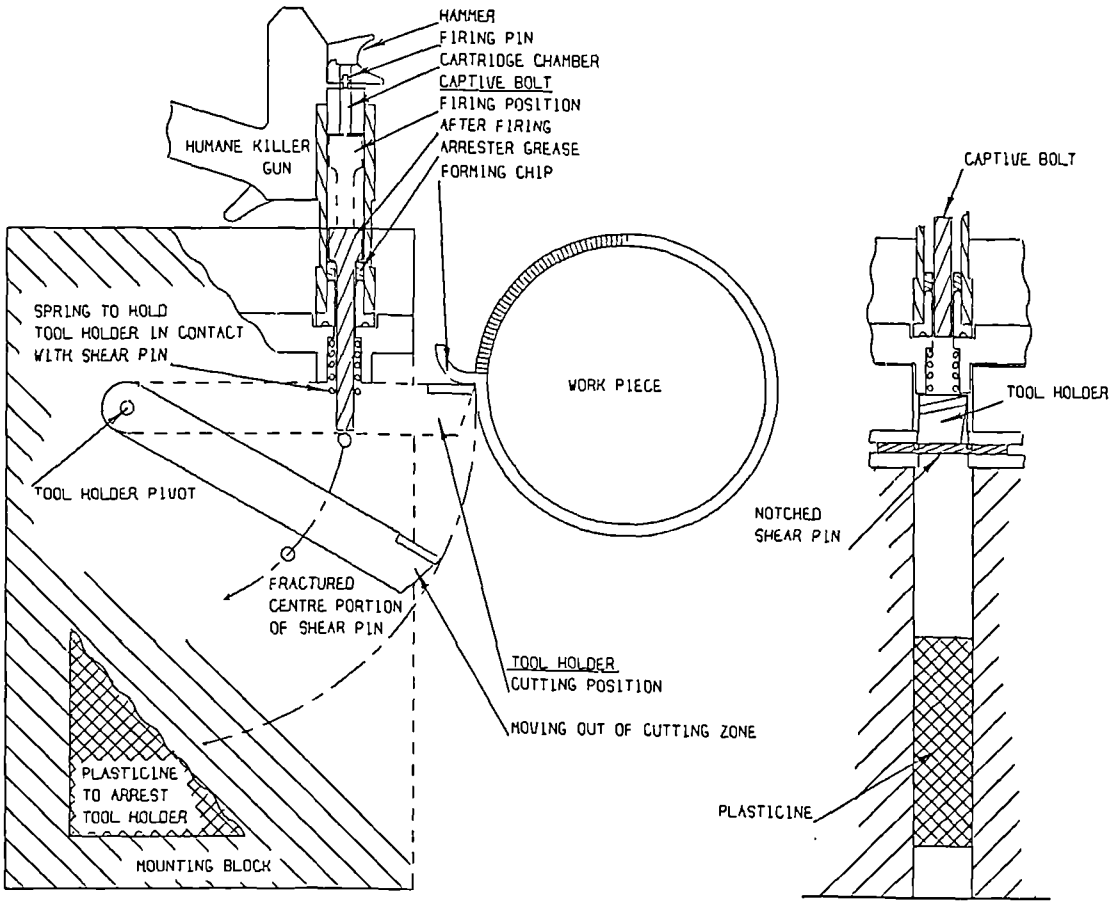

Fig 3.4 The "Quick-stop" device utilising a humane killer to disengage the tool from the workpiece rapidly leaving the flow of metal in the chip undisturbed.

these devices led to a more quantitative understanding of cutting tool performance. The dynamometers were designed to meet certain requirements in order to measure the force components to high accuracy. The primary requirements are high sensitivity and good stability. Cutting forces should not be influenced by external vibration and no interference between different force components should occur during a machining operation.

The forces involved in the cutting operations performed on the Churchill lathe were measured by a Kistler Type 925A-SN 40505 turning dynamometer It was mounted to the tool holder and attached firmly to the lathe saddle.

The measurements were carried out directly from the tool deflections produced as traces against cutting time. The deflections were measured in millimetres and multiplied by the sensitivity indices which were pre-set in Newtons per millimetre. The sensitivity adjustments were made according to the magnitude of each force component, ie increased sensitivity for low force and reduced sensitivity for high force. After measurement the force values were given as Newtons.

3.4.4 THE RANK TAYLOR-HOBSON TALYSURF

The surface measuring instrument employed to assess the quality after the finish machining operation was a Model 3 Rank-Taylor-Hobson 'Talysurf'. It had a pick up unit with a stylus of small radius of curvature that traversed across the surface by means of a motorised driving unit. The vertical movements of the stylus were converted into corresponding changes in an electric current which was amplified and then used to drive the Roughness Average meter which shows the centre line average (CLA) index of all irregularities within a standard length of surface.

The surface quality of the machined workpieces was tested after every finishing operation using the Talysurf. Due to the variation in the surface quality of the workpieces that were usually observed during most of the cutting operations, a careful method of measuring the surface finish was adopted. Readings were taken at three different distances along the workpiece, and at each distance three readings were taken circumferentially by rotating the workpiece at each sampling location. The average readings at each of the three locations were added together and the overall average was considered to represent the surface finish.

3.4.5 SCANNING ELECTRON MICROSCOPY

During the current work, investigation of microstructures was carried out by a Scanning Electron Microscope (Cambridge Instrument's Models 200 and 360), from which information regarding texture, porosity, size and shape were obtained. The relationships between different phases were studied and where possible identification of phases was carried out.

3.4.5.1 SAMPLE PREPARATION

Scanning Electron Microscope (SEM) studies were made on the polished QS specimens. The specimens were then coated with a conductive material, either carbon or gold, in the evaporative coater. Coating was carried out for two reasons:

i) Non-conducting specimens build up a surface charge through which secondary electrons are unable to penetrate, which could affect the image at both levels (ie either at signal level or at image form).

ii) To provide a surface layer that produces a higher secondary electron yield than the specimen material.

Normally the coating is very thin (up to 200 Å), and does not hinder the identification of specific phases.

3.4.5.2 INSTRUMENTATION

The SEM consists of an electron optical column and an electronics console. The coated specimen is placed in the sample chamber and which is then evacuated to high vacuum (10^{-5} bar). Instead of light (as the case in optical reflected light microscope), the SEM image is formed by an internally generated electron beam. This beam is produced by heating a very thin tungsten filament in the electron gun until it emits the electrons. The electrons are accelerated through the column by a 0.2-40 KV accelerating voltage. They are then demagnified and focussed through a series of electromagnetic lenses into a finely focussed beam, which bombards the sample. Final diameter of the beam is typically 100 Å in most commercial SEM's. Additional components include a stigmata for controlling the shape of the beam and an aperture to minimize the lens defects (aberrations), which severely limit resolution in optical light microscope. The interaction of the primary electron beam with the sample produces various forms of radiation; eg. secondary electrons, characteristic X-rays, Auger electrons and back scattered electrons. All these reactions occur simultaneously, and it is therefore possible to both observe and analyse the elemental composition of an isolated phase in a matter of seconds.

3.4.5.3 USE OF SCANNING ELECTRON MICROSCOPE

The most widely used technique to study microstructures of different phases is a reflected light optical microscopy. In case of industrial diamonds the reflectivity

of various phases is very similar and especially so in pure industrial diamonds. Some of the minor phases are very small in size, and higher magnification than the optical microscope range is necessary. The actual three dimensional grain relationships and details of the microstructure were outside the range of the optical microscopes. The introduction of the SEM has enabled us to identify minor impurity phases and to examine their distribution as well as their microstructures. Apart from significantly higher magnification other advantages of the electron microscopes are the greater depth of field and resolution.

3.4.5.4 SECONDARY ELECTRON (SE) EMISSION

Free electrons which leave the specimen, liberated by the elastic scattering reaction, are known as secondary electrons. These electrons do not have any relationship with the material from which they were liberated and have an energy less than 50 electron volts. The energy of the incident electron beam, at conventional scanning electron microscope accelerating voltage does not play any part in relation to the number of secondary electrons emitted by the elastic scattering reaction. At these high voltage levels the relationship between the material making up the specimen and the emission of secondary electrons is fairly constant. Only at very low atomic numbers does the secondary emission relate to atomic number.

3.4.5.5 BACKSCATTERED ELECTRON (BSE) EMISSION

Backscattered electrons are incident beam electrons that have been re-emitted from the specimen through multiple scattering. They have an energy up to the incident beam energy, and are usually very near to that energy. The emission of backscattered electrons from a specimen is related to the atomic number of the

material involved. The higher the atomic number, the higher is the backscattered coefficient. The emission of backscattered electrons also relates to the energy of the incident electron beam. The higher energy of the incident electron energy, the greater is its ability to move through the specimen material, and the higher is the probability of it emerging as a backscattered electron.

3.4.5.6 THE SCANNING ELECTRON MICROSCOPE MICROGRAPHS

The three dimensional image (SEM micrograph) is formed by collecting the secondary electrons generated by the primary beam. These are low energy electrons, so only those formed near surface (50-500 Å deep for insulating materials such as rocks) are able to escape. The electrons emitted are collected by a secondary electron detector mounted in the SEM (sample) chamber and subsequently processed into the familiar SEM image. This image is either continuously displayed on a VDU screen or photographed with an attached camera. The backscattered mode works on a similar principle, but the images obtained are the microstructures in only two dimensions.

3.4.5.7 PREPARATION AND EXAMINATION OF SPECIMENS

The specimens which were examined, fall into two categories, the chips and the tool, and the investigation has dealt with both these categories. The chips have been inspected so that the interpretation of the tool results may become more obvious. The preparation of the tool for examination varies depending upon whether the tool is of carbide or ultra-hard (polycrystalline diamond (PCD) or cubic boron nitride (CBN)) type.

After the carbide tools had been used for cutting, the tools were now encapsulated in Araldite cold curing resin such that the cutting edge was vertical and the tool nose uppermost. After the Araldite had hardened, the top surface of the specimen was ground away on a coarse diamond impregnated copper lap, until 0.5 mm had been removed from the tool. This creates a section halfway along the depth of cut of the tool perpendicular to the cutting edge. By sectioning the tool in this manner it was hoped that a chip flow pattern approaching that produced by machining would be revealed. The specimen has then lapped on a finer copper lap, with final polishing being carried out on flat plate vibratory polishers using nylon clothes impregnated with diamond paste and a suitable lubricant. This method of specimen preparation has been found to give a minimum of rounding at the edges of the tools. The carbide tools were etched for 2 to 4 minutes in an aqueous solution of alkaline potassium ferricyanide, freshly made up from equal parts of 20% aqueous solutions of sodium hydroxide and potassium ferricyanide. The etched tools were then examined by optical microscopy and photographs taken at various magnifications to illustrate any salient features.

The titanium chips which have been examined have either been those found to be attached to the tools after the termination of cutting, or those specially produced by the Quick Stop technique. Chips attached to the tools were already sectioned along their centre line and therefore only had to be polished and etched. The Quick Stop chips were removed from the parent bar together with a part of the bar. These were then examined using the SEM or mounted in Araldite so that they could later be sectioned. The chips were sectioned halfway through their width, parallel to their direction of travel in a plane perpendicular to the bottom of the chip; this was done by grinding away excess Araldite and chip material using a surface grinder. Preparation was completed by grinding on finer papers ranging from 250 to 600 grade, followed by hand polishing on cloths impregnated with 6 μm and 1 μm diamond paste. The polished chips were etched in a solution of 0.5 ml hydrofluoric acid, 0.5 ml nitric

acid and 99 ml of water. Great care was necessary when handling the etchant, due to the highly corrosive properties of hydrofluoric acid. The etched chip sections were examined and photographed to illustrate the formation of the chips and the built up edge.

After cutting titanium, some of the worn tools were examined under the SEM but it was clear that the wear features were masked by adherent iron and other machining impurities. Consequently, it was decided to carry out light chemical cleaning of the tool surfaces. Before cleaning all the tools, a trial was undertaken to ensure the stability of the structures. All the tools were then cleaned in 50% diluted HCL in an ultrasonic bath for 5 minutes and then they were prepared for examination.

CHAPTER 4

PRESENTATION OF RESULTS

4.0 PRESENTATION OF RESULTS

4.1 INTRODUCTION

This chapter contains the results of the two experimental techniques used for the present investigation. The first section has the data obtained by the quasi-static technique during the point loading, while the second section has the results collected from the machining process.

4.2 QUASI-STATIC ADHESION RESULTS

4.2.1 INTRODUCTION

In recent years, a modified indentation technique has been developed to study the deformation of hard materials by softer 'indenters' (174). For example, it has been shown that tungsten carbide single crystal can be plastically deformed, ie slip lines are produced, due to the contact pressure developed beneath a copper cone at low temperature (174). In this work, the 'soft indenter' technique has been applied using cone made from the titanium alloy to deform the various tool materials over a range of temperatures. Above a certain critical temperature, strongly welded junctions were formed. In Table 4.1 the critical adhesion temperatures determined in this way are summarised, together with the relevant contact pressure developed over the contact area, for these materials.

Invariably, when these welded junctions were separated the fracture face was through the cutting tool material. The following sections give further detail and the relevant micrographs represent additional evidence in support of that observation. It should be noted that this measured contact pressure is not simply related to the

Tool material	Critical temperature (°C)	Nominal contact presure (GPa)
Polycrystalline diamond	760	0.142
Cubic boron nitride Amborite	900	0.146
Coated carbide (KC850)	740	0.234
Coated carbide (KC910)	820	0.267
Uncoated carbide (K68)	800	0.294

Table 4.1 Critical adhesion temperatures

hardness of the metal cone but it is also influenced by the friction at the metal ceramic interface.

4.2.1.1 POLYCRYSTALLINE DIAMOND (PCD)

As a result of separation strongly adhered PCD cutting tool material remains attached to the titanium alloy cone (Fig 4.1) and the corresponding pit on the rake face of the cutting tool is shown in Figure 4.2. The obvious roughness of the fractured surface indicates that failure has occurred around particles rather than through them but this needs to be verified. A longitudinal section of the ground and polished indenter (Fig 4.3) shows the adhered layer which is 8 - 10 microns thick (Fig 4.4).

4.2.1.2 CUBIC BORON NITRIDE (CBN)

A difference in the behaviour between the rake and flank faces of CBN is apparent in the table. The following observations reinforce that evidence:

(a) Rake Face

Once the adhesion test was completed, the separation of the welded junction was made. Figure 4.5 shows the result of separation of a junction formed between the titanium alloy and the cubic boron nitride such that a pit has formed in the original surface where a hemispherical fragment was removed with the titanium cone (Fig 4.6). It is apparent that the fracture surface is somewhat less rough than the corresponding PCD surface (Fig 4.1) and this observation is consistent with the size of particles - ie 1-2 microns and 10 microns respectively. Finally, after the separation

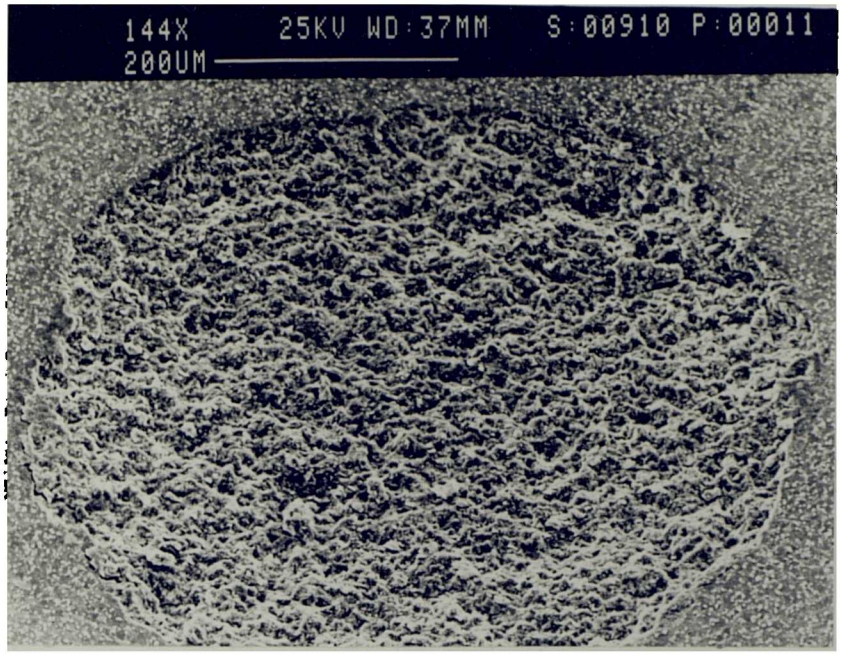

Fig 4.1 Crater formed in polycrystalline diamond tool after separation of welded junction.

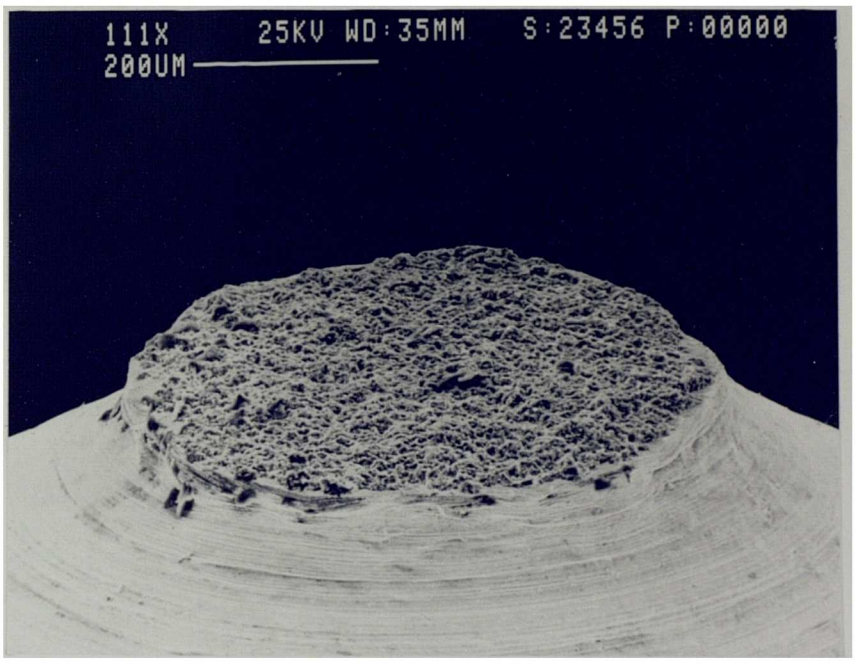

Fig 4.2 Titanium alloy indenter with strongly adherent polycrystalline diamond after fracture within bulk of tool material.

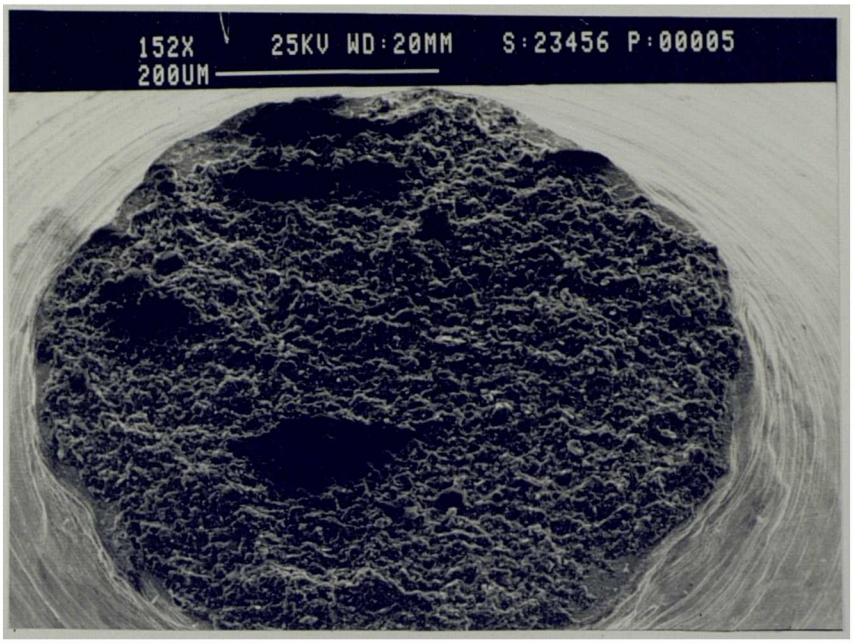

Fig 4.3 An enlarged view of area shown in Fig 4.2.

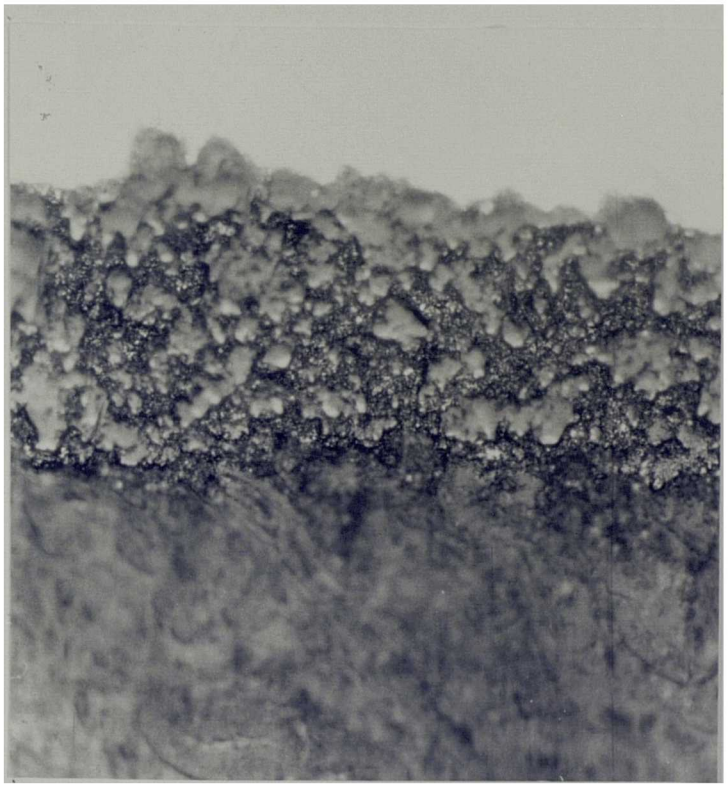

Fig 4.4 Longitudinal section through titanium alloy:tool welded junction showing toolpiece particles from PCD. X400

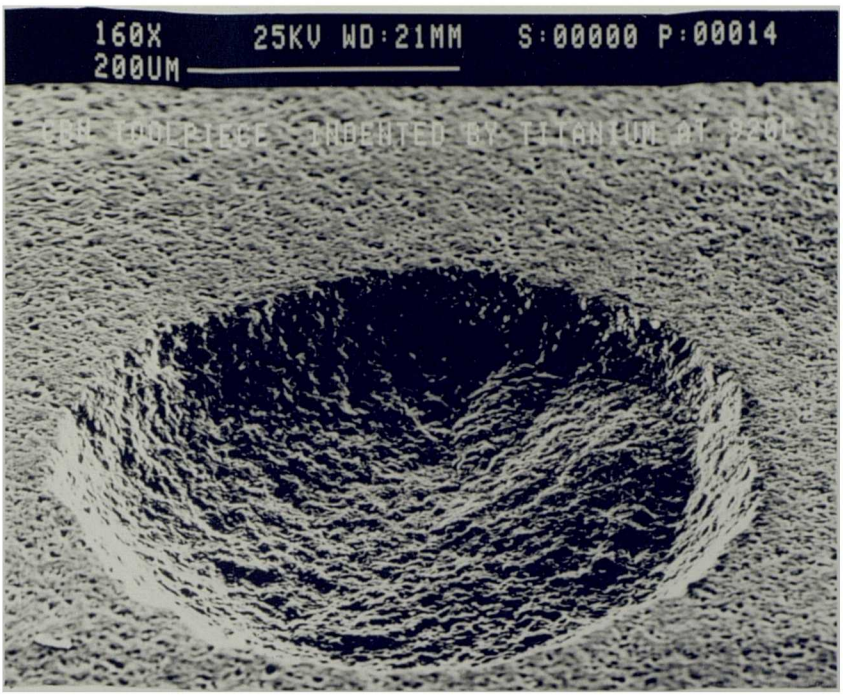

Fig 4.5 Crater formed in cubic boron nitride tool after separation of welded junction.

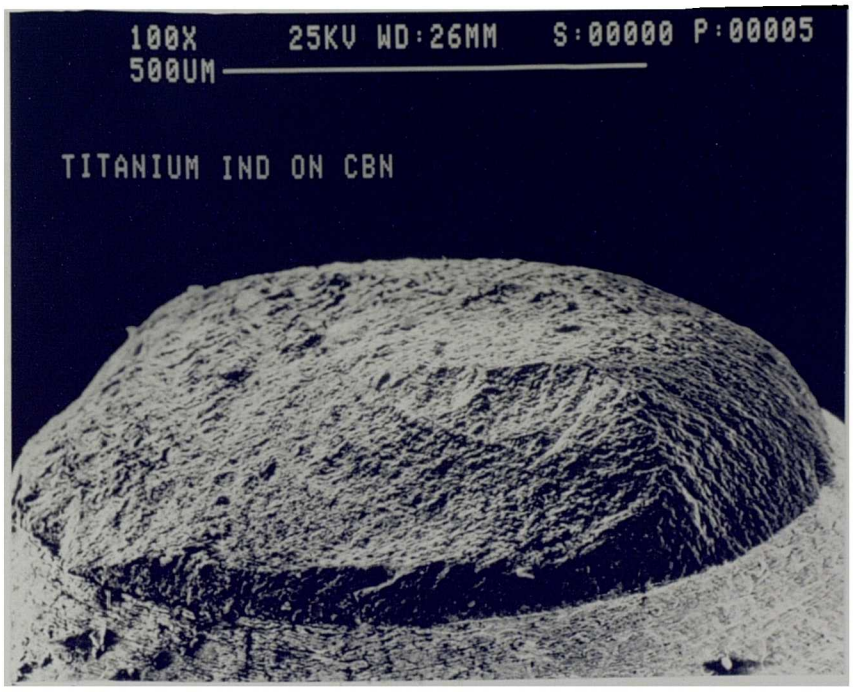

Fig 4.6 Titanium alloy indenter with strongly-adherent cubic boron nitride after fracture within bulk tool material.

of welded junction, the indenter was ground and polished to show the entire welded junction (Fig 4.7) in to the cutting tool attachment.

(b) Flank Face

Because of the marked difference in the behaviour of the flank face a large number of indentation tests were carried out on this. The same detailed procedures as of rake face was adopted for all the tests which were carried out on the flank face. After completion of each test, the indenter was removed and it was discovered that the indenter was severely deformed without the normal welded junction being formed. (Fig 4.8). Even at higher temperatures, with a corresponding increase in the extent of deformation, there was no evidence of significant adhesion (Fig 4.9). Whilst an explanation of this particular effect is now possible at the time, there are three points which should be made.

This observation underlines the importance of the role of friction at the interface. Here, due to lack of adhesion, the contact pressure becomes remarkably low and so residual impressions are made on the tool face - the flow of con material is such as to accurate replicate surface features and structure on the hard material, ie note scratch marks on rake face replicated on blunt end of con in Figure 4.8.

Differences in the cutting performance for rake and flank faces of CBN are discussed in Chapter 5.

4.2.1.3 COATED CARBIDE KC850

Due to point loading after the removal of welded junction, a large crater was found on the rake face of toolpiece (Fig 4.10). This crater is roughly circular in shape and encompasses areas of uneven thickness. Depth of indentation is clearly visible which shows three distinct coatings and the material from the substratum (Fig

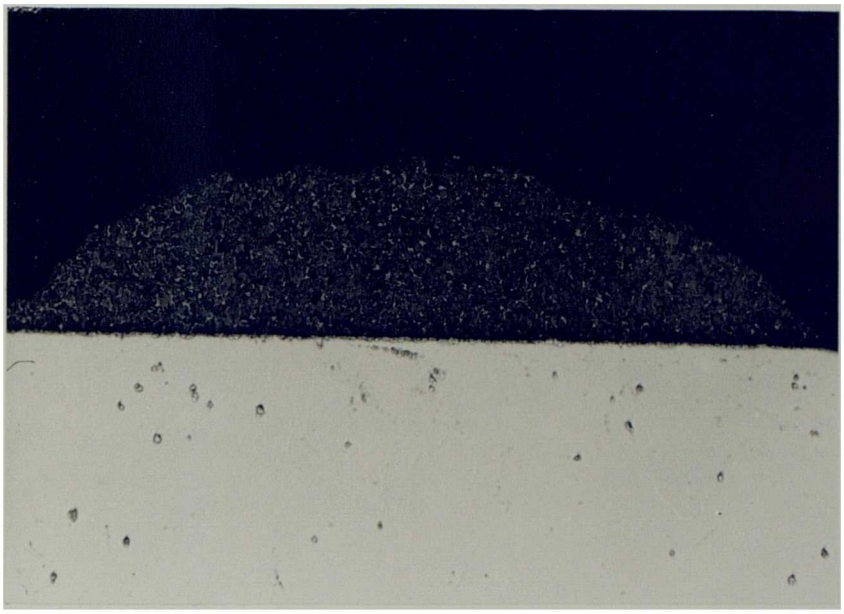

Fig 4.7 Longitudinal section through titanium alloy:tool welded junction showing toolpiece particles from CBN.

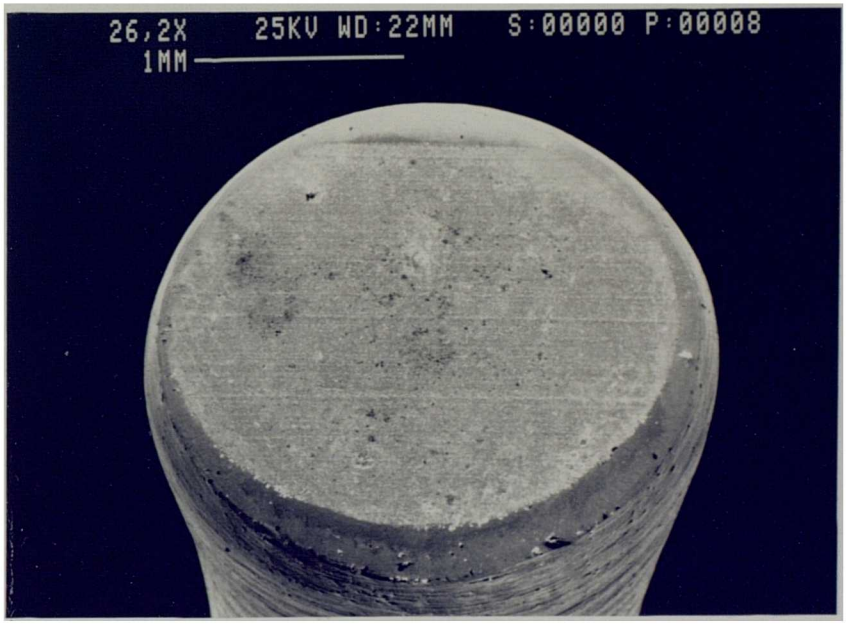

Fig 4.8 Titanium alloy indenter on the flank face of cubic boron nitride tool, showing no sign of adhesion.

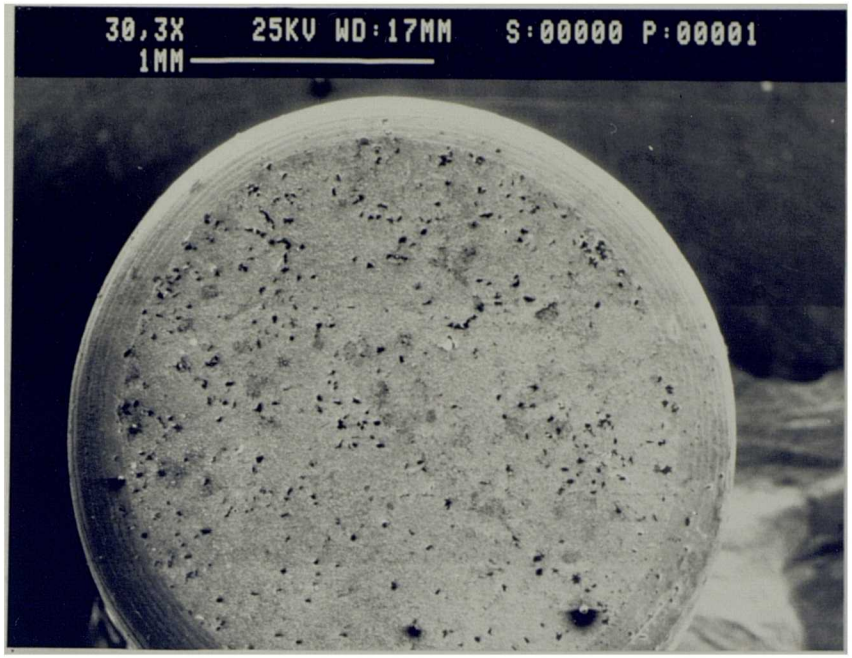

Fig 4.9 Titanium alloy indenter on the flank face of cubic boron nitride tool at high temperature.

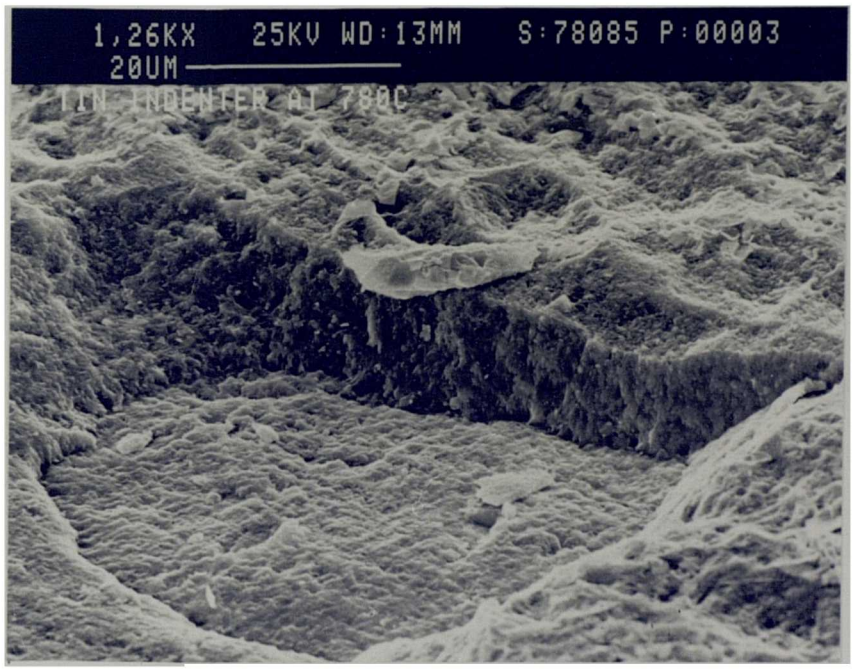

Fig 4.10 Crater formed in coated carbide tool (KC850) after separation of welded junction.

4.12). This crater is approximately 17 microns deep while the total thickness of all three coatings is 12 microns. From this, it is evident that all three layers were removed along with some parts of substratum, thus, exposing tungsten carbide particles (Fig 4.12). Cracks and fractures were also developed around the perimeter of the pit. The cracks range from 2-4 microns in width and may have been caused during the point load process (Fig 4.13). The surface of the cone was flattened after the separation of welded junction, and was seen to closely resemble the shape of impression made on the tool. The cone had adhered strongly to the material of the carbide tool (Fig 4.14). A closer view of the cone reveals a coating of titanium carbide layer in association with a few tungsten carbide particles scattered randomly over it (Fig 4.15). To elucidate the nature of the welded junction, a cone was first sectioned, and then ground and polished (Fig 4.16). Results of X-Ray analysis confirmed the presence of tool and workpiece material.

4.2.1.4 COATED CARBIDE KC910

Upon separation of the welded junction, a pit in the original tool surface was formed as the hemispherical fragment was plucked out by the titanium con (Figs 4.17, 4.18). The periphery of the pit is somewhat broken and cracked, and enlarged view of this shows the presence of microcracks and microfractures (Fig 4.19). Finally, an indenter with adhering tool material was ground and polished to show the coated layers and substratum (Fig 4.20). Also to confirm the composition of particles from the tool, several X-Ray analyses were made at various places on the welded junction. In all the cases, analysis confirmed the presence of elements similar to that of tool.

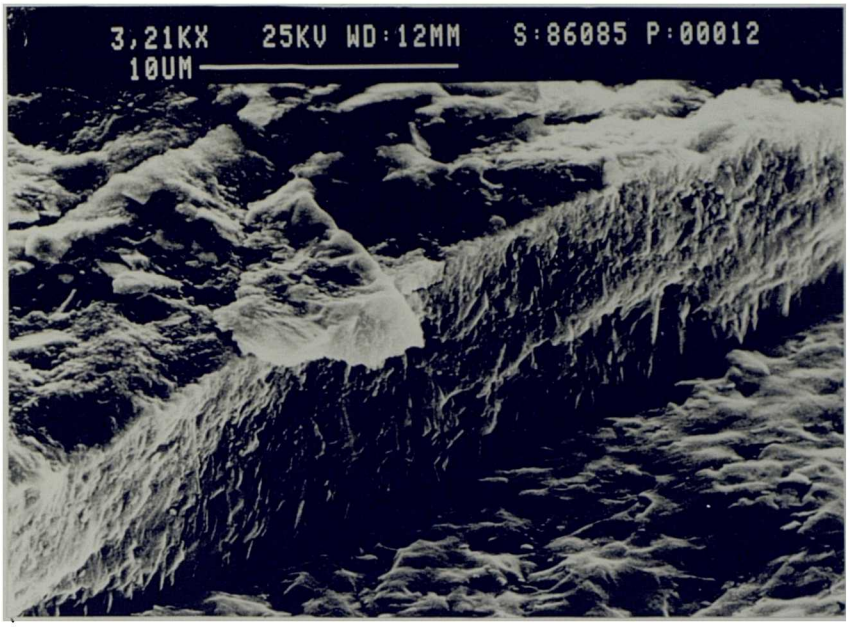

Fig 4.11 SEM micrograph of carbide tool (KC850) rake face showing the exposed coated layers & substrate particles.

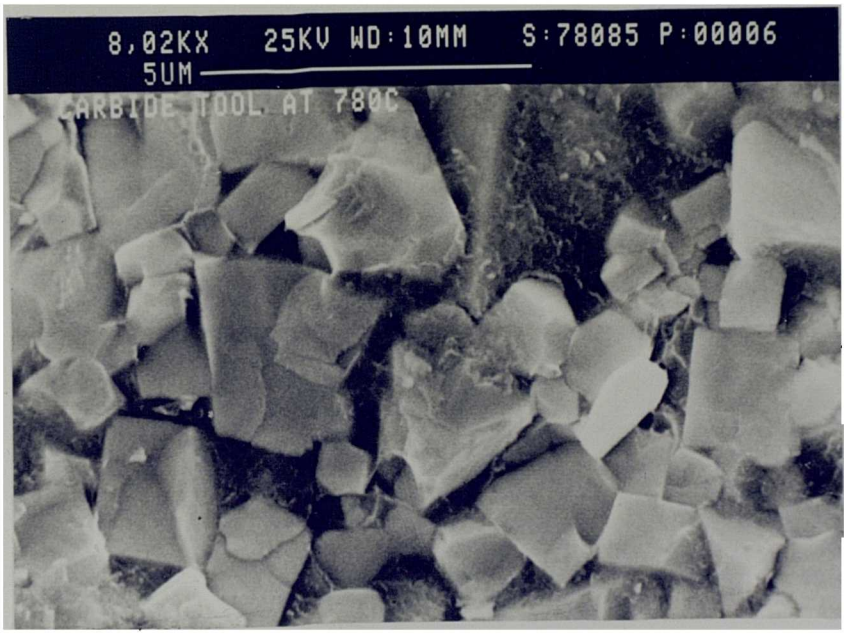

Fig 4.12 SEM micrograph of exposed carbide substrate after fracture of welded junction (ref Fig 4.13).

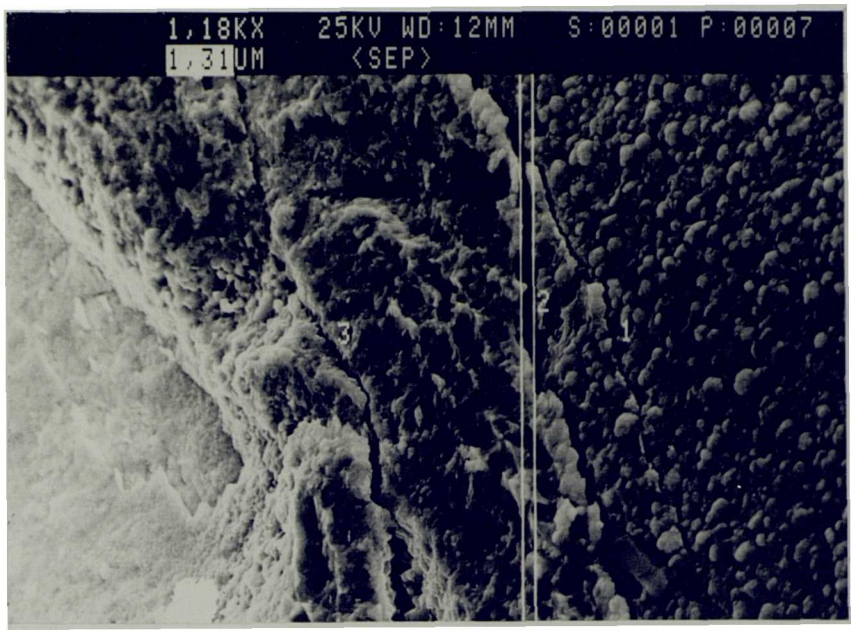

Fig 4.13 **Formation of crater during the point loading on the carbide rake face (KC850).**

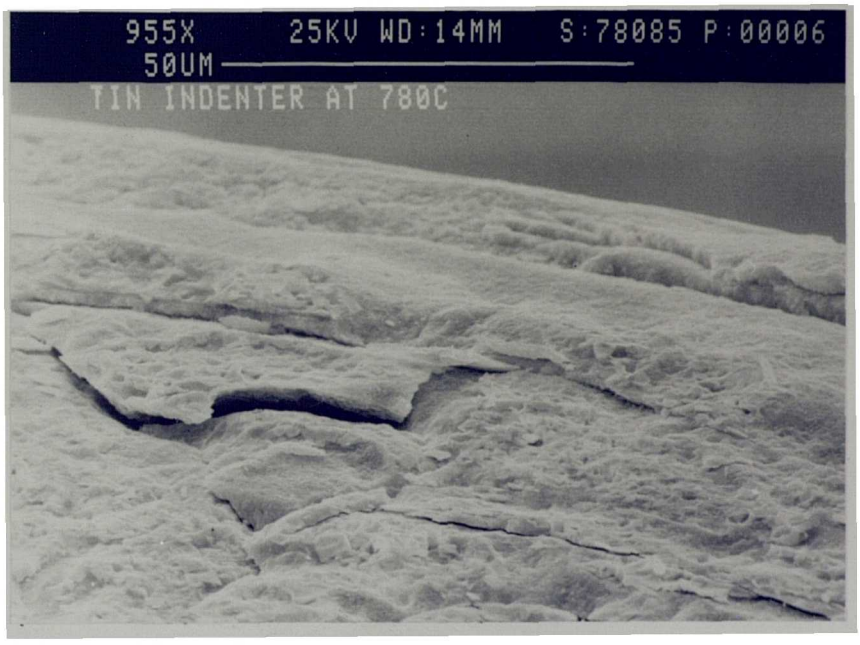

Fig 4.14 **Titanium alloy indenter with strongly-adherent carbide (KC850) after fracture within bulk tool material.**

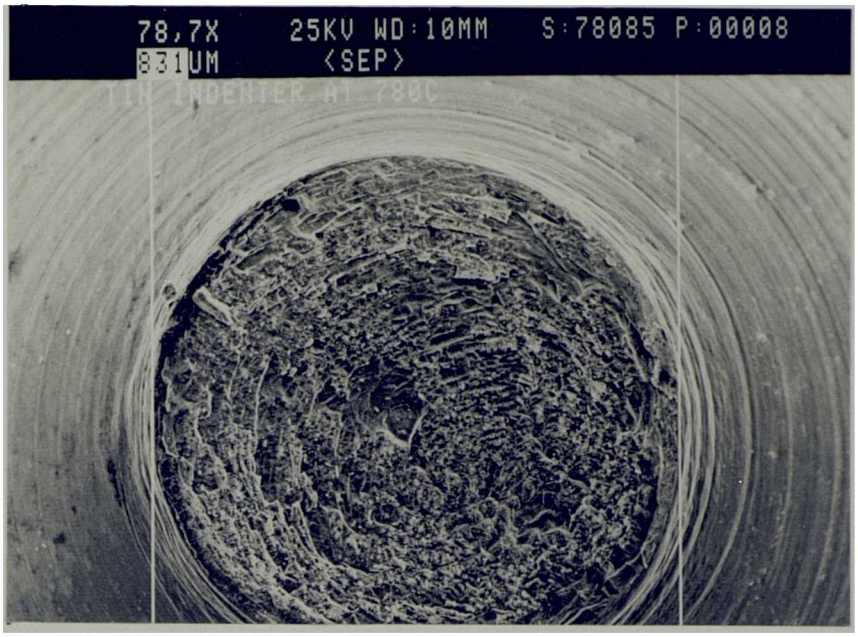

Fig 4.15 Coated layers of carbide tool (KC850) attached to a titanium alloy indenter.

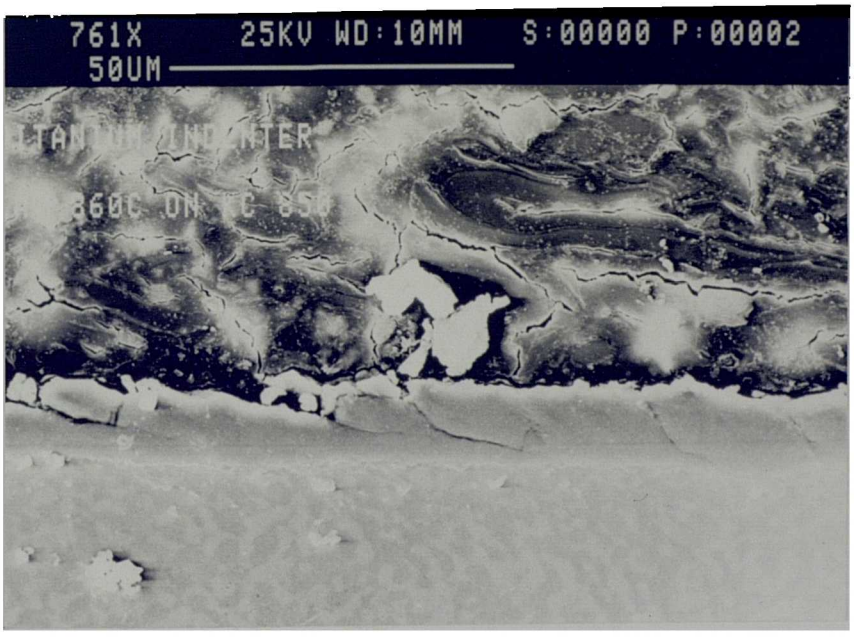

Fig 4.16 Longitudinal section through titanium alloy:tool welded junction showing layers from coated carbide (KC850) specimen.

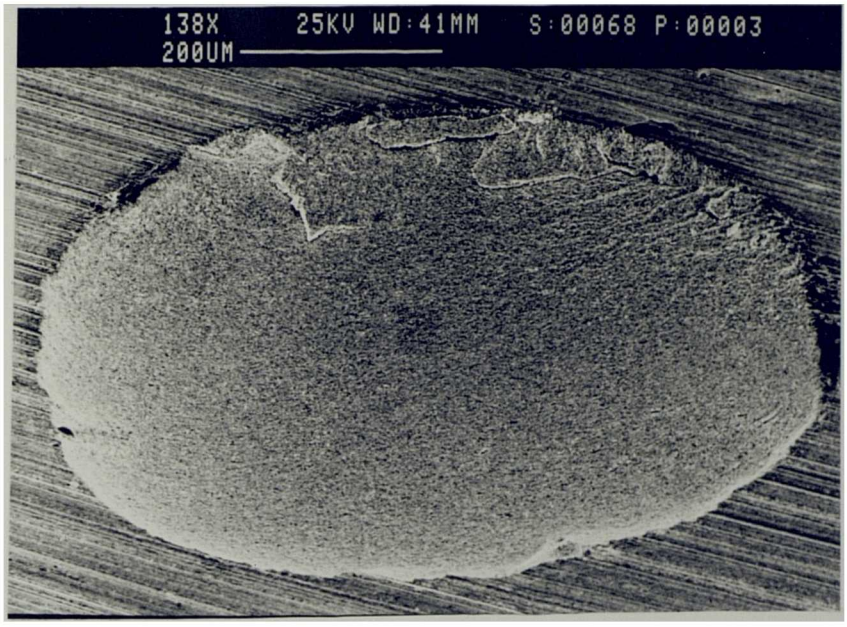

Fig 4.17 Crater formed in coated carbide (KC910) tool after separation of welded junction.

Fig 4.18 Titanium alloy indenter with strongly-adherent coated carbide (KC910) tool after fracture within bulk tool material.

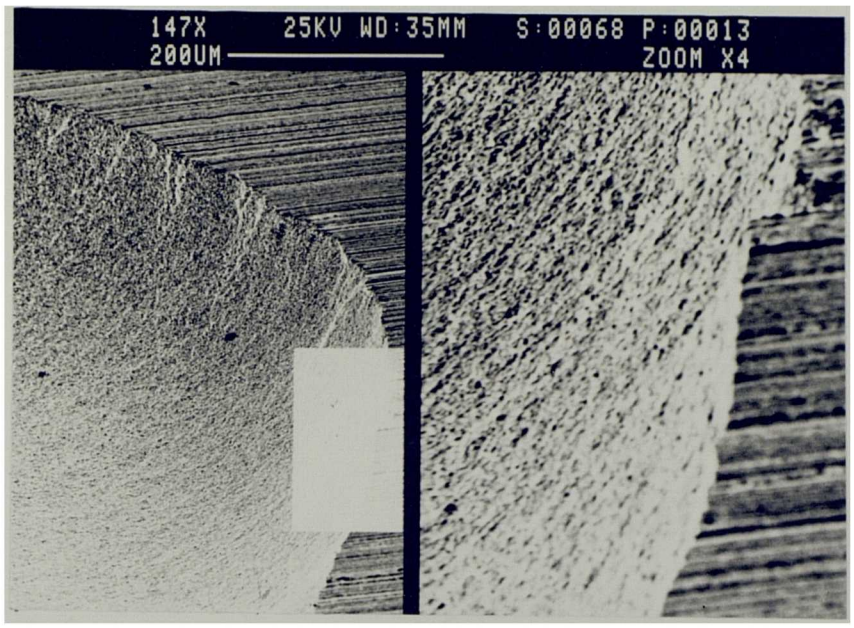

Fig 4.19 An enlarged view of Fig 4.17.

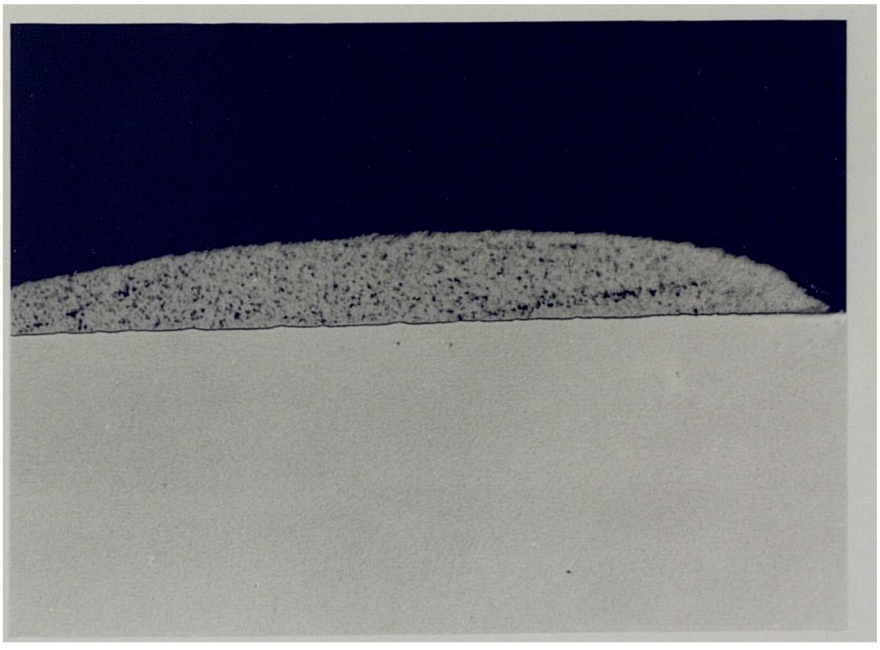

Fig 4.20 Longitudinal section through titanium alloy:tool welded junction showing toolpiece particles of coated carbide (KC910) tool.

4.2.1.5 UNCOATED CARBIDE K68

The observations on this tool material were virtually the same as those for coated tools. First, a shallow depression formed on the rake face of the cutting tool (Fig 4.21) which was the result of separation of the welded junction. Removal of tool material by the cone is illustrated in Figure 4.22. An enlarged view of the same is given in Figure 4.23, where the plucked out tool material extends beyond the edge of the cone. A sectioned an polished view of this cone indicates strong welding between it and the tool (Fig 4.24).

4.2.2 RELEVANCE OF QUASI-STATIC TESTS TO METAL CUTTING EVALUATION

At this stage two important aspects of the method can be identified as being important to the subsequent metal cutting tests.

First, that the critical temperatures for adhesion and welding will generally be exceeded at the interface during metal cutting conditions. Second, that once formed, the welded attachment of workpiece to tool withstands forces of separation and failure invariably takes place within the bulk of the tool.

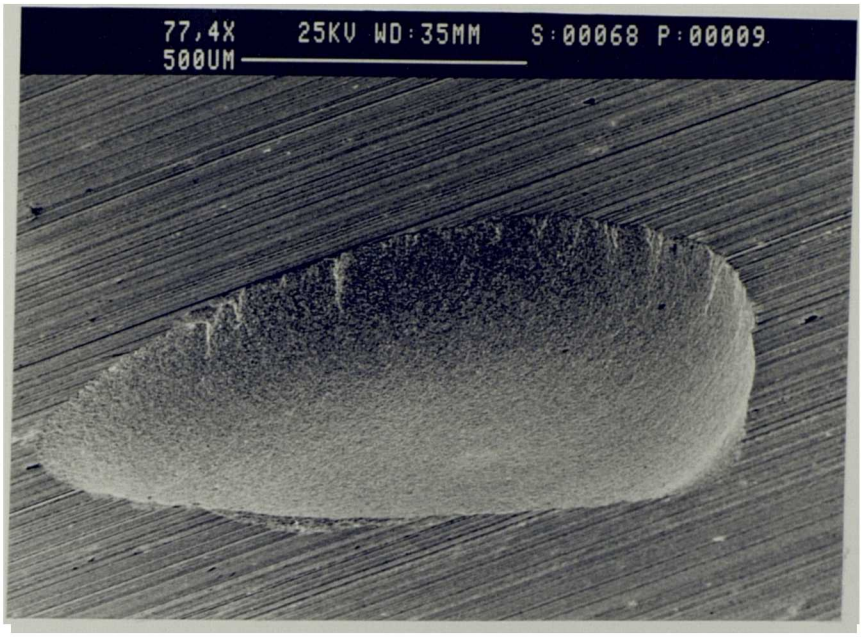

Fig 4.21 Crater formed in carbide (K68) after separation of welded junction.

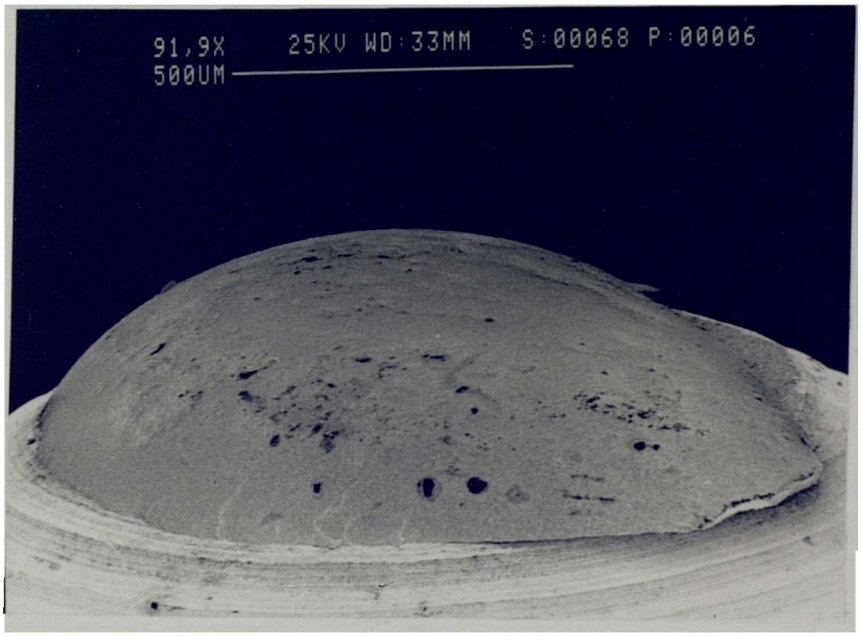

Fig 4.22 Titanium alloy indenter with strongly-adherent carbide tool (K68) after fracture within bulk tool material.

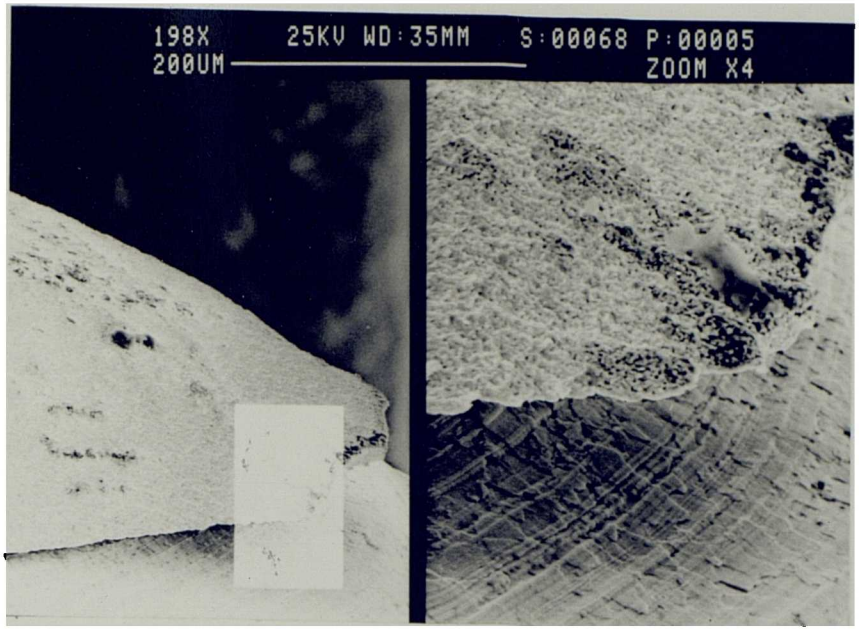

Fig 4.23 An enlarged view of Fig 4.22.

Fig 4.24 Longitudinal section through titanium alloy:tool welded junction showing toolpiece particles of carbide (KC68) tool.

4.3 SURFACE MORPHOLOGY AND STRUCTURE OF CARBIDE TOOLS

4.3.1 SURFACE MORPHOLOGY

4.3.1.1 CARBIDE TOOLS

Figure 4.25 shows a typical surface of KC910 consists of a three dimensional array of 'hills' and 'valleys'. The vertical distance between 'hill' peak and 'valley' floor, for each of these coatings varied from 2-3 microns whilst the horizontal distance between individual spheroids was nearly 1 micron.

Some of the KC910 inserts used in the early parts of this research contained additional blister-like features which stood nearly 6 microns above the main surface of the insert and were nearly 10-15 microns in diameter. Such features (which were approximately hemispherical in shape) were found to be hollow and were quickly worn through revealing small voids after cutting at 100 m/min for 60 seconds (Fig 4.26). These blister features were observed on most of the coated specimens and it may be presumed that they represent unsatisfactory coating technique.

The KC850 inserts also had a similar hill and valley topography but the surface was found to comprise a random array of fine rectangular shaped protrusions approximately 4-5 microns in size. The Al_2O_3 coated inserts were found to have an irregular surface consisting of numerous elliptical nodules, whose dimensions were about twice those of the spheroids seen in KC910 surface. Furthermore, no finer surface features were observed.

The KC910 inserts had a dark grey surface which on lightly polishing, revealed the bulk of the TiC and Al_2O_3 layers having a white/silver grey and light grey colours respectively. The surface of the KC850 inserts were also lightly polished and the original yellow appearance of the TiN layer was found to be slightly

Fig 4.25 SEM micrograph of coated carbide tool rake face surface.

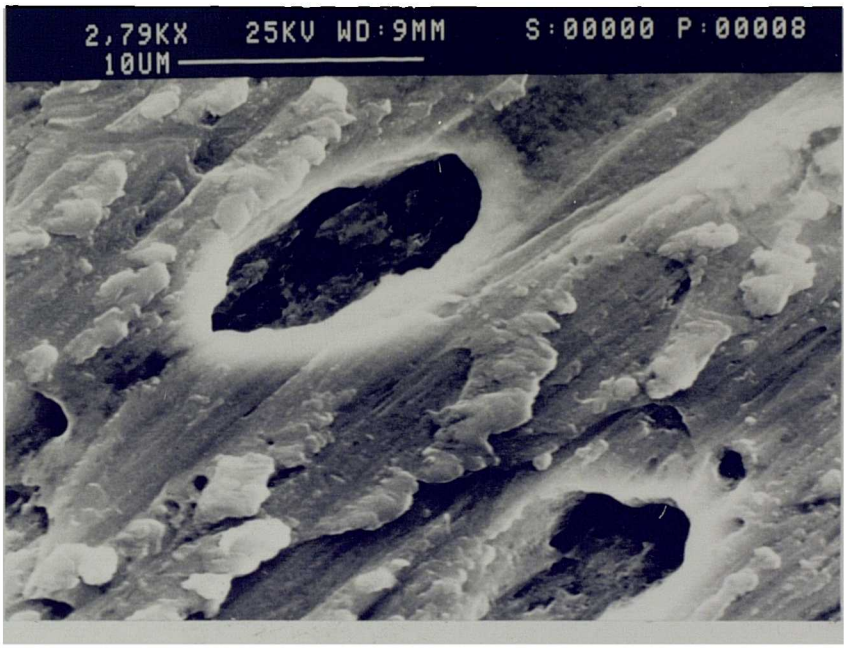

Fig 4.26 Appearance of small voids on the rake face of coated carbide (KC910) at speed of 100 m/min.

darker than the bulk of other layers. These observations suggest that the surfaces of these coatings are contaminated, perhaps by oxygen or carbon, after the deposition process was completed.

4.3.2 STRUCTURAL ASPECTS OF COATED CARBIDE TOOLS

4.3.2.1 CARBIDE TOOL

A similar metallographic section through KC850 is shown in Figure 4.27 and, again, the individual layers of the coating are clearly seen (Figs 4.27 and 4.28). The grains which were quite small in size were visible in the as polished condition. The reason for this phenomenon is not clearly understood but it is possible that the TiC grain boundaries become outlined by the carbon and other debris collected during the preparation process. However only a small proportion of the TiC layers were outlined in this fashion and it is not thought that this constitutes porosity detrimental to its preformance.

The whole substrate of KC850, including the TiN layer, successfully etched in an acid/water mixture [5% HF, 20% HCL, 20% HNO_3, and 55% water (by volume)].

Longitudinal sections through the Al_2O_3 coated inserts (Fig 4.28) clearly revealed the two layers of coating as shown in Figure 4.28 and also presence of an intermediate layer between the TiC and the substrate. Closer examination of this layer showed that it is comprised of many crystals nearly 2 microns across, which appeared to have a similar colour to that of the mixed carbide phase in the substrate and was often contiguous with that phase.

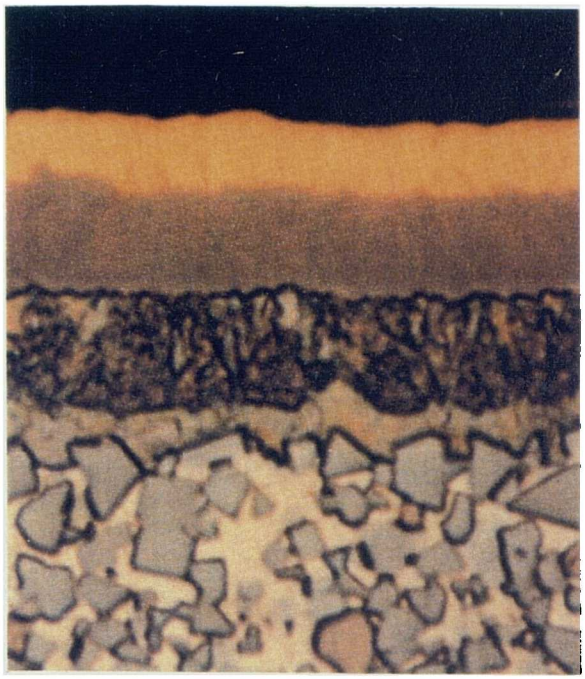

Fig 4.27 Longitudinal section through coated carbide tool (KC850) showing the interface of coated layers & the substrate.

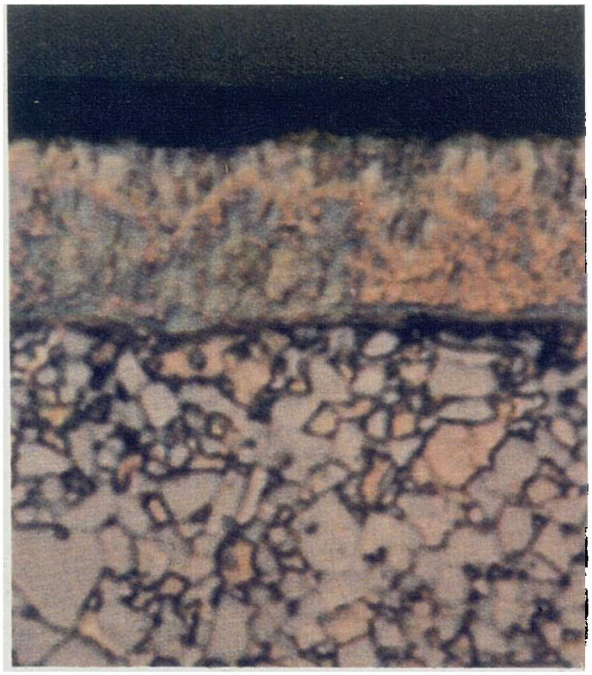

Fig 4.28 Longitudinal section through coated carbide tool (KC910) showing the interface of coated layers & the substrate.

The observed wide variations in the constitution of the coating/substrate interface suggests a poor control of carbon level in the substrate prior to, and during, deposition of the coatings.

4.3.2.2 STRUCTURE OF PCD AND CBN TOOL MATERIAL

The surfaces of these materials were prepared by mechanical polishing and reflect the structure of the sintered aggregates.

Syndite polycrystalline diamond consists of fully dense, sintered diamond powder with bonding between adjacent diamond crystals via a cobalt binder phase. This cobalt binder plays an important role in the synthesis of PCD at temperatures in the region of 1400 $^{\circ}$C and applied pressure of the order of 60 Kbar. Without the presence of the cobalt, the intergrowth between diamond grains, which gives polycrystalline diamond its toughness, would not be as extensive. However, if the composite is over-heated during tool manufacture, the cobalt will have an adverse effect on the material's resistance to thermal degradation.

Figure 4.29 is a micrograph of a polished and unetched diamond aggregate. In this micrograph cobalt phase can be distinguished as the lighter phase.

Figure 4.30 is an aqua-regia etched scanning electron micrograph of a diamond aggregate at a higher magnification. This micrograph mostly shows the microstructure of the etched diamond aggregate and also the diamond-diamond intergrowth and bridging. The cobalt, which is the matrix material, had been leached out by the etching to reveal the continuous skeleton of the compact. The diamond particles which form most of the material are not attacked by the etching and are seen to be quite large and well bonded to each other, both by direct sintering and by significant diamond to diamond bridging.

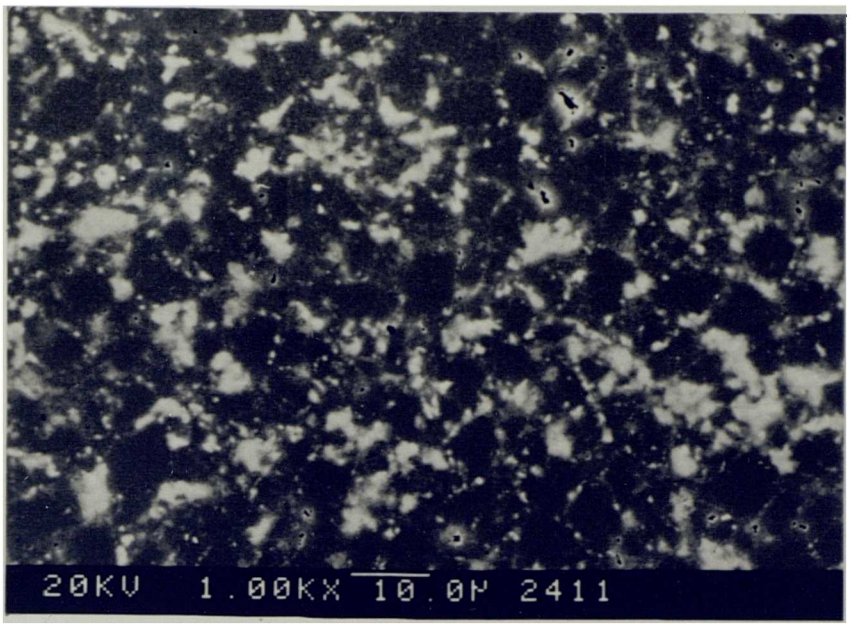

Fig 4.29 SEM micrograph of polished surface of aggregate diamond tool.

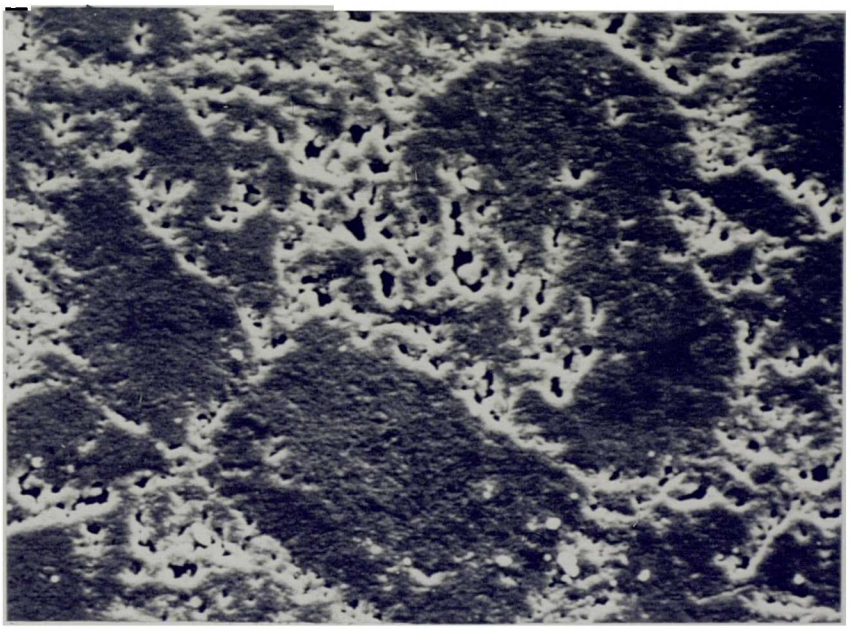

Fig 4.30 Microstructure of aqua-regia etched diamond aggregate showing diamond-diamond intergrowth and bridging.

Figure 4.31 is a scanning electron micrograph of the etched diamond aggregate, revealing the close network of fine grained diamond aggregate. The skeleton shows porosity of some degree, which throws light on the durability of this diamond aggregate as cutting tools.

Cubic boron nitride is manufactured by using very fine, randomly oriented, and carefully graded boron nitride particles at high temperature and pressure in the presence of metal to form a ceramic binder phase. Under these conditions the composite mass of particles develops into a dense polycrystalline structure. Amborite is an aggregate of synthetic cubic boron nitride in which the boron nitride particles are surrounded by a thin case of aluminium nitride in a continuous matrix consisting of aluminium diboride.

The micrographs of polycrystalline tools are similar to those presented in the work carried out by Brookes et.al (123). Figure 4.32, is a micrograph of CBN structure in which some grains have broken into two or more fragments between which the binder has penetrated. In the regions between the larger distinct CBN grains, smaller CBN fragments are present. In some cases these are grouped together in such a way that they are remnants of a larger grains which have completely shattered during consolidation. Some may be single fragments from the grains that have otherwise remained intact.

There are two particularly important differences in the microstructure of material based on diamond when comparisons are made with other tool material aggregates (ie. tungsten carbide, cermet). Firstly, the particle size is much larger than the 1-5 microns commonly used in cermets. Diamond aggregates are available with particles sizes ranging from 10 to 25 microns, whilst the average size of boron nitride particles is 10 microns. Secondly, junctions are formed by the secondary diamond growth during the manufacture of this material. This will ensure the formation of a

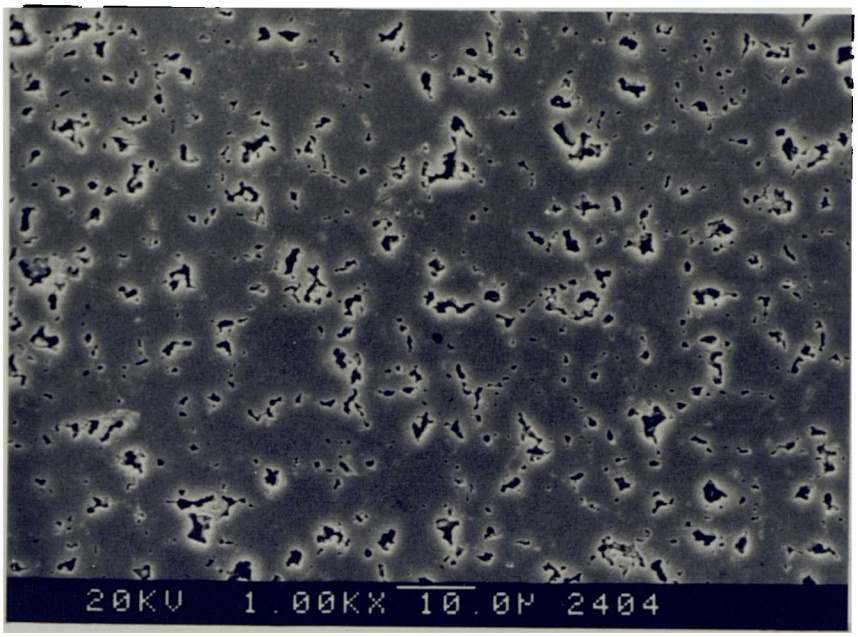

Fig 4.31 SEM micrograph of polished diamond aggregate tool etched with acid.

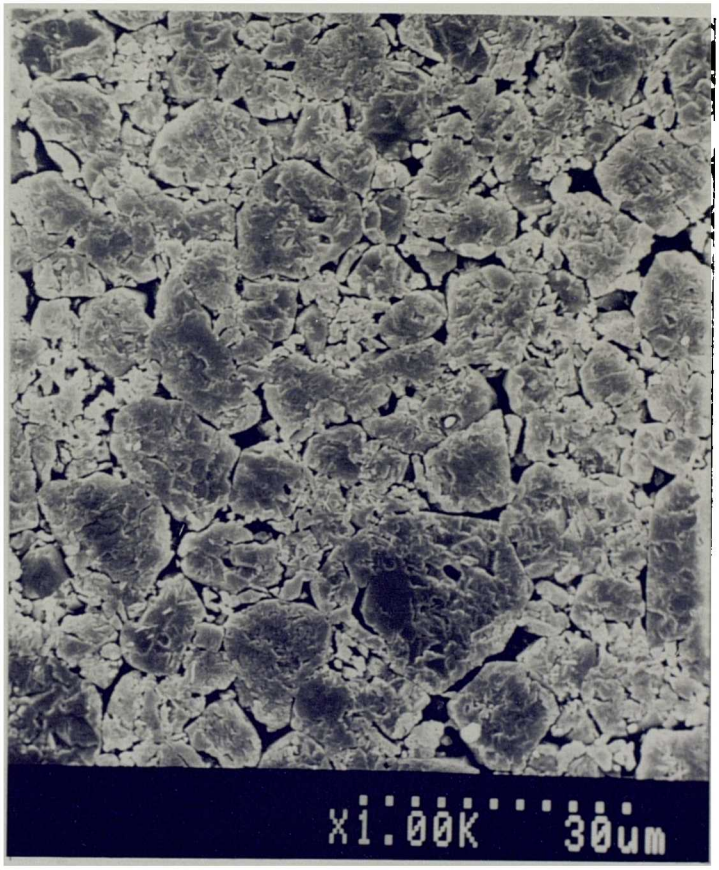

Fig 4.32 SEM micrograph of cubic boron nitride tool.

formation of a continuous skeleton of the particle phase and the certainty of its deformation or fracture when sufficiently high stresses are developed.

In the case of CBN tool material, again the particle size is larger than for conventional tool materials, eg. 10 microns. But it should be noted that, as in the case of WC:CO cermets, primary particles are separated by the second phase, in this case aluminium nitride.

4.4 TOOL WEAR

4.4.1 INTRODUCTION

The results which were obtained by the aforementioned experimental techniques are presented in two sections. The first contains the results when machining with different tool materials and their performance. The second section the results obtained from the chip produced when machining in conjunction with the Quick Stop Tests.

4.4.1.1 COATED CARBIDE TOOLS

There is much published evidence that chemical vapour deposition (CVD) coatings greatly increase the resistance to wear of carbide tools. This evidence has normally been presented in the form of measurements of the depth of wear on the tool flank and the depth of crater formed on the rake face of tool (similar to the procedure used for measuring wear of uncoated tool) as function of cutting speed, or cutting time for different types of coating. In the present work attention is focused on the mechanisms which operate to cause wear of the tools, in the main regions shown in Figure 4.33.

In general, wear in the main rake face contact area is most rapid at its centre. On the flank face the coatings are first worn through below the tool edge. Deep grooves are often worn through the coatings at both extremities of the depth of cut (regions C & D; Fig 4.33). Coatings are first worn through precisely on the tool edges, with the wear extending along the rake and end clearance faces as cutting is continued.

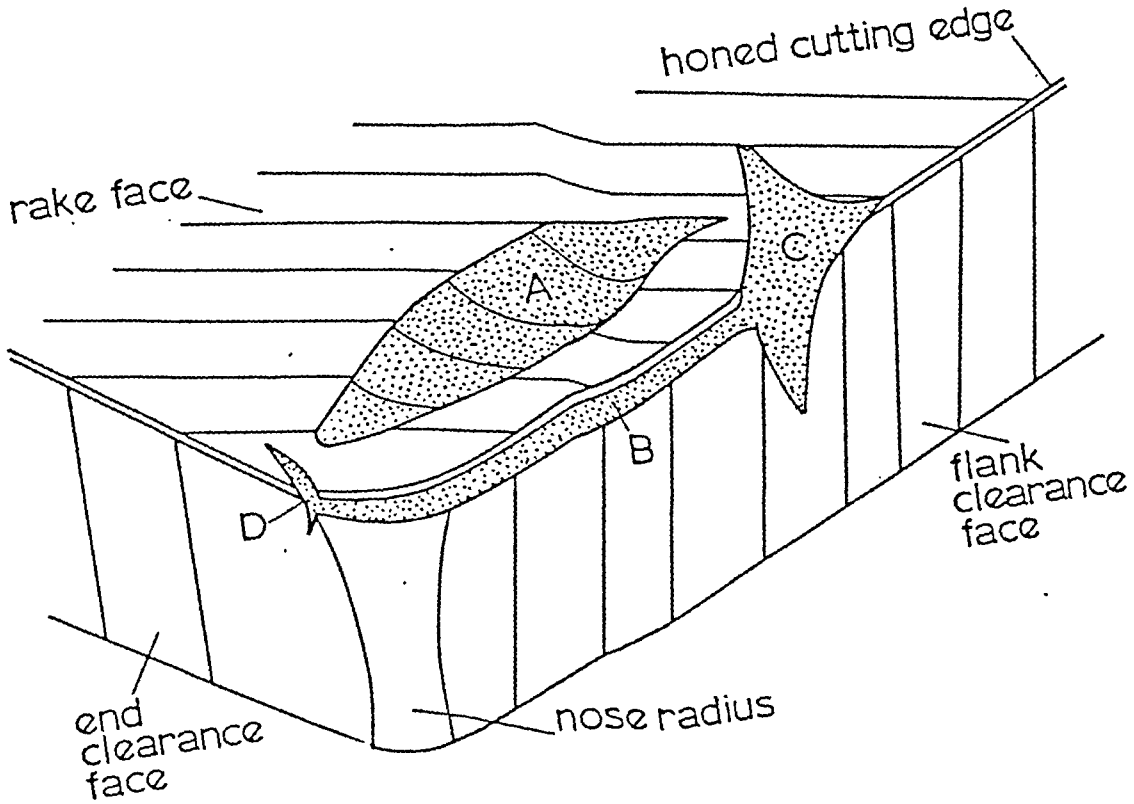

Fig 4.33 Schematic diagram of worn coated tool showing principal areas of wear.

These features of wear, established in previous studies, were essetially observed in this work. More details of the wear for individual cutting tools are given in the following sections.

4.4.1.2 CUTTING PERFORMANCE OF KC850

At a cutting speed of 50 m/min, measurable flank wear began after 30 seconds of machining the TA48 grade with KC850 tools. The first sign of crater formation was distinguishable, at 'A' in Figure 4.34, the surface layers coating having been removed. At the cutting edge, each of the layers in coating were exposed -- see position 'B', 'C' and 'D' in Figure 4.34. Therefore, there are regions where the TiN layer is still intact ('B'); the intermediate layer TiC/TiN is exposed ('C'); and the TiC layer is visible ('D'). The flank face had undergone a mixed wear process due to diffusion and attrition resulting in both smooth wear and irregular surfaces. On the flank wear land some faint ridges can be seen running away from the cutting edge, apparently caused by the removal of TiN and Ti(C,N) particles resulting in attrition.

After cutting for a period of 2 minutes, the irregular surface of flank land became completely smooth, exposing the TiN/TiC layer and the deterioration of the cutting edge sharply increased (Fig 4.35). The failure of the cutting edge took the form of flaking and chipping as a result of the increased stress in this zone due to increased cutting forces. The nose deformation and rake face wear were considerably accelerated with the increase in contact area between the tool and chip on the rake face (Fig 4.36).

After cutting for 8 minutes the tool was completely worn at both extremities of the depth of cut. Figure 4.37 illustrates a large notch which formed on the clearance face of the tool. The surface of this notch was smooth due to diffusion

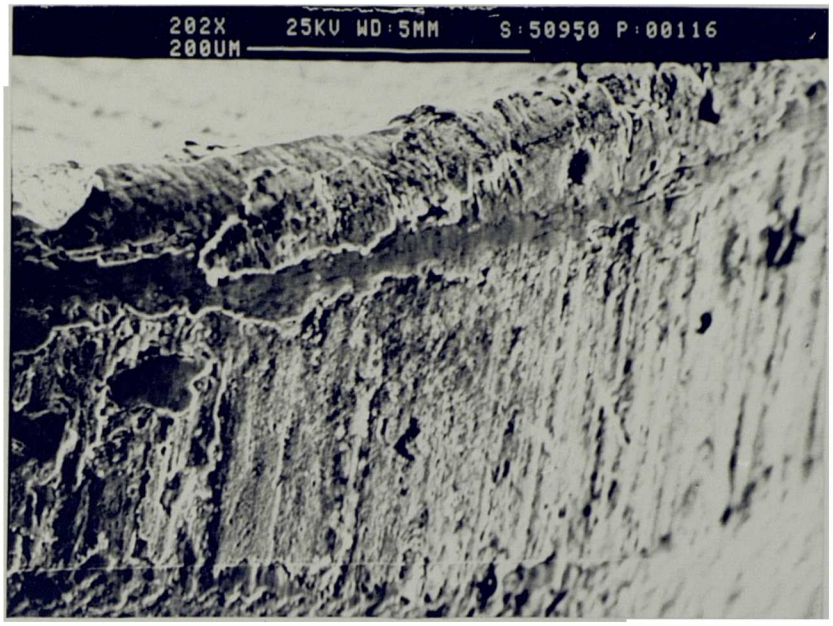

Fig 4.34 Worn surface of KC850 due to the diffusional/attrition wear.

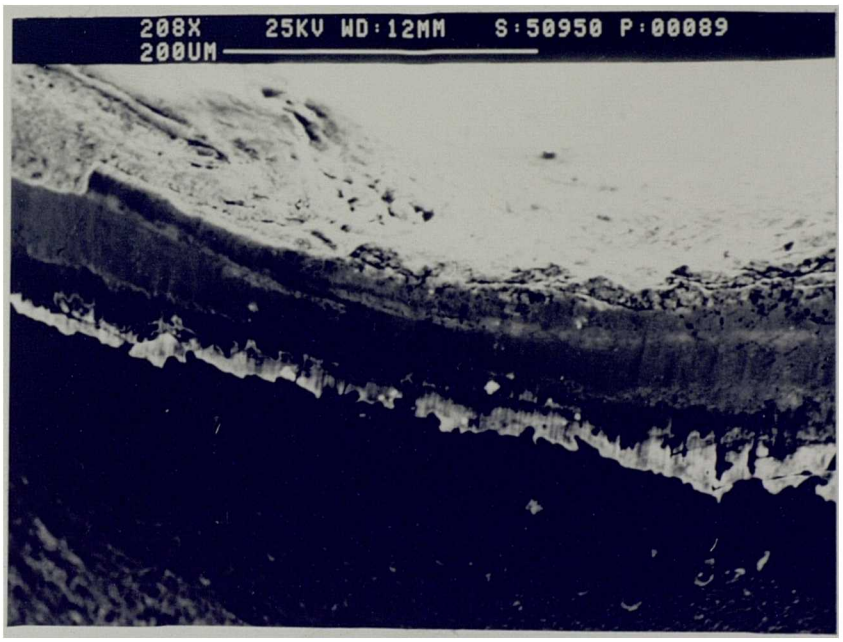

Fig 4.35 Chipping off portions from the cutting edge of KC850.

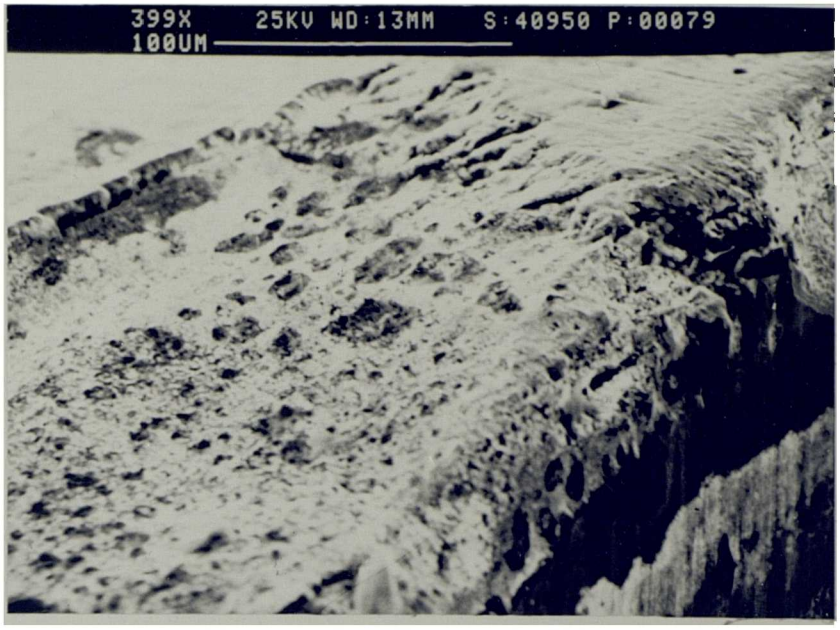

Fig 4.36 Worn surface on the rake face of KC850.

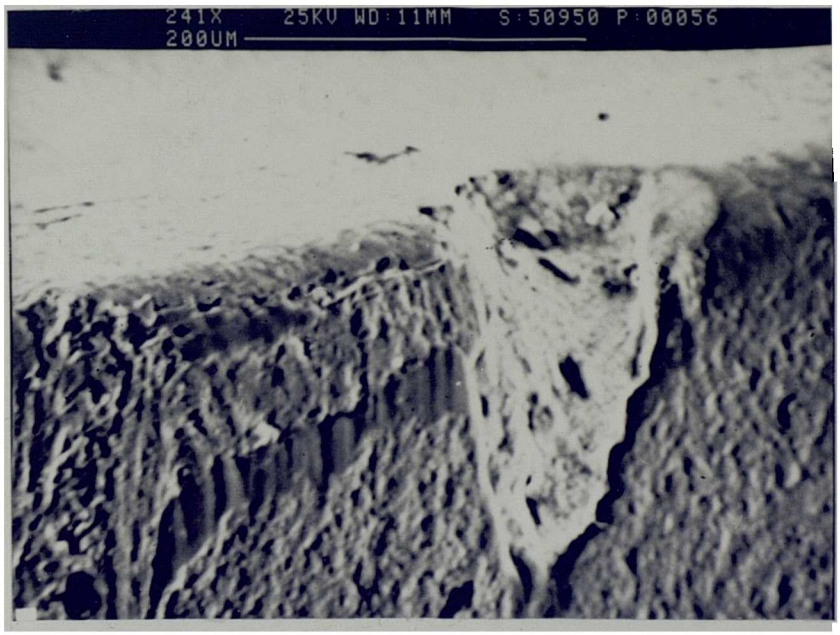

Fig 4.37 Formation of notch wear at the clearance face of the coated carbide tool (KC850).

mechanisms dominanting, but with some evidence of attrition wear. At this stage of wear the tool would have been rejected due to the rough surface finishing.

After cutting at the speed of 75 m/min for 4 minutes, the flank and the rake face of the tool showed similar patterns of wear to the ones already observed at low speed (Fig 4.38). The wear of the coating around the cutting edge in region 'C' zone (Fig 4.33) was much higher than that of those found in region 'D' (Fig 4.33) and were formed exclusively by a smooth wear process. The flank and rake surfaces which were similar in appearance to those described earlier which were worn by a diffusion/dissolution process . However, in contrast to the earlier case, cracks were running normal to the chip flow direction. The craters were formed as a conseqence of undermining of the coating and exposure of large material substrates (Fig 4.39). Two mechanisms of wear are thought to operate on the rake face of the tool. The condition of rake face is consistent with wear occuring by the initial removal of the coating , followed by diffusion wear on the exposed substrate. The other process is that of attrition wear as a result of large fragments being frequently broken away and adhering to the underside of the swarf and subsequently carried away along the rake face.

When cutting TA48 at the speed of 100 m/min for 1 minute, the coatings were found to be rapidly removed. Once the coating was undermined and the substrate exposed, wear proceeded by a diffusion/dissolution mechanism. Evidence for the latter can be seen in Figure 4.40, which shows typical tool wear. The figure shows that the triple coated layers on the rake face have been removed leaving behind the exposed WC substrate. The TiN and intermediate Ti(C,N) layers were also removed from the flank face exposing the underlying layer of TiC. Numerous ridges were seen to be present on the flank face running normal to the rake cutting surface. Close examination of these ridges at high magnification (Fig 4.41) shows the smooth worn

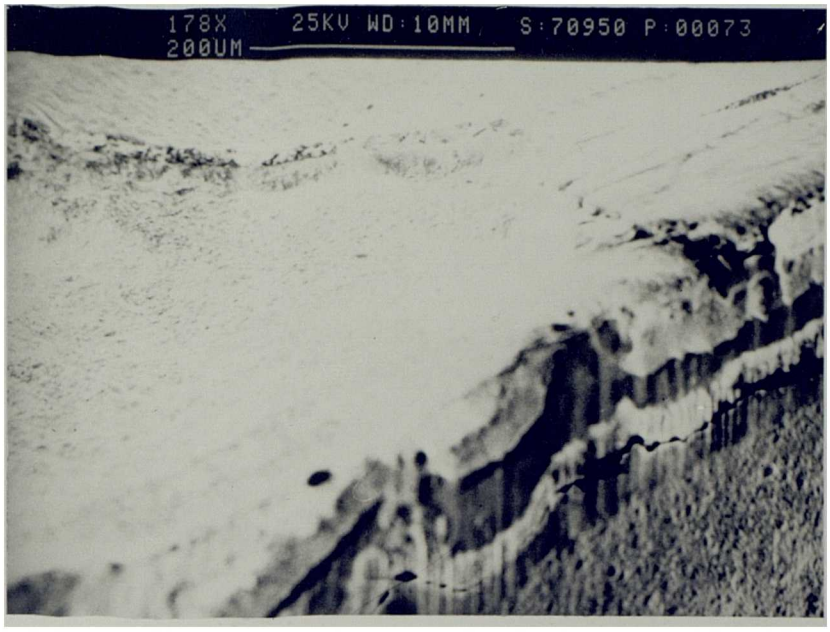

Fig 4.38 Wear on the rake face of coated carbide tool (KC850) as a result of attrition at speed of 75 m/min.

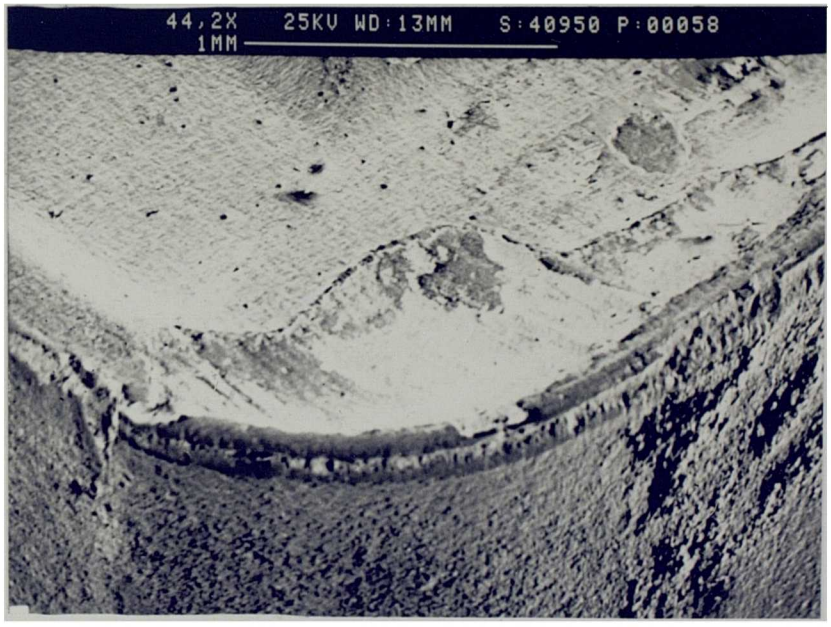

Fig 4.39 Formation of crater on the rake face of coated tool (KC850).

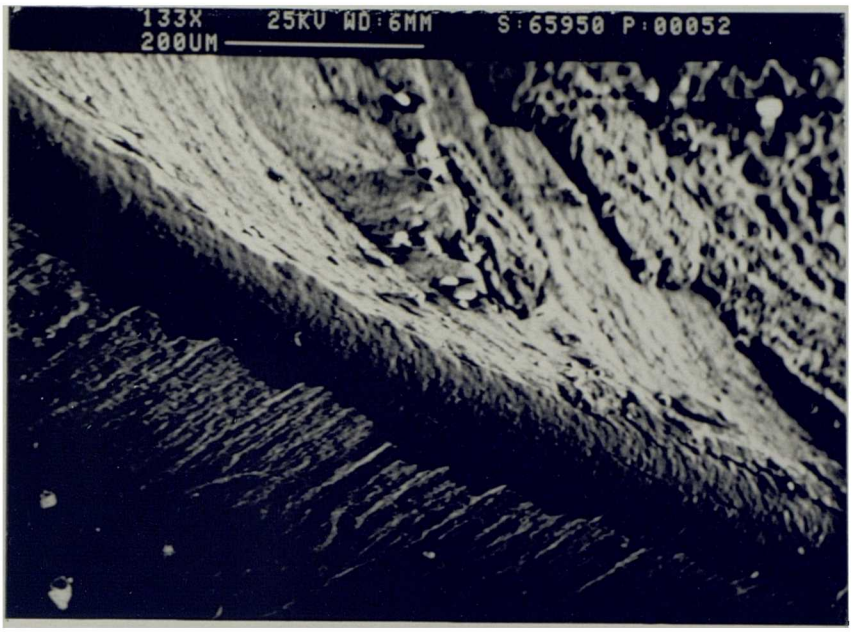

Fig 4.40 PLucking at the rake face, while the cutting edge still intact.

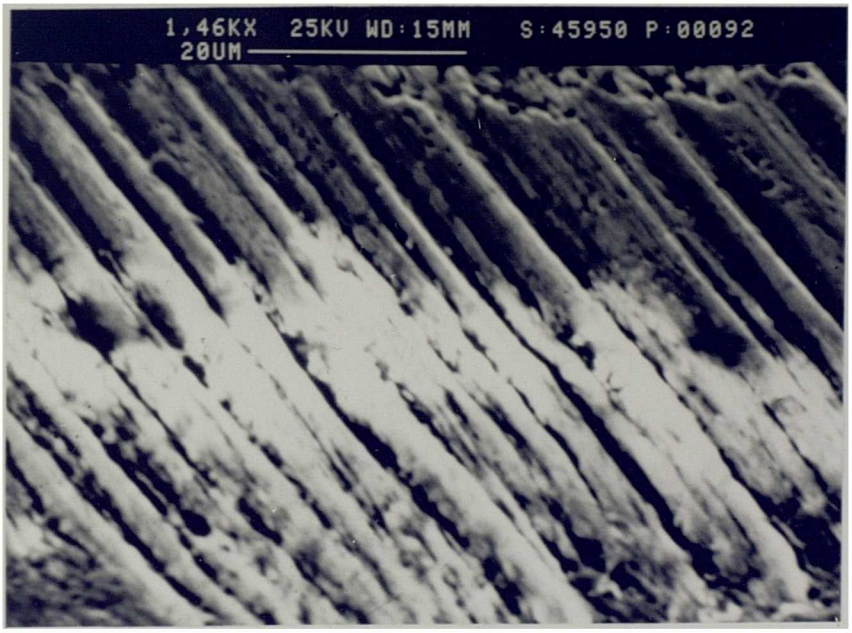

Fig 4.41 Ridges formed on the rake face of KC850 tool.

surface of these ridges. The lighter area of this region indicates exposure of the substrate while the darker area represents the intact TiC layer.

After cutting for a period of 2 minutes, the wear on the flank face occurred at rates comparable with those seen on the coated KC910 inserts. On the flank face blister features were observed. Such features (which were approximately hemispherical in shape) were found to be hollow and were quickly worn through revealing small voids (Fig 4.42). It was surprising to observe that the coating was still firmly attached to the substrate in a few places at the cutting edge, with the original surface topography ie. the 'hills and valleys', still visible (Fig 4.43). Examination of this tool after 6 minutes cutting shows a crater within which there are remains of some metallic surface layers (Fig 4.44). Close examination of this crater at high magnification (Fig 4.45) shows the surface to be smoothly ridged. The pitch of the ridge is approximately 20 microns, and their surface appearance is consistent with a fine scale progressive wear of the carbide substrate. This wear is manufect by parallel scoring in the direction of chip flow. The pitch of the ridges is significant larger than carbide substrate. This is felt to represent evidence for the ridges being produced solely by the movement of workpiece material over the tool substrate, and not by carbide being carried over the tool by the workpiece.

Figure 4.46 shows a magnified view of severe notching at the end of the depth of cut. This figure also shows some tool material being plucked out at the notched region. This notch could be responsible for the rapid deterioration of the surface finish of the machined workpiece.

After cutting at the speed of 150 m/min for 60 seconds all the coated layers were removed from the rake face of the tool. On the flank face the coated layers of TiN and Ti(C,N) were removed leaving the TiC layer exposed (Fig 4.47). This figure shows the regular and smoothly worn surface of flank face, while the rake face

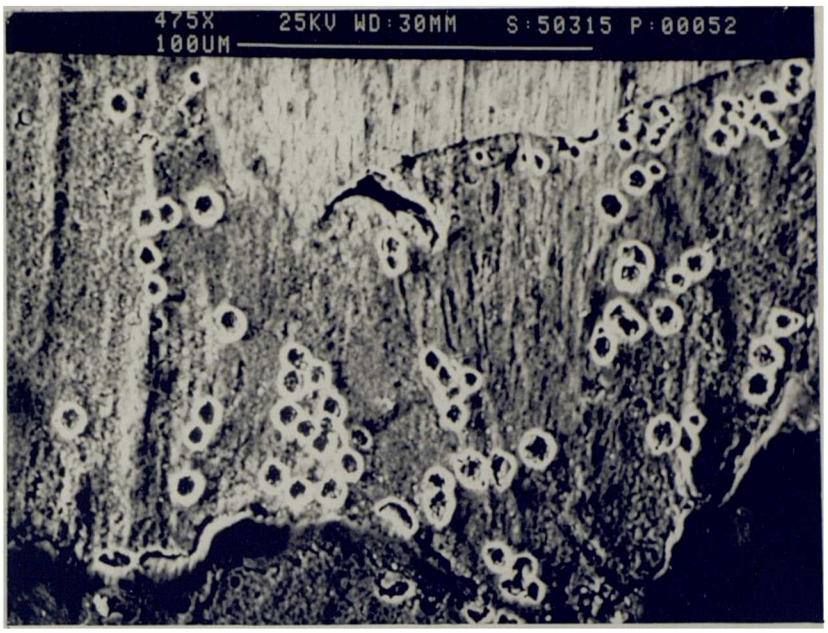

Fig 4.42 Regions of exposed WC particles on the flank face.

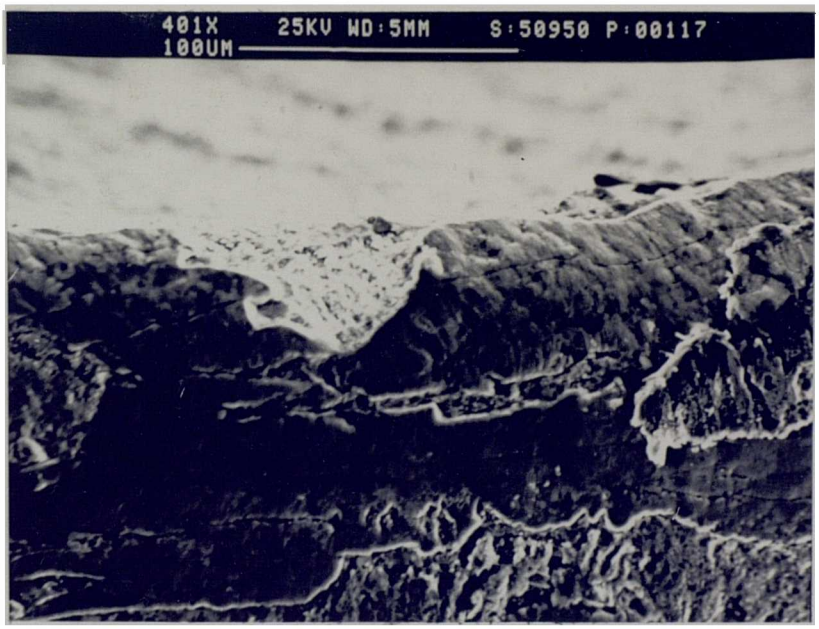

Fig 4.43 Chipping at the periphery of intact coated layers.

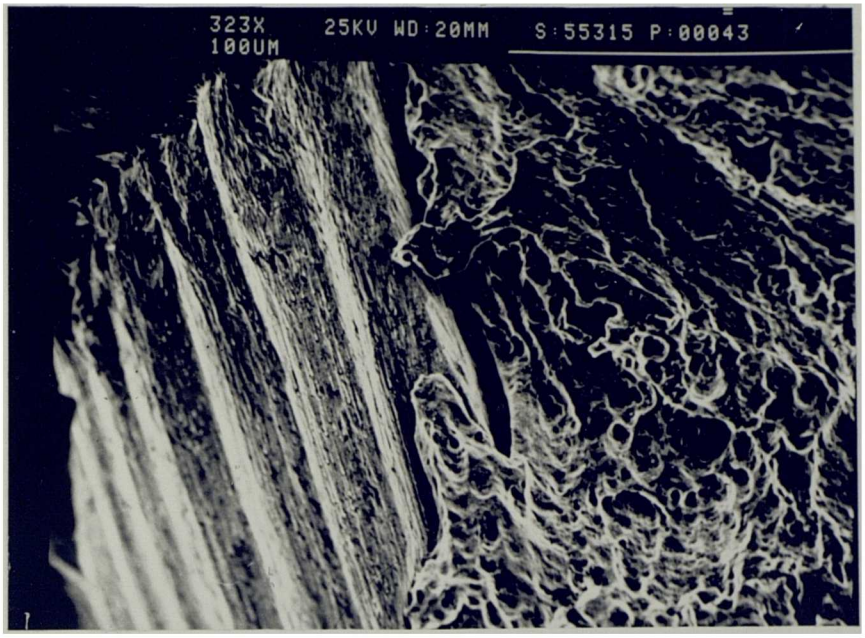

Fig 4.44 View of coated carbide tool (KC850) with smooth rake face crater and remains of adherent metal layer.

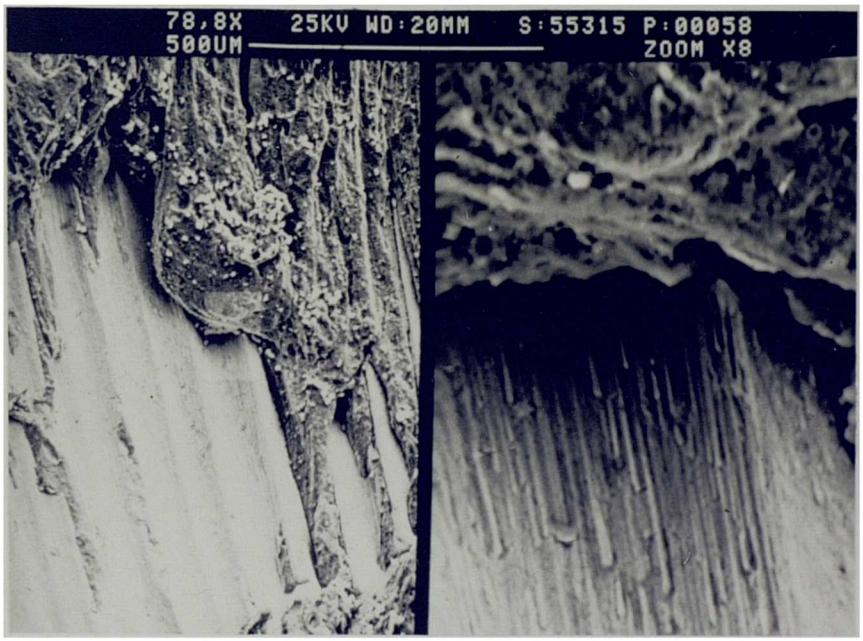

Fig 4.45 Close-up view of rake face crater wear showing smooth ridges with fine scoring in the direction of chip flow.

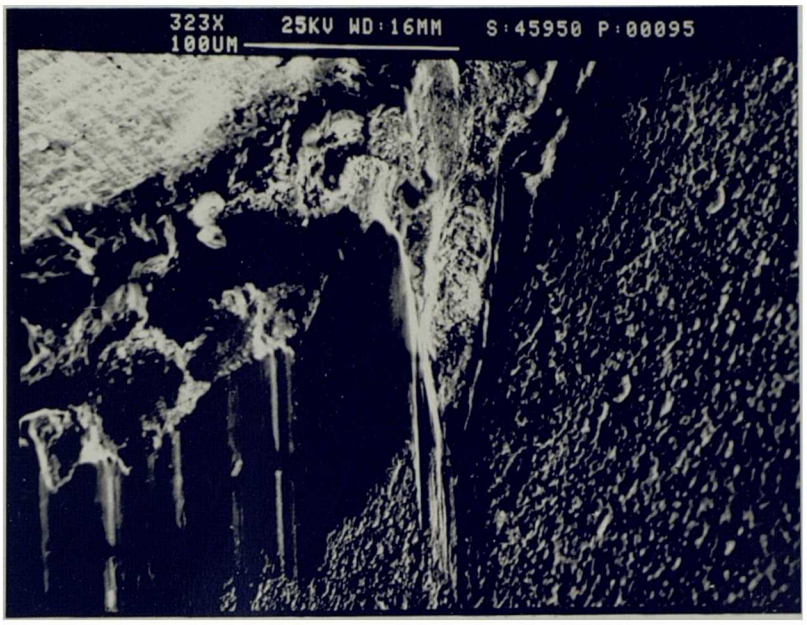

Fig 4.46 Formation of notch wear at the end of depth of cut.

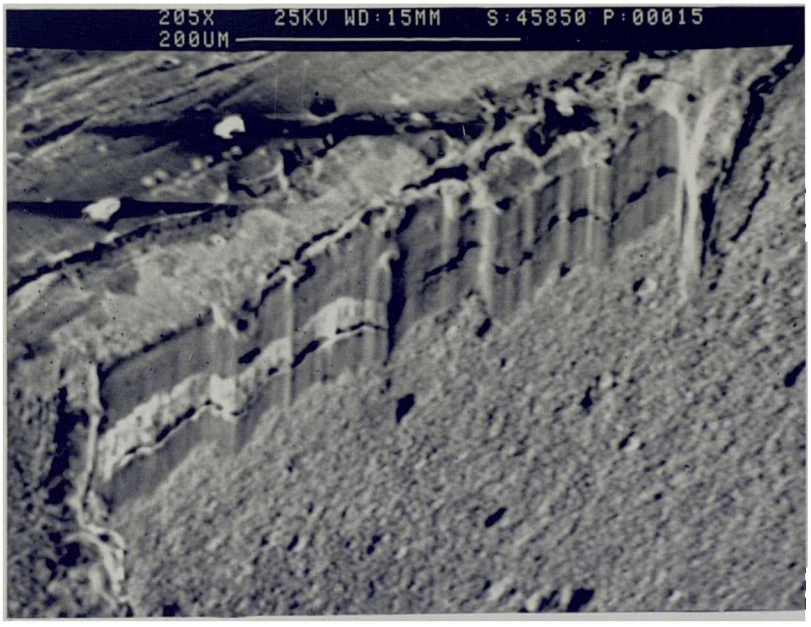

Fig 4.47 Exposed coated layers on the flank face.

shows the formation of a crater which is worn by mechanisms based on attrition. Although evidence of smooth light wear was observed at high magnification, the wear on cutting edge was similar to the previous tool at lower speed (Fig 4.48). This figure shows the coating at the edge still firmly adhering to the substrate, with a large region of exposed substrate (white zone) observable along the adjacent flank land. After 6 minutes cutting, this tool was rapidly worn at both extremities of the depth of cut (regions 'C' & 'D', Fig 4.33). The wear grooves, which were formed during cutting, were found to have been formed by a smooth wear process. However, the wear grooves later widened due to a diffusion/dissolution mechanism. This type of mechanism is clearly visible on the regions of the exposed substrate lying adjacent to main contact area (in the vicinity of the side cutting edge), where a fine surface texture is visible (region 'D'; Fig 4.49). The groove at the outer-most edge shows the similar finely worn surface (Fig 4.50).

After cutting for 30 seconds at a speed of 200 m/min, the tool was severely worn on the cutting edge, whilst the flank and rake experienced a fine smooth wear due to diffusion/dissolution as a result of high temperature operation. Figure 4.51 illustrates a regularly worn surface on the flank land with the absence of all coated layers. Similarly a smooth surface could be observed in the crater formed on the rake face, where numerous fine ridges are running parallel to the direction of chip flow. This worn pattern appears to be a result of a process in which particles from the tool have diffused into the workpiece material and are carried away in the workpiece or swarf as they pass over the tool.

When cutting time was increased to 2 minutes, rapid and severe wear was observed with the nose radius plastically deformed (Fig 4.52). This figure illustrates cracks which are running normal to the direction of the newly formed workpiece surface. Mixed particles (mainly WC and TiC) are seen to have moved down from the flank face away from the cutting edge (Fig 4.53). These large and small

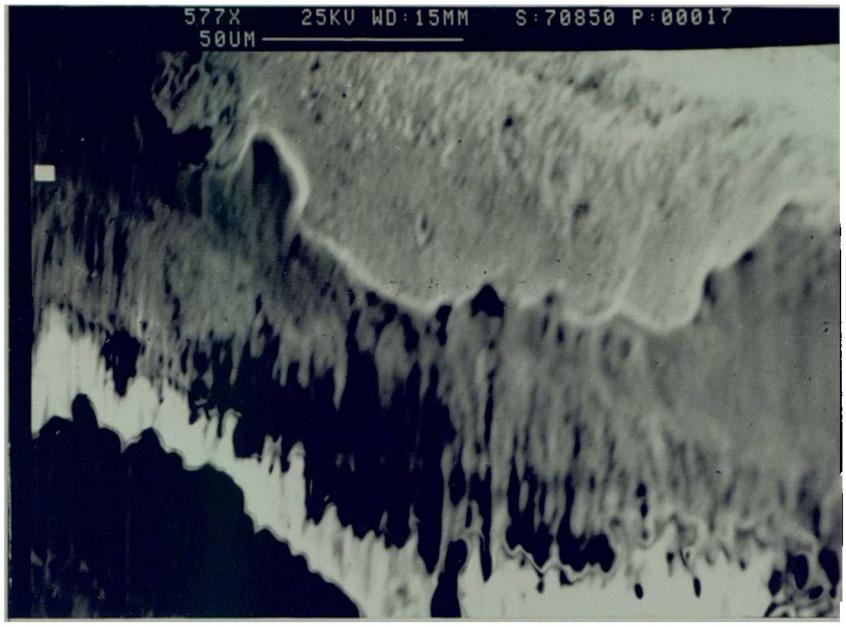

Fig 4.48 **Smooth wear on the flank face of KC850.**

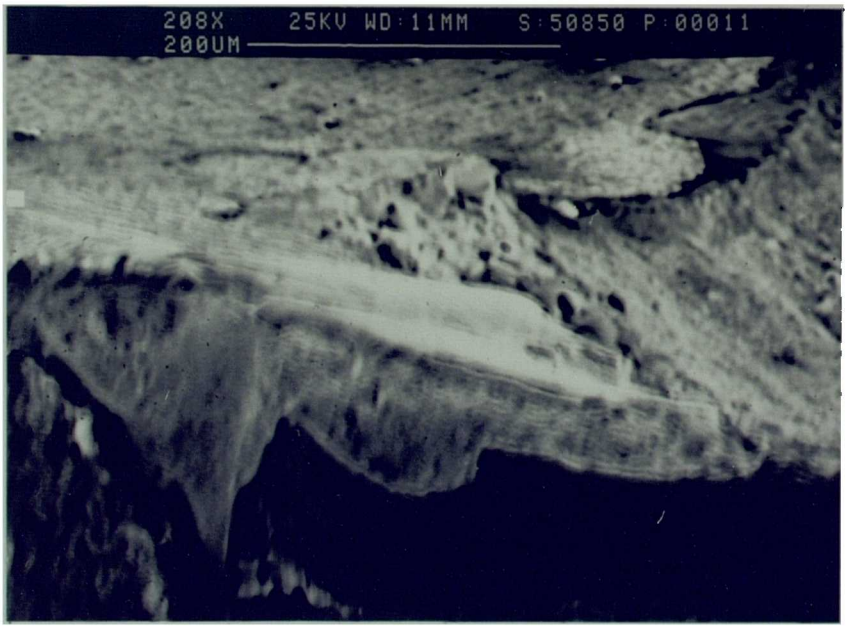

Fig 4.49 **Formation of notch wear at the end of depth of cut.**

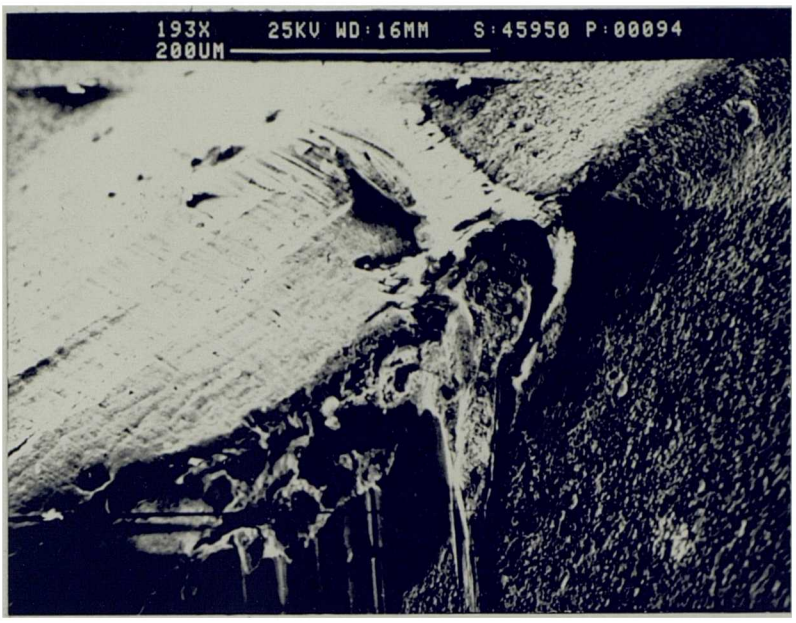

Fig 4.50 **Formation of smooth ridges on the rake face of coated carbide tool (KC850).**

Fig 4.51 **Smoothly worn crater surface by diffusion/dissolution wear.**

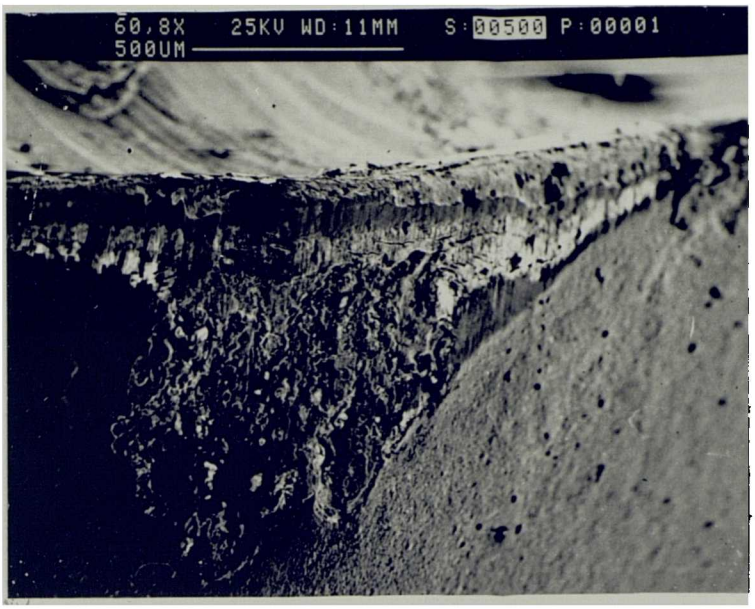

Fig 4.52 Severe wear on the flank face.

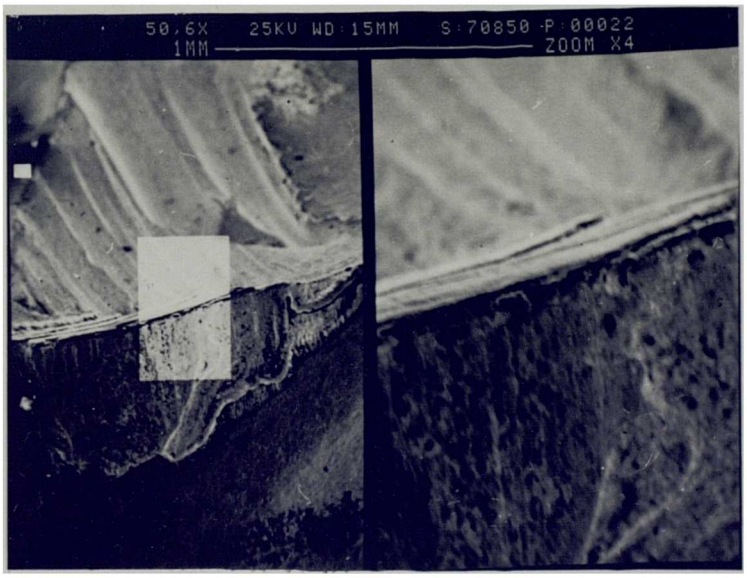

Fig 4.53 Magnified view of ridges formed on the rake face of KC850 tool.

fragments which have been broken and pulled out of the tool would be due to the intermittent action between the flank face and newly cut surface.

Figure 4.54 shows two different types of worn surface on the rake face. The first is surface in which very large fragments of tool coating have been removed in the region at the end of depth of cut, outside the crater. The surface of this area suggests that attrition wear was dominant in this region. The second surface is a classical form of crater wear, where the surface has formed as a result of plucking out particles adhering to the underside of the swarf and then carried away in the chip flow direction. This surface is smoothly worn and ridged.

After 4 minutes machining, the cutting was stopped due to imminent catastrophic failure of the tool and formation of large size notch, at the side cutting edge (Fig 4.55).

4.4.1.3 CUTTING PERFORMANCE OF KC910

After cutting TA 48 for 30 seconds at a speed of 100 m/min, the Al_2O_3 layer on the flank face was removed by a smooth wear process, whilst all the coated layers on the rake face around the cutting edges were removed and dragged along the surface of the crater region (Fig 4.56). Ridges were observed on the undulation formed on the rake face which lay parallel to chip flow direction. At some distance away from the tool edge traces of exposed TiC ridges (ie. the whiter regions) could be detected.

After cutting for 2 minutes the entire Al_2O_3 coating layer on the flank face was removed from a substantial part of the contact zone thus exposing the TiC layer beneath. Both layers were smoothly worn (Fig 4.57 at 'A') on the flank face, yet the mixed coating of Al_2O_3/TiC is still present on the cutting edge (Fig 4.57 at 'B'). The

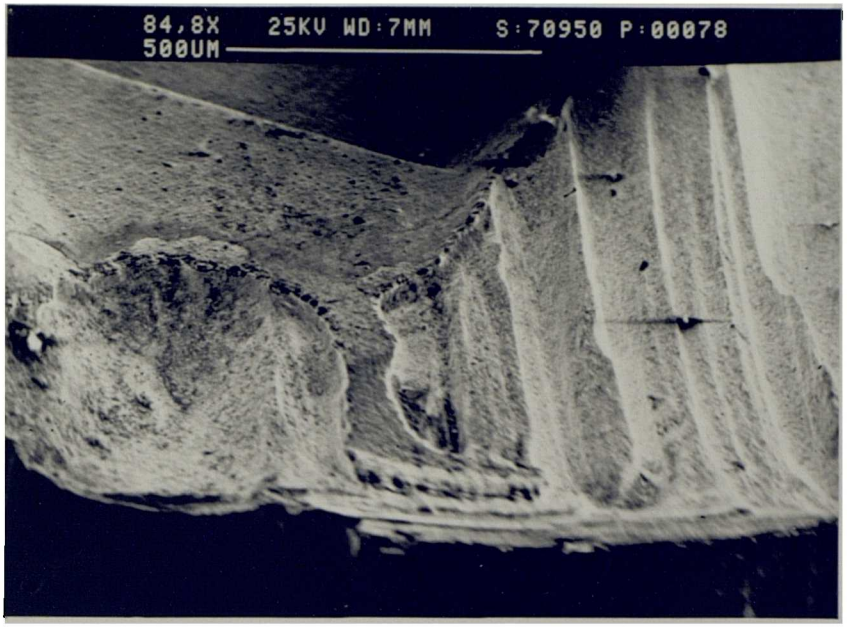

Fig 4.54 Formation of crater on the rake face worn by attrition.

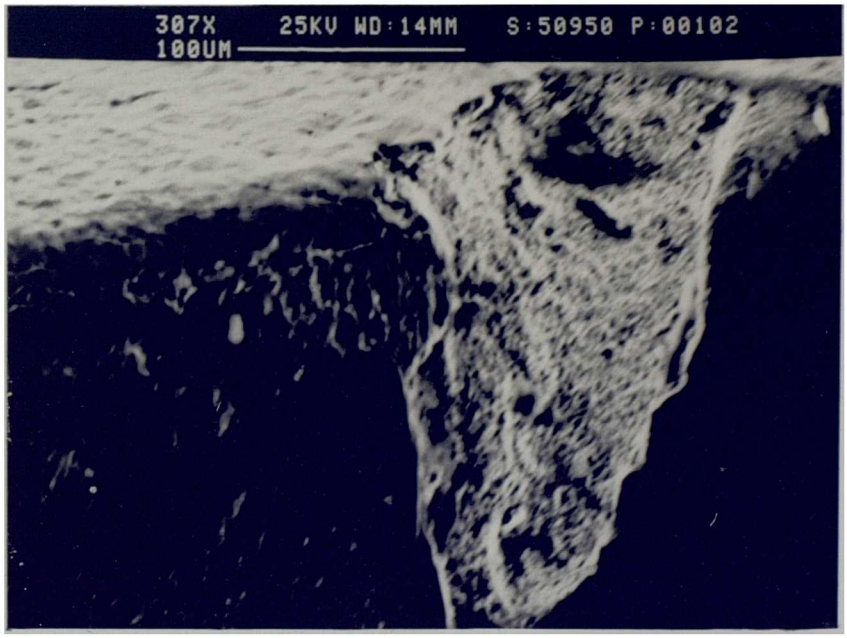

Fig 4.55 Notch surface wear indication of diffusion/attrition.

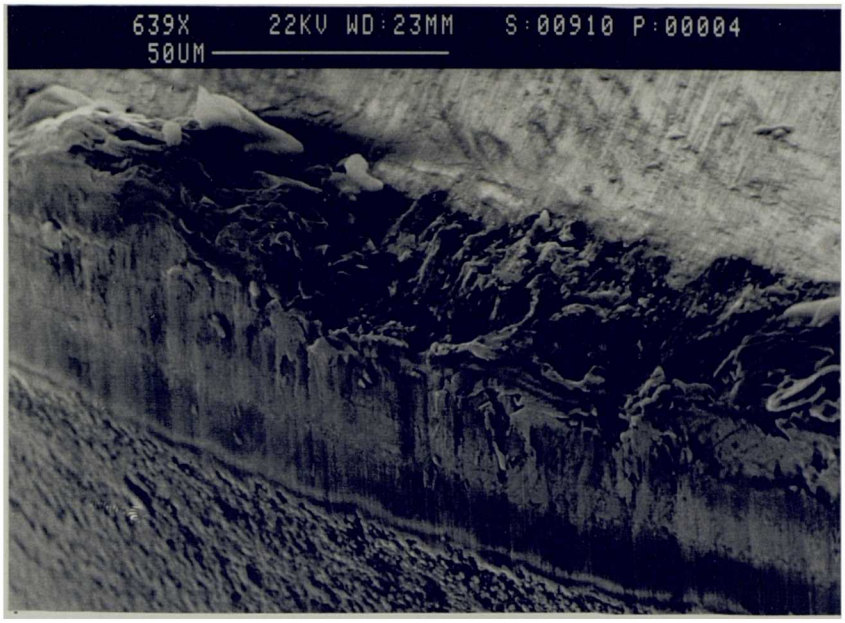

Fig 4.56 Smoothly worn flank face of KC910 tool.

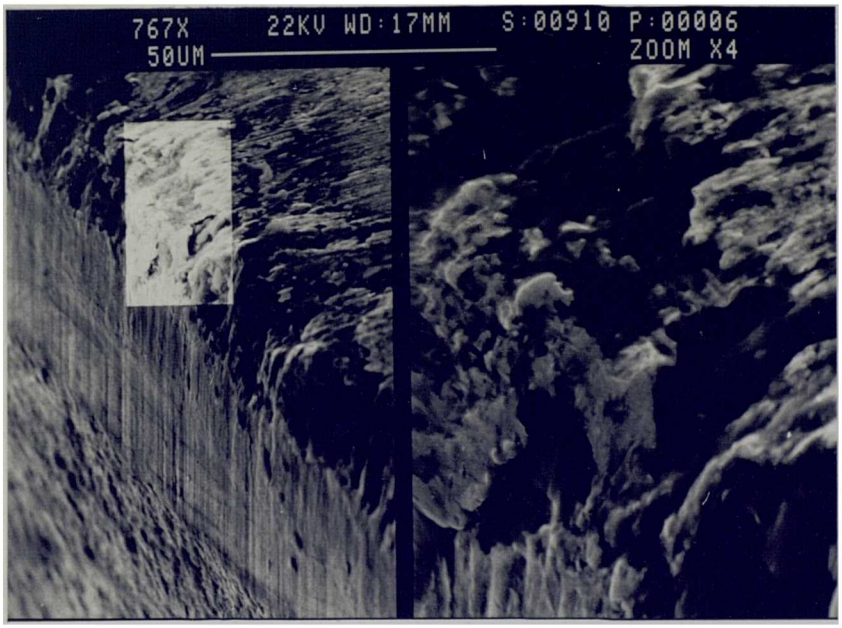

Fig 4.57 Removal of coated layers from the cutting edge.

exposed TiC coating layer on the flank face is still attached to the substrate, even though slight deformation of the tool edge has occurred.

After cutting for 5 minutes the entire cutting edge experienced severe wear becoming very blunt. Figure 4.58 shows the severity of this damage on the rake face. As the cutting time was extended to 7 minutes, the substrate which had previously been exposed showed a fine smooth surface with WC grains on the rake surface surrounding a cluster of tool piece. A large piece of tool material has been removed from the rake face of the tool near the cutting edge (Fig 4.59). The tool particles were then dragged along the rest of the rake face where the contact is made with the chip during the cutting operation. The cutting was then continued for a further 1 minute, during which time the crater surface developed a rough surface in association with cracks which ran parallel to the tool edge. Typical of these cracks is the one shown in Figure 4.60.

After machining for 9 minutes the trend towards notch wear became far more noticeable and as a result, the flank face was found to be extensively deformed and the tool failed catastrophically (Fig 4.61). This notch has appeared on the side cutting edge of zone 'C' (Fig 4.33). Within the surface of the smoothly worn notch, the cobalt phases and protruding mixed carbide grains were also seen. Thus, the worn tool rake and flank surfaces were consistent with those which are generally accepted to be formed due to atomic diffusion of the WC and cobalt phases (2, 143).

Upon increasing the speed to 150 m/min the wear of the tool became visible after machining for only 30 seconds. The wear which developed on the rake face caused the surface hills to become smoothly worn, whilst the valley regions in this zone were slightly worn. Examination of wear zones after cutting with the same tool for a further 30 seconds revealed that both hill and valley were worn through, and

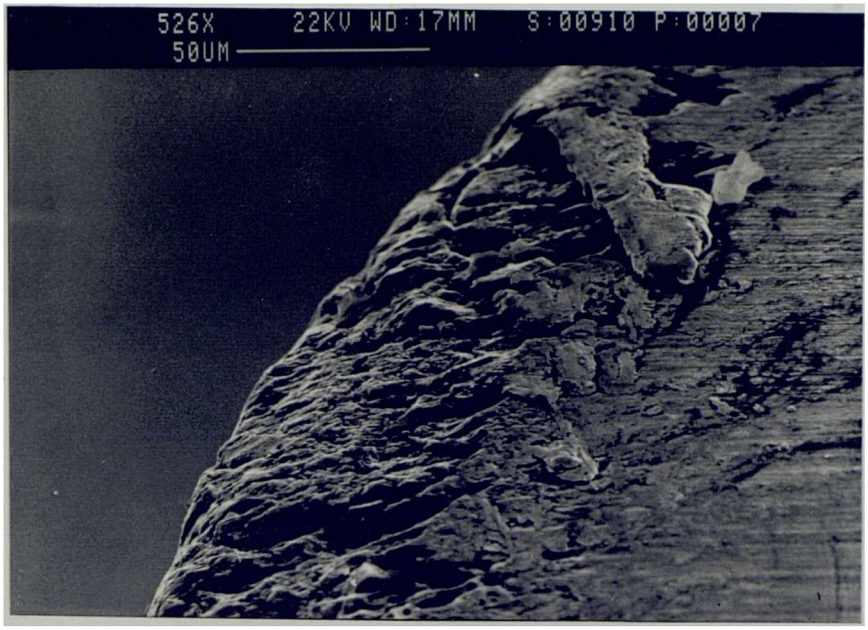

Fig 4.58 Plucking about to take place on the rake face of carbide coated tool.

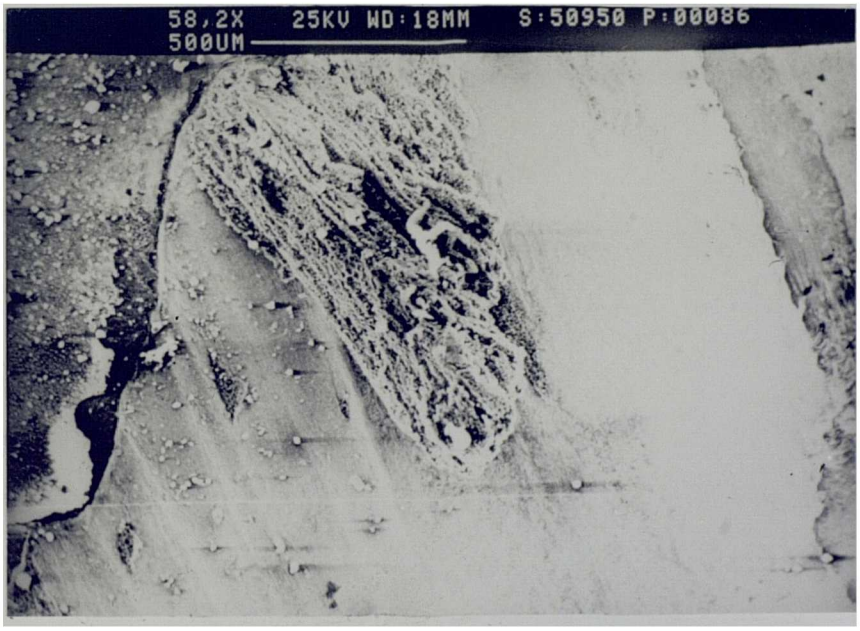

Fig 4.59 Crater smoothly worn with the remains of adherent metal layer.

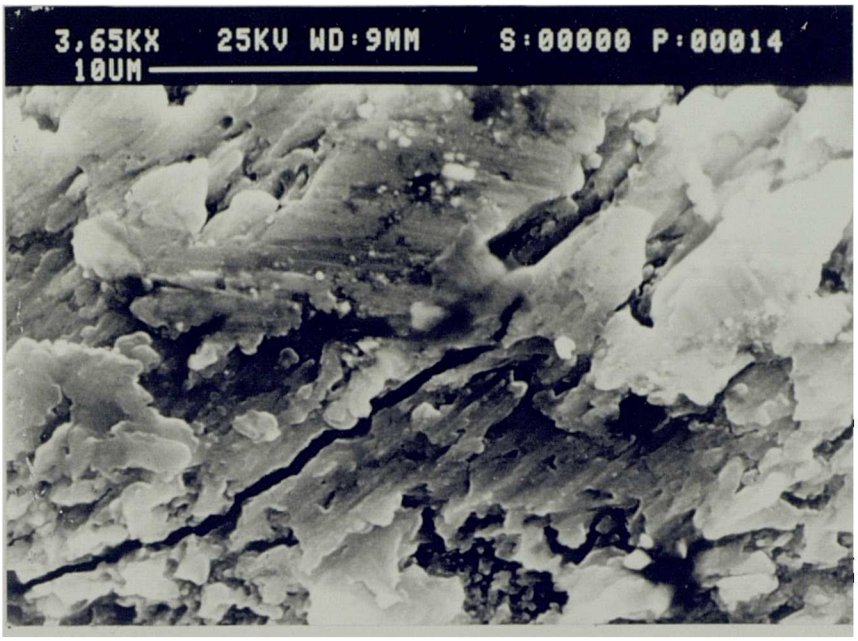

Fig 4.60 Crack on the worn rake face of coated carbide tool (KC910).

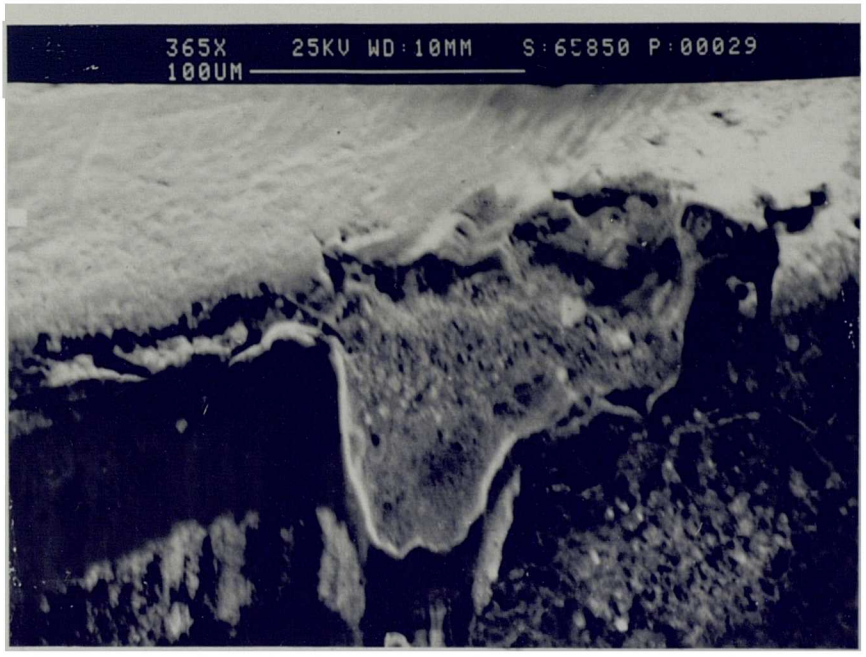

Fig 4.61 Notch wear produced on the flank face KC910.

plucking out of the coated layers at the tool edge had taken place (Fig 4.62). Furthermore, the exposed substrate could easily be seen in certain regions.

On cutting with this tool for a further 1 minute the flank face was smoothly worn and the coated layers were gradually worn through on the flank face leaving behind the exposed substrate (Fig 4.63). This photograph shows severe and irregular wear on the rake face, especially near the cutting edge. Also seen is a piece of the coating (A) which has been plucked out and moved towards the back of rake face, in the area where the crater formation can be distinguished. It was notable that, within a limited area along the rake face, the coating has been practically unworn and the original topography is still intact.

Upon examining this region of the rake face of the tool after cutting for a further 4 minutes, the crater was seen to be smoothly worn (probably as a result of dissolution) compared to that of relatively unevenly worn flank land (Fig 4.64). After the total machining time was increased to 7 minutes, it was found that the shape of the tool edge was further deformed and the size of the wear notch (Fig 4.65) at the side cutting edge was far more pronounced than with the similar tool at lower speed.

As the cutting speed increased to 200 m/min, so did the rate of tool wear. The coating was removed and nose deformation and the flank wear became measurable after 30 seconds accompanied by an increase in crater size (Fig 4.66), relatively higher than the one noticed previously for the same period cutting time at the lower speed (Fig 4.56). Wear increased when cutting was continued for another 30 seconds, and a close examination of the crater region indicated that numerous ridges existed running parallel to the chip flow direction. Although the worn surfaces on both sides of the crater rake face appeared similar, the region adjacent to the leading edge experienced severe wear (Fig 4.67). After increasing the total cutting time to 2 minutes it was not surprising to observe that the tool became heavily worn in several

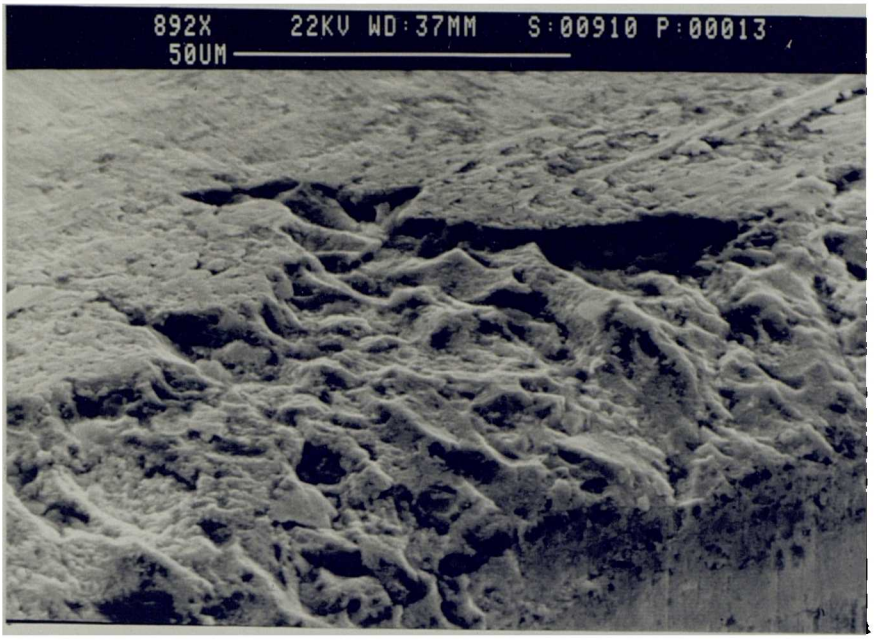

Fig 4.62 Removal of coated layers from the rake face surface.

Fig 4.63 Smoothly worn flank face with plucking at the rake face.

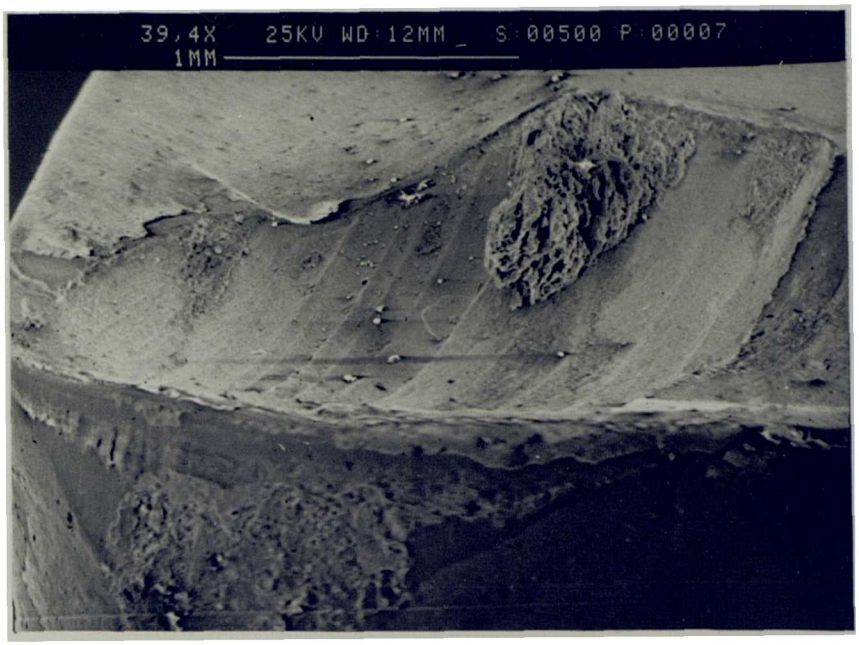

Fig 4.64 Smoothly worn crater surface by diffusion/dissolution with remains of adherent metallic layer.

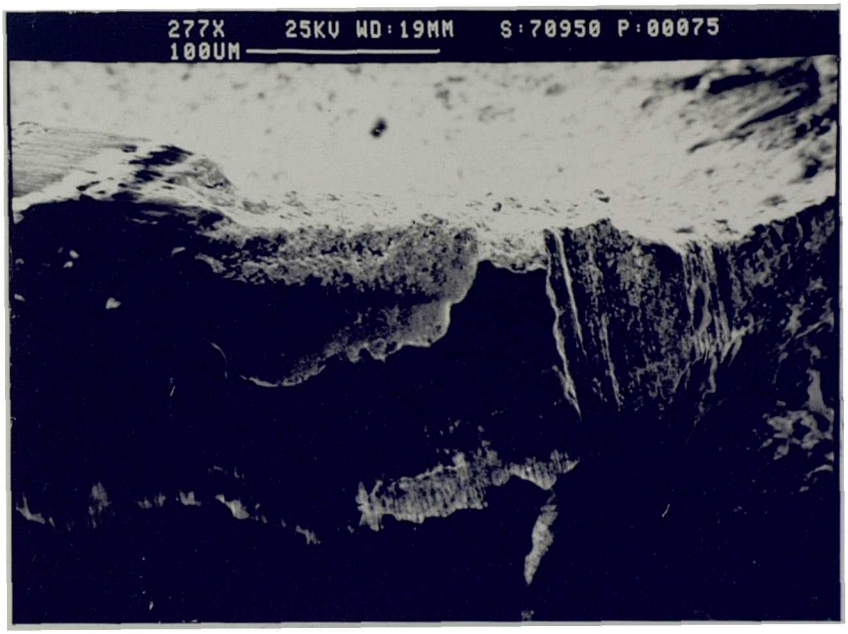

Fig 4.65 Enlarged view of wear at the end of the depth of cut.

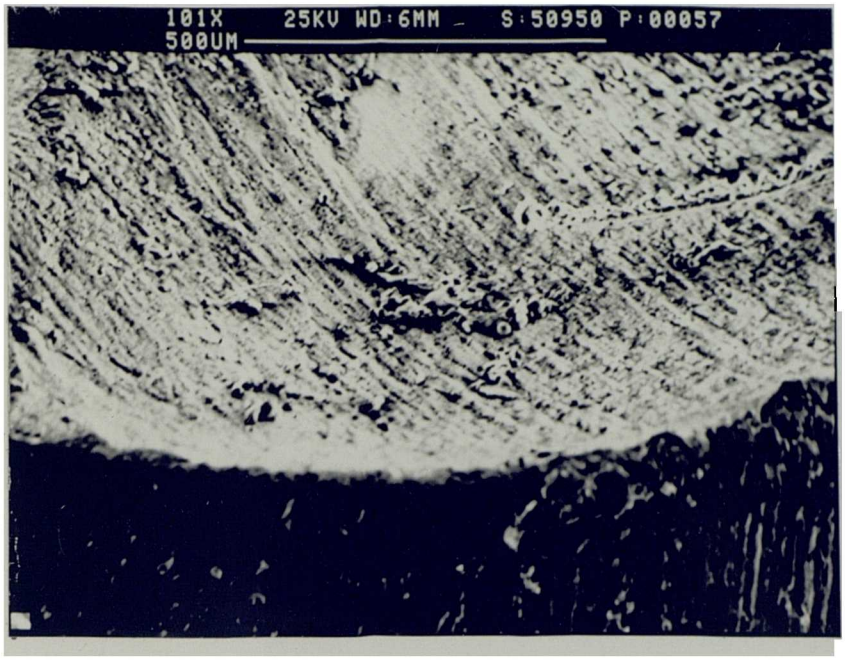

Fig 4.66 A severely worn crater surface on the rake face of KC910 carbide insert.

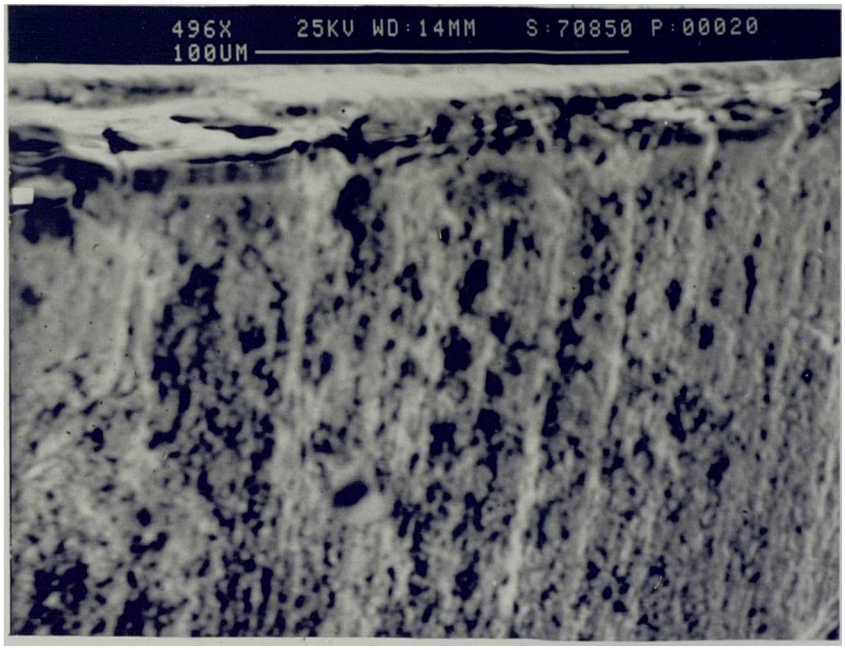

Fig 4.67 A worn flank face of KC910 carbide insert after machining for 30 secs at speed of 200 m/min.

places in the crater zone with elongated fragmentation on the rake face in the direction of chip flow (Fig 4.68). An enlarged crater was observed on the rake face of the tool after cutting for a further 3 minutes. A magnified view of the crater showed an area which had smoothly worn as the result of diffusion wear at high temperatures (Fig 4.69). From this micrograph it can be seen that a large piece of tool debris has been removed from the rake face, ready to be swept away by the next cut. The notch at the side cutting edge showed an increase in size with prolonged cutting time (total of 4 minutes). Figure 4.70 shows the region in which tool material has been plucked out from the notch zone. The exposed substrate within the wear notch revealed the mixed crystal phase which stood out prominently on the notch surface. An enlarged view of this area is shown in Figure 4.71.

After cutting TA48 with KC910 at a speed of 250 m/min, the mechanism of wear and the nature of the worn surface were directly comparable with those observed at the lower cutting speeds but the rate of wear accelerated. Figure 4.72 shows wear on the flank face and particularly noticable are the numerous voids produced on the substrate of the tool. At a point such as 'A' in this figure it is apparent that a void is about to be produced. Figure 4.73, which should be compared with Figure 4.68, illustrates smooth diffusional wear on the rake face together with firmly adherent workpiece material.

4.4.1.4 CUTTING PERFORMANCE OF K68

At the speed of 50 m/min after 6 minutes, an uneven wear pattern was observed on the flank face (as a result of a increase in cutting forces), which then led to the sudden failure of the tool by fracture as cutting continued for further 1 minute. Figure 4.74 shows a crack produced under these conditions. Fragments of the tool,

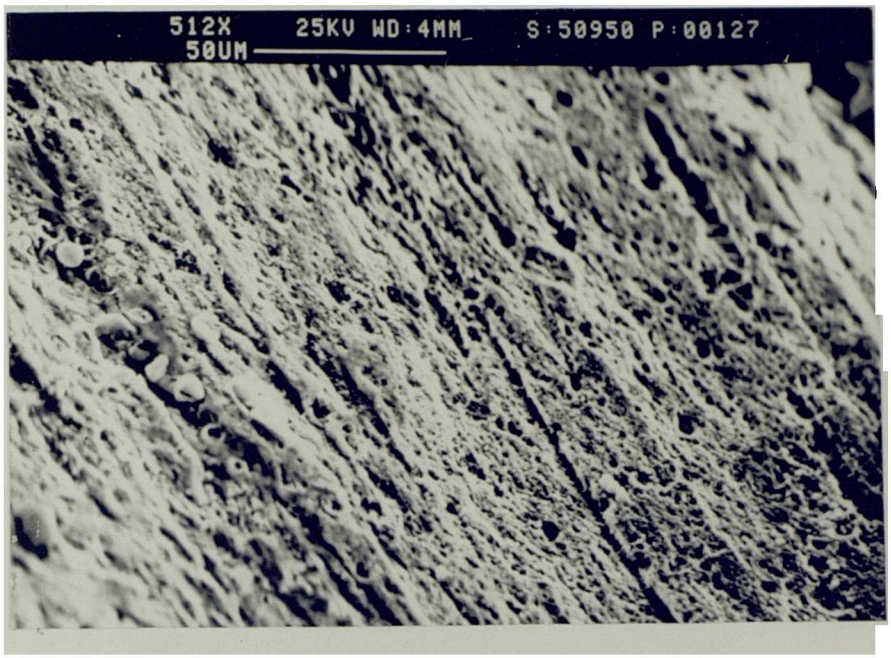

Fig 4.68 Formation of grooves on the rake face running parallel to chip flow direction.

Fig 4.69 Smoothly worn rake face with evidence of plucking.

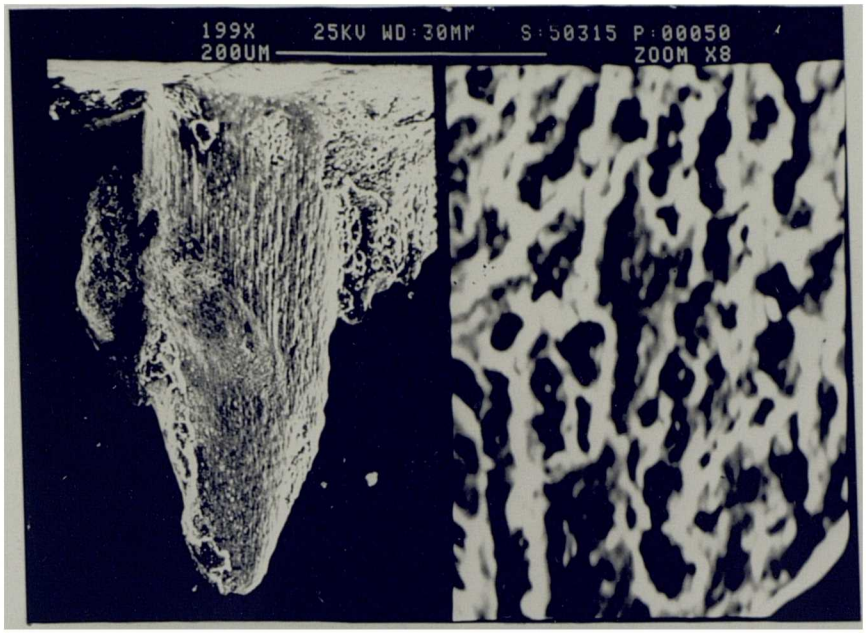

Fig 4.70 Enlarged section of notch wear on the flank face of the KC910 insert.

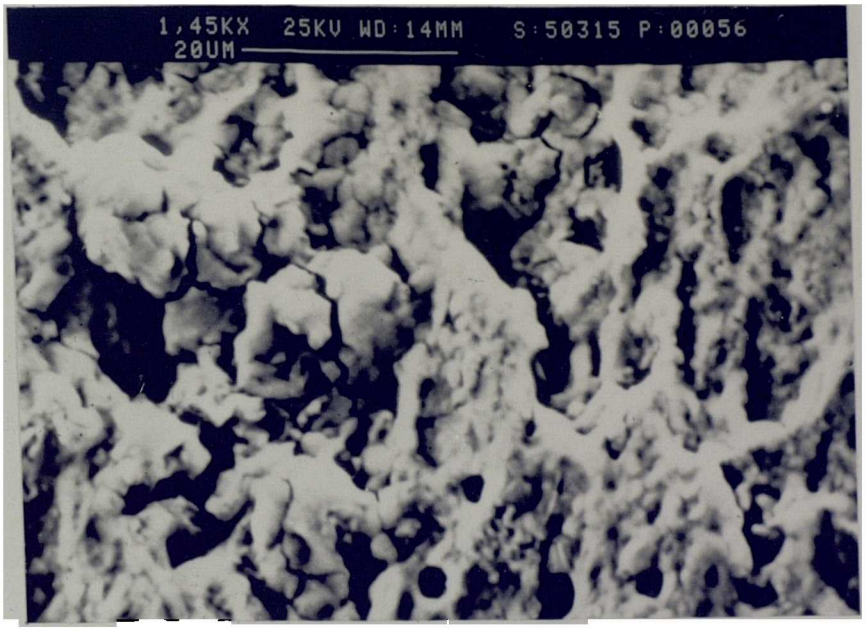

Fig 4.71 Enlarged view of smoothly notch wear surface.

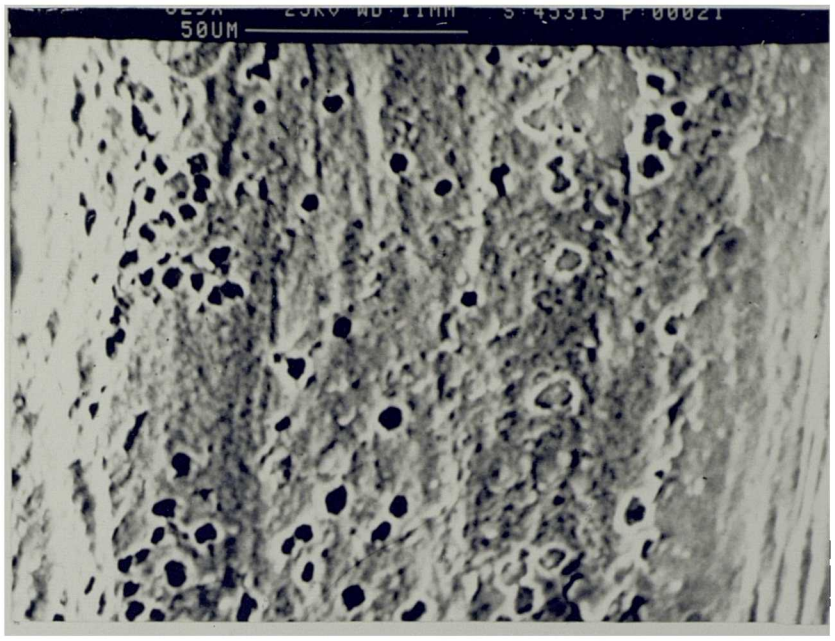

Fig 4.72 Appearance of viods on the flank face of KC910 insert machining at high speed.

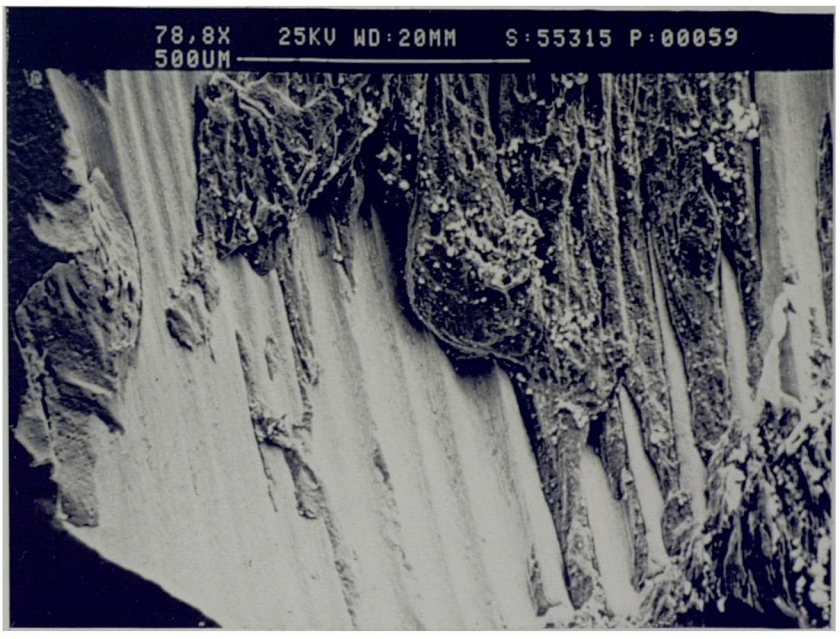

Fig 4.73 View of KC910 carbide insert with smooth ridged crater surface & remains of adherent metal layer.

plucked out during cutting, were seen towards the bottom of the worn region on the flank face (ie. 'A' on Fig 4.74).

Figure 4.75 shows the K68 tool after 4 minutes cutting at the speed of 75 m/min, showing the flank face surface has worn unevenly developing equal sized grooves. The light coloured particles are WC and have been dragged away off the cutting edge.

As the cutting time increased for a further 4 minutes, the flank face was severely worn. At this point the tool life was terminated as the rake face crater intersected with the grooves formed at the cutting edge. By this time the tool began to plastically deform and chipping near the tool edge, at the nose radius, took place (Fig 4.76).

In Figure 4.77 grooves or ridges can be seen on the worn flank face and holes are apparent in the zone close to the grooves where the WC particles were plucked out due to removal of either microscopic grains or aggregates of them. Severe plucking out has occurred on the nose radius resulting in several ridges running away from the cutting edge. The nature of this wear surface is consistent with a high level of adhesion and partial seizure.

A significant crater was observed on the rake face of the tool at a speed of 100 m/min after machining for 4 minutes. A considerable amount of the workpiece material was firmly attached to both the crater and flank wear lands. In addition, the bottom of the crater is grooved presumably by plucked out tool particles as they were swept away in the formation of the chip. Chipping may have taken place as a result of K68 hard tool particles which were plucked out and moved into the tool/chip interface. Figure 4.78 illustrates typical removal of hard particles into the worn areas at the bottom of the crater zone.

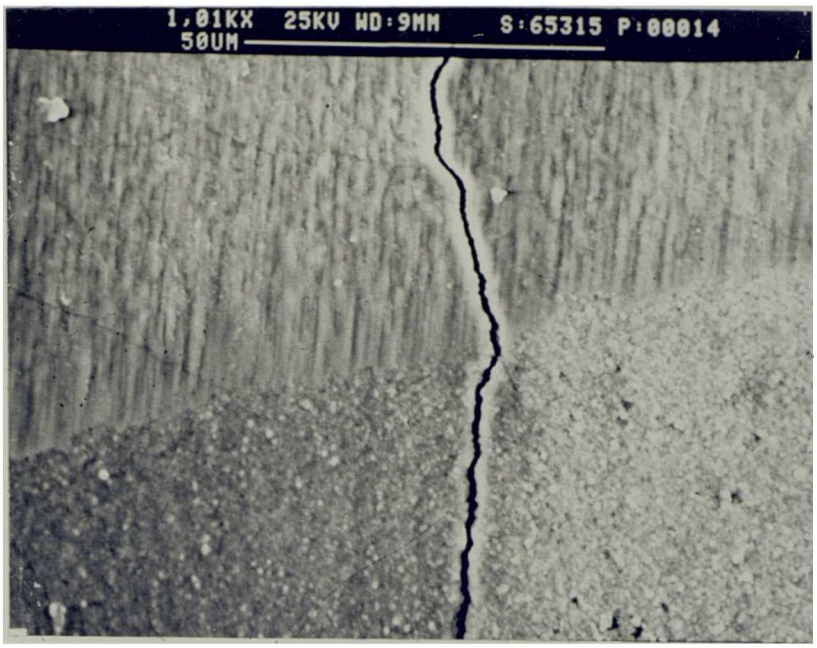

Fig 4.74 Crack on the worn flank face of K68 after cutting at speed of 50 m/min. Note that the cutting edge is at the top of the micrograph.

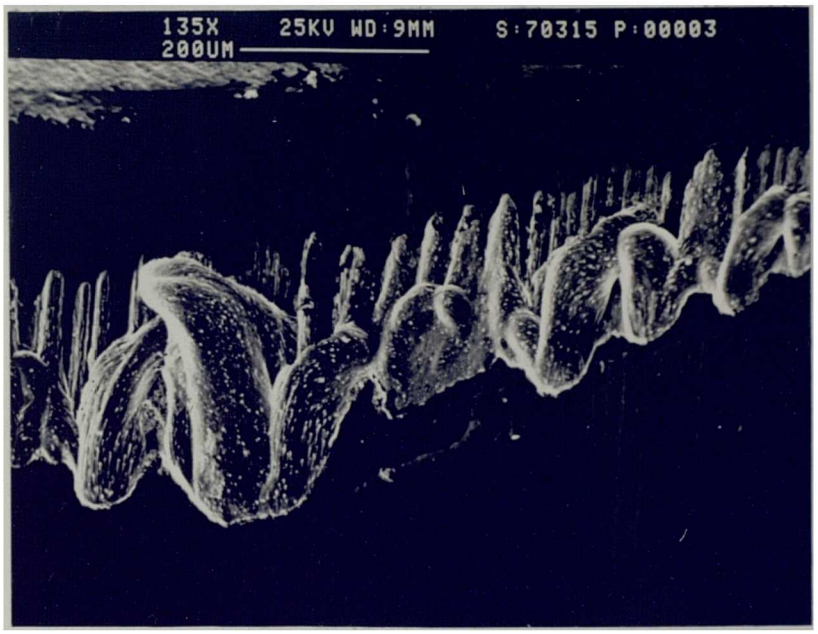

Fig 4.75 Showing WC particles detached from the cutting edge on to the flank face.

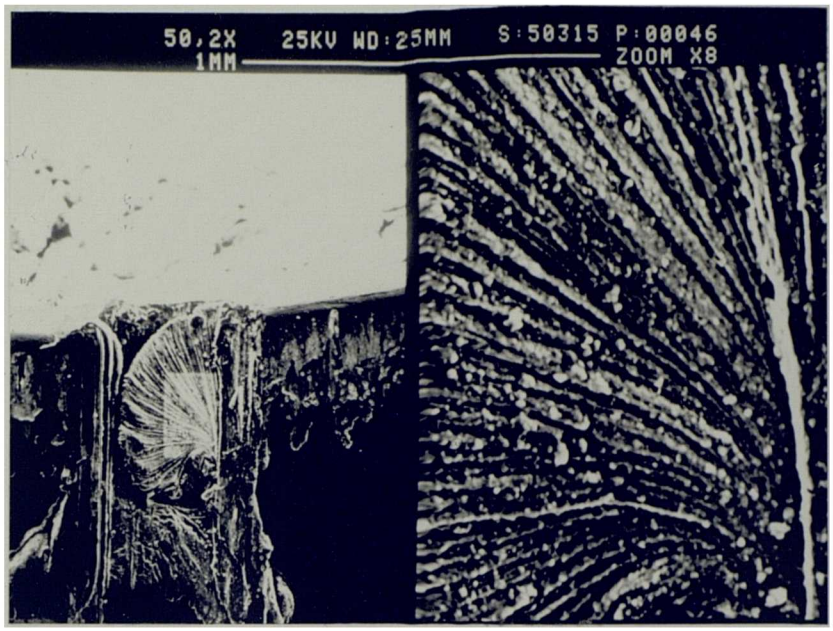

Fig 4.76 Enlarged section view of flank face wear.

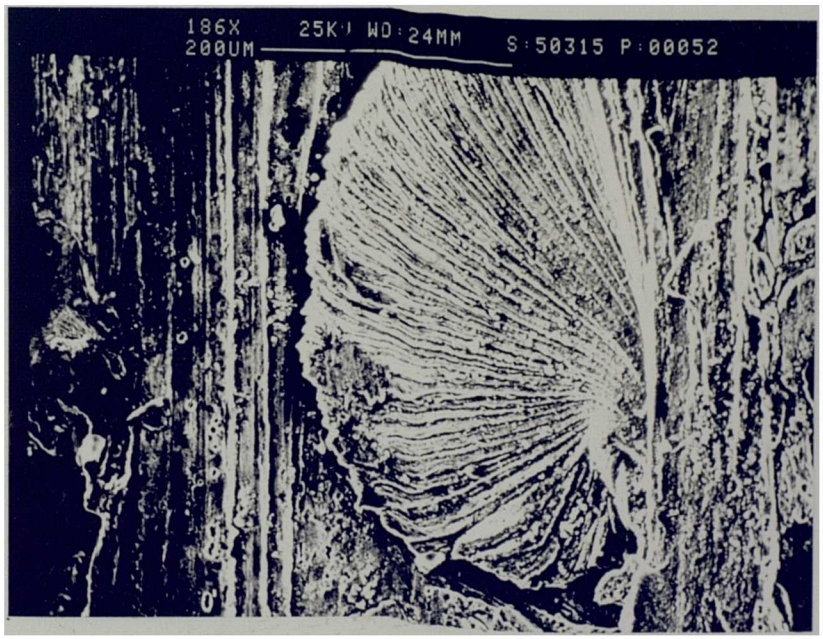

Fig 4.77 Plucking off microscopic particles and formation of ridges on the flank face.

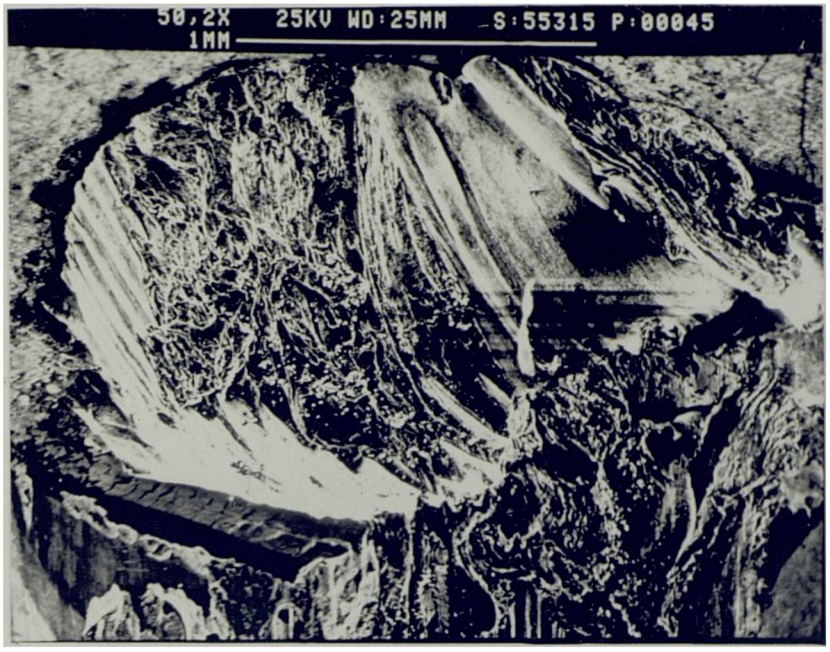

Fig 4.78a Crater surface smoothly worn as a result of diffusion/dissolution wear.

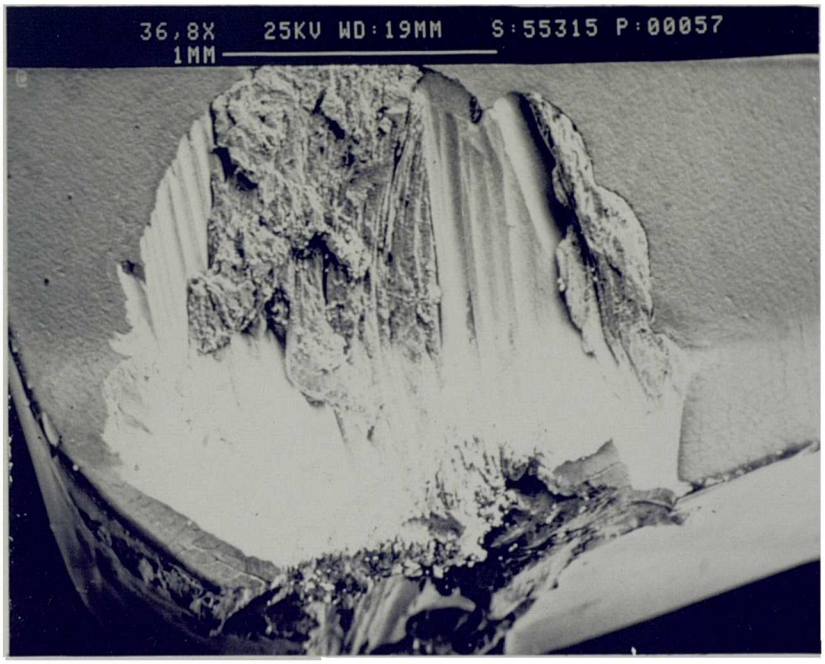

Fig 4.78b General view of tool wear with evidence of plucking.

The worn rake face of K68 after machining at the speed of 100 m/min for a further 2 minutes was not significantly different to Figure 4.78a, but here (Fig 4.78b) the worn rake face has a typical plucked appearance and a few clusters of tool particles standing prominently ready to be plucked out are evident. The plucked out particles have gathered at the crater formed around the tool nose from where they descend through the notch via the tool nose into the interface between the tool and work material.

As the cutting speed increased to 125 m/min for 4 minutes, so did the flank wear and the extent of edge deformation. In addition, pronounced notching wear became evident. Figure 4.79 shows this effect and also evidence of tool particles moving out of the plucked zone on the flank face and into the rake face, with signs of severe deformation and wear. When the cutting time was increased by a further 1 minute the rate of wear also increased rapidly (Fig 4.80). Both the rake crater and the flank wear land were then rapidly developed and grooves were produced at the both extremities of the depth of the cut (Figs 4.81 & 4.82). These figures show the cutting edge intact which suggests that the chip formed some distance away from the cutting edge. High magnification of the notched wear of Figure 4.80 revealed the surface appears to have be worn by a mechanism of diffusion/dissolution (Fig 4.83).

Under this condition, particularly smooth crater wear occurred on the rake face at the cutting edge of the uncoated carbide tool (Fig 4.84). Figure 4.84 is an enlarged view of the crater showing the smooth wear on the rake face connecting the flank face to form a joint where the crater meets the wear notch. The smoothly worn surfaces are the result of dissolution and diffusion of the tool material into the workpiece material.

An enlarged view of the rake face of the K68 tool at the cutting speed of 150 m/min after 4 minutes shows loosely bound tool particles which are sandwiched

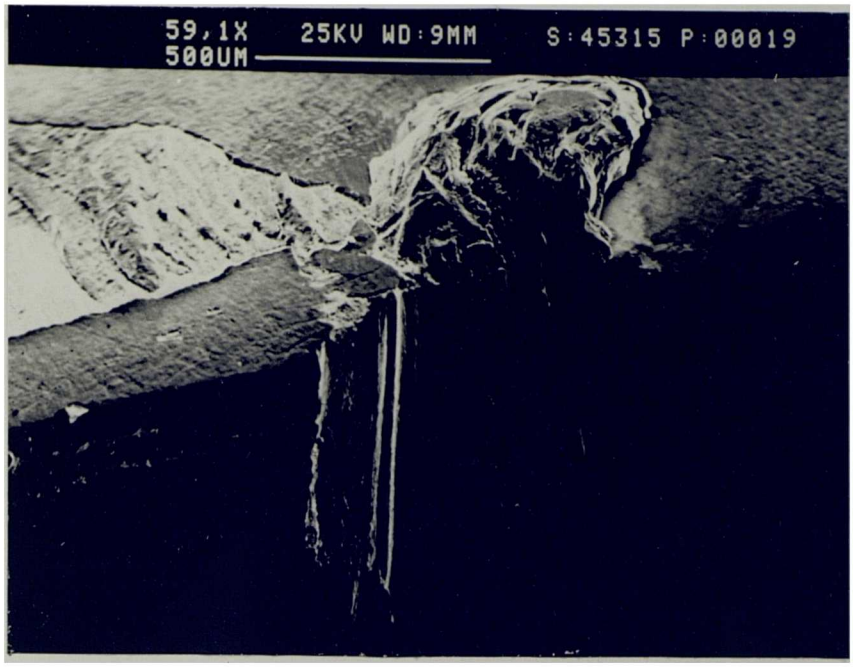

Fig 4.79 Development notch wear at clearance face with chipping at the cutting edge.

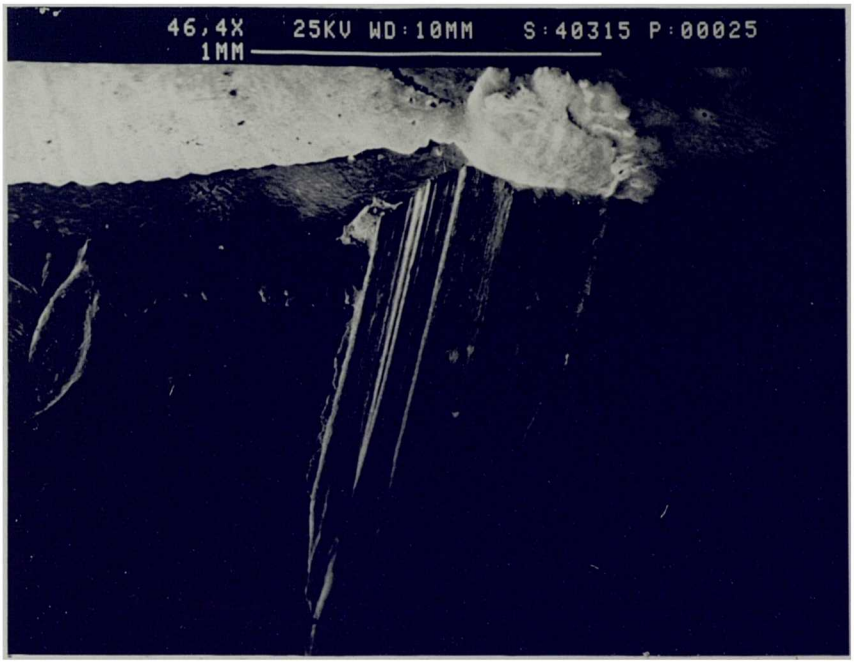

Fig 4.80 Smoothly worn surface ridges within the notch.

Fig 4.81 Development of notchs at the both extremities of the depth of cut on the flank face.

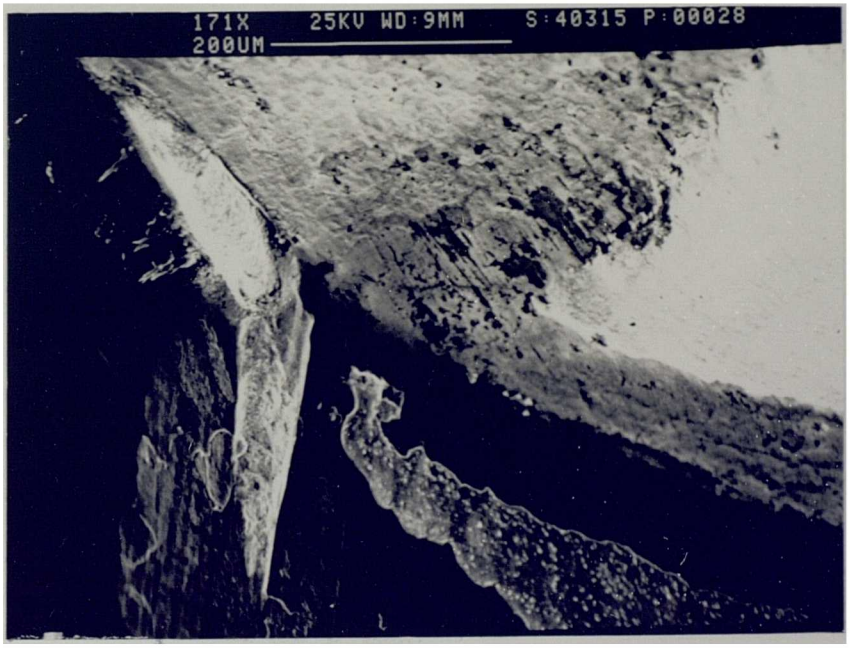

Fig 4.82 Formation of notch wear at the end of the depth of cut with evidence of plucking of microscopic tool particles on the flank face.

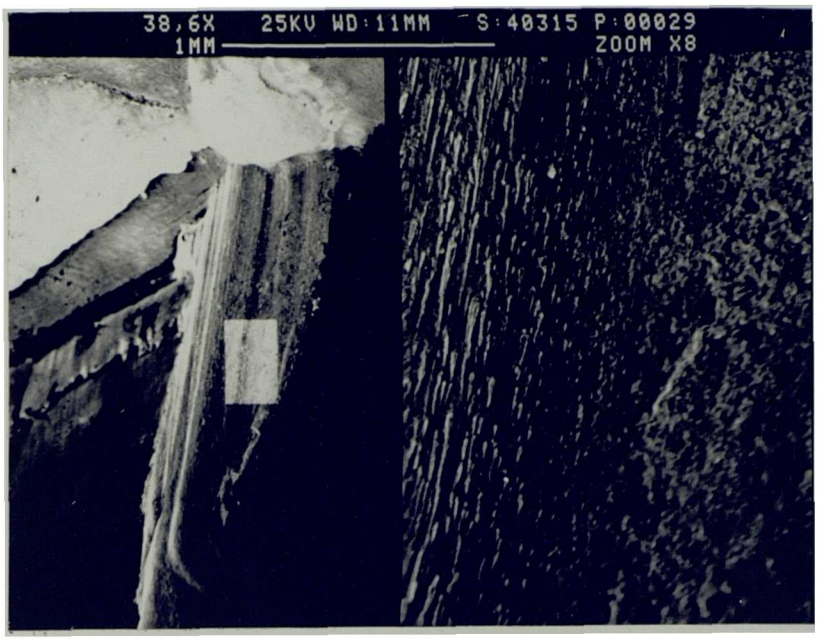

Fig 4.83 Enlarged view of smoothly worn of notch surface.

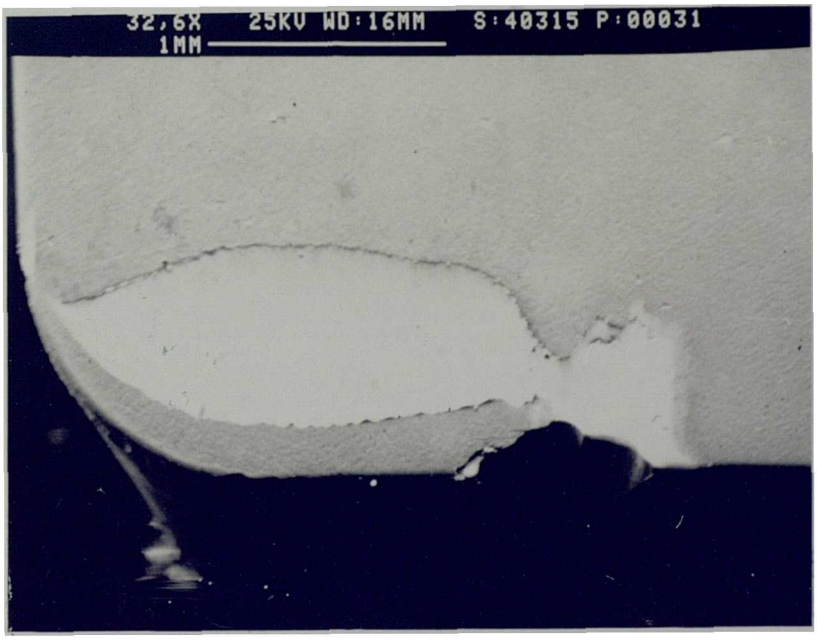

Fig 4.84 Smoothly worn crater surface evidence of diffusion/dissolution wear.

between the tool rake face and fast-moving swarf. These particles mostly stick at the under side of the chip surface and are swept along the rest of the rake face. They remain in contact with the swarf during the cutting until deposited at the trailing edge of the crater (Fig 4.85). This type of wear is accelerated by the high temperatures which are generated during high speed machining. Further machining with this tool could lead to enlargement of the crater as the trailing edge breaks down further. The premature failure of the tool under these conditions may be the reason for the poor surface finish which has been recorded at high speed (Figs 4.160 and 4.161).

As the cutting time was increased by further 1 minute, the crater became somewhat broader and deeper but the grooved surface remained similar in appearance (illustrated in Figure 4.86). It is interesting to note, by comparison with Figure 4.84, that cutting at this higher speed deepens and extends the crater, but that the pronounced notching formed at 125 m/min was not developed.

As the cutting speed was increased to 200 m/min, the crater was again broadened and deepened within for 2.5 minutes (Fig 4.87), and the substrate was exposed to revealing a smooth surface. Further increase in cutting speed resulted in futher increase in flank wear with massive adhesion of workpiece material to the flank face. Figure 4.88a shows flank wear of K68 at a speed of 250 m/min and after machining for 1 minute. The wear on the flank face was extremely uneven rough and extensive. Plucking out of the tool material was observed on the worn flank face and smooth grooves were also produced in this zone.

When cutting time was increased to 2 minutes, a very large notch was developed (Fig 4.88b). At this point, the tool was found to be severely deformed and the surface finish of the workpiece had completely deteriorated (see Fig 4.160).

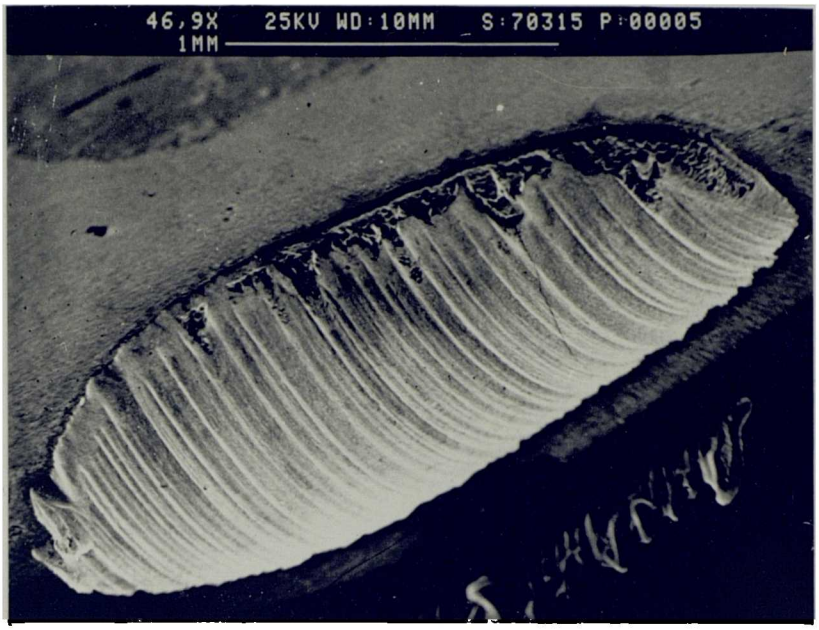

Fig 4.85 Crater surface smoothly worn within remains of loosely bound tool particles at the bottom of the rake face.

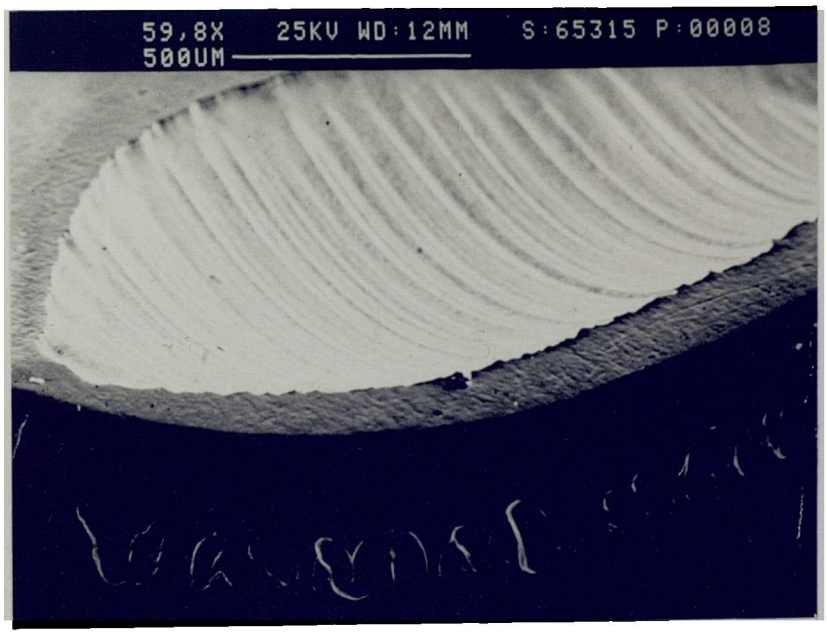

Fig 4.86 Rake face crater smoothly ridged by diffusion/dissolution wear process.

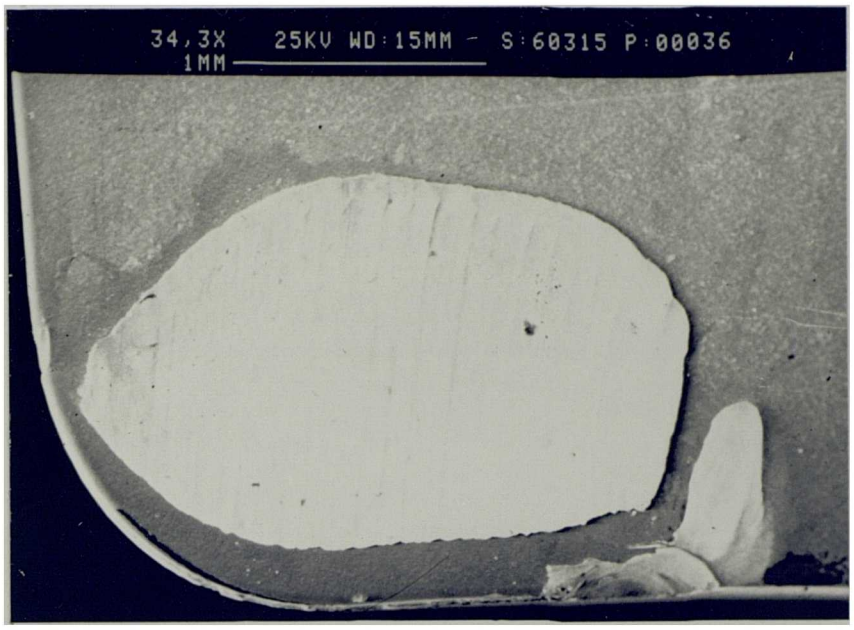

Fig 4.87 Crater rapidly broaden & deepen while machining at high speed (200 m/min).

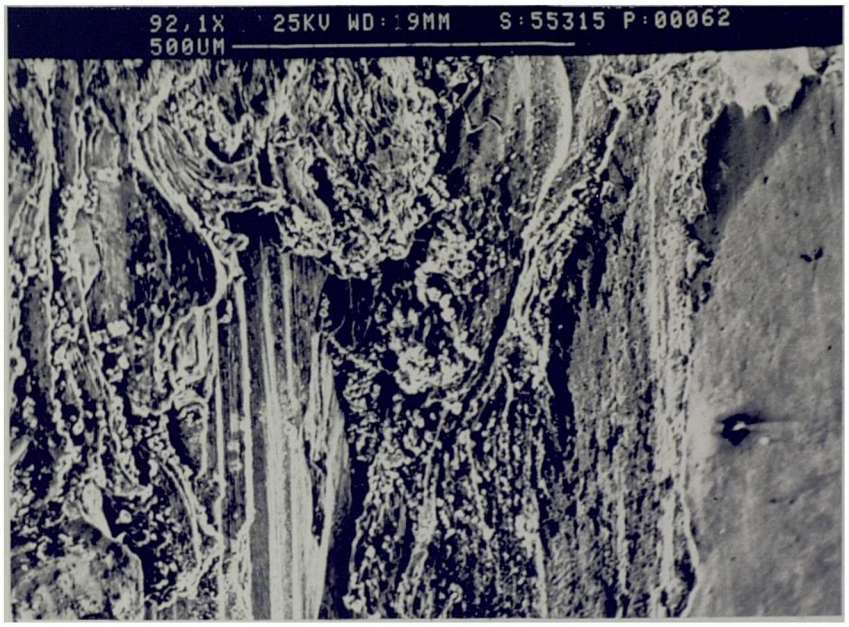

Fig 4.88a Rapid wear on the flank face of K68 insert with appearance of plucking.

4.4.1.5 CUTTING PERFORMANCE OF CBN

a) CBN WITH NORMAL ORIENTATION

The S.E.M. examination of the tool used for cutting at a speed of 50 m/min is presented in Figure 4.89, which shows the rake face and cutting edge of an Amborite tool after cutting for 3 minutes. The worn surface exhibites severe wear, suggesting that in the wear region a high normal stress was present. The rake and flank face show numerous grooves with an approximate width 10 microns. This suggests that these grooves were formed as a result of particles from the cutting edge adhering to the underside of swarf (possibly due to intense contact at the interface), and subsequently sliding over the crater.

Figure 4.90 shows the flank wear surface of the CBN tool, revealing many grooves and an appreciable amount of adhered workpiece as verified by SEM/EDX.

Upon further cutting for 6 minutes, the CBN tool has undergone severe chipping wear at the side of the cutting edge in a scalloped form (Fig 4.91). This scalloped type of rake wear is seen in diamond tools (120), but it is rather unusual in CBN tools. The worn zone appeared to be abraded and the discontinuous, scalloped form of wear can be seen clearly in Figure 4.91. As the cutting time increased, so did the rate of wear (Fig 4.92).

A large amount of wear took place on the rake face with prolonged cutting (ie. 8 minutes) and a relatively rough and chipped cutting edge was formed. Evidence of fragmentation was seen from where the tool particles had been removed. The worn rake surface exhibites regions which have been worn consistent with a process of etching and attrition wear (Fig 4.93). The process of etching wear involves an increased rate of chemical attack of those highly dislocated areas which are continuously developed on the rake face and their subsequent removal as oxides

Fig 4.88b Formation of large size notch wear at the flank face.

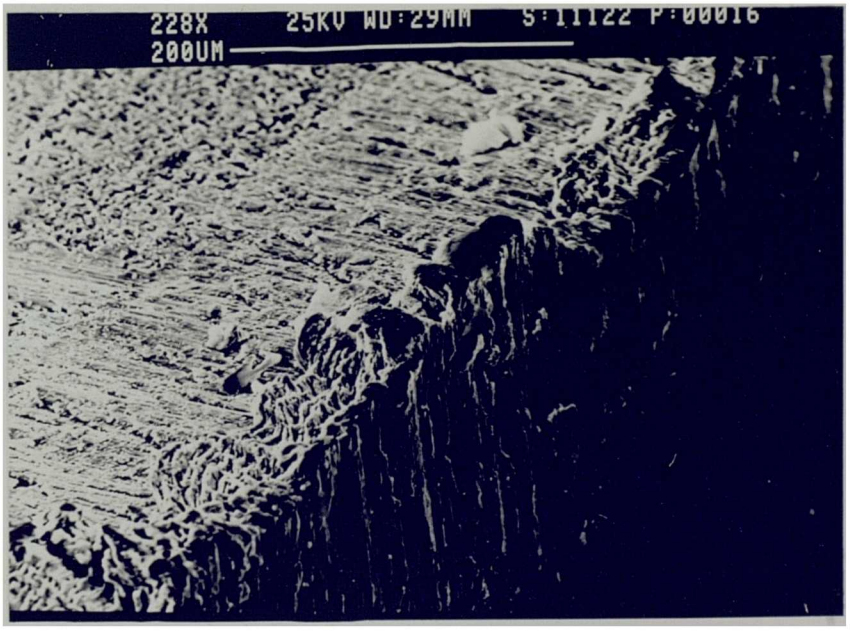

Fig 4.89 General view of cubic boron nitride tool wear.

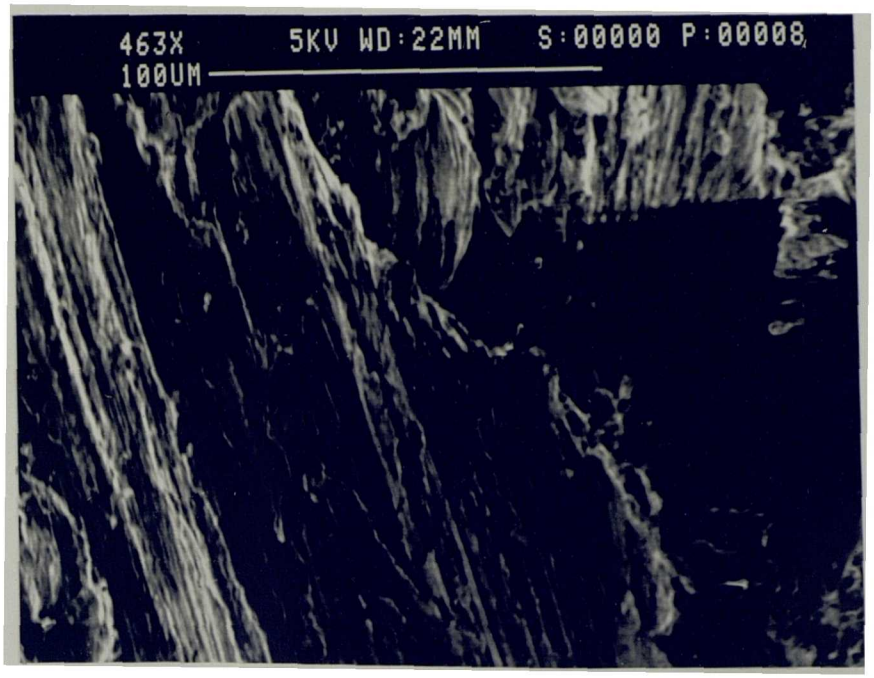

Fig 4.90 Enlarged view of flank face wear.

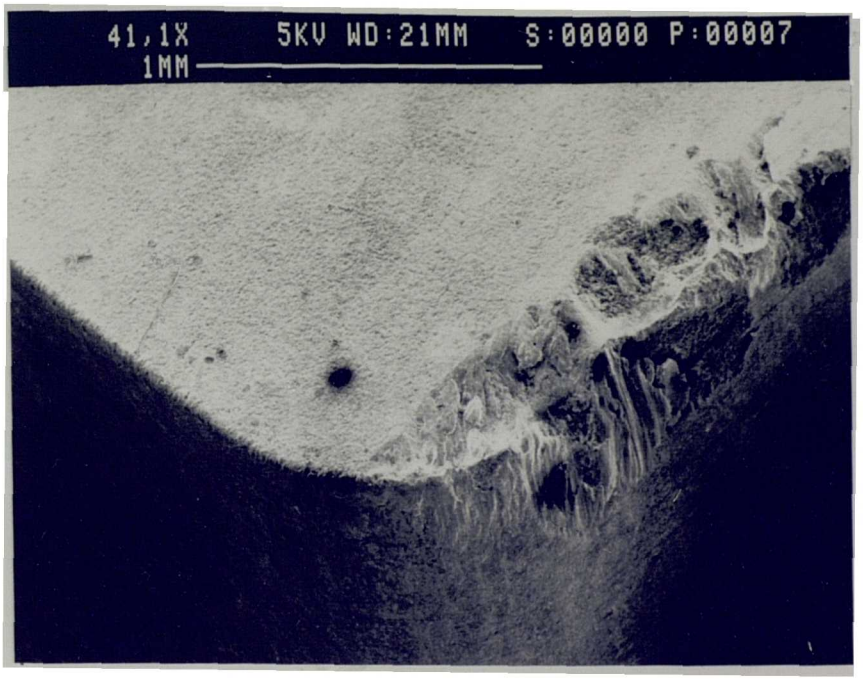

Fig 4.91 Chipping at the cutting edge of cubic boron nitride insert.

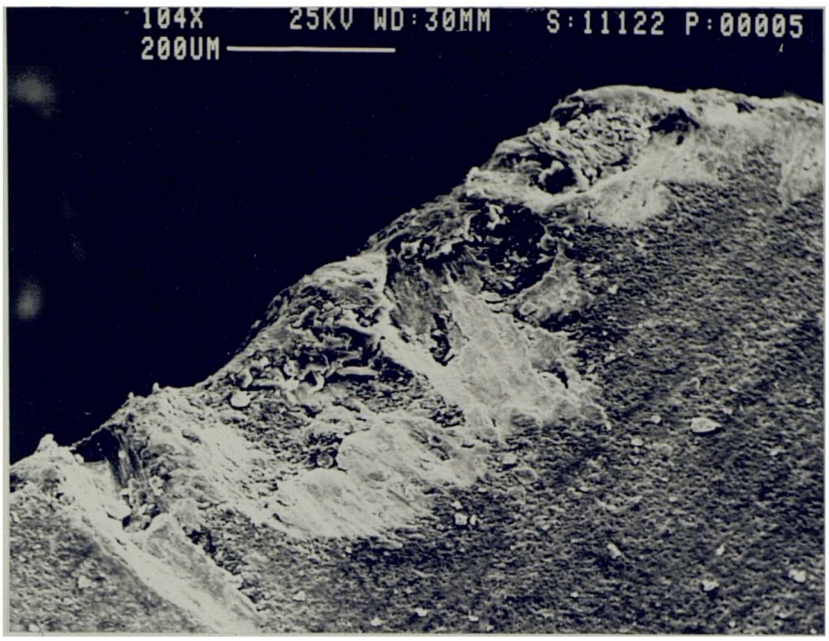

Fig 4.92 View of tool wear on the rake face of cubic boron nitride tool.

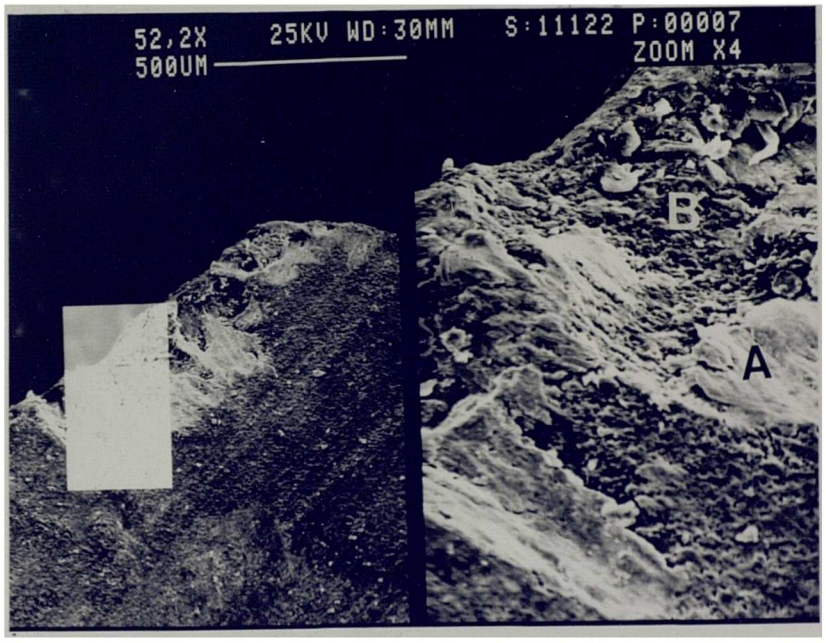

Fig 4.93 The rake surface Amborite exhibit regions worn by a process of etching & attrition wear.

(175-176). This chemically based process tends to produce a smooth surface (region 'A'). Attrition shows characteristics of a wear process in which microscopic fragments of tool material are torn away adhering to the rake face (region 'B') and to the swarf. Further evidence to support this suggestion is given later (Fig 4.153).

As the cutting time was raised to 10 minutes, the tool completely failed at the cutting edge (Fig 4.94).

Examination of tool inserts after cutting at a speed of 100 m/min, revealed a pattern of wear similar to that observed with PCD tools and described in the next section, where a metallic layer was seen on the rake face of the tools. Figure 4.95 shows the rake face of a CBN tool, after 2 minutes of cutting, which is entirely covered with a thin metallic layer. Energy dispersive X-ray (EDAX) analysis of this layer has shown that it contains the components of the titanium workpiece alloy. These layers did not prove to be strongly bonded to the top surface of the tool. Furthermore, their formation is time dependent. After 4 minutes of machining, the layer was found to be adhered to the underside of the swarf, and subsequently this process of uneven wear in the contact region between tool/chip, which contributed to the wear of the tool by attrition (Fig 4.96), became severe. Prolonging the machining time to 6 minutes revealed a scalloped form of wear on the rake face of the tool where numerous ridges have developed into the flank region (Fig 4.97).

After cutting for 8 minutes, a classic form of crater was formed on the rake face of the tool, similar to the crater formed on the carbide tools. The process of wear leading to formation of this crater is thought to involve dissolution of tool material by diffusion into the adjacent zone of the chip and workpiece (177), (Fig 4.98). Again plucking out of the tool material can also be seen to have occurred on parts of the worn rake face.

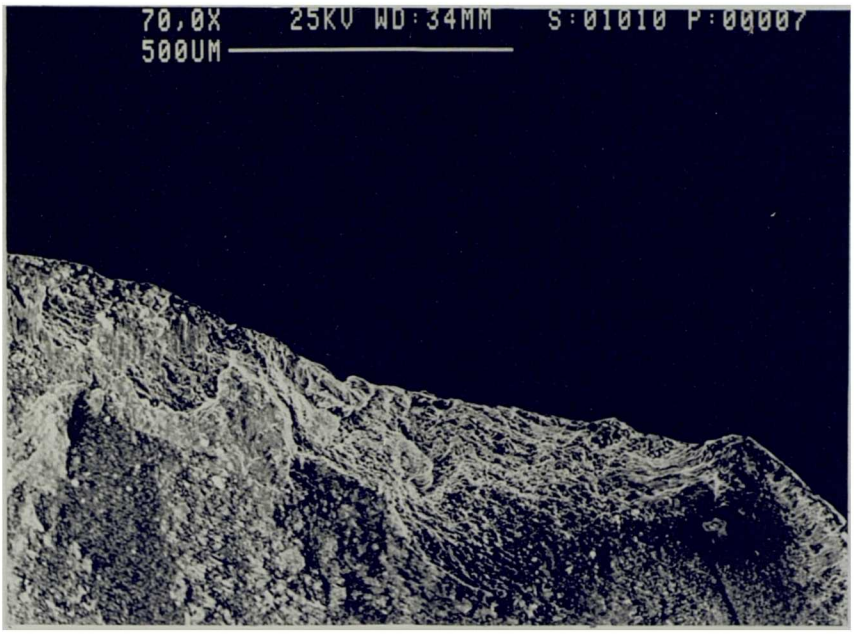

Fig 4.94 Plastic deformation of cubic boron nitride tool at the cutting edge.

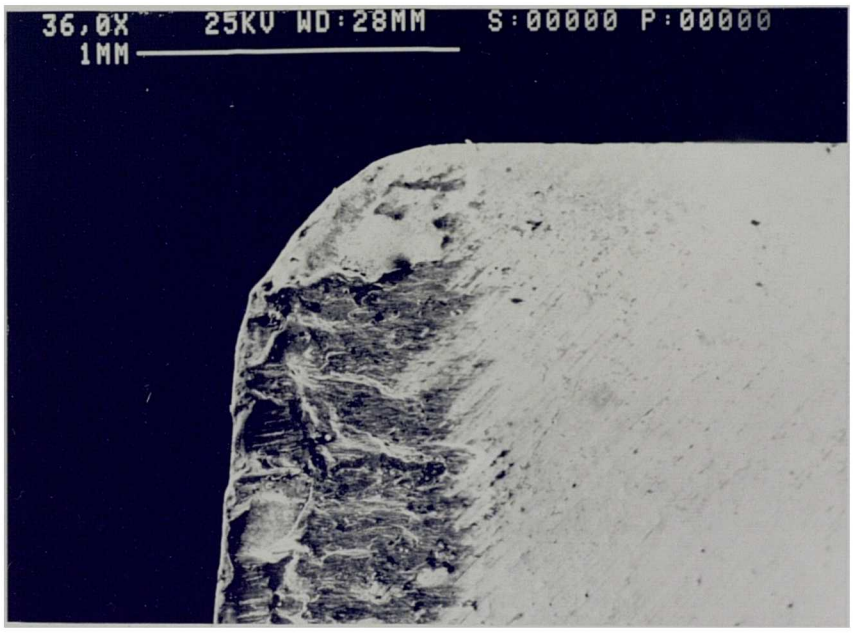

Fig 4.95 Deposited metallic layer on the rake face of cubic boron nitride tool.

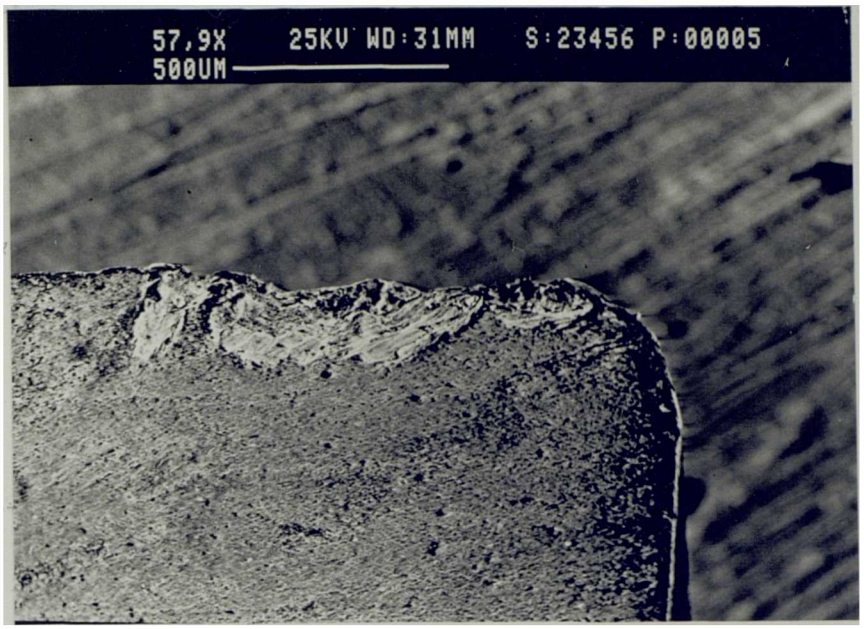

Fig 4.96 Evidence of chipping at the cutting edge of cubic boron nitride tool.

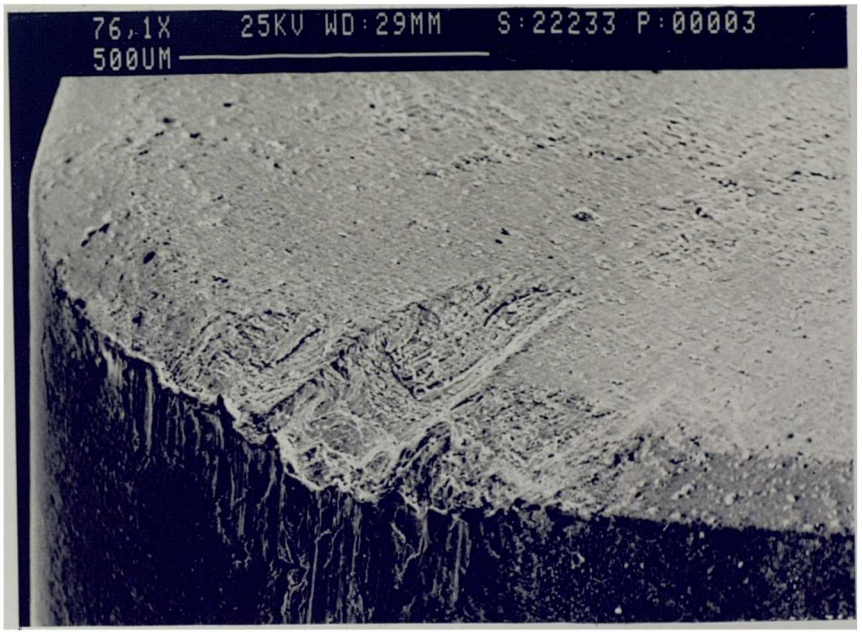

Fig 4.97 Worn surface of flank & rake faces of Amborite machining at speed of 100 m/min.

Figure 4.99 shows the condition of the rake face of a CBN insert after cutting for 10 minutes. Although gross wear of the insert has occurred due to fracture, it is still possible to clearly see part of a smooth worn crater on the rake face. Such wear, which is clearly similar in form to that of carbide tools, was most likely due to dissolution wear. The combined effects of the flank and rake face wear gave rise to an unsupported section of the cutting edge which lead to subsequent plastic deformation of the tool with increased cutting time (Fig 4.100). At this point the tool was rejected due to fracture after 11 minutes of cutting.

Figure 4.101 illustrates an Amborite cutting tool which has been used for the machining of the titanium alloy, at the speed of 150 m/min for 2 minutes. Several layers of workpiece material have been deposited on the rake face, and the surface of these adhered layers is smoothly ridged as a result of tool fragments which have been chipped out of the cutting edge and travelled through the crater zone.

The edge depression continued to increase with time and the build up material was greatest in the vicinity of nose radius (Fig 4.102), whilst the flank land is evenly worn. Higher magnification of worn regions on the rake face, illustrate the adherent layer is ready to be moved by the next cut and, beneath it, the surface is smoothly grooved (Fig 4.103). An increase in cutting time led to the introduction of several types of wear. Essentially three regions (Fig 4.104) on the rake face of this tool were identified as follows:

Region 'A' spattered with molten material from the workpiece. This region is extremely smooth as the result of the diffusion/dissolution wear process.

Region 'B' in which an adhered layer covered the entire cutting edge. The surface of this layer is smoothly worn (not as smooth as region 'A'), within it there are numerous fine streaks running in the direction of chip flow.

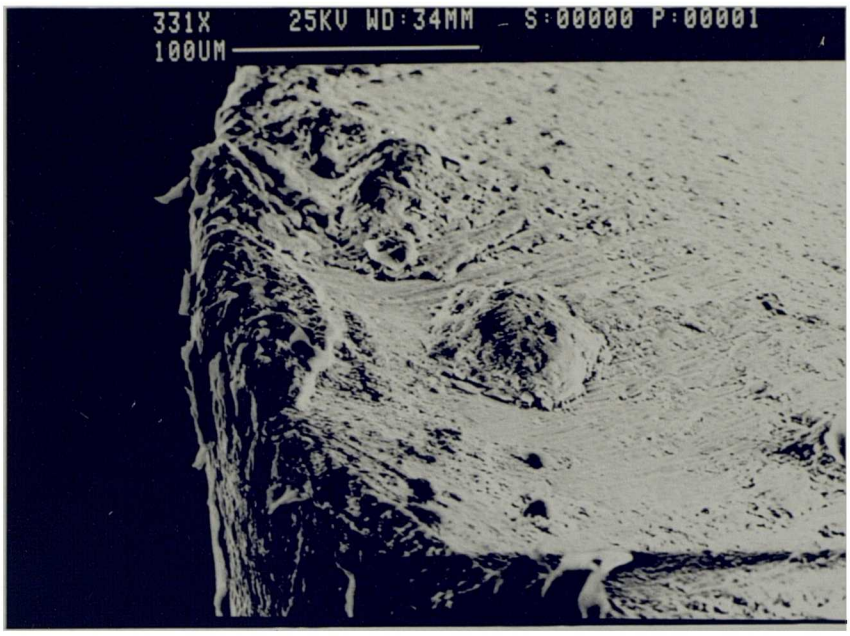

Fig 4.98 A plucked area on the rake face of Amborite within the smooth crater surface.

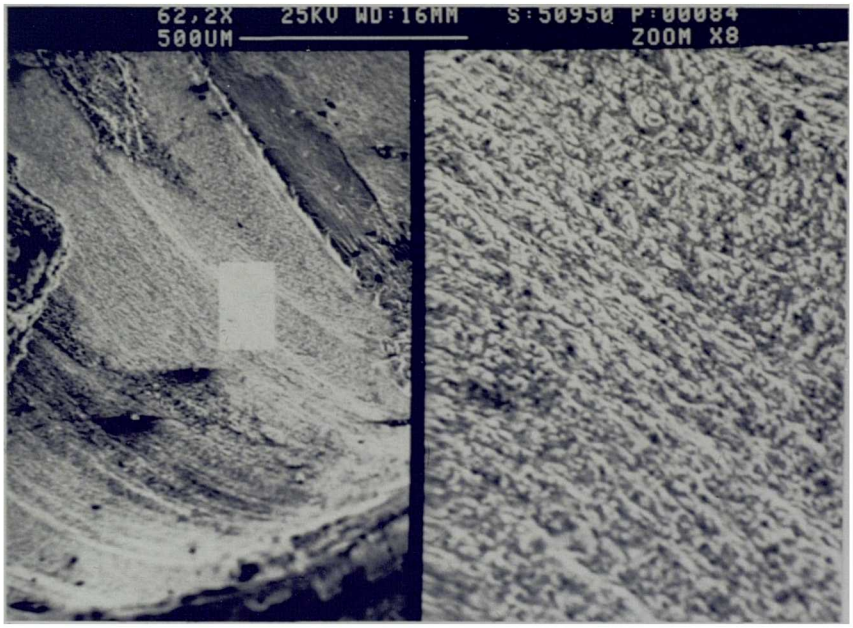

Fig 4.99 Close-up views of rake face crater wear of cubic boron nitride tool.

Fig 4.100 Chipping off portion of the rake face of cubic boron nitride tool.

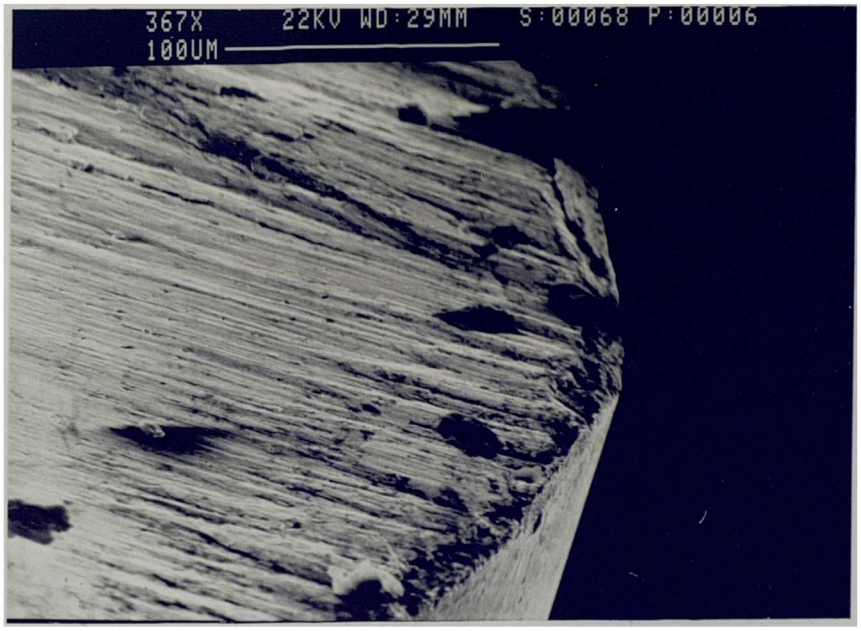

Fig 4.101 Smoothly ridged surface of adhered layers on the rake face of Amborite tool.

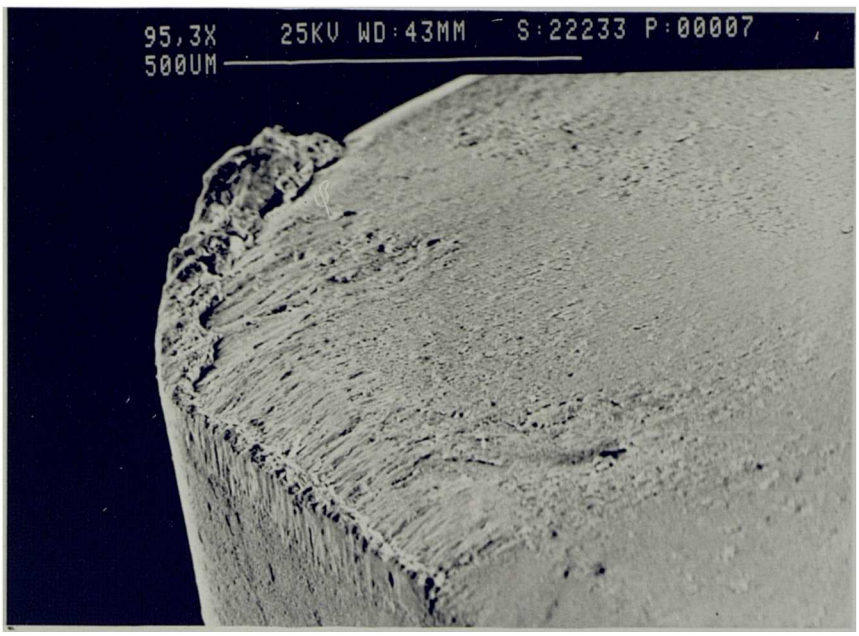

Fig 4.102 Built up material in the vicinity of cubic boron nitride tool.

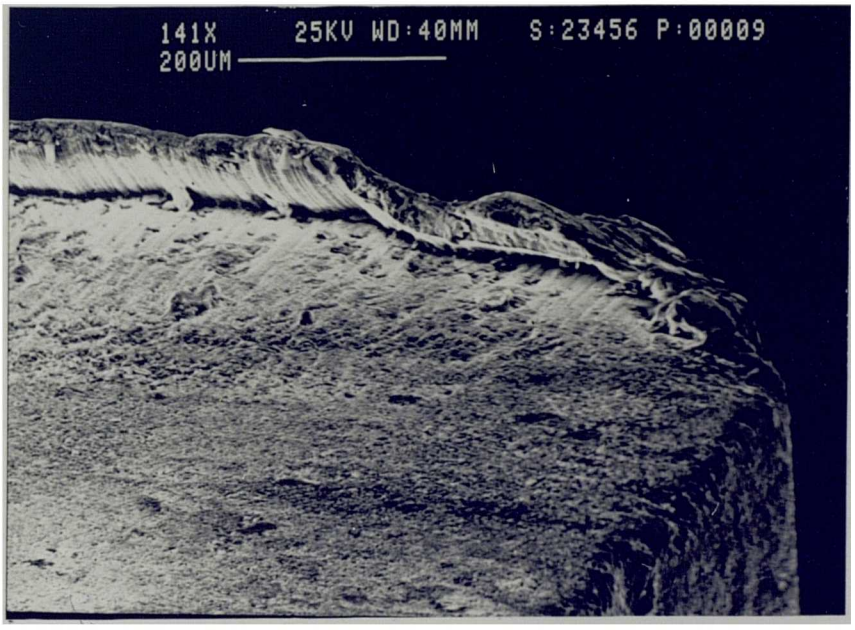

Fig 4.103 Smoothly ridged surface beneath the adhered layer on the rake face of Amborite tool.

Region 'C', a fluted surface in the crater similar to the wear observed in carbide tools. No evidence of the adhered workpiece material was found.

The tool was removed after 10 minutes machining in order to avoid catastrophic failure by fracture. Based on the earlier experience, this type of wear will certainly lead to complete failure of the tool.

As the cutting speed was increased to 200 m/min for 1 minute, cratering became more evident. Temperatures in excess of 1000 $^{\circ}$C had apparently been produced over part of the tool/chip interface during the machining. A white-etching region close to the cutting edge, could be detected (Fig 4.105). In this figure the crater zone is smoothly worn, suggesting a mechanism of diffusion/dissolution is active at this region. Furthermore, build up of material in small quantity could be seen adhering to the cutting edge. Upon increasing the machining time to 6 minutes, it was found that the crater slowly broadened and deepened, while the flank face was evenly and smoothly worn. A similar smooth type of wear was observed in the crater zone (Fig 4.106). This figure illustrates a similar pattern of wear to that of the carbide tools, where the crater area is smoothly grooved.

Figure 4.107 shows a details from Figure 4.106 at higher magnification. The tool particles could be seen on the rake face which have been removed from the region close to the cutting edge. These particles were loosely attached and their periodic removal by adhesion to the chip has contributed to the wear of the tool by attrition. It might be noted that edge retention was surprisingly good despite significant wear of both the rake and flank faces.

The CBN tool was rejected after machining for 3 minutes at a speed of 250 m/min. A micrograph of the worn tool suggests that the plastic deformation of the

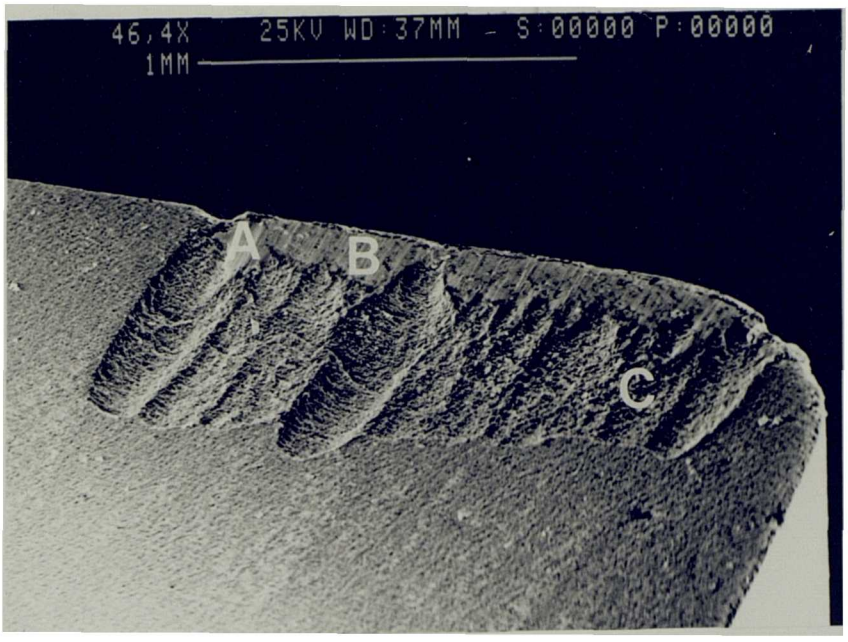

Fig 4.104 Rake face of cubic boron nitride tool showing regions of wear.

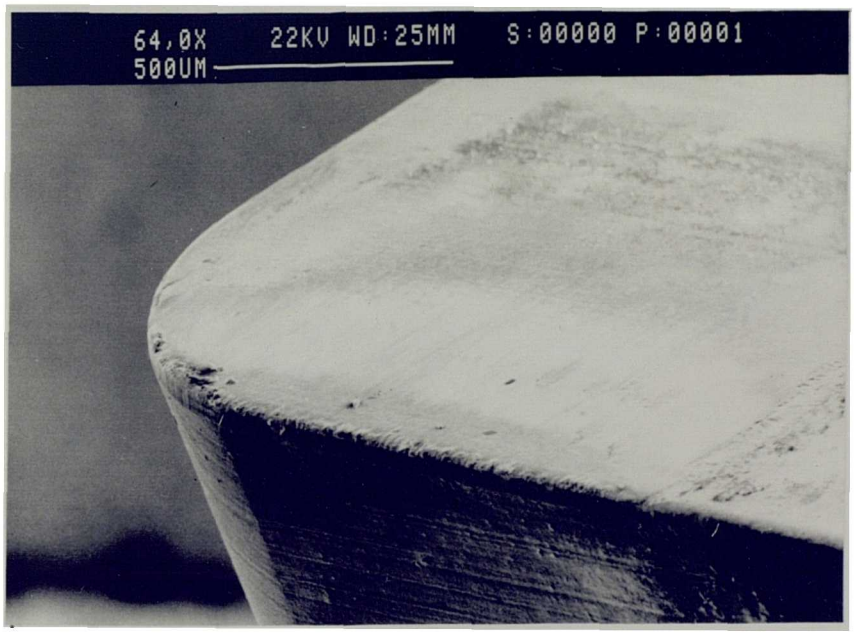

Fig 4.105 Smoothly worn rake face of cubic boron nitride insert evidence of diffusion/dissolution wear.

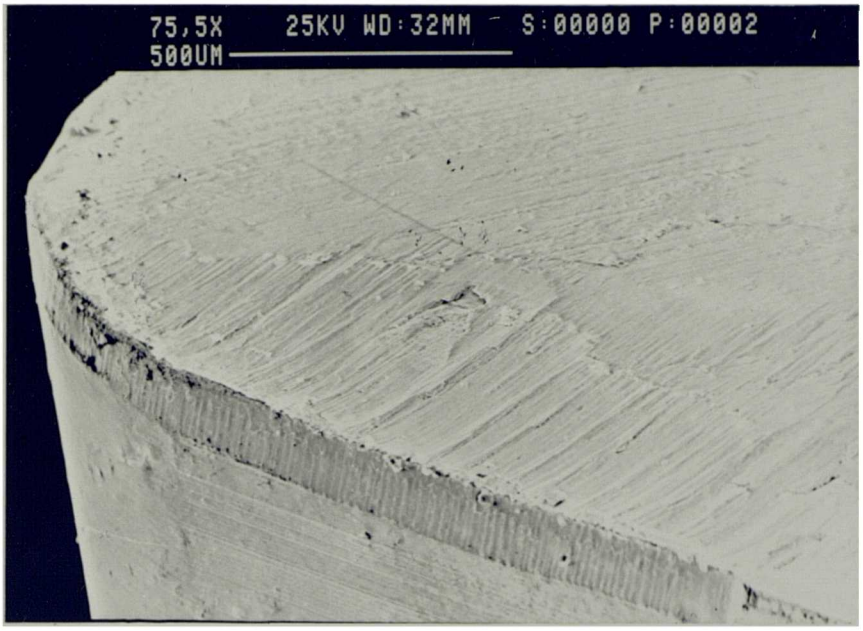

Fig 4.106 Worn surface of flank & rake faces of cubic boron nitride tool.

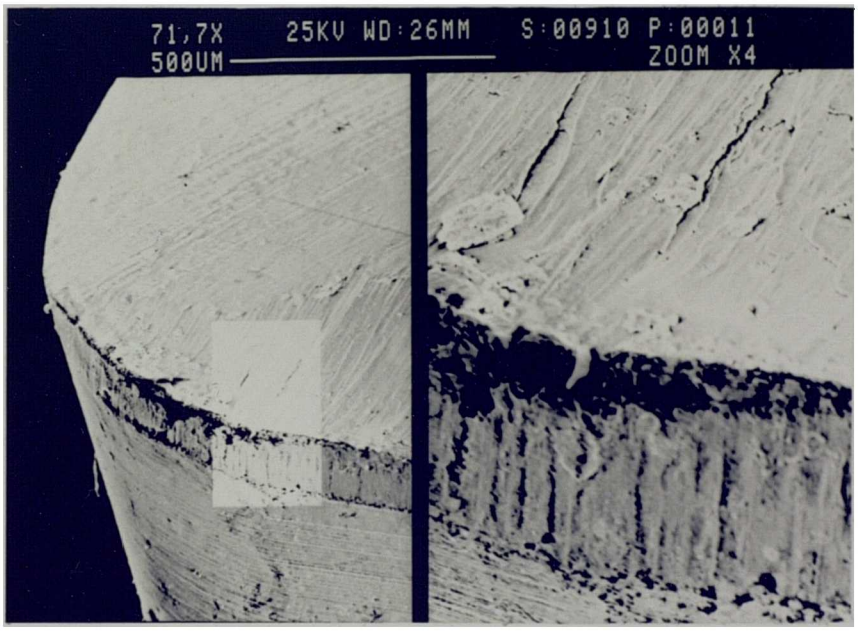

Fig 4.107 Close-up views of flank & rake face wear of cubic boron nitride tool.

cutting edge led to the catastrophic failure. Furthermore, it is possible that large particles of tool were being removed mechanically at the contact area (Fig 4.108).

b) MODIFIED CBN TOOL

The remarkable behaviour of the flank face of the Amborite tool in the earlier quasi-static adhesion tests prompted examination of its use as the rake face of a tool during the cutting process.

Upon using the modified Amborite tool (CBN2), for machining titanium alloy at the speed of 100 m/min, the mechanism of wear was seen to be very different from that of normally oriented (CBN1) tools. Figure 4.109 is an SEM micrograph of the cutting tool which has been used for the duration of 2 minutes and should be compared with the corrosponding micrograph in Figure 4.95. There is hardly any wear established on the rake face and a relatively sharp cutting edge is retained with no evidence of fragmentation or chipping.

The overall rate of wear was far less than that of the normal CBN tool under similar cutting conditions. Consequently, the cutting time required to produce an equivalent amount of wear was much longer. After 6 minutes cutting, the crater region was still intact, whilst on the flank face, adhered layers were developed in the vicinity of cutting edge (Fig 4.110). These adhered layers were found to be unstable and their periodic removal by adhesion caused a deterioration in the surface finish of the workpiece (Fig 4.160).

A wear groove formed around the cutting edge after 12 minutes is shown in Figure 4.111. It seems that this wear notch was caused by fracture. Although the surface of the wear had formed at a relatively large flank land, the nose radius was

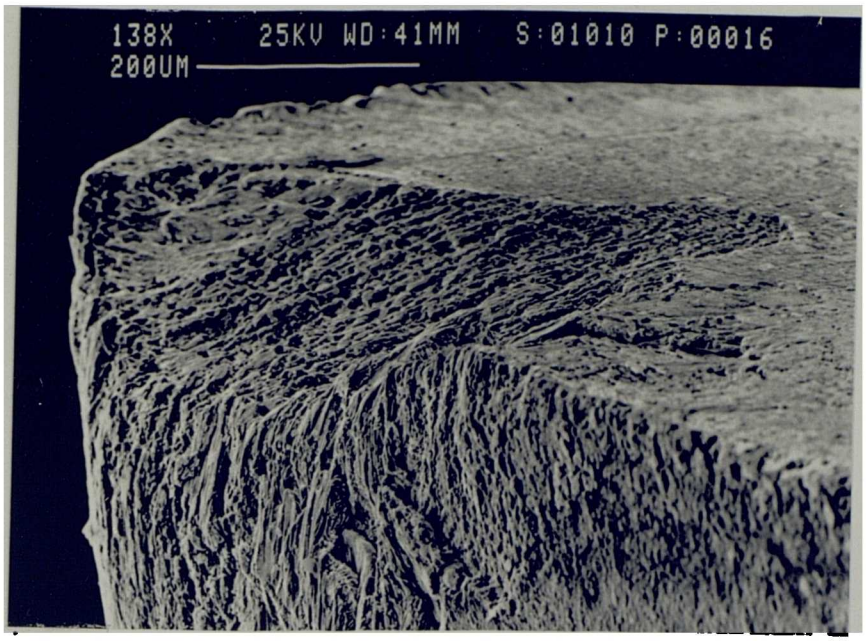

Fig 4.108 Plastic deformation at the cutting edge of cubic boron nitride tool.

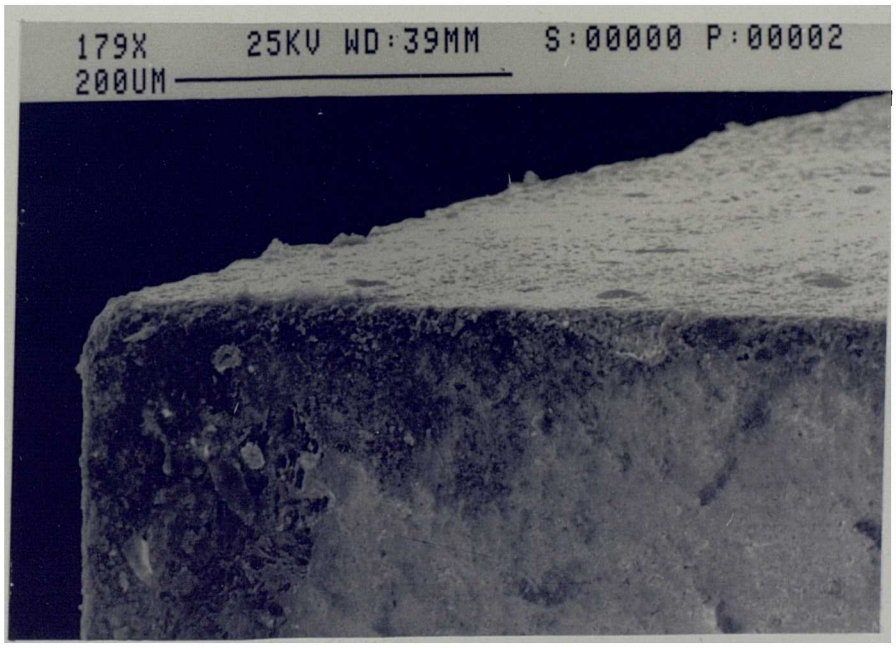

Fig 4.109 Minimum wear observed on the modified cubic boron nitride insert.

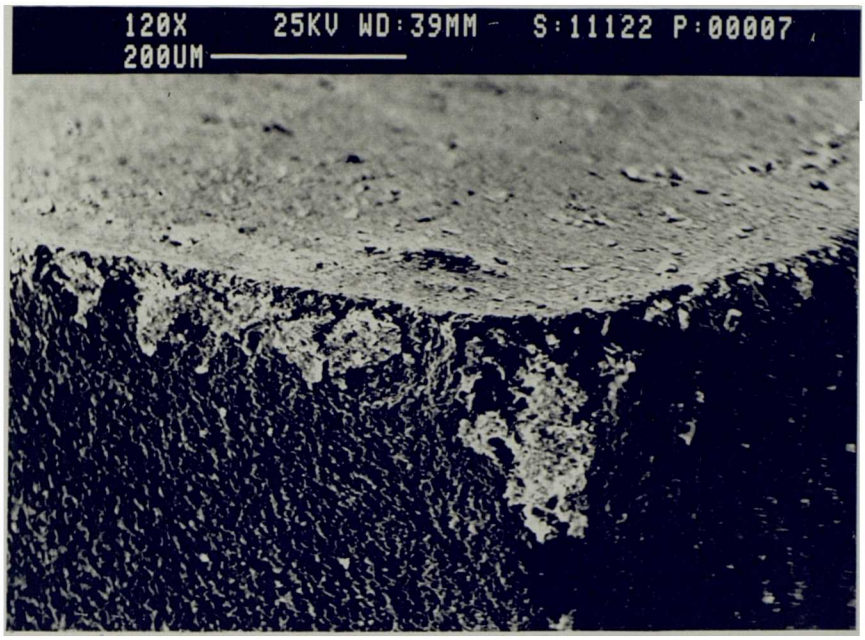

Fig 4.110 Metallic layer on flank & rake face of tool near cutting edge.

Fig 4.11 Wear grooves formed around the cutting edge of modified tool wear.

found to be smoothly grooved (Fig 4.112). The extent of wear never approached that of the normally oriented CBN1 tools (see Fig 4.98 for a comparison).

Neither the flank face nor the rake face of the modified CBN tool showed any appreciable grooving wear after 16 minutes cutting. There was no indication of cracking. Furthermore, there was only little evidence of severe wear upon increasing the cutting time to 18 minutes (Fig 4.113). On closer examination at higher magnification (Fig 4.114) it was evident that the present flank face (that is normally the rake face) had undergone greater wear than the rake face. It also shows less resistance to attrition wear. The difference in behaviour of these two faces may well be attributable to adhesion as indicated by the quasi-static method described in earlier section.

The workpiece surface finish obtained with the CBN2 tool was extremely rough and deteriorated during all the cutting procedures. Nevertheless, the recorded tool life was twice that of the normally oriented cubic boron nitride. This unusual orientation-dependent behaviour of polycrystalline CBN material has not been reported previously. However, manufacturing processing involving hot pressing tends to induce a degree of preformed orientation in the resultant microstructure which may then lead to anistropic effects.

4.4.1.6 CUTTING PERFORMANCE OF PCD TOOLS

Figures 4.115-4.117, illustrate the PCD used to cut titanium alloy at the speed of 50 m/min for a duration of 10 minutes. These figures, whilst representing the condition when disengaging the tool, consistently indicate the high level of adhesion between the workpiece and the tool that is developed under these particular conditions. Figure 4.115 shows the most extreme case of build up with the workpiece material smearing over the relief surface. Figure 4.117 illustrates the

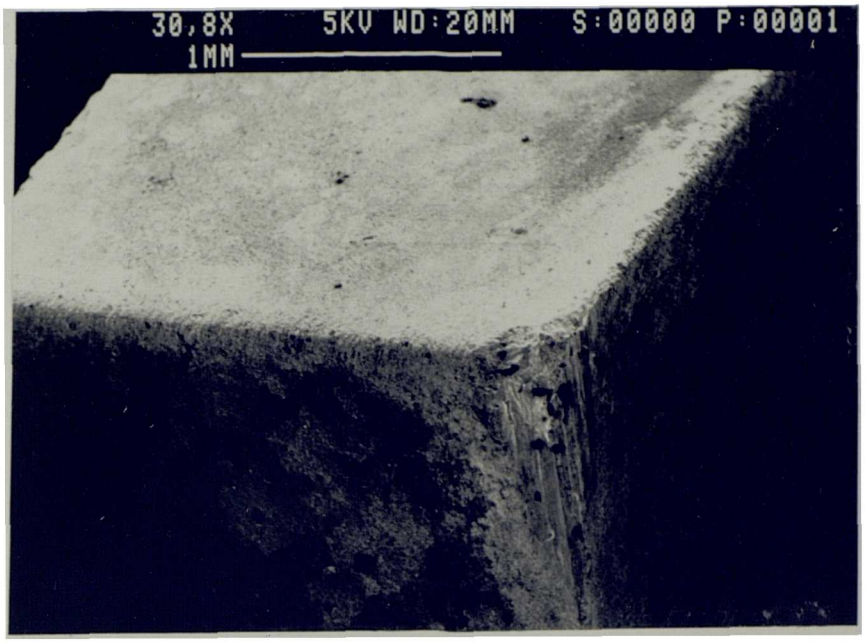

Fig 4.112 General view of CBN modified toolwear.

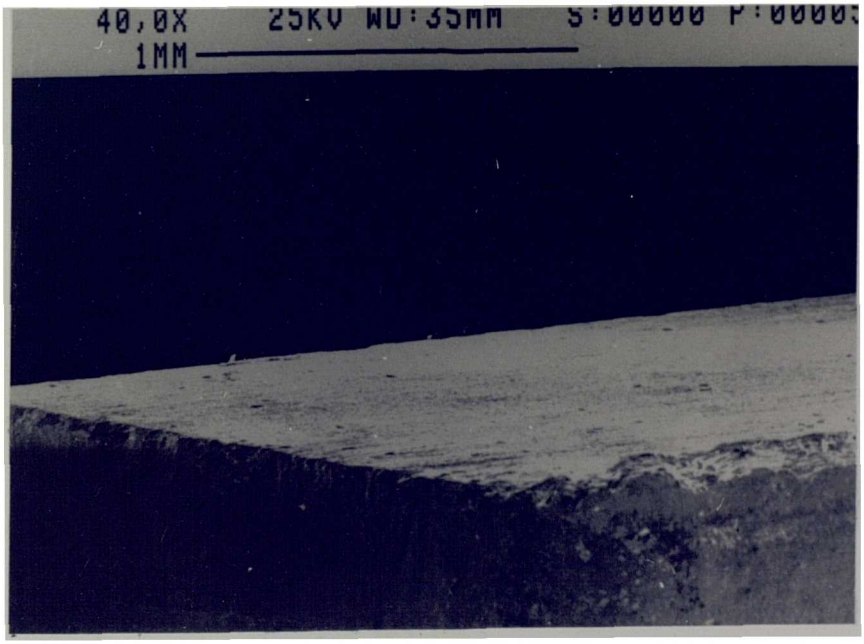

Fig 4.113 View of surface worn of modified CBN insert.

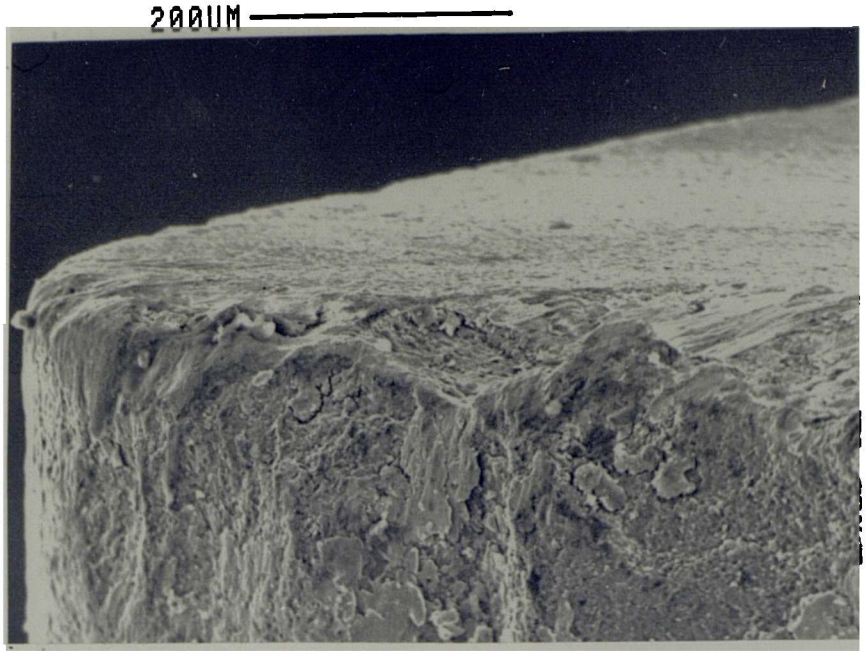

Fig 4.114 Severe wear observed after 18 mins cutting with CBN modified tool at speed of 100 m/min.

Fig 4.115 Build up of workpiece material smearing on the relief surface of PCD insert.

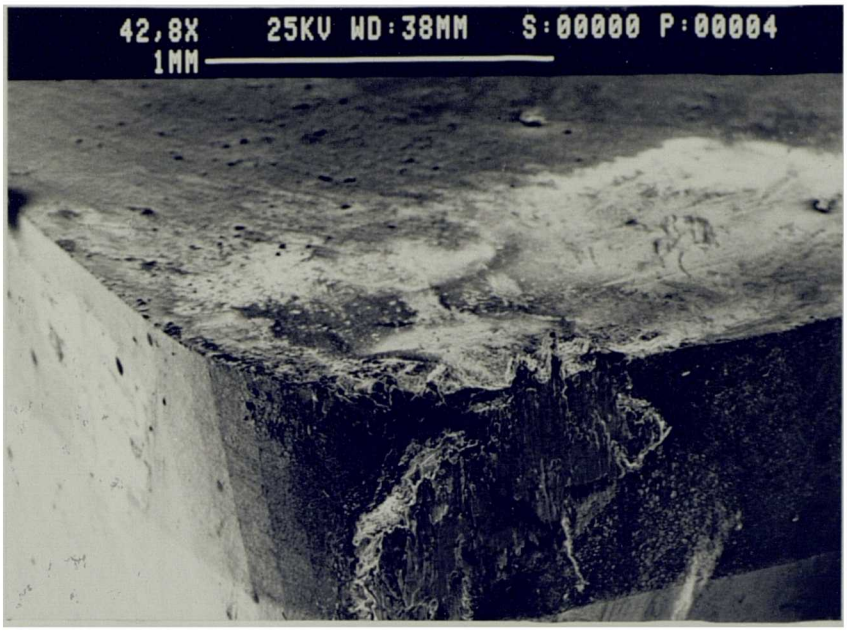

Fig 4.116 Irregular wear on the flank face of PCD insert machining at low speed (50 m/min).

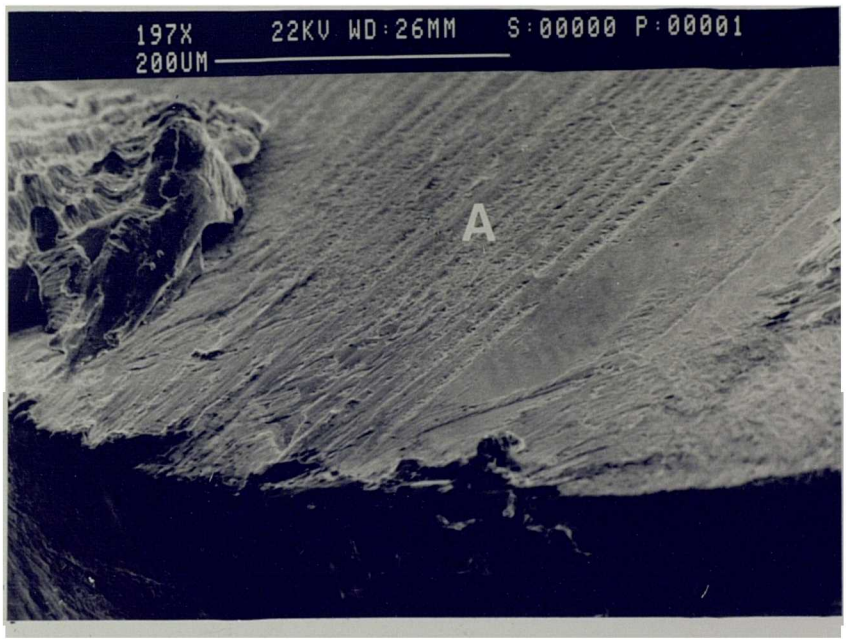

Fig 4.117 Formation of smoothly ridged deposited layer of workpiece on the rake face of PCD insert.

formation of a metal layer of workpiece adhering to the rake face of the tool. This layer occurred in the area of engagement of tool/chip interface.

After cutting for 20 minutes, fracture occurred at the cutting edge and the formation of cracks running parallel to the direction of swarf can be seen in Figure 4.118.

At the speed of 100 m/min the PCD tool showed a similar wear pattern to the one earlier observed at lower speed. Figure 4.119 shows the built-up material of workpiece smearing on the rake face of the tool, and this material has completely covered the edge clearance face. Higher magnification of this built-up material revealed that it comprised adhered layers deposited on top of one another (Fig 4.120). Upon further cutting for 16 minutes, the size of the layers was seen to have increased (Fig 4.121).

As a result of increasing the cutting time by a further 2 minutes, the built-up layers were removed from the top surface leaving behind a very stable and thin adhered layer. Figure 4.122 shows such an adhered layer of titanium alloy workpiece on the rake face. From this figure it can be seen that the surface of this layer becomes very smoothly grooved. This is probably the result of particles breaking loose from the metal layer at the cutting edge, adhering to the underside of the chip, and being dragged away in the direction of swarf flow. A further 2 minutes cutting results in breaking of the adhered layer and removal of tool material from the cutting edge. Examination of the worn surface at higher magnification (Fig 4.123) indicates that small scale chipping has taken place at the edge of cut.

A significant change in behaviour became obvious after cutting for a total of 22 minutes. Cracks were developed on the face of brazed WC material substrate, initiating normal to the cutting edge, and the size of these cracks increased with cutting time . Figure 4.124a illustrates the formation of these cracks on the flank face

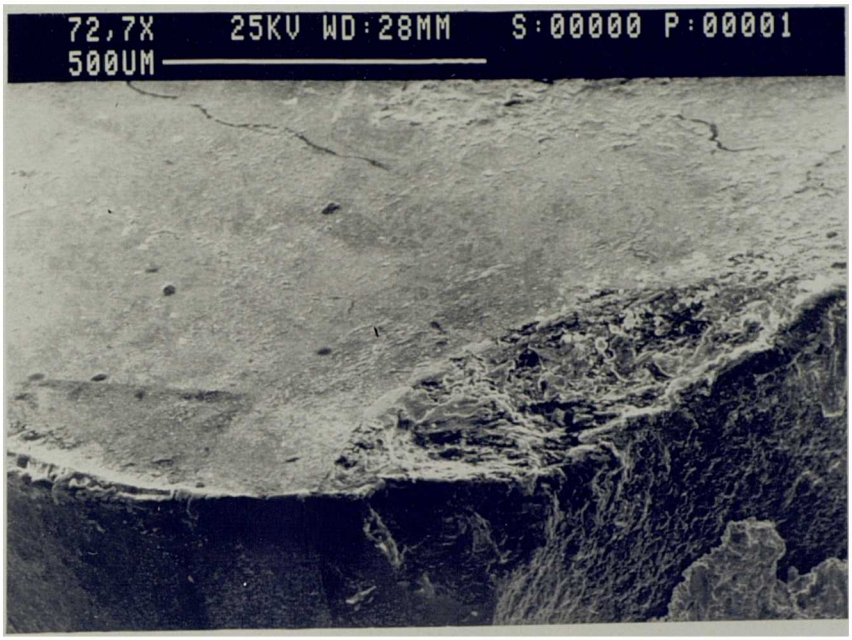

Fig 4.118 Development of cracks running parallel to the direction of chip flow on rake face of PCD insert.

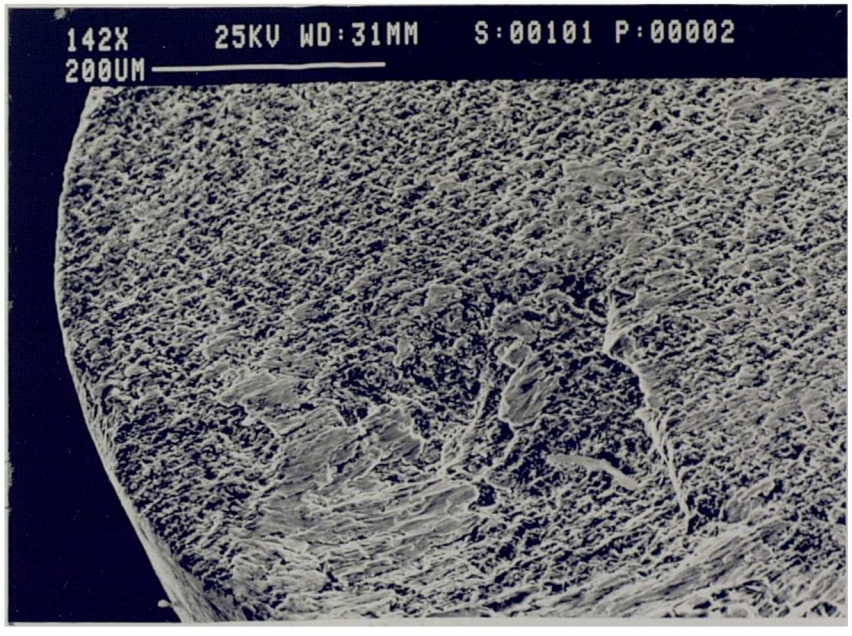

Fig 4.119 Formation of protective layer on the rake face of PCD insert.

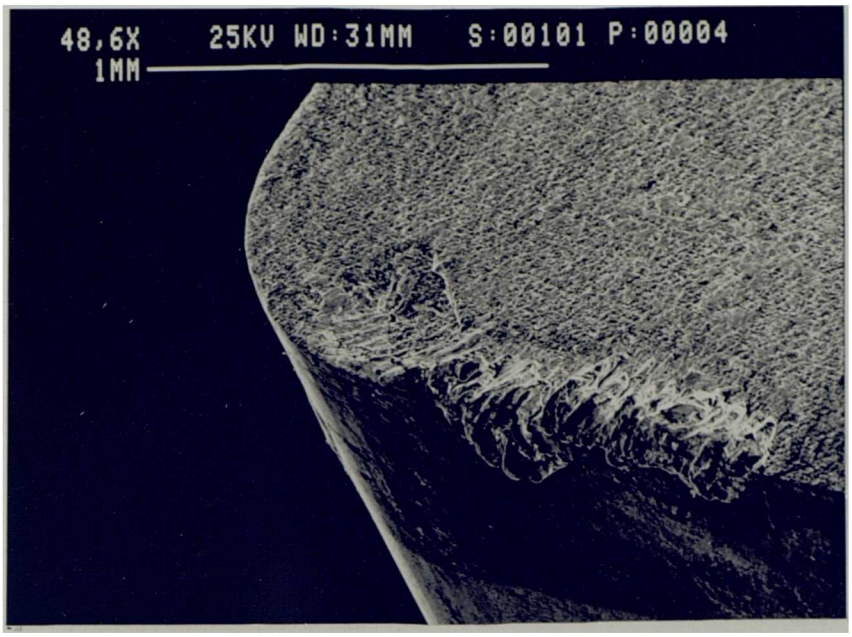

Fig 4.120 Further increase of protective layers on the cutting edge of PCD insert.

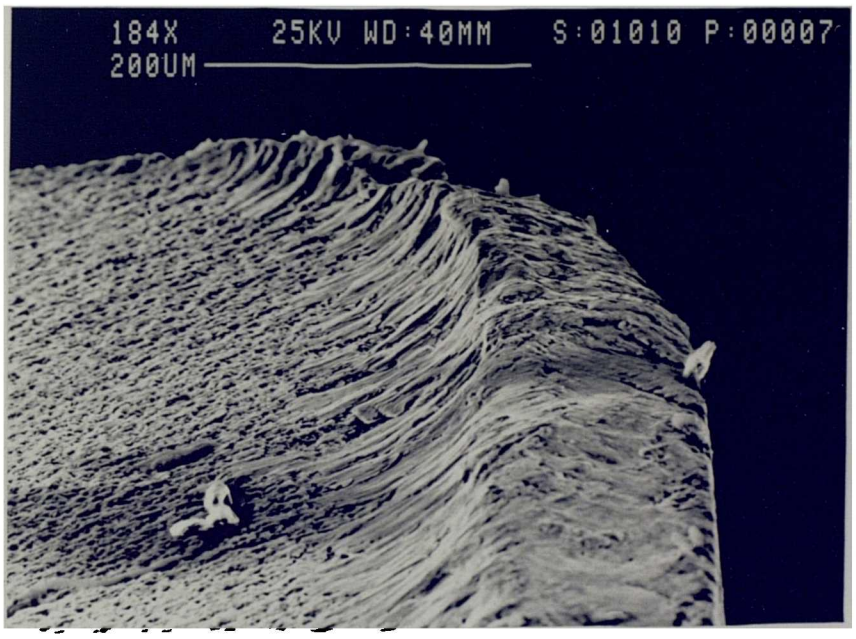

Fig 4.121a Formation of adhered layers deposited on rake face of PCD insert at speed of 100m/min.

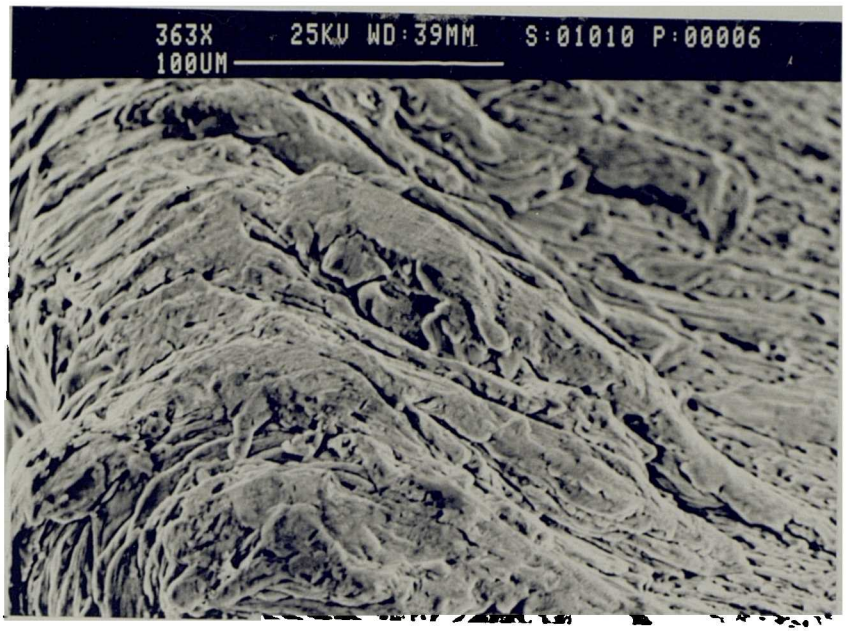

Fig 4.121b Close-up view of Fig 4.121a.

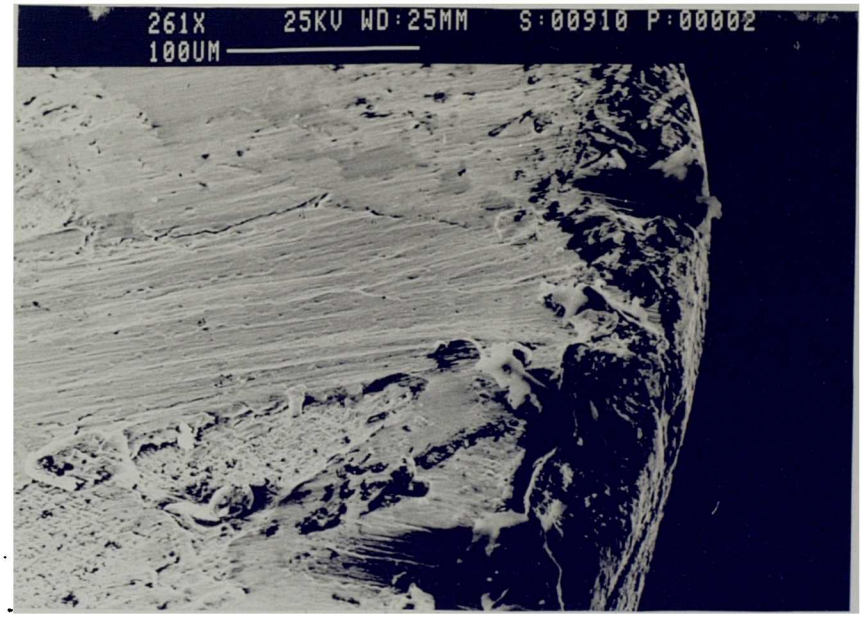

Fig 4.122 Formation of thin deposited layer of workpiece on the rake face of PCD insert.

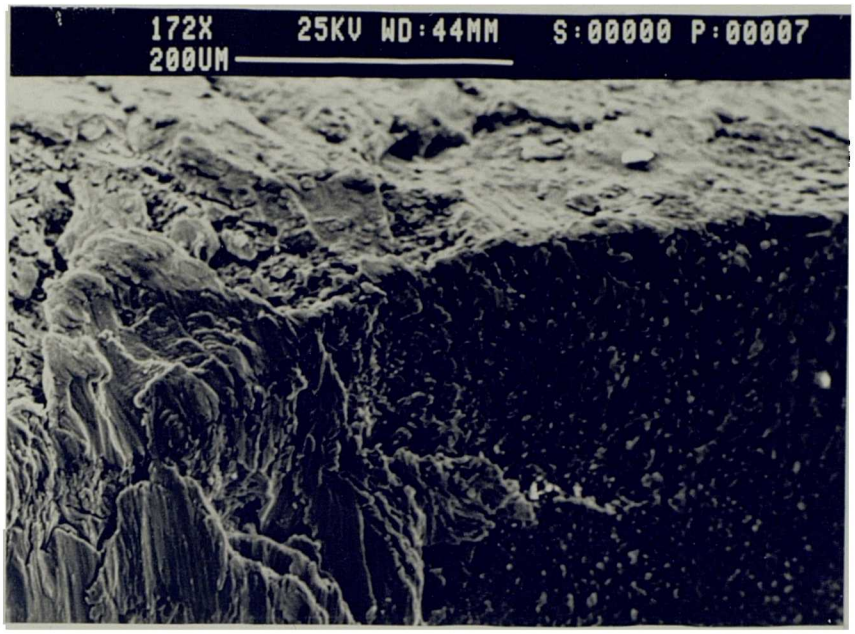

Fig 4.123 Chipping at the cutting edge of PCD insert machining at speed of 100 m/min.

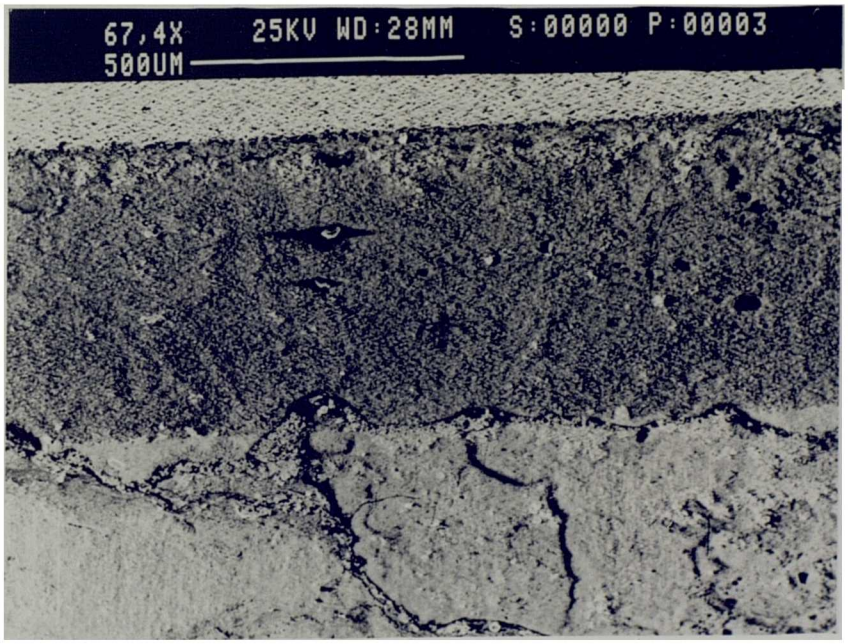

Fig 4.124a Development of cracks on the flank face of brazed WC material.

of brazed carbide which have been unable to penetrate through the diamond layer situated above it, and are deflected along the interface. The mechanism responsible for these cracks is considered to involve diffrential thermal expansion. This crack formation mechanism rapidly increased at the higher temperature, and the evidence for this hypothesis is collated and discussed in the following section.

After machining for a total of 24 minutes at the speed of 100 m/min, the cracks which were earlier seen on the WC brazed material have penetrated through the diamond layer, running towards the cutting edge (Fig 4.124b). At this point it was decided to stop the cutting, even though the tool still could be used.

Profile traces across the flank face of the tool showed no apparent tool wear after 5 minutes cutting at the speed of 150 m/min (Fig 4.125). A micrograph (Fig 4.126) of the rake face illustrates an adherent layer of titanium alloy which appears to be covering the entire surface (Fig 4.126). As the cutting proceeds up to 9 minutes, the sharp edge of adhered layer becomes flattened on the rake face (Fig 4.127). Furthermore, small fractures of the tool have occurred close to the nose radius. After extending the machining process a further 8 minutes, there was no significant increase in wear of the flank or rake face, apart from the crack development on the flank face (Fig 4.128). No doubt this cracking was initiated in the brazed material and then extended to the diamond layer as a result of thermal effects. The cracking is running normal to the chip flow direction in a wavy line and it could be due to the crack propagating between the primary particles. From this time onwards, crack development was relatively rapid. Figure 4.129 shows multiple cracks on the flank wear surface 50 microns and 100 microns below the cutting edge. Chipping has taken place on the end clearance face edge (Fig 4.130). Higher magnification of the worn surface reveals that a large portion of tool/workpiece has been plucked out of the cutting edge (Fig 4.131).

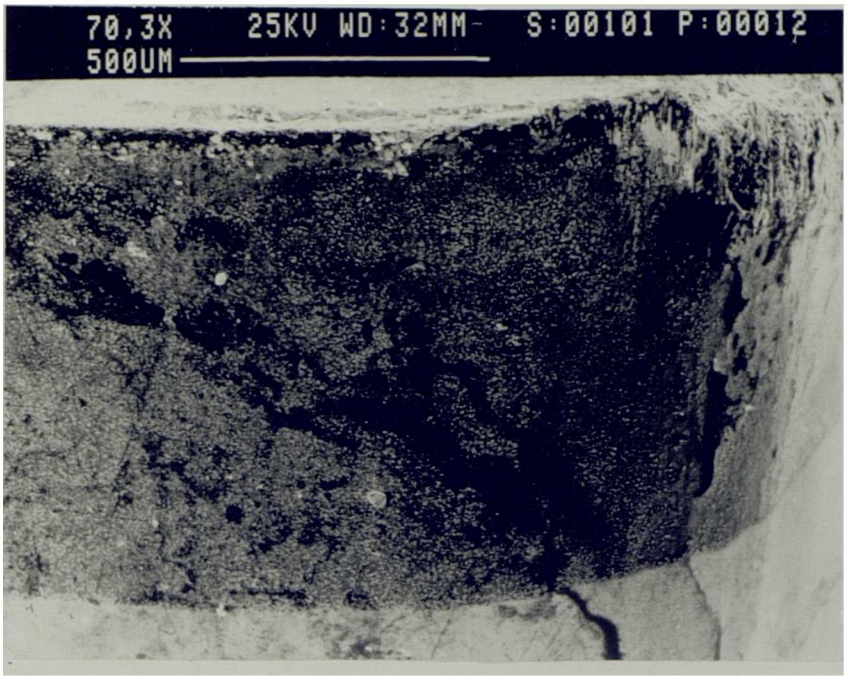

Fig 4.124b Penetration of cracks from brazed WC material into the PCD layer.

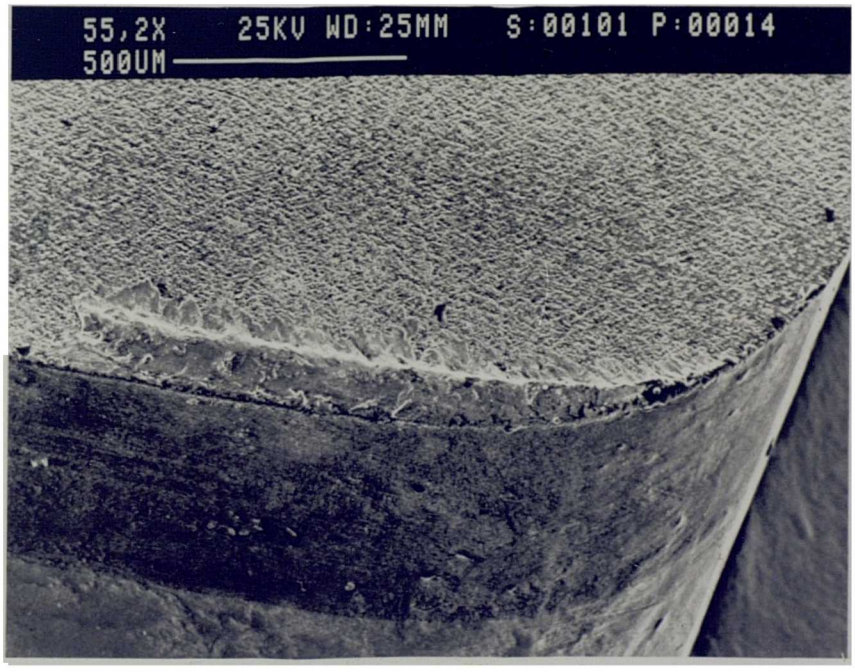

Fig 4.125 Formation of protective layer on the rake face of PCD insert machining at speed of 150 m/min.

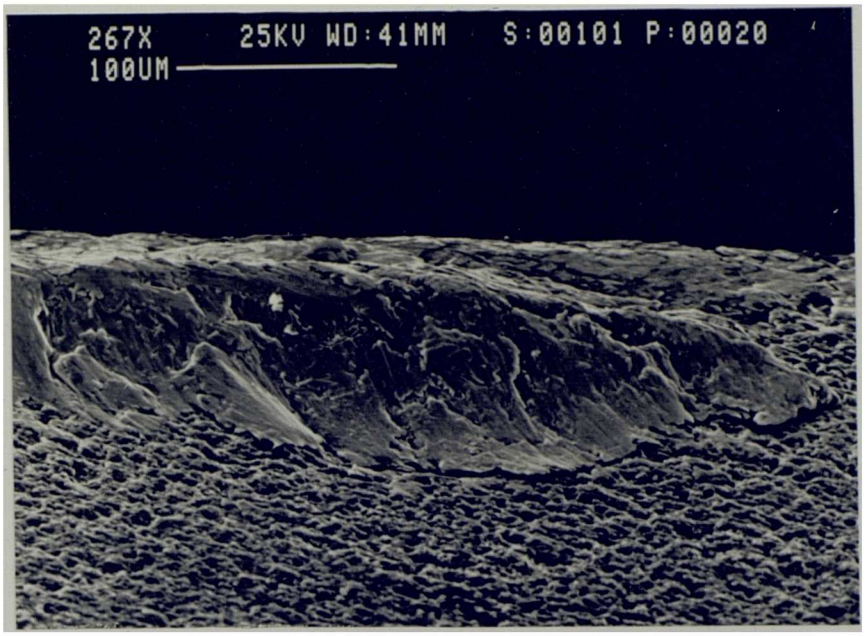

Fig 4.126 Deposition of adhered layers covering the entire surface of the rake face.

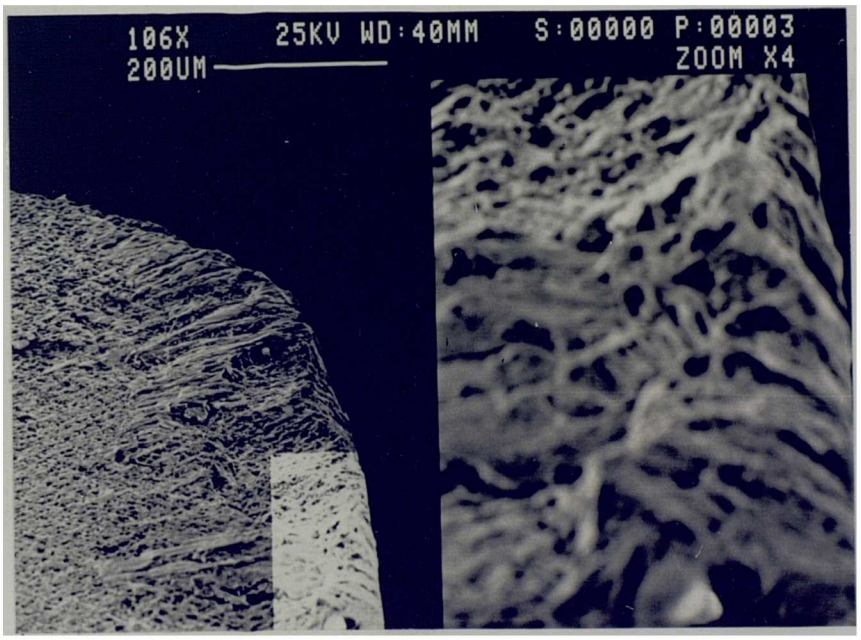

Fig 4.127 Section views showing the PCD insert machining at the speed of 150 m/min after 14 mins cutting.

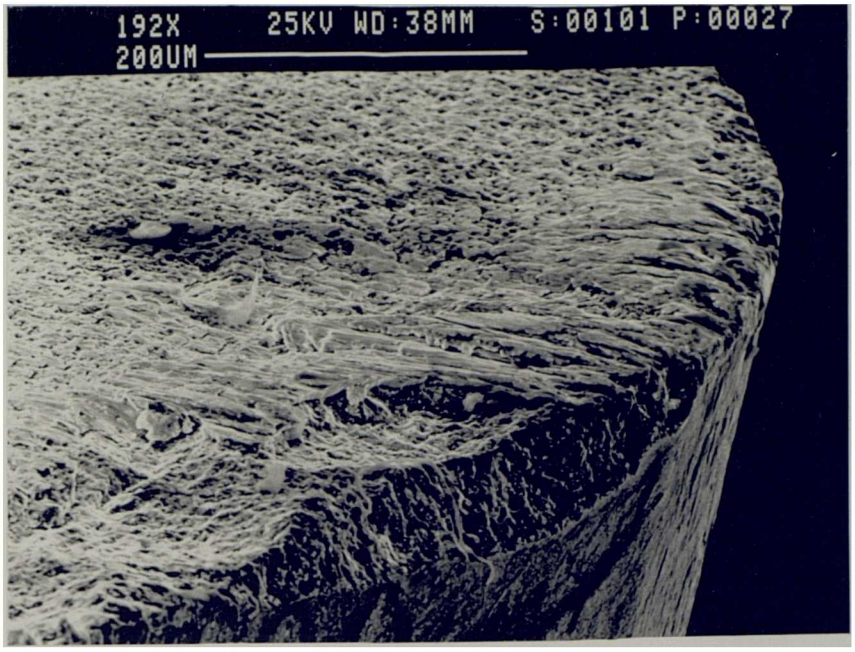

Fig 4.128 Development of crack on the flank face of PCD insert.

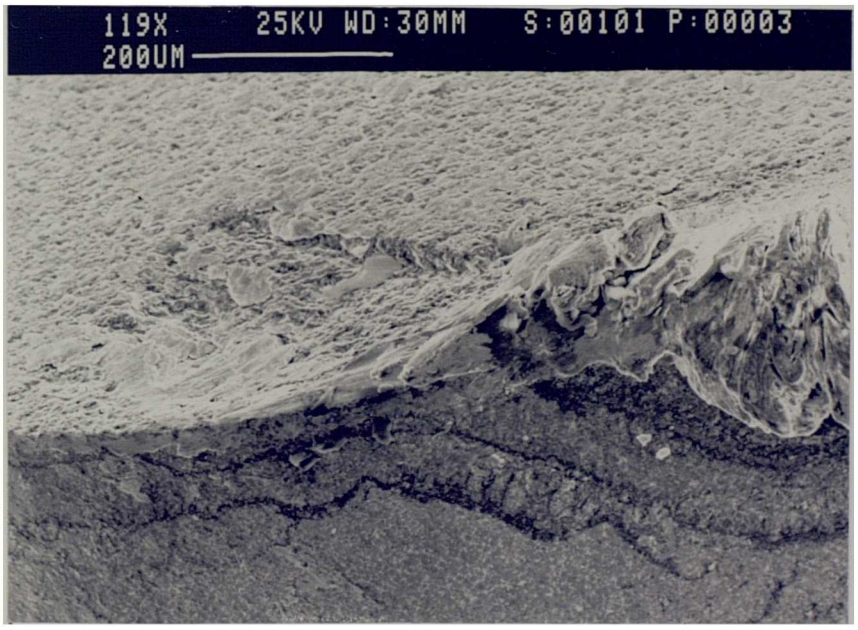

Fig 4.129 Formation of cracks on the flank face parallel to the cutting edge.

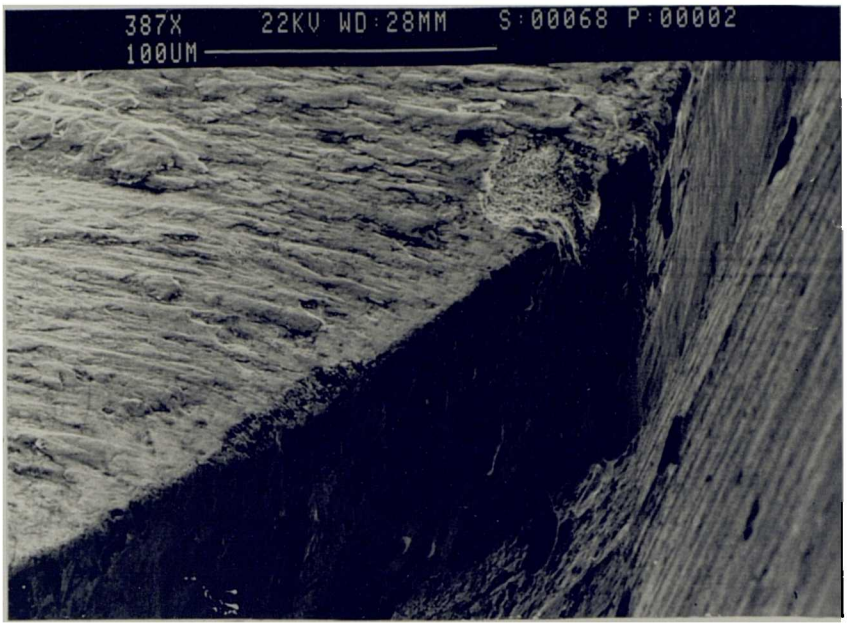

Fig 4.130 Chipped portion of the cutting edge of PCD insert.

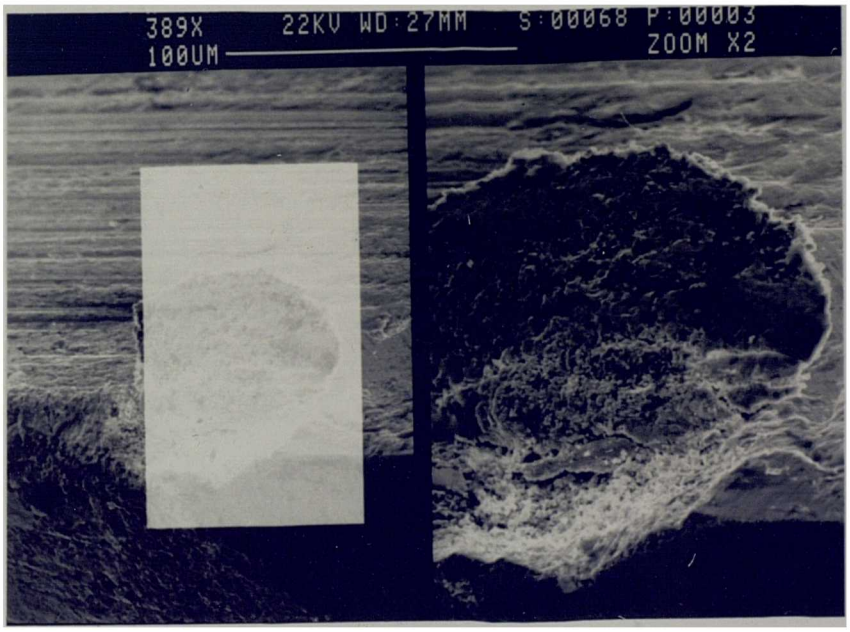

Fig 4.131 Close-up views of PCD insert shown in Fig 4.130.

After cutting for a total 20 minutes, a large portion of tool has been plucked out in the area where cracks have previously existed. This wear phenomenon is a result of widening of the crack (high temperature, high speed) and thereby weakening of the edge, followed by subsequent fracture (Fig 4.132). Examination of the wear surface at higher magnification showed evidence of relatively smooth wear (Fig 4.133).

Upon increasing the cutting speed to 200 m/min, similar wear to that observed earlier at the lower speed developed. Adhered layers of workpiece material were deposited on the rake face of tool. After 8 minutes cutting, the adhered workpiece layers on the top surface were flattened, and close examination of this region showed the presence of fine scale grooves which ran parallel with the direction of chip travel (Fig 4.134).

The adhered layers thickened and became more stable as a result of prolonged cutting time (total 16 minutes). Figure 4.135 is a micrograph of these layers and illustrates a fine surface with slight development of grooves.

After 20 minutes cutting, a fracture wear surface formed around the end cutting edge in the vicinity of tool nose radius, this was found to have formed by three distinct wear processes (Fig 4.136). The first zone indicated by 'A' was quite smoothly worn, while the region in zone 'B' is smoother than that of 'A'. The third zone 'C' showed a similar form of wear produced by attrition This type of wear could be clearly seen in Figure 4.137. Within the worn area a large portion of workpiece material could be seen ready to be lifted off by the next cut. Furthermore, fragments of workpiece material were seen adhering to the exposed substrate. At this stage of cutting, the tool was withdrawn in order to conserve the limited amount of workpiece material.

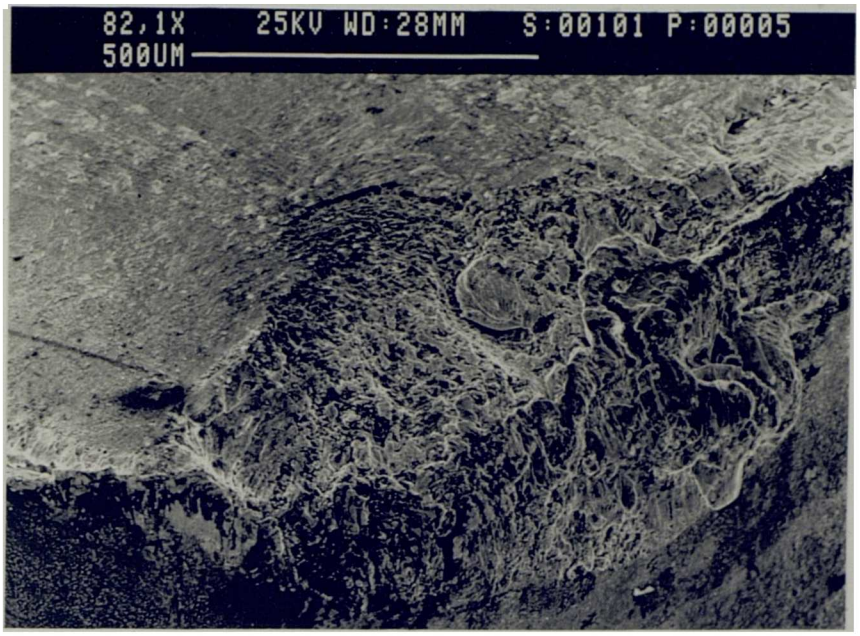

Fig 4.132 Evidence of fracture at the cutting edge of PCD insert.

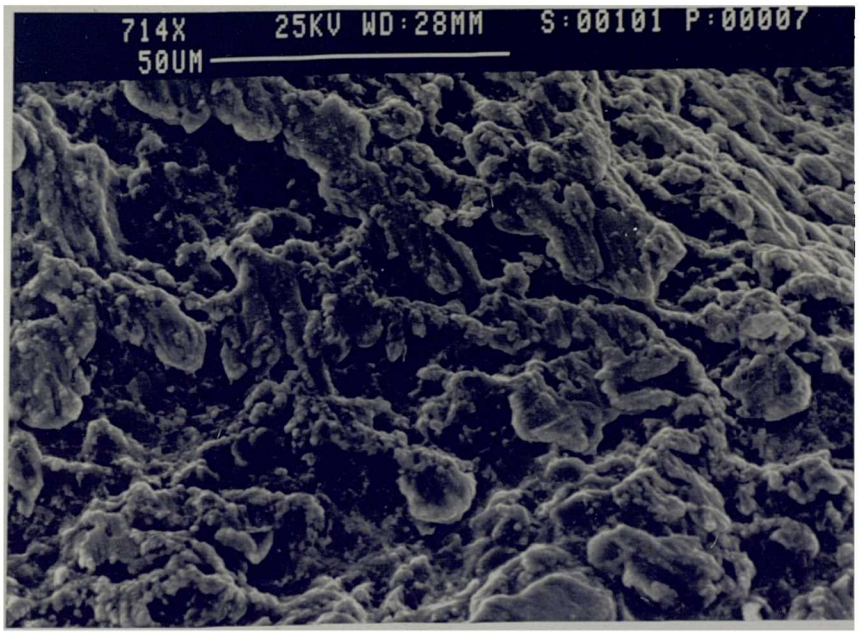

Fig 4.133 SEM image of fractured surface at high magnification showing evidence of smooth wear.

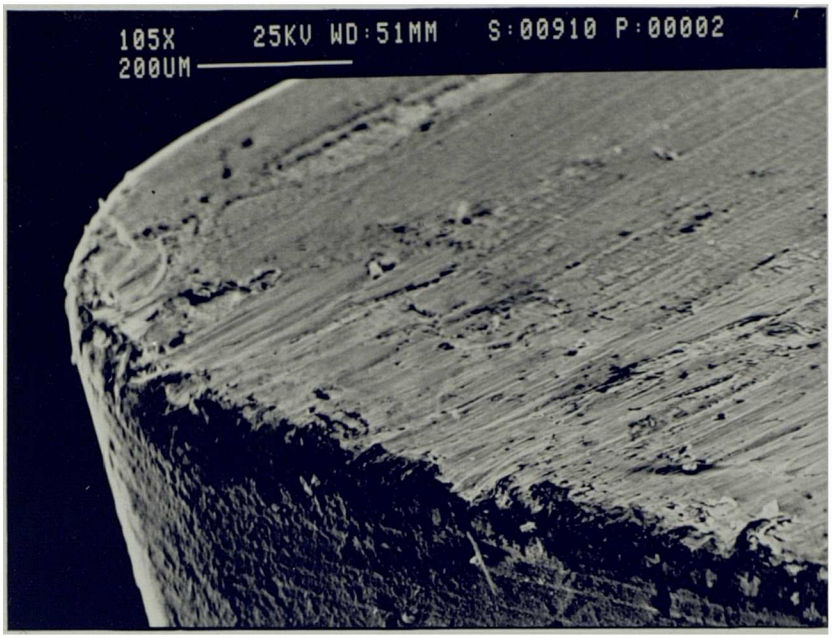

Fig 4.134 **Presence of fine scale ridges on the rake face running parallel to the chip flow direction.**

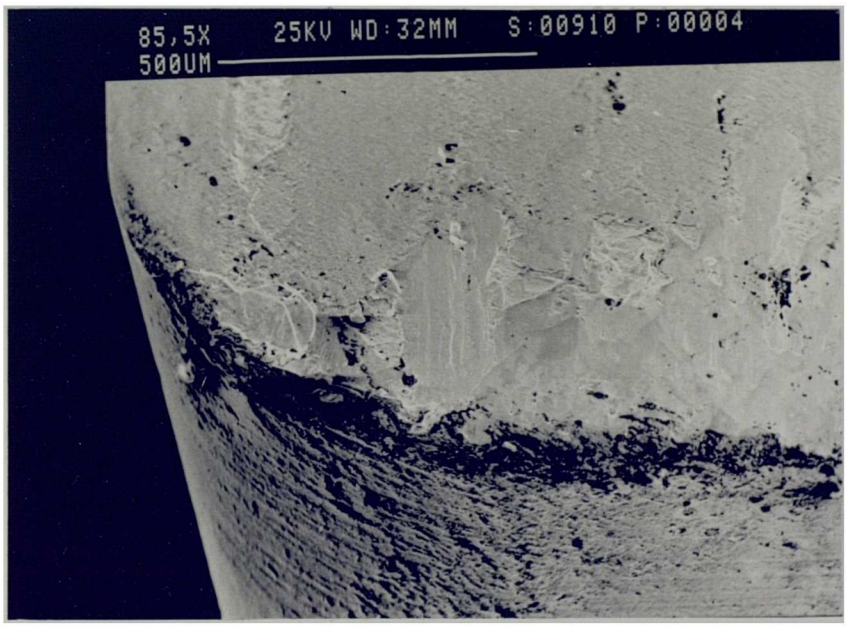

Fig 4.135 **Evidence of smooth wear on the rake face of PCD insert.**

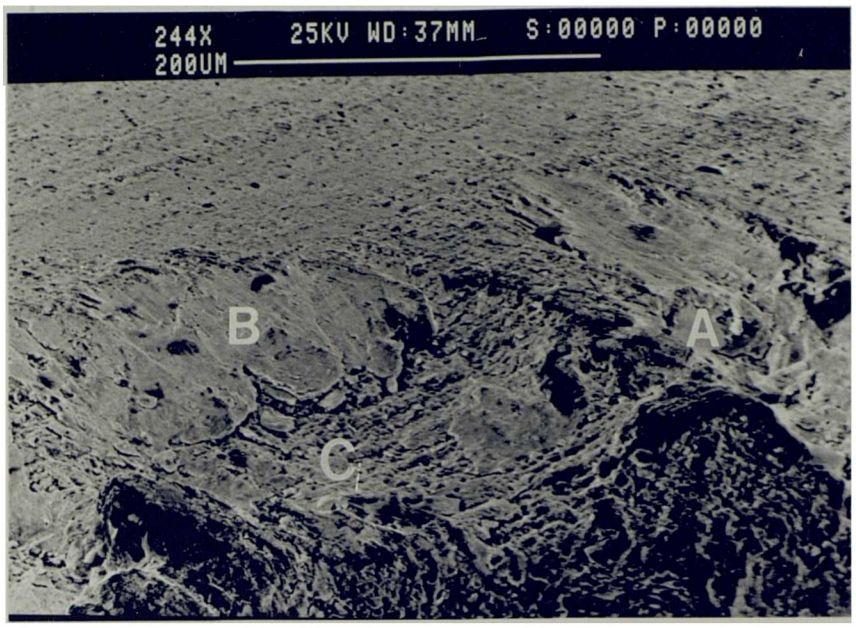

Fig 4.136 Micrograph showing regions of wear on the rake face of PCD insert.

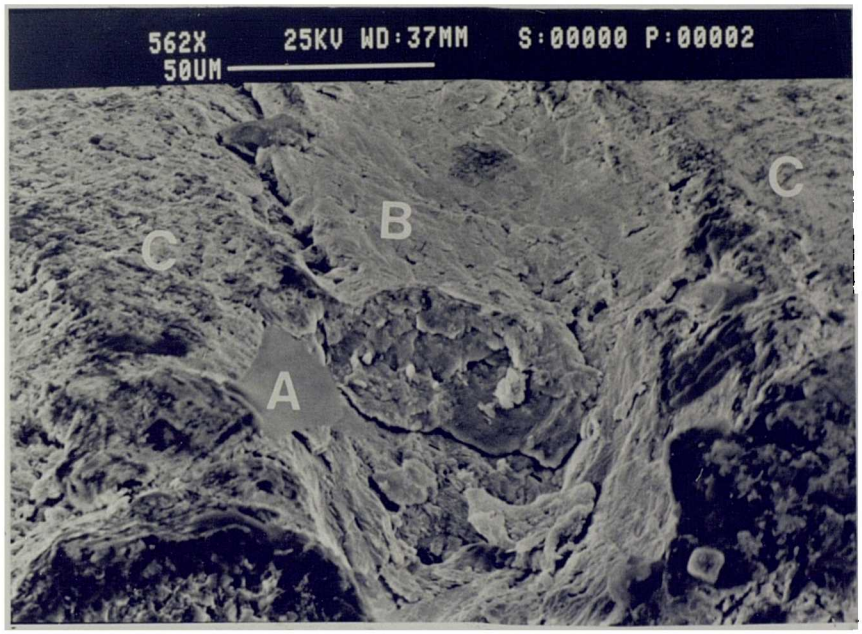

Fig 4.137 Enlarged view of Fig 4.136.

The overall rate of wear at the speed of 250 m/min was slightly greater than at 200 m/min, and consequently the cutting times required to produce an equivalent amount of wear were shorter. After 3 minutes cutting, a smooth topography was visible in the crater zone, where workpiece material is adhered to form a protective layer (Fig 4.138).

After cutting for 10 minutes, the tool produced identical patterns of wear to that observed on a tool at lower speed, where the previously formed metallic layers flattened over the entire contact area (Fig 4.139). The layers of workpiece material have elongated in the direction of chip flow. Further increases in cutting time (total 17 minutes) lead to the removal of the adhered layer with fractured particles of tool and workpiece being dragged away along the rake face (Fig 4.140).

Again it was decided to terminate the cutting procedure after 22 minutes cutting in order to conserve the limited amount of workpiece and to avoid the failure of tool by fracturing since numerous cracks were developed in the brazed material (Fig 4.141).

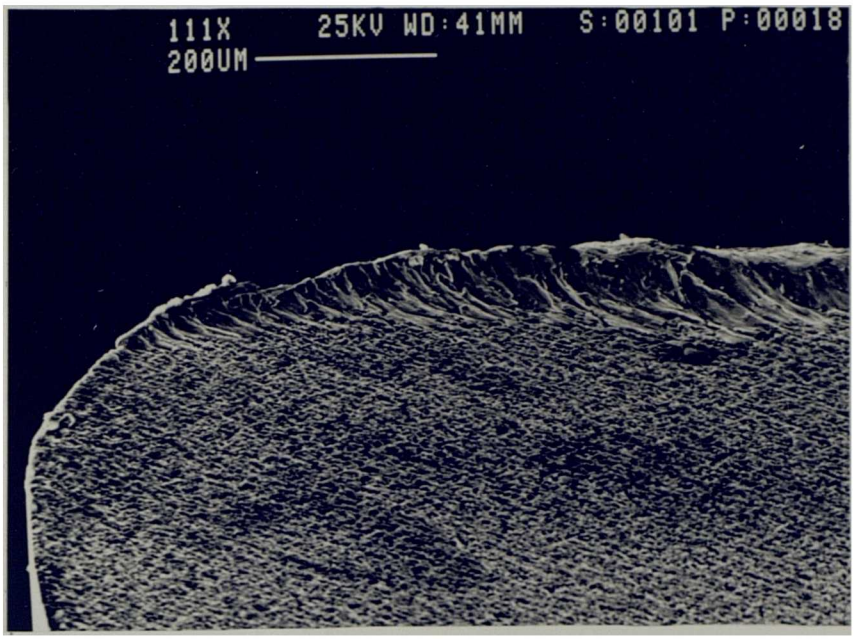

Fig 4.138 Formation of deposited layers on the rake face of PCD insert machining at the speed of 250 m/min.

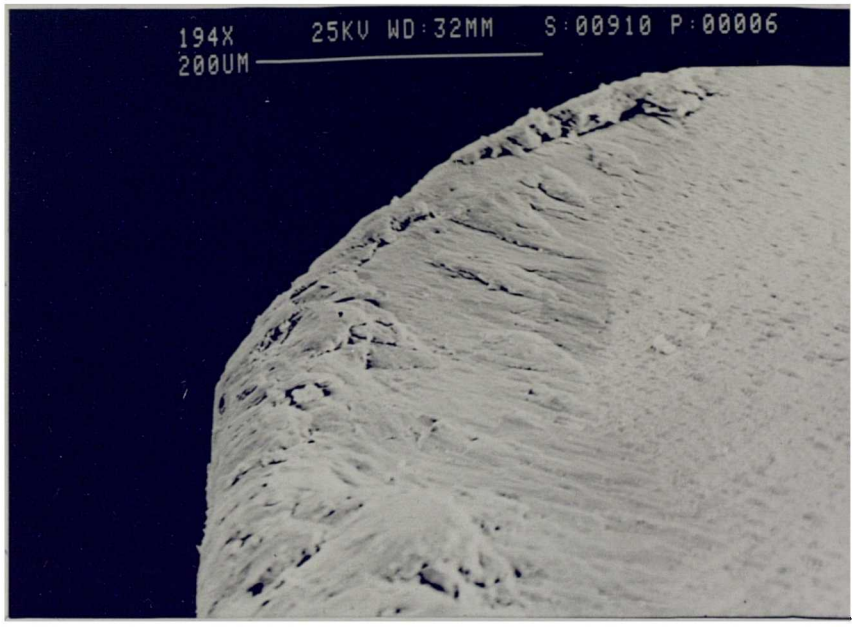

FIg 4.139 Flattening of deposited layers on the rake face of PCD insert.

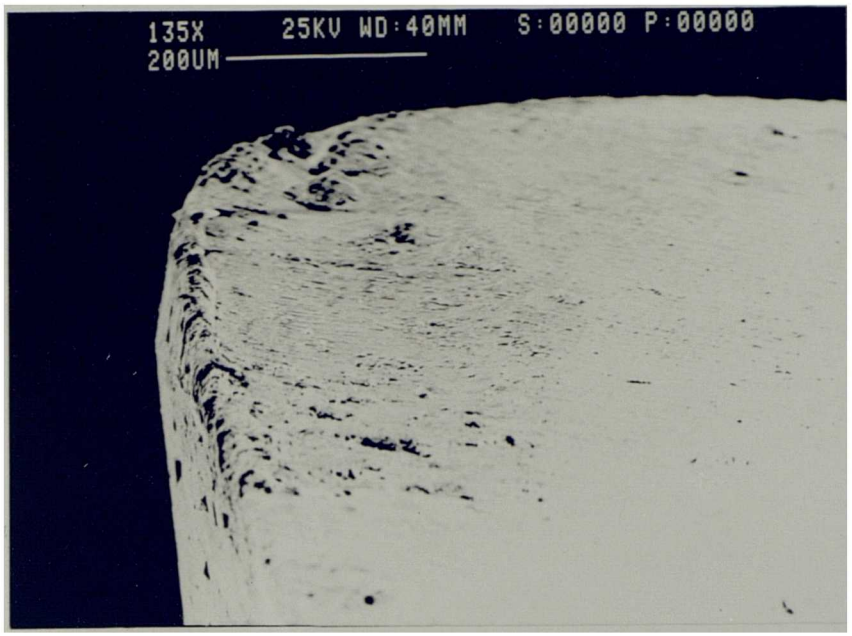

Fig 4.140 Smooth wear observed on the rake face of PCD insert.

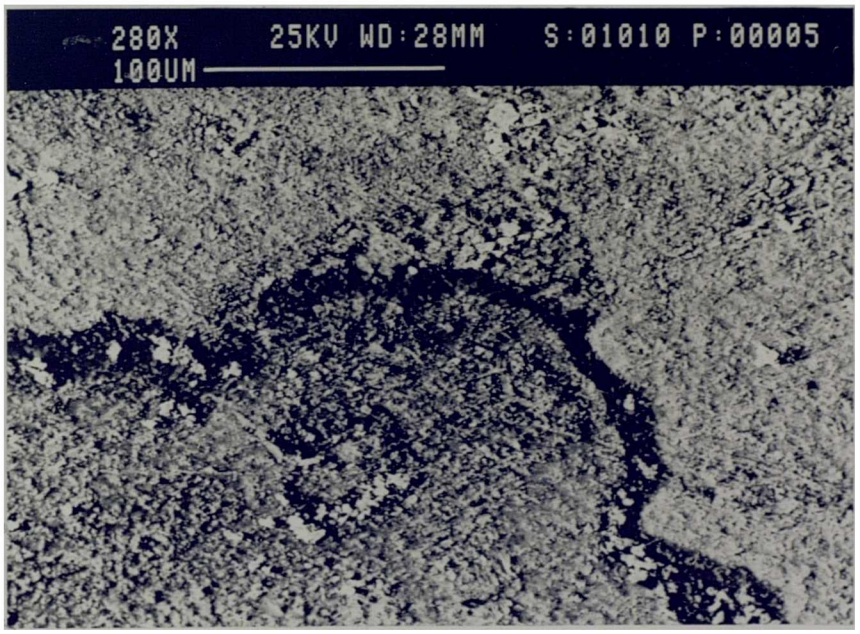

Fig 4.141 Development of crack on the brazed WC material due to thermal expansion.

4.5 QUICK STOP RESULTS

4.5.1 INTRODUCTION

The majority of quick stop samples were taken whilst cutting titanium alloy at a speed of 100 m/min with carbide and polycrystalline inserts. Quick stop swarf samples were examined in addition to the swarf collected during the normal machining.

Both quick stop samples and corresponding chip specimens were examined by S.E.M and optical microscopy so that adhesion conditions obtaining in the chip/tool interface could be assessed. Furthermore, special attention was paid to the nature of chip segments.

4.5.2 EXAMINATION OF CHIPS PRODUCED WHEN MACHINING TA48

In this work many representative chips were examined to establish a possible explanation of tool wear mechanisms by the form and flow of the chip. All but one chip sections illustrated in this work were produced with the quick stop technique (see Chapter 3). The remaining one (as shown in Figure 4.142) was obtained by sectioning pieces of swarf, produced during normal machining. It was not easy to produce good quick stop chip specimens when cutting titanium alloys. The chip had a tendency to remain adhered to the tool and be torn away from its root on the workpiece. The chip sometimes also became detached from the tool. In some cases, it was necessary to repeat the tests, because of these problems.

When machining titanium alloys, samples of the chips were produced by sawing to measure the average thickness. The thickness of chips was measured only approximately due to their complex curly forms. A second characteristic of the

titanium alloy was the saw-tooth shape, especially visible at the top of the chips. The estimation of the thickness of the chips was carried out by averaging several values obtained from the measurement of chips with a micrometer. This method did not seem to be very accurate, with the thickness varying between 0.2 and 0.3 mm (0.25 mm being the most frequent value). There is however, a tendency for chips to become slightly thinner with increasing cutting speeds. The chips formed by PCD were curly and long, and remained the same throughout the cutting ('A' at Fig 4.143). While using carbide and CBN tools the chips remained straight ('B' and 'C' at Fig 4.143), with only a small amount of curling at low cutting speeds, in terms of the speed range of the titanium alloy being machined. At higher speeds (100 m/min), the curl was still slight, but the swarf took the form of the chip, curling away from the tool nose. With a further increase in machining speed for the titanium alloy, the chips tended to be tangled in form and, at very high speeds above 200 m/min, they became flat and straight. Reasonably flat and straight chips were again subjected to thickness measurement by using optical microscopy. This method gave similar values to those obtained with the micrometer. The general chip form is segmented comprising narrow bands of intense shear between which there is deformation of the structure, such that the Alpha (α) grains are elongated in the direction of chip flow (Fig 4.144).

Quick stop experiments conducted on all of the tool inserts used in this work caused the tips to fracture such that the cutting edge and part of rake face of the tool remained bonded to the chip underside (Figs 4.145-4.148).

The quick stop experiments confirmed that bonding across the majority of the chip/tool interface was essentially similar for carbides (coated and uncoated) and CBN tools. Metallographic sections of the carbide and CBN tools revealed a continuous segmented chip form, with a well developed flow zone adjacent to the

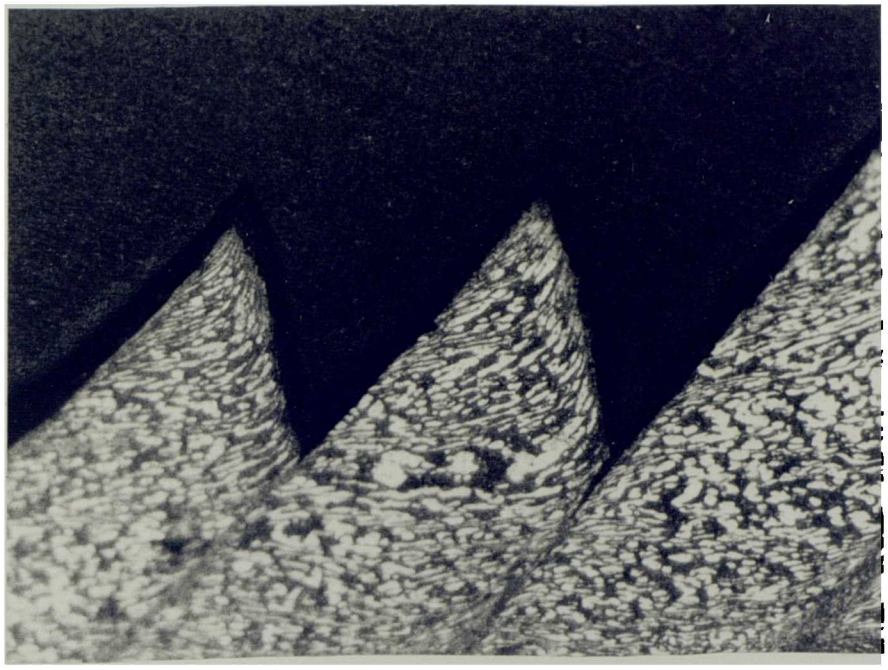

Fig 4.142 Section through forming titanium alloy chip, showing saw-tooth type of chip mode.

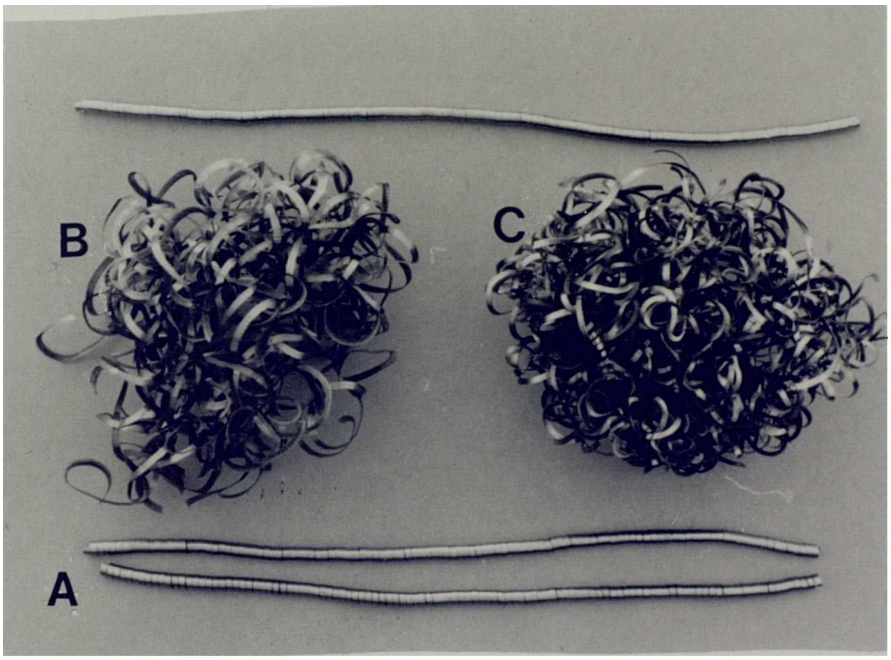

Fig 4.143 Chip shapes produced during machining of titanium alloy.

chip underside (Figs 4.144, 4.145c, 4.146b and 4.147b). The bond strength across the chip/tool interface is less for the polycrystalline insert than for the carbide tools.

Examination of the newly-formed workpiece surface which had been in contact with the flank face revealed a rougher surface than that of the PCD insert quick stops. There was obvious evidence of flank contact area with carbide tools (Figs 4.145b and 4.147b).

A normal section cut back to half the depth of cut from the quick stop between CBN and titanium alloy, revealed that a substantial part of the chip flow zone had been removed by the separation of the tool, confirming that separation between chip and tool occurred at the interface rather than above it. Evidence of loss of workpiece material from the secondary new surface was seen, which indicates a strong bonding between flank face and the workpiece (Figs 4.147b,c).

The PCD chips were continuous but they fractured with little area of contact between the tool/chip since the contact length remains at a low level. Thus the machining will take place at low energy consumption, and from the practical machining point of view, PCD is probably the most satisfactory tool material. It machines with low energy consumption, gives form of chips, which is important in chip disposal, and produces an excellent workpiece surface finish.

Figure 4.142 reveals the structure of the chip more clearly, where the saw-tooth form of the top of the chip is typical. The grains of the workpiece material have been stretched out at an angle of about 15 $^{\circ}$ to the bottom of the chip. While the adiabatic bands of intense shear are elongated at an angle of 45 $^{\circ}$. However, a close examination revealed certain regions to be more deformed than others. Notably an apparently structureless layer at the bottom of the chip has experienced intense shear. A layer of material rich in titanium exists between the tool and chip in the region of contact (Figs 4.145c and 4.147b).

Fig 4.144 Alpha (α) grain elongated in direction of chip flow (1000X).

Fig 4.145a Section through 'quick stop' specimen showing part of coated carbide (KC850) tool adhering to underside of chip (100X).

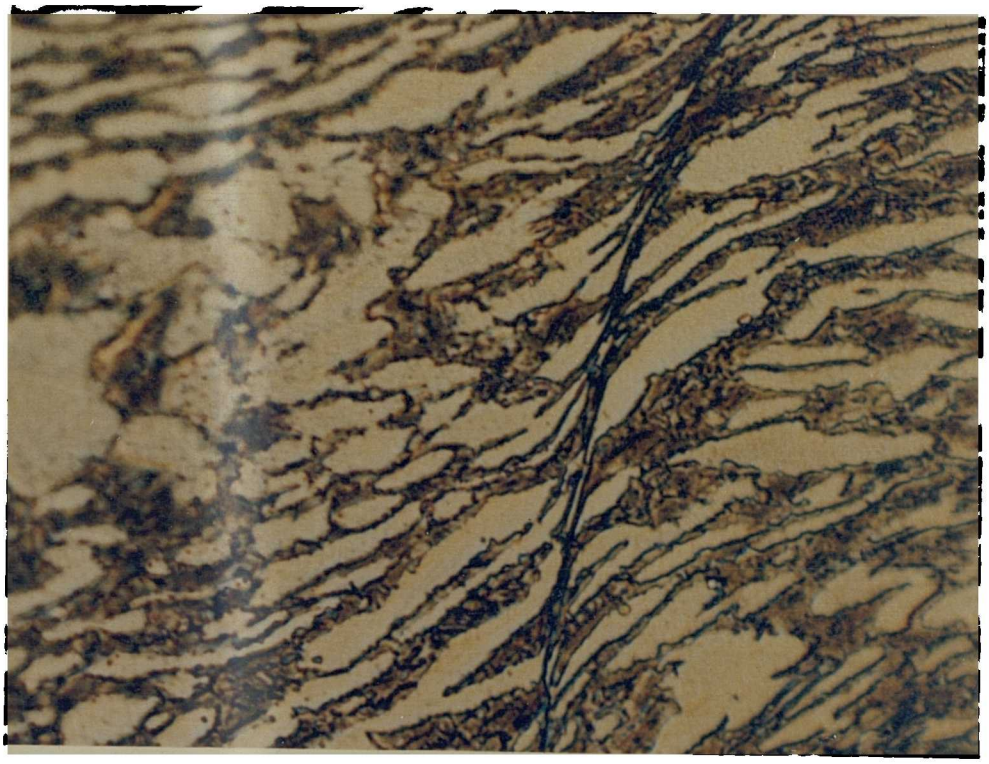

Fig 4.144 Alpha (α) grain elongated in direction of chip flow (1000X).

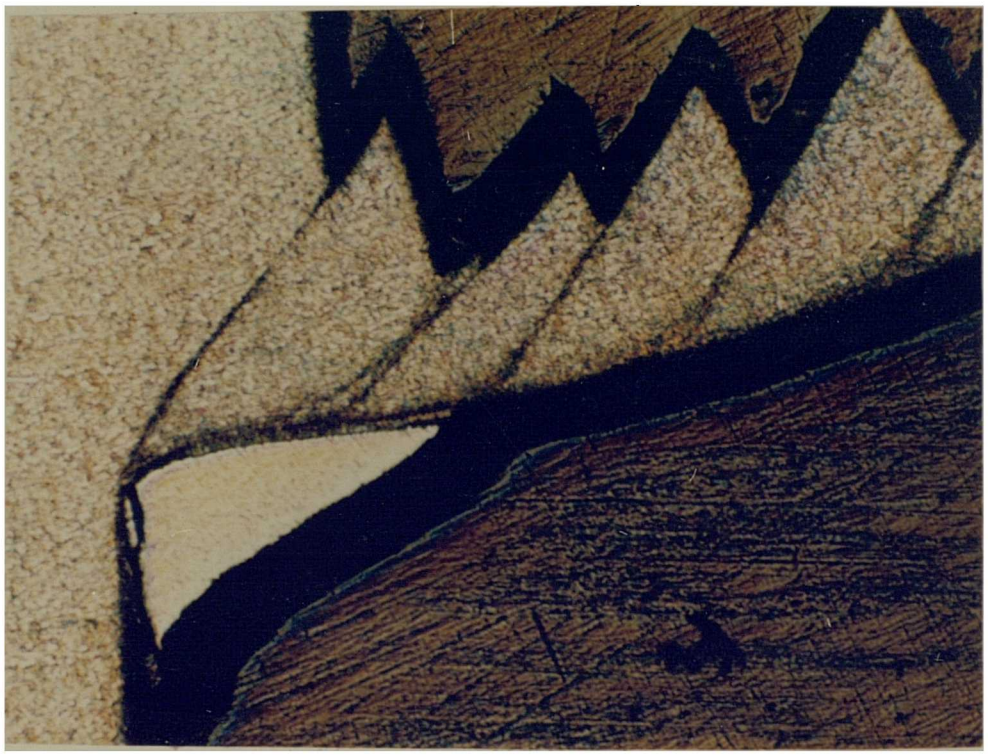

Fig 4.145a Section through 'quick stop' specimen showing part of coated carbide (KC850) tool adhering to underside of chip (100X).

Fig 4.145b Enlarged view of (a) showing tool particles attached to the newly surface formed (400X).

Fig 4.145c Flow zone on the rake face of coated carbide (KC850) tool (200X) .

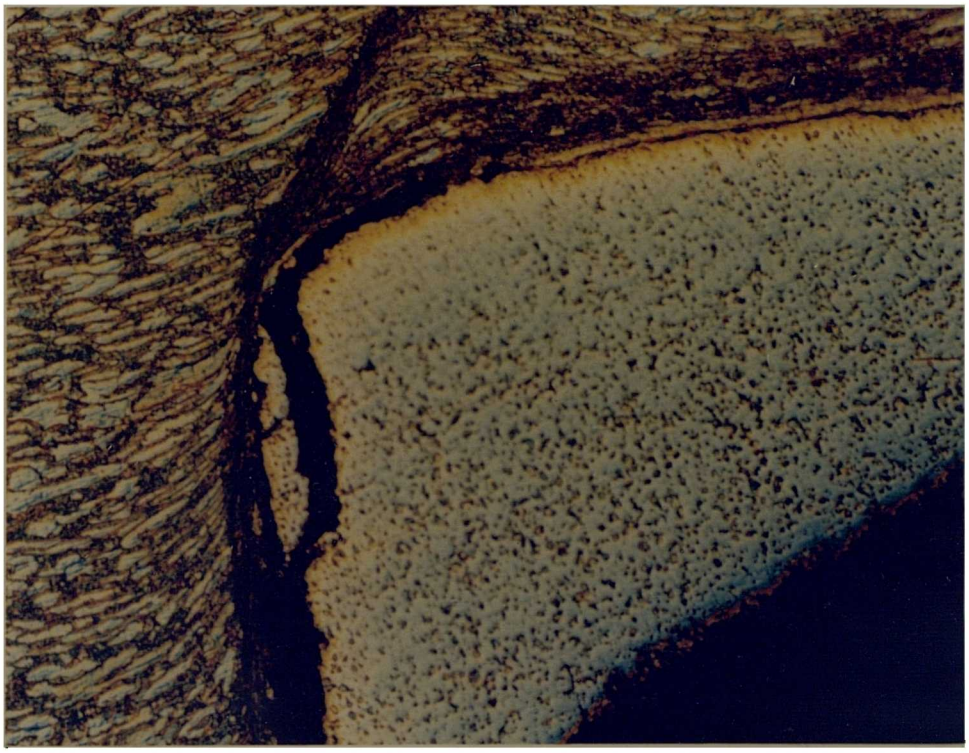

Fig 4.145b Enlarged view of (a) showing tool particles attached to the newly surface formed (400X).

Fig 4.145c Flow zone on the rake face of coated carbide (KC850) tool (200X) .

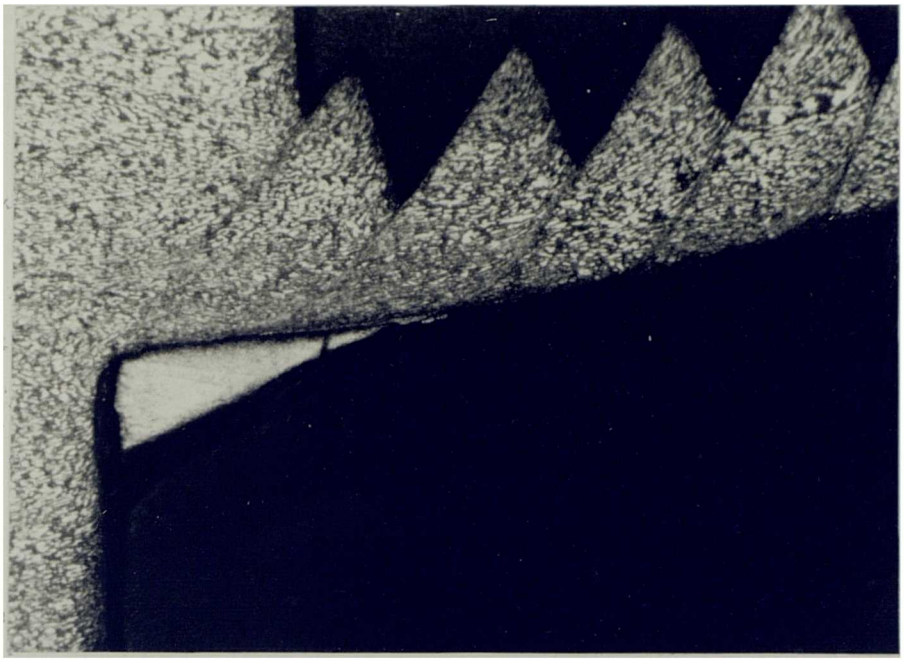

Fig 4.146 a) Section through 'quick stop' specimen showing part of carbide (K68) tool adhering to underside of chip.

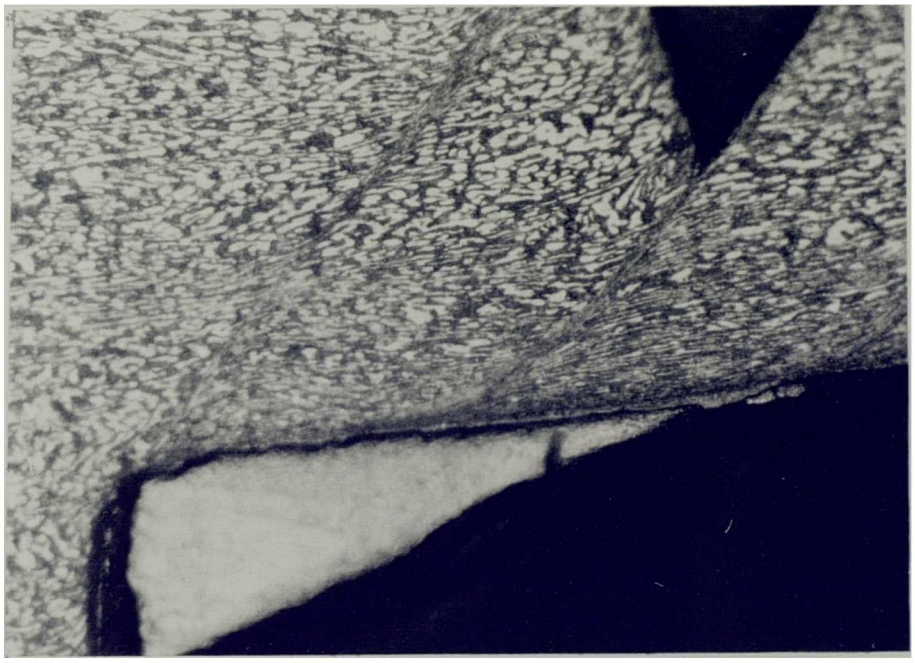

b) Close-up view of a) showing a flow zone region.

Fig 4.147a Section through 'quick stop' specimen showing part of cubic boron nitride tool adhering to underside of chip (100X).

Fig 4.147b Enlarged view of (a) showing CBN tool particles attached to the newly surfac formed (400X).

Fig 4.147a Section through 'quick stop' specimen showing part of cubic boron nitride tool adhering to underside of chip (100X).

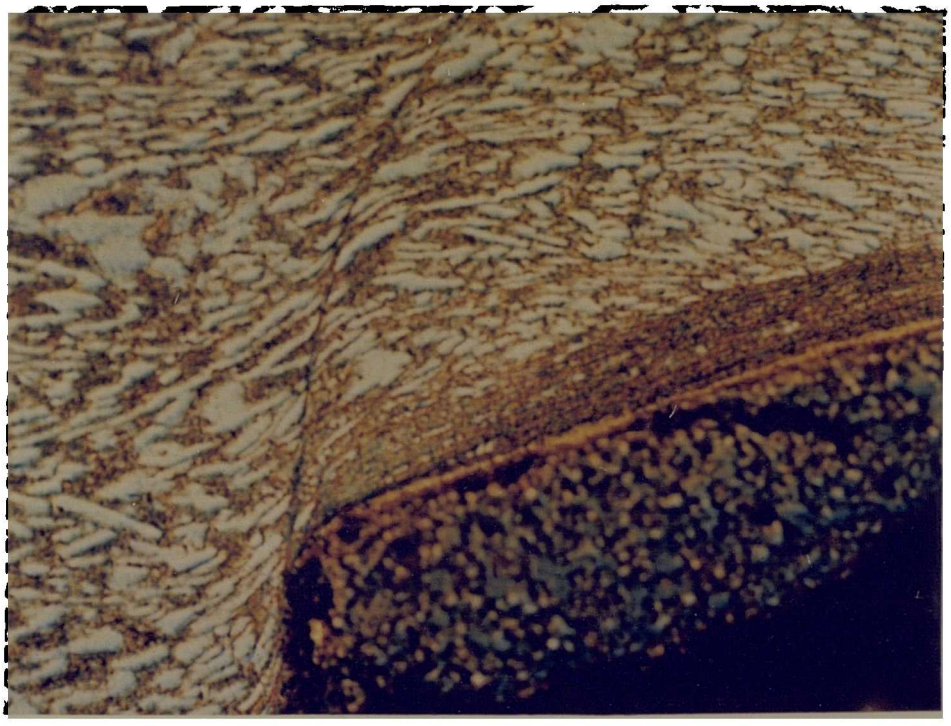

Fig 4.147b Enlarged view of (a) showing CBN tool particles attached to the newly surfac formed (400X).

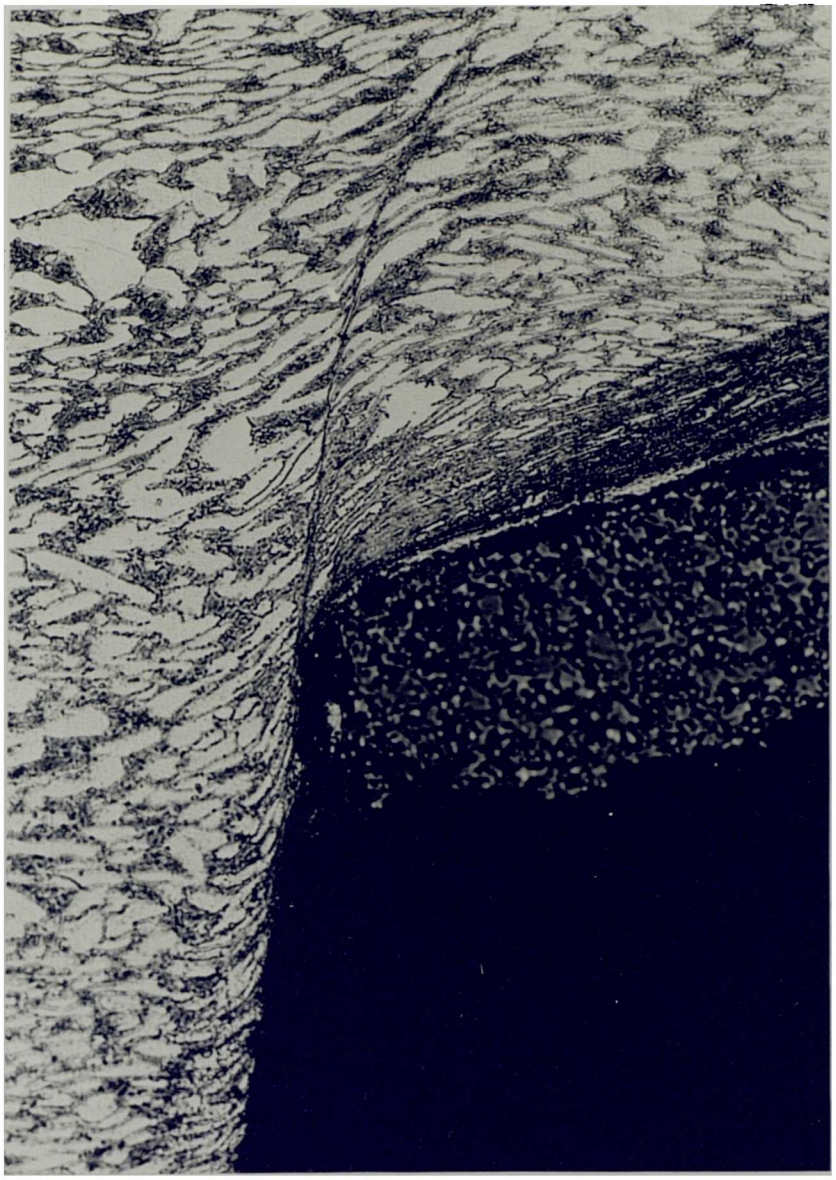

Fig 4.147c **Close-up view of a)**

Fig 4.148a Section through 'quick stop' specimen showing fragments of PCD tool adhering to underside of chip (50X).

Fig 4.148b Close-up view of (a) (200X).

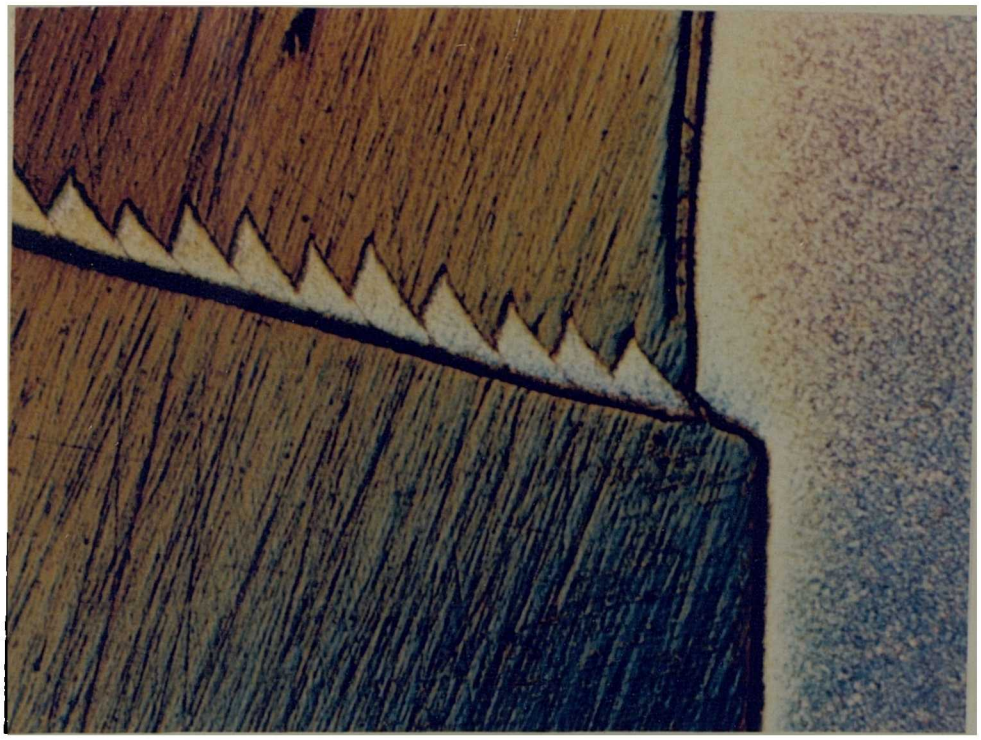

Fig 4.148a Section through 'quick stop' specimen showing fragments of PCD tool adhering to underside of chip (50X).

Fig 4.148b Close-up view of (a) (200X).

The examination of coated carbide tools after quick stop tests indicates that the coated layers were rapidly removed after cutting for only 10 seconds. It seems that, due to the effect of high temperature, the coated layers were removed by the underside of swarf leaving the WC substrate vulnerable for cratering wear. Furthermore, the TiC layer did not act as a diffusion barrier as earlier reported (2). In order to observe the coated layer more clearly, the specimen of carbide with double-coated layers was produced, using the quick stop technique. This specimen was photographed in the unetched state, and Figure 4.149 illustrates the strong bond between the chip and tool rake face, where the workpiece chip is penetrating the rake face, forming a crater. This was done after removal of coated layers and exposing the substrate, at a distance away from the cutting edge. A similar pattern of wear was observed with KC850 carbide triple coated layers.

Upon increasing the depth of cut at a higher speed (100 m/min), the form and shape of chip changed. While using the PCD tool it remained the same as that of one observed at lower speed and lower depth of cut, where the chip was curling and long (see Figure 4.150). The CBN tool showed an almost identical form of chip to the one produced at the lower depth of cut.

There were significant differences in the performance of the carbide tools in term of chip formation as the depth of cut was increased. Due to the existence of high interface temperatures the swarf becomes very brittle and then becomes friable, after only 10 seconds cutting. This behaviour is clearly illustrated in Figure 4.151.

The newly generated underside of the chip surfaces were also examined for evidence of detached carbides or polycrystalline tool material. In Figures 4.152 and 4.153 such particles of carbide and Amborite could be seen adhering to the underside of swarf, aligned in the direction of chip flow.

Fig 4.149 Section through 'quick stop' unetched specimen showing part of KC910 tool adhering to underside of chip(400X).

Fig 4.149 Section through 'quick stop' unetched specimen showing part of KC910 tool adhering to underside of chip(400X).

Fig 4.150 Chip form by cutting tools under high speed & large depth of cut.

Fig 4.151 Chip formation of Carbide tools at high speed (high temperature).

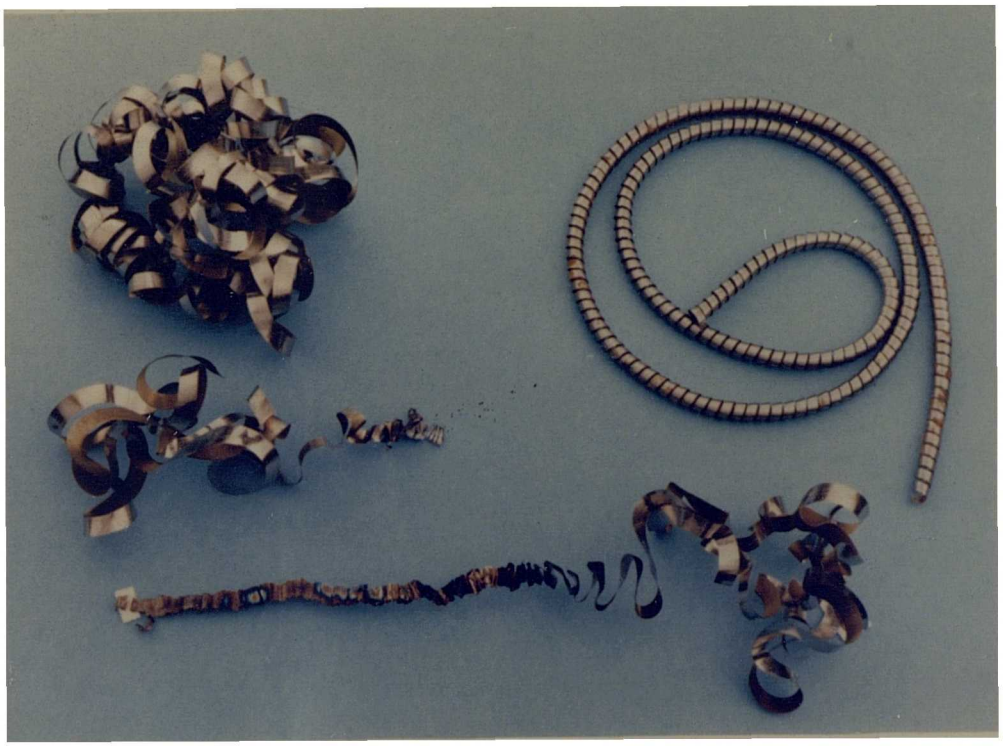

Fig 4.150 Chip form by cutting tools under high speed & large depth of cut.

Fig 4.151 Chip formation of Carbide tools at high speed (high temperature).

Fig 4.152 Clusters of CBN particles adhering to underside of chip form during cutting.

Fig 4.153 Carbide tool particles adhering to underside of chip form during machining.

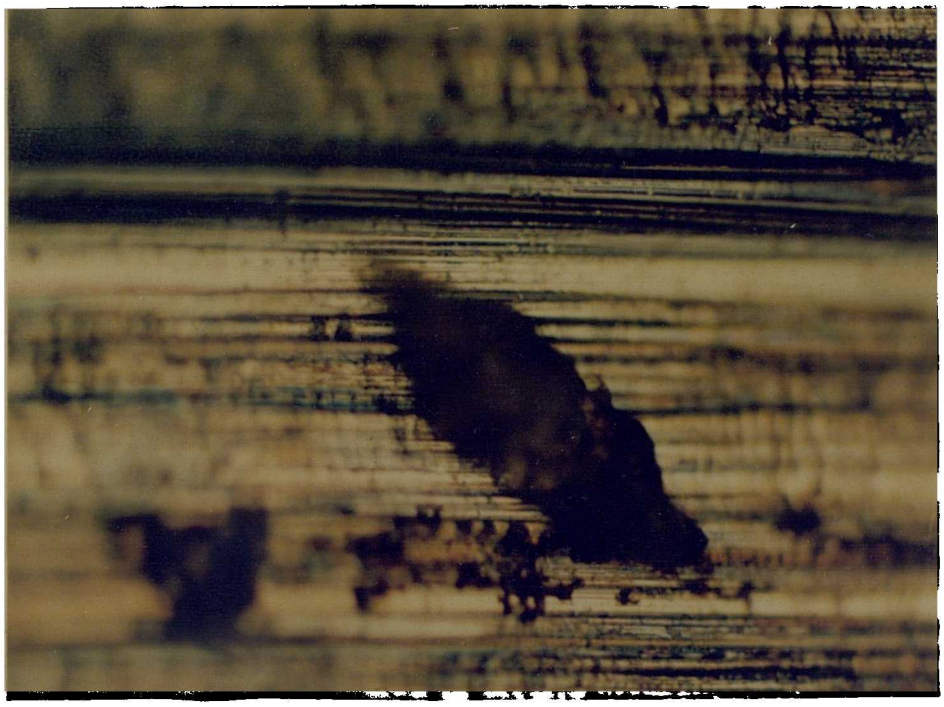

Fig 4.152 Clusters of CBN particles adhering to underside of chip form during cutting.

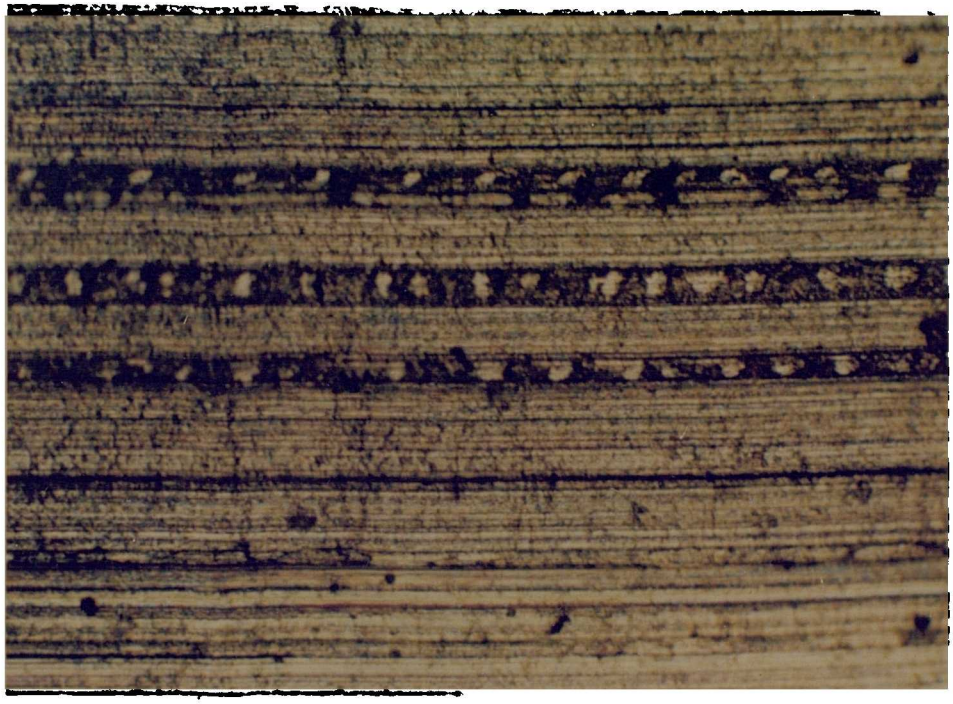

Fig 4.153 Carbide tool particles adhering to underside of chip form during machining.

4.6 FORCES GENERATED DURING MACHINING

Three components of force were recorded during the machining tests, the normal force, feed force and radial force (Fig 4.154a).

A plot of the recorded components of force at various cutting speeds when machining titanium alloy with all cutting tools are presented in Figures 4.154-4.159. These figures show that the normal force is greater than the feed and radial forces under all the cutting conditions (Figure 4.154-4.156). The radial force is always higher then the feed force but lower than the normal force. All the forces increased with cutting speed up to 50 m/min and then either decreased significantly, or (less often) remained constant.

The highest values of cutting forces were recorded at the speed of 50 m/min when using coated and uncoated carbide tools (Figure 4.154-4.156). The increase in the forces at the cutting speed of 50 m/min compared to speed of 25 m/min, could be due to the presence of a built up edge.

The lowest forces were recorded when using PCD at all cutting speeds, and it was followed by KC850 up to the speed of 100 m/min, where further increase in speed resulted in the reduction forces for CBN tool, and an increase for the KC850 insert. This is followed by KC910 and K68 carbide tools. Close values of cutting forces were recorded for coated and uncoated tools at the speed of 200 m/min. This effect could be due to the removal of coated layers, and cutting with direct contact with substrate.

Figures 4.157-4.159 illustrate the cutting forces which were generated at the speed of 100 m/min, after 30 seconds machining. Again the PCD showed the lowest cutting forces.

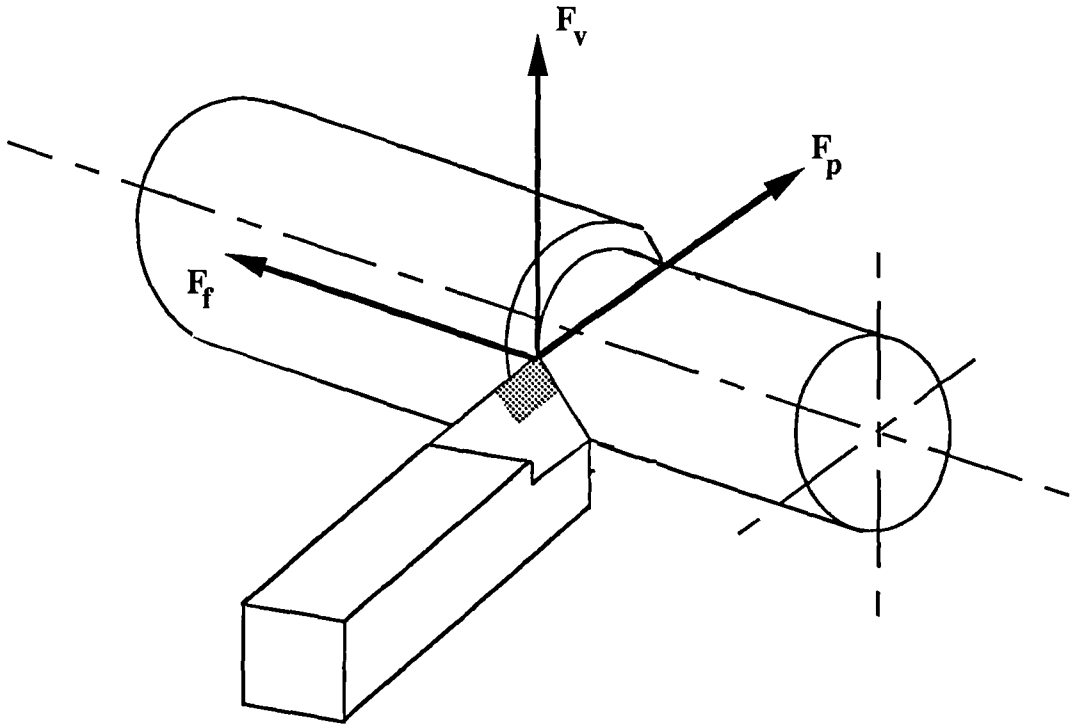

Fig 4.154a Cutting forces in conventional turning

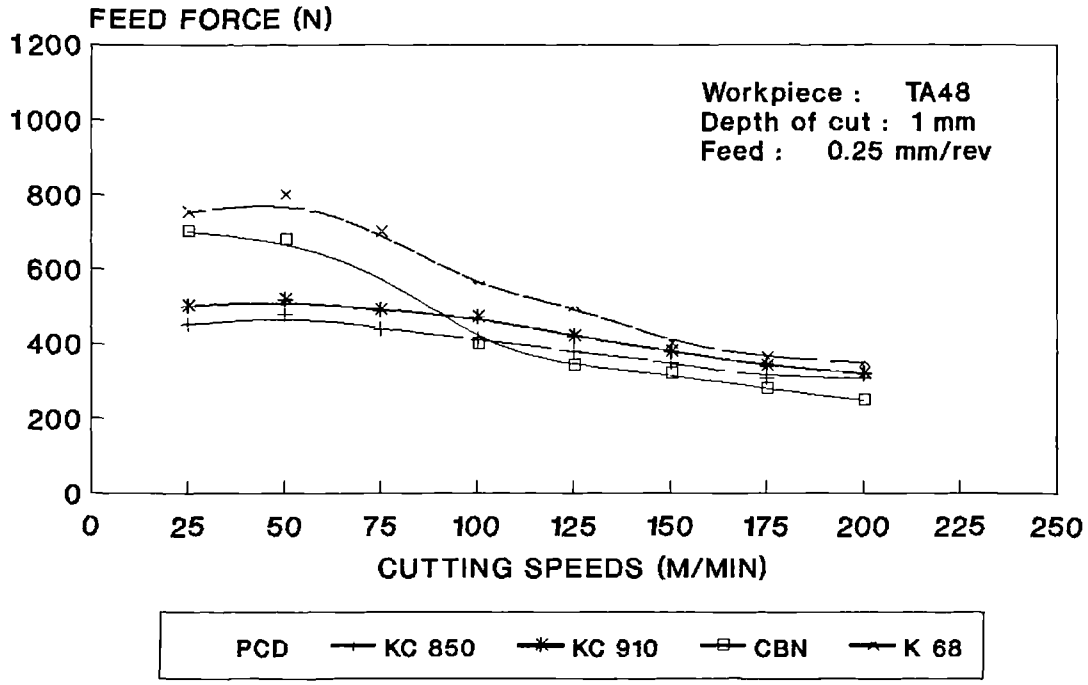

FIG 4.154 FEED FORCE VS. CUTTING SPEEDS

RADIAL FORCE (N)

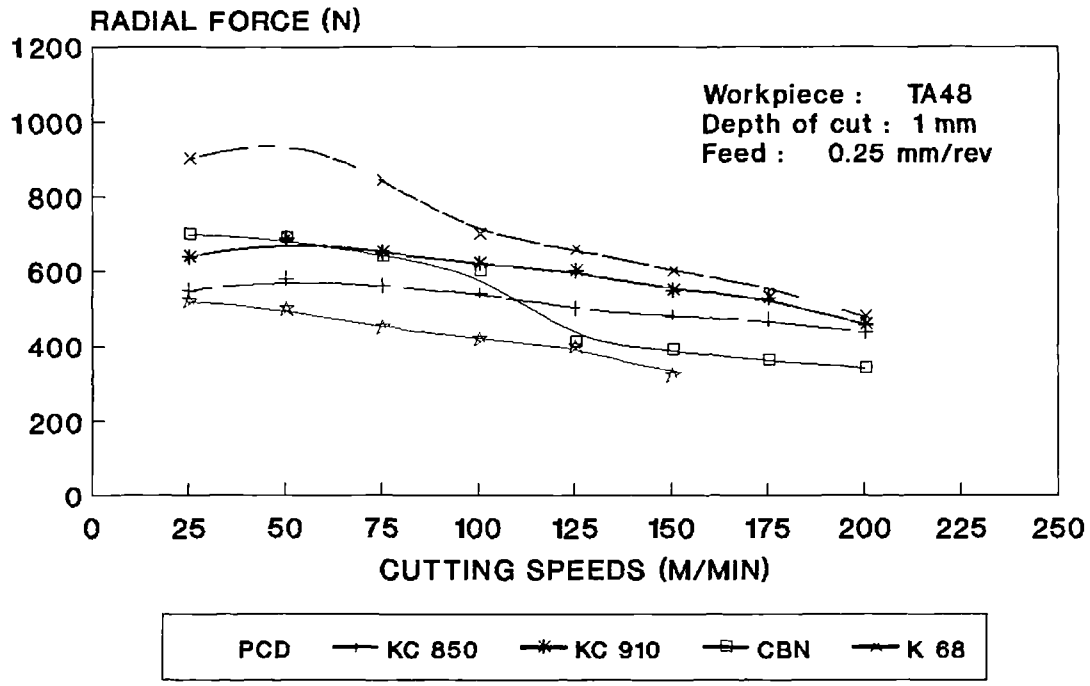

FIG 4.155 RADIAL FORCE VS. CUTTING SPEEDS

NORMAL FORCE (N)

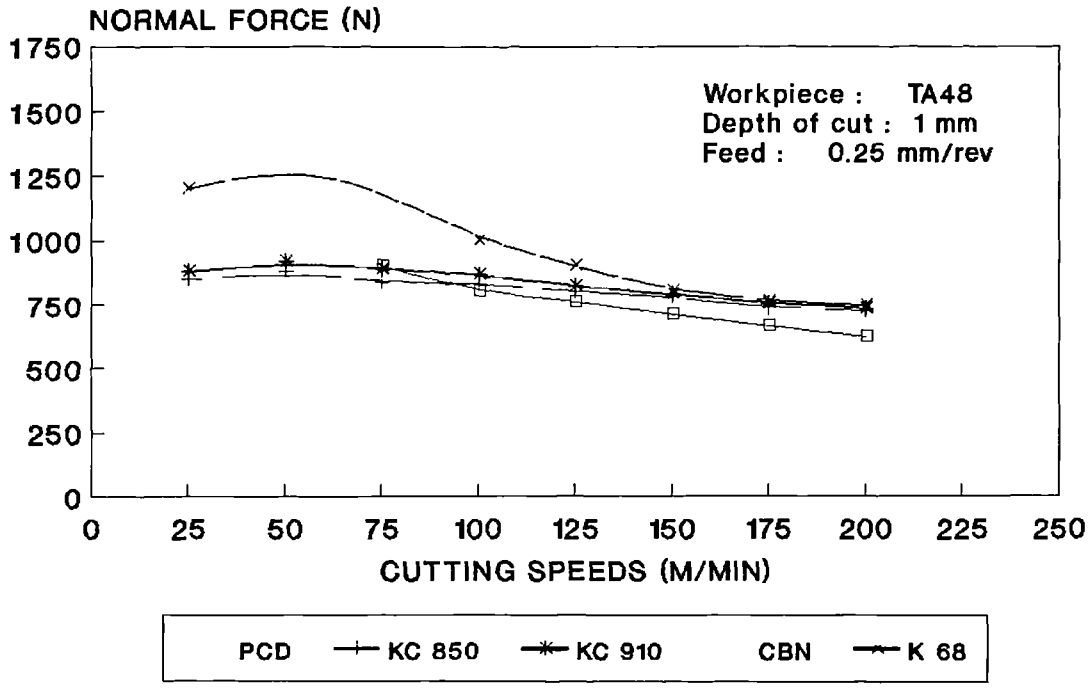

FIG 4.156 NORMAL FORCE VS. CUTTING SPEEDS

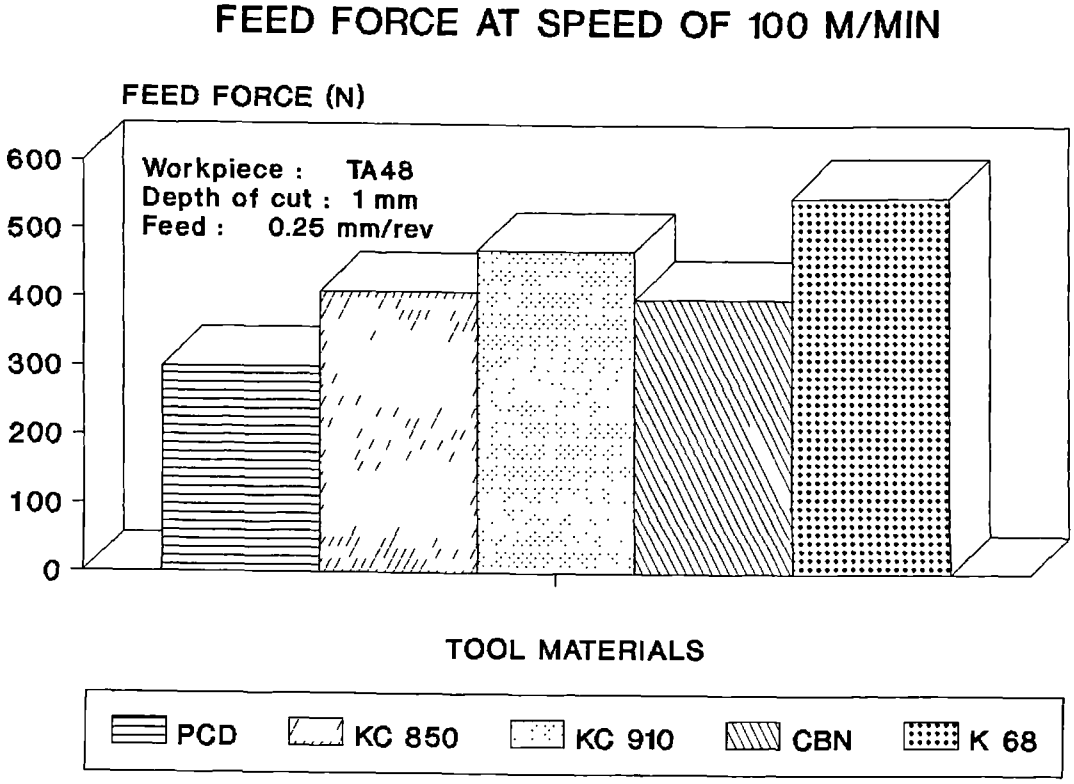

FIG 4.157 FEED FORCE VS. CUTTING SPEED OF 100 M/MIN

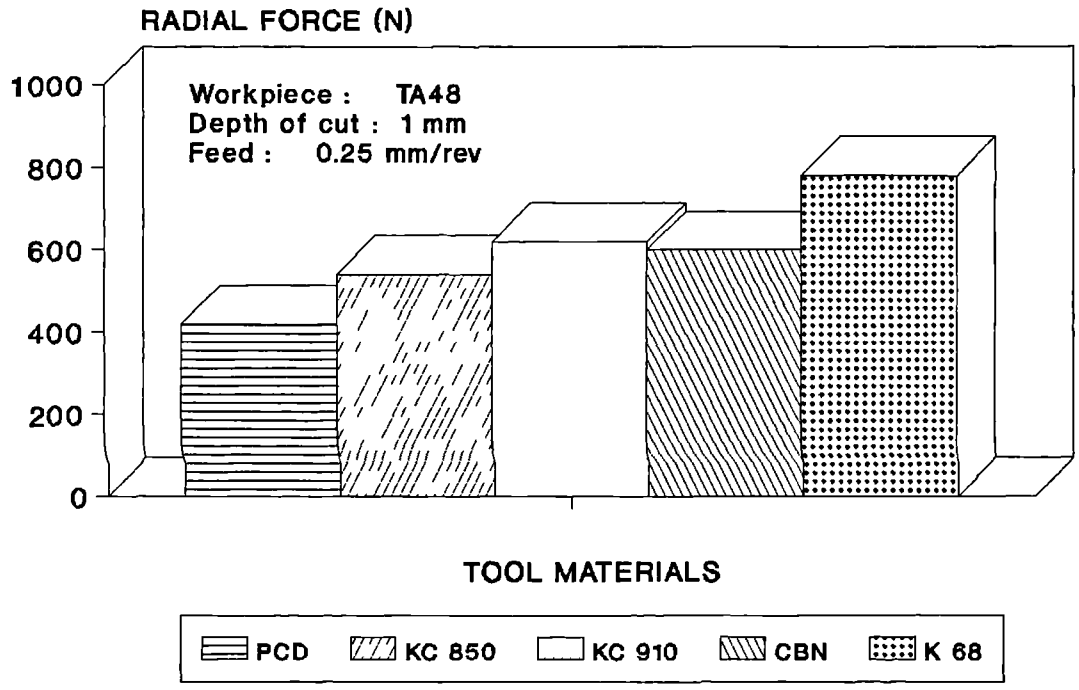

FIG 4.158 RADIAL FORCE VS. CUTTING SPEED OF 100 M/MIN

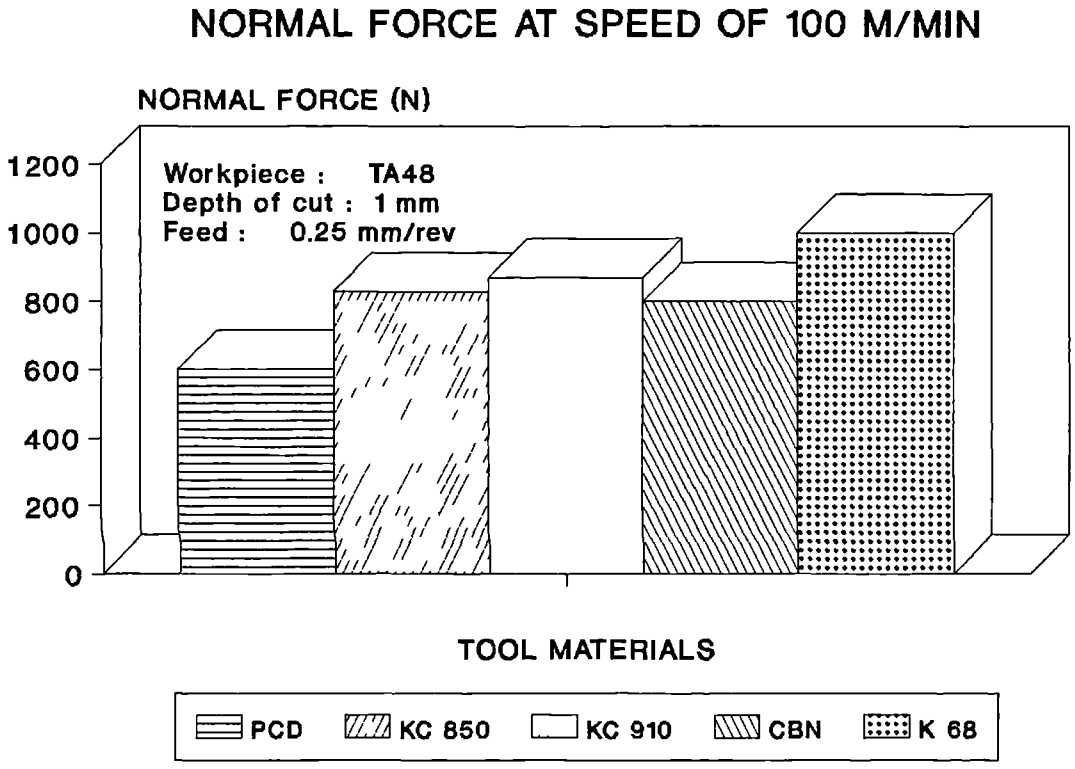

FIG 4.159 NORMAL FORCE VS.CUTTING SPEED OF 100 M/MIN

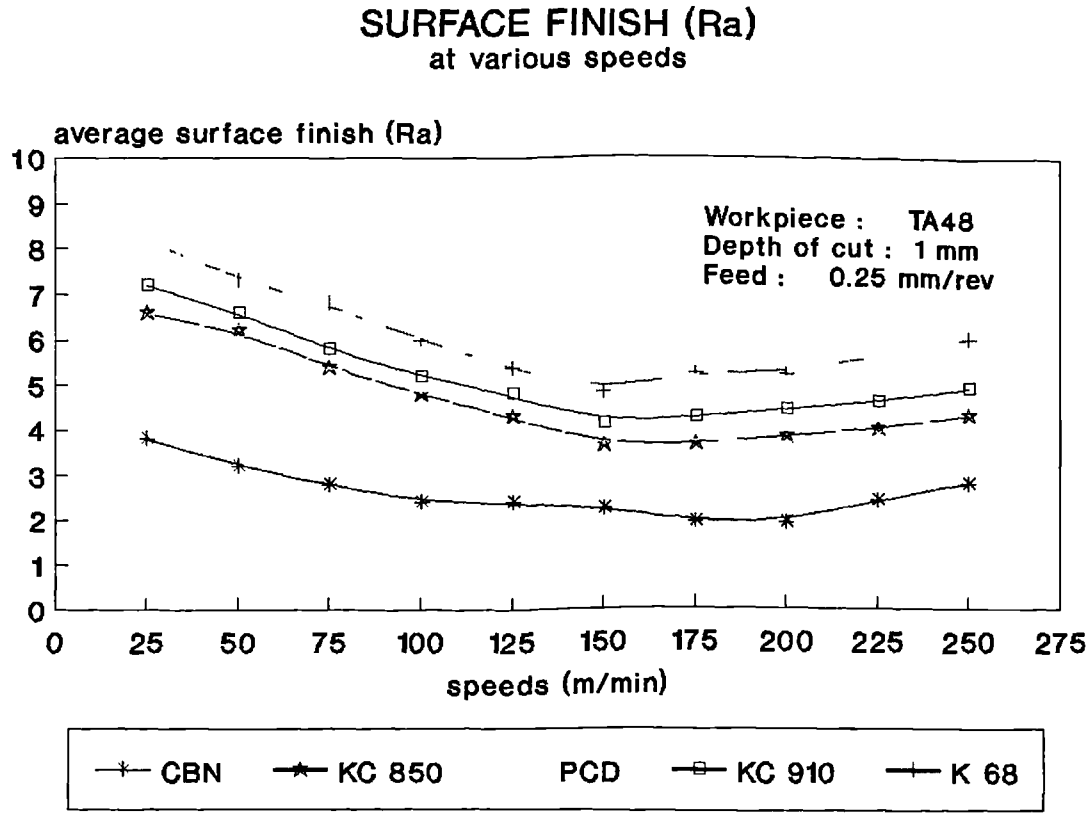

Fig 4.160 cutting time vs. roughness

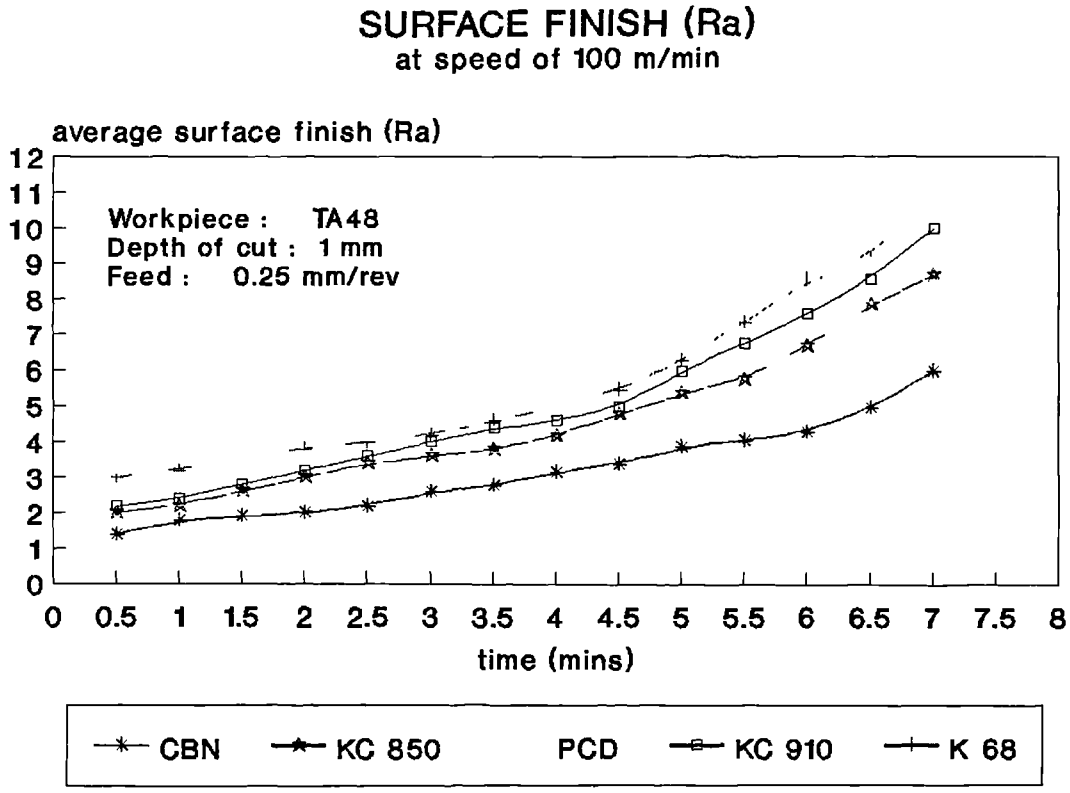

Fig 4.161 cutting time vs. roughness

There was a significant difference in forces when carbide tools were used in contrast to polycrystalline tools. The cutting forces generated when cutting with carbide tools is far more than those obtained when cutting with the polycrystalline tools. This means that the power consumption by the lathe when cutting with the PCD and CBN is significantly lower than that when cutting with carbide.

4.7 SURFACE ROUGHNESS

The roughness of a machined surface can be of importance due to its direct influence on the fatigue performance of stressed components and the wear of counter faces. Surface finish, measured as a function of the cutting speed was determined along the workpiece as described in Chapter 3, for carbide (coated and uncoated) and polycrystalline tools (PCD and CBN). The tests were carried out with the feed of 0.25 mm/rev and depth of cut of 1 mm. The results are presented in Figure 4.160. This graph shows that high surface finish values were recorded at low cutting speeds with K68 at speed of 25 m/min.

The effect of cutting speed on the surface finish generated when machining titanium with PCD can be seen in Figure 4.160. Increasing the cutting speed led to gradual improvements in the surface roughness as the speed increased from 25 to 200 m/min.

Cubic boron nitride (CBN) shows a similar pattern to PCD, and the best surface finish value of 2 micron (Ra) was recorded at the speed of 200 m/min. There was a gradual improvement in the surface finish as the speed increased.

Coated carbide tools gave a relatively poor surface finish at low speeds (Fig 4.160). The surface quality was improved with the increase in speed. The best surface finish of 3.6 microns (Ra) was recorded at the speed of 175 m/min with KC850, and further increase in speed (200 m/min) resulted in deterioration of the surface finish. Double coated layer carbide tools (KC910) showed a gradual improvement in surface roughness as the speed increased from 25 to 200 m/min. Uncoated carbide tools showed a sharp deterioration in the surface finish as the speeds were increased from 150 to 200 m/min.

Summarizing the data shown in Figure 4.160, it can be seen that the best finish of 1 μm (Ra) was observed at speed of 200 m/min for PCD and the corresponding values for the other tools were:

CBN ..... 2 μm at speed of 200 m/min.
KC 850 ..... 4 μm at speed of 150 m/min.
KC 910 ..... 5 μm at speed of 150 m/min.
K 68 ..... 6 μm at speed of 150 m/min.

Figure 4.161 shows the deterioration of surface quality in response to increasing cutting time. In this figure, a graph of surface finish against cutting time at the speed of 100 m/min is plotted. From these curves it can be observed that the PCD produced a better surface finish compared with other inserts at the same speed. Cubic boron nitride is the second best to the diamond in producing a good surface finish. As the cutting continued, the PCD and CBN showed an increasing and constant rate of surface deterioration whilst the carbide tools have an accelerating rate after about 4 minutes cutting time.

CHAPTER 5

DISCUSSIONS

5.0 DISCUSSIONS

5.1 WELDED JUNCTIONS

The use of workpiece:tool adhesion tests to evaluate candidate cutting tool materials appears promising in that both the critical welding temperature and the failure of the bulk or substrate material were identified. It also enables detailed chemical analysis of interfacial reaction between tool and workpiece to be carried out using SEM/EDX techniques.

When the junctions formed between the workpiece and polycrystalline tools are subsequently broken. there are three possible routes for crack propagation - ie through the workpiece, the interface or the bulk of the tool material. However, there are a greater number of possibilities for the coated carbide tool since failure might also take place within the coating or at its interface with the substrate. In the event, in this work, failure was always through the bulk of the polycrystalline or tungsten carbide tools (Figs 4.1, 4.5, 4.10 and 4.21). At higher magnifications (Fig 4.13) it can be seen that the cracks in the tungsten carbide had propagated around the hard particles - presumably through the cobalt phase. In other work in this laboratory, primarily designed to measure the critical resolved shear stress of ceramic crystals, the incidence of sub-surface lateral cracking (sometimes referred to as 'venting') in the bulk of the harder crystal is quite common - even at temperatures in the region of 1000 $^{\circ}$C. In normal indentation studies, such cracks are thought to be formed at the elastic:plastic boundary as a result of tensile stresses developed by the recovery of compressive plastic strain as the load is removed. On the assumption that the critical resolved shear stress of tungsten carbide is comparable with that of titanium carbide at 800 $^{\circ}$C, ie 0.25 GPa (178), the contact pressure applied by the titanium alloy cone might have been sufficient to produce a degree of plastic deformation. Therefore it is possible that, under the conditions obtaining in this study, lateral cracks are initiated

during unloading at the welding temperature and are then propagated through to the surface when the junction is pulled apart at room temperature. Such crack formation with PCD or CBN is less likely since the critical resolved shear stress would be considerably higher - eg. about 1 GPa for diamond (179).

A more likely crack initiation mechanism is now thought to be associated with the differential thermal contraction of the titanium and the cutting tool materials. When the weld cools from the critical temperature, tensile stresses will be induced in the tool materials around the periphery of the weld contact area due to the greater rate of contraction of the titanium. This situation is currently being modelled to determine whether these tensile stresses could be of sufficient magnitude to account for the observed fracture (180).

It is considered significant that the failure of the substrate material, as observed using this technique, was consistently reflected in failure of the bulk material during the quick stop investigation (see Section 4.5).

5.2 TOOL WEAR

5.2.1 PRE-MACHINING STUDIES OF TOOLS

5.2.1.1 CARBIDE TOOLS

The substrates of two types of coated tungsten carbide tools, and the substrate of an uncoated tool, were examined. The examination revealed that the most distinguishable features which were expected to affect tool performance were as follows:

i) Size and distribution of porosity

ii) Grain size, distribution and uniformity of microstructure

iii) Size and distribution of carbide particles in the binder (cobalt), and

iv) Chemical composition.

All the above factors may have an influence on tool performance and thus contribute to variations in tool wear. The first three factors were detected easily by the scanning electron micrographs of cross-sections through each tool, while the chemical composition revealed by the EDX analysis gave semi-quantitative results with considerable inaccuracy due to the wide variation in composition from area to another.

A cutting tool substrate must be strong and tough. Strength is needed for wear-resistance and toughness for resistance to fracture by thermal shock and mechanical impacts. It is worth noting that these two basic requirements usually tend to be mutually exclusive such that one can only be achieved at the expense of the other. Consequently, an adequate balance must be achieved by a compromise between the two properties. This is one of the main factors that has led to the alloying of the substrates and to the advancement of surface coating technology.

It is known that the toughest tungsten carbides are those of large particle size alloyed with a high percentage of cobalt, and the most wear resistant are those with small particles and a low percentage of cobalt. Turning insert users and researchers are used to practice machining and investigating tool performance in the absence of reliable information, for a large number of commercially available tools. The lack of hard information in the technical data supplied by the various manufacturers may be deliberate in order to avoid disclosing proprietory aspects of production techniques, or it may be due to ignorance about the behaviour of their products in wide and ill-defined fields of application. It should be emphasised that this imprecise information may provide an adequate guide for production engineers, but is not satisfactary for research purposes (181-183).

The structure of the substrates of the KC910 and KC850 grades were expected to be similar but porosity was much in evidence in the former and less so in the latter.

The effect of the bulk material properties of the tool on the machining performance is more likely to be apparent either in very rough operations, or in later stages of a normal cutting operation. However, wear may be accelerated if substrate defects are close to the interface with the coating layers, or a localised defect lies under them.

The part of the tool that comes into direct contact with the work material and which is subjected to the high heat generation and frictional force is obviously its surface, and this needs to be protected from the wearing conditions encountered in metal cutting. Coated or uncoated, the surface of the tool must have the minimum number of defects because almost any kind of surface defect can have an effect on wear, and consequently on the cutting performance and tool life.

Pre-machining inspection of the surfaces of the experimental tools revealed significant surface defects. These were related to the topography of the rake face, the cutting edge and the nose radius condition.

The uncoated tools were generally free of defects other than the scattered voids on the nodular surfaces. On the other hand, the coated tools showed more than one type of surface defect. These included voids, nodules, surface irregularities, microcracks, surface inclusions and roughness.

The quality of the coating systems and the conditions of the coating/substrate interface of the coated tools are important aspects that contribute directly to the performance of the coating and life of the tool. Irrespective of the properties of a specific coating material, performance of coated tools will be influenced largely by the existence of defects within the coating layers or at the interface with the substrate. Such defects usually occur as a result of inadequate preparation of the substrate prior to the coating process, or as a result of chemical interaction during the process which should be operated under careful control.

The scanning electron microscopy study carried out on the carefully prepared cross-sections of the coated tools has revealed various defects which could have a significant influence on tool wear during machining.

All the coated tools appeared to have an additional layer between the substrate and the bottom layer of TiC. This layer, which could easily be mistaken for the TiC layer on top of it, was shown by chemical analysis to consist of tungsten and cobalt, the main constituents of the base material, in addition to titanium. This layer is termed the 'eta' phase and has been discussed by several investigators (184-186). It is a brittle layer which is formed due to the decarburization of the substrate surface during the early stages of the deposition of TiC coatings. Besides the occurrence of this brittle decarburization phase at the base material/coating interface, regions of

microporosity and localities of high void concentration were also evident in some tools. The zones of void concentration represent weak areas under the brittle layers where damage to the coating may be initiated and accelerated to result in total tool failure at early stages of machining. However, coating defects may be present even before commencing a cutting operation. Microscopic examination has revealed different forms of serious cracking of some coatings, mainly in the brittle layer zone at the coating/substrate interface. The KC910 tool had the highest frequency of these defects and was the one with most surface defects, as mentioned earlier. The tool with the least number of defects was KC850 which was coated with thin layers of TiC/Ti(C,N)/TiN. The coating itself seemed to have some porosity.

5.2.1.2 PCD AND CBN TOOLS

Generally, the integrity and microstructure of these materials were consistently free of significant defects.

5.2.2 WEAR OF CARBIDE TOOLS

5.2.2.1 FAILURE OF COATINGS

The coating and/or substrate wear processes that occurred during turning tests are illustrated in Fig 5.1. During the initial stage of cutting (inset (a) of Fig 5.1) the chip slides across the coated insert. The temperature is sufficiently low during the initial stage that the substrate is not softened and the coated insert can support the loads imposed by the cutting process. The wear at this stage is due to abrasion or dissolution. With time, however, the heat generated from the shearing of the workpiece, and from the sliding friction that occurs between the chip and coating, softens the substrate to an extent that the coating and underlying substrate cannot

support the cutting loads. At this point (as illustrated in inset (b) of Fig 5.1) the coating fractures as the substrate is plastically deformed in a manner similar to that observed in HSS inserts with CVD coatings (187). The fractured coating is eventually transported away with the moving tool chip (Figs 4.43, 4.51 and 4.58), leaving the underlying substrate exposed to the tool chip. The heat generated continues to soften the substrate and consequently the region of softened substrate expands to underlying regions of coating that are still intact. Eventually, the substrate under the coating adjacent to the crater is softened to such a degree that it cannot support the cutting forces, and the coating at the edge of the crater fractures (inset (c) in Fig 5.1). In this manner, the coating is gradually chipped away to expose more and more substrate giving way to crater formation. An example of this "chipping" effect is seen in Figures 4.40, 4.59 and 4.64.

5.2.2.2 RAKE FACE AND CRATERING

Cratering was relatively more significant when cutting with the K68 tools as can be seen from the Figures 4.78, 4.84 and 4.87. The effect of the significant crater observed on the K68 tools is to undermine the cutting edge and eventually cause its collapse (Fig 4.78). It has been suggested that the TiC in the mixed phase of K68 has a dual effect on the tool in that it increases the wear resistance of the tool and also moves the crater closer to the cutting edge (110). The increase in resistance to crater wear is to some extent counteracted by the crater being closer to the cutting edge. Then less wear can be withstood before the cutting edge is undermined and collapses. Rake face wear was of major importance in causing failure when machining titanium with the K68 tools. The weakening and subsequent collapse of the tool edge caused by increased cratering explains why a high flank wear rate was recorded when cutting with the K68 at higher speeds. The collapse of the cutting edge tends to eliminate the clearance angle and increases the area of the flank face in contact with the work

material (Figs 4.76 and 4.77). The high flank wear rate may also be due to the strong affinity of TiC present in the mixed phase of the tool material to the workpiece - since it has been shown that a similar affinity is demonstrated in ferrous materials (110). It is therefore reasonable to suggest that TiC in carbide tools promotes diffusion. The TiC makes the tool material more susceptible to chipping and to subsequent failure of the cutting edge. Plucking out also occurred on the rake face of the K68 tools when cutting at low and high speeds (Figs 4.79 and 4.88). This effect may perhaps be aggravated with intermittent contact and also unstable cutting conditions. Grooves were observed on the rake face of the K68 tools when cutting at the speed of 100 m/min (Fig 4.77). Plucking out of tool particles was also observed at the periphery of the chip-tool contact length on the rake and flank faces when cutting at high speeds (Fig 4.79). The severe plucking of tool material suggests plastic deformation as the major wear mechanism under such conditions.

The formation of the crater on the rake face initiates from numerous small voids in the coatings at the chip/tool interface (Figs 4.37, 4.62 and 4.67). These small voids are the result of plucking out of tool material by the chip (Figs 4.63 and 4.69) flowing over the surface at high temperatures. They then join up and form a line of craters parallel to the cutting edge with further cutting (Figs 4.44 and 4.45). These will then taper to a wear pocket by a smooth wear mechanism. Once the coating(s) is penetrated at the centre of the crater, the rate of wear increases rapidly due to the higher solubility of the substrate in the workpiece (ie. dissolution). Coating fragments can then be broken off the crater on each side of the chip and taken away with it. This process of crater formation is illustrated in Figures 4.73 and 4.85. Numerous grooves running parallel to the chip flow direction and craters running parallel to the primary cutting edge can be seen in this figure. The size of these grooves differ being the largest on K68 and on the Al_2O_3 layer of KC910 and shallowest on the TiC layer, with TiN of KC850 lying intermediate. In this context it

may be noted that TiC is harder than TiN which in turn is harder than Al_2O_3, ie. TiC 3300--4000 HV, TiN 2500--3000 HV, and Al_2O_3 1900--2400 HV (188). More grooves and cracks were observed at higher speeds, and the existence of the smooth and shiny craters, numerous ridges, cracks and grooving wear are illustrated in Figures 4.41, 4.50 and 4.60.

When machining titanium, discontinuous chips are formed. The location of the highest temperature exposure is on the rake face where the chip runs over and across the surface. These temperatures have been reported to be as high as 1000 $^{\circ}C$ (189). Based on extensive study of the topographical features of the carbide inserts employed in this work, it can be seen that crater wear takes place by a combination of chemical (diffusion) and attrition wear, the atoms of the coatings being dissolved in the work material flowing over them. At times, the mixed crystal particles, present in carbide tool materials, which do not wear as rapidly as the WC and cobalt, are plucked out and dragged across the flank face of the tools causing grooves (Fig 4.66). More abrasive wear can be caused by fragments of the coating broken off the tool by the workpiece material.

Grooves may also be formed by a combination of oxidation and attrition. The larger grooves (notchings) at the two extremities of the depth of cut suggest wear under sliding conditions at these places allowing oxygen to penetrate in the area of work/tool interface. The penetrated oxygen is believed to react with the work/tool material causing an oxide film of the tool material on the rake face which is then mechanically removed by the work material. The smaller ridges in between the two extremities of the depth of cut give evidence of seizure taking place at this area. It can be seen that the ridges start at the cutting edge, where numerous small holes are present, and extend across the width of the crater (Fig 4.68). The deepest and shallowest parts of the ridges are on Al_2O_3 and TiC layers respectively. This suggests that these are formed by hard particles of the coatings, which have least

effect on the harder TiC and greatest effect on the softer Al_2O_3. This can clearly be seen in Figure 4.58.

Close examination of established grooves revealed that they often tapered to a point, which always pointed in the direction of chip travel (Figs 4.45 and 4.68). This evidence, coupled with plastic deformation of the original surface asperities (Fig 4.25), suggests that the grooves may be formed as schematically depicted in Figure 5.2, sequence 1-4. Groove formation involves plastic deformation only of the near surface and probably does not extend further than about a few microns beneath the surface. For this reason, the term "discrete plastic deformation" has been ascribed to this process. It is postulated that groove formation culminates in ductile fracture of the ridge towards its tail end (position 4 in Fig 5.2), resulting in the tapered groove shown in Figure 4.45. The fracture fragment is then removed by the adherent chip.

The extent of groove formation was more marked when cutting with KC850 than when cutting with KC910. This suggests that rake face shear stresses may have been higher with the former, since rake face temperatures were similar for the coated tools when cutting TA48 material. It is not known whether higher temperatures or higher stresses were responsible for the more marked groove formation when cutting with KC850.

Although no tests were made to measure the temperature on the rake face of the tools, it is expected that the magnitude of the maximum rake face temperature and size of heat affected zone would be larger for uncoated rather than for coated carbide tools. The maximum rake face temperatures of 900 and 1200 $^{\circ}$C were recorded with coated and uncoated tools when cutting steel at 150 m/min (190). The poor thermal conductivity of TA48 will enhance rake face temperature and will lead to higher temperatures than those experienced when cutting steel. Furthermore, the temperature distribution for KC910 coated tools would not differ significantly from that of

KC850, since all the coated tools had more or less similar chip/tool contact lengths regardless of the coating material (Fig 5.3). This is a further indicator of temperature similarity since it was demonstrated (191) that temperature distribution and magnitude is proportional to the chip/tool contact length.

It has been previously reported that the improved behaviour of coated inserts continued after the coating had worn away in the crater region (192-193). Two mechanisms have been proposed to explain this phenomenon. Colding (192) suggested that the bulk of the stress on the insert in the crater region was supported by the sides of the crater which remain coated after the substrate had been exposed at the crater base, and, additionally, the flow of swarf over the crater enabled some TiC to flow from the coated regions into the uncoated areas thus prolonging life. Sproul and Richman (193) disagreed with this explanation and suggested that the 'δ' phase beneath the coating acted as an additional diffusion barrier hence prolonging insert life. The current work has shown no significant difference in the crater wear behaviour of inserts with differing amounts of δ phase and no evidence has been found to suggest that in commercial inserts the δ phase prolongs life after the coating has been removed. Similarly, with the indication of coating removal in the form of small particles, the explanation in terms of flow of TiC into the crater where it acts as a diffusion barrier is also unlikely.

5.2.2.3 FLANK FACE GROOVING

The flank wear in coated tools appeared to be an abrasion process similar to that in uncoated tools. In general the flank wear of the coated inserts appeared to develop less quickly than did the rake face crater. Occasionally a piece of the flank coating would chip after short cutting times and this may be one of the reasons for the reported inconsistent performance of coated inserts. In Figures 4.34 and 4.43 an

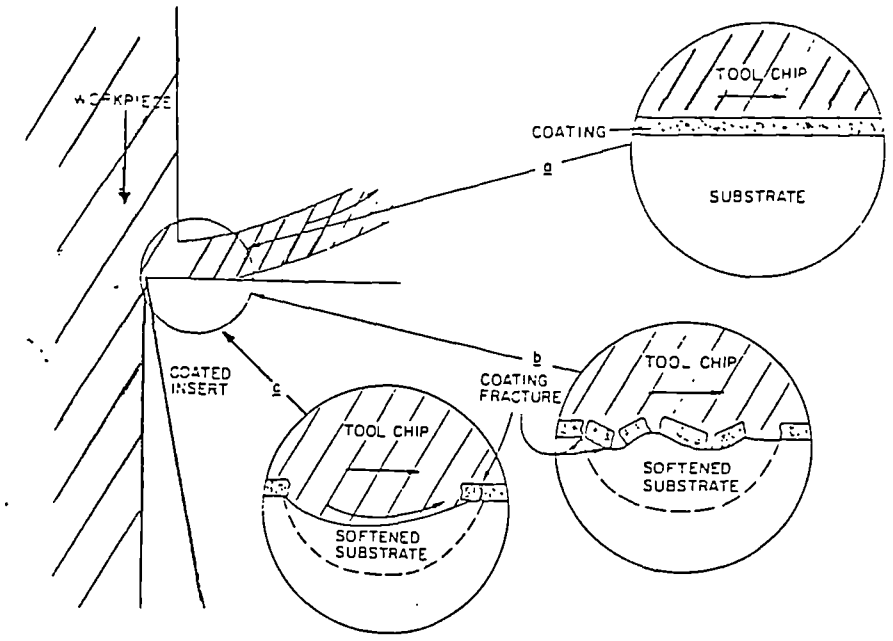

Fig 5.1 Schematic diagram of coating wear modes observed during machining of Aerospace alloys.

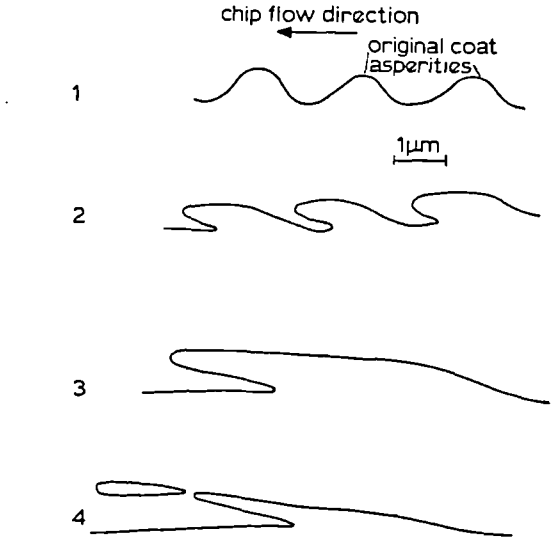

Fig 5.2 Schematic diagram of ridge formation on surface of coatings (sequence 1-3), culminating in ductile fracture (4).

FIG 5.3 CONTACT LENGTH VS. CUTTING SPEEDS

insert shows how most of the coating on the flank is intact whereas the coating in the crater has been completely removed. The only two areas where the coating had been removed on the flank were probably the result of chipping of the coating in that region.

The coating on the flank face wore by an abrasive mechanism due to the rubbing of the flank on the workpiece. Breakdown of the coating in this region was slower than in the crater and one of the reasons for this was the absence of thermal cracking. The coating of the flank broke through just below the cutting edge probably because of slight bulging in this region as the result of plastic deformation of the insert. Once the coating had been removed from the flank the mechanism of wear appeared to be based on attrition and diffusion/dissolution.

A combination of attrition (Figs 4.36, 4.38 and 4.49) and diffusion (Figs 4.47 and 4.56) wear mechanisms do take place when cutting at intermediate speeds. This can be shown by the smoothly worn and plucked surfaces observed on the carbide tools under such conditions. A diffusion wear mechanism is highly probable at higher speeds because of the large diffusible surface area in the lattice of the carbide tools (Figs 4.47 and 4.56). There seems to be metallic attraction of carbide to the titanium work material and the forces holding the surface grains in place are lessened by the heat generated at high speeds. The carbon in the workpiece may be likely to dissolve in the TiC of the mixed phase and thus weaken it by causing a volume change.

The mechanism based on diffusion increased the flank wear rate of coated carbide tools rapidly as the cutting speed and temperature increased, thus forming a smooth surface. Various workers (194-195) have shown diffusion as being the dominant wear mechanism at high temperatures. This suggests that the increased smooth wear on the flank face of the coated carbide tools is probably controlled by

temperature generated during machining and the chemical reaction at the interface. For example, Ham and Narutaki (196) have reported the existence of diffusion wear on the flank surface of coated carbide tools when machining AISI-4340 steel due to the diffusion of some elements such as calcium and silicon from the workpiece. The diffused elements react with the atmosphere to form their oxides (CaO, SiO_2, etc) which in turn react with the alumina (Al_2O_3) to form an unstable glass-like composite (spinel) which has a low melting point (191-192). This reaction would weaken both the flank and rake faces of the carbide tools thus accelerating wear.

Diffusion wear on the KC910 tools used for machining titanium may well occur when iron (Fe) and silicon (Si) diffuse from the work material into the chip-tool interface where they oxidize to form FeO and SiO_2. However, there was no evidence to suggest that these oxides react with the alumina (Al_2O_3) to form spinels, since the coated layer of Al_2O_3 was rapidly removed at high speed. Some of the Fe and Si in the interface which did not oxidize will invade the tools by diffusion and may soften the tool matrix. This action would weaken the coated tools and accelerate wear.

The hole(s) observed on the flank face of the KC850 and KC910 tools (Figs 4.42 and 4.72) after cutting at very high speed suggest plucking out of WC particles from the flank surface at high temperature. The hard WC particles are plucked out of the flank face leaving voids behind and move out to the interface between the flank face and the freshly cut surface causing rapid deterioration of the surface finish generated. Furthermore, they tend to weaken the tool nose and may further cause the deformation at the cutting edge. Plastic deformation does not necessarily depend on the extent of the rake face (and flank) wear but does depend on the conditions of temperature and stress acting on the tool nose. Bond strength is the controlling factor in this process; the bond energy between the WC and the mixed phase must be exceeded before this type of wear can take place.

5.2.2.4 NOTCHING WEAR

Notching was observed when machining titanium with the carbide tools. This type of failure mode was the cause of tool rejection when cutting with the KC850 and K68 at the speed of 100 m/min and at higher speed of 200 m/min (Figs 4.37, 4.55 and 4.86b).

The formation of notch wear starts off by breakage and plucking of bits of the coating/coatings from the flank face at the tool edges. These were then dragged by the workpiece along the surface of the tool, giving rise to small shallow grooves (Figs 4.37, 4.79 and 4.82). The breakage of the coating/coatings is helped by the cracks on the rake face, as can be seen in Figure 4.60. The propagation of the grooves then involves oxidation and attrition taking place simultaneously, with the alumina coating (KC910) probably wearing totally by attrition. Interaction between the tool and the oxygen in the surrounding atmosphere, under sliding conditions, produces an oxide film which is rapidly removed mechanically by the workpiece. This is accompanied by continuous plucking of the coating/coatings which takes place at the bottom of the notches giving rise to more voids (Figs 4.46 and 4.61). Finally, diffusion is held responsible for the smooth and shiny surfaces produced. The above process is illustrated in Figures 4.80 and 4.83.

Sharp increases in the depth of notch occurred throughout the cutting periods. Topographical examination of the tools at these points showed that a rapid increase in the notch depth occurred when the crater band on the rake face joined up with the groove at the end of the depth of cut (Fig 4.79). This often resulted in weakening of the tool edge at this point with consequent chipping taking place (Figs 4.80 and 4.84). Thus, more room was provided for oxygen to penetrate giving rise to severe notching by accelerated oxidation.

The amount and rate of notch wear was higher for the K68 than the TiC/Al_2O_3 coated KC910. The superiority of KC910 over K68 is marked at high speed, where the highest temperatures are produced. Furthermore, when cutting with K68, notches consistently occurred in zone C (Fig 4.33) of the flank faces of which there were only small traces when cutting with KC910. Having established that oxidation is the cause for notch wear and is generally more severe at higher speeds where higher temperatures are produced, it is tempting to suggest that the superiority of KC910 over K68 is because of the aluminium 'oxide' (Al_2O_3 or alumina) coating overlay. It is easy to appreciate that Al_2O_3 would be unaffected by an oxidation process, since it would simply not be oxidized. The rates of notch wear at 50 m/min, where an abrasive wear mechanism is more likely, were approximately the same for K68 and KC910. This suggests that Al_2O_3 layer on KC910 was probably worn through by a mechanical wear mechanism.

Generally notch wear was most marked at the outside edge of the depth of cut (zone 'C' in Fig 4.33). This was observed with all carbide tools (Figs 4.46 and 4.55), and the notch sizes were greater with the uncoated carbide tool (Figs 4.81 and 4.88b). The sliding conditions prevailing at the periphery of the tool-chip interface seem the likely cause of the notching. It has been mentioned by various authors that notching is worse at slow speeds since sliding action between the tool and the chip is prevalent under such conditions, and sufficient time is available for chemical reaction to take place. Results obtained from the experiments did not agree with this view since the notch at the depth of cut increased steadily with speed. This trend may be caused by the high temperature generated when cutting at higher speeds, which may have accelerated chemical reaction (dissolution wear) at regions of intermittent contact around the periphery of the tool-chip interface in a shorter time than when cutting at slower speeds. Titanium always produces a discontinuous chip and thus atmospheric attack could always occur. The explanation therefore shows that notching could take

place when cutting at high speeds due to the acceleration of chemical reaction (diffusion/dissolution) enhanced by high temperatures generated under such conditions, despite the lesser time available for the tool/chip interface to be exposed to atmospheric air. The notch observed at the tool nose when cutting with the K68 at various speeds is always smaller than the ones at the end of depth of cut (Figs 4.82 and 4.83). This may be due to the inaccessibility of the tool nose to sufficient atmospheric air since it is always buried in the work material during the cutting operation. The limited access or complete absence of air at the tool nose might prevent chemical reaction at this zone, and hence cause a reduction in the length of the notch formed. Significant notches observed when cutting with the carbide tools did, however, govern the tool life indirectly by affecting the surface finish generated on the work material.

Ansel and Taylor (197) have reported that notching at the tool nose and depth of cut is, among other things, caused by stress concentration at the edges of the tool during the cutting operation. The stress concentration at the boundaries of the loaded surface is independent of the cutting conditions (i.e. whether a BUE is present or not) and can be increased by the work hardening of a surface layer on the work material from a previous cut leading to an increase in the notch wear. Solaja (198) has related the severity of notch wear to the hardness of the tool when machining 0.25 %C steel with carbide tools at a speed of 150 m/min, whilst harder tool materials tend to have an increased resistance to notching. The relatively high hardness of carbides therefore explains the cause of the notch wear which occurred when machining at high speeds since the work hardened layer can abrade the tool at the periphery of the chip-tool interface.

5.2.3 WEAR OF POLYCRYSTALLINE TOOLS

5.2.3.1 PCD TOOLS

Within the time scale of these cutting tests, no significant wear due to cratering, notching attrition or plastic deformation was observed. The absence of such wear processes is consistent with the excellent cutting performance described in Chapter 3.

PCD has a low thermal conductivity coefficient in the temperature range typically achieved during high speed machining. Investigations carried out by Bex (199) when machining AISI-1045 steel with carbide tools show that thermal conductivity of a cutting tool material plays a significant role in the wear rate. The absence of fracture or catastrophic failure when cutting with PCD at slower speeds (Figs 4.117 and 4.118) may be due to the low temperatures generated under such conditions since PCD tools are known to resist thermal shock, due to their extremely low coefficient of thermal expansion. This means that the PCD tools have greater ability to resist heat transfer from the cutting zone, resulting in lower temperatures of the inserts and therefore minimal and evenly distributed stress on the cutting edge. The low cutting force imposes a relatively low compressive stress on the rake face of the tool when cutting at very high speeds thus minimising the level of stress concentration which might lead to the catastrophic failure of the tool, by fracture.

Following a high speed (200 m/min) cutting test with PCD inserts on a titanium alloy workpiece, two striking structural defects were observed. Firstly, a number of small cracks typically 15 μm in length were seen in the bulk of the PCD layer and, secondly, longer more continuous cracks were found at the PCD/WC interface. Both types of cracks are thought to occur as a consequence of disparities in the coefficients of expansion of material constituents in the inserts (199). For example, the coefficient of volume expansion of Co is about five times that of

diamond at over temperature range 20--1000 °C (Fig 5.4). At the high temperatures involved in the present tests (>1000 °C) this is thought to be particularly significant.

The small cracks within the PCD for instance are thought to develop as a consequence of the expansion of the Co binder phase forcing apart the diamond grains (Fig 5.6). A contributory factor may also be the increase in volume associated with the diamond to graphite transformation, which is also possible at these temperatures.

Konig (200) relates the formation of such cracks in a PCD tool during rubbing of titanium to the thermal over-loading of the PCD compound. The PCD aggregate structure is characterized by diamond grains connected with each other by various diamond bridges which are created under the catalytic influence of cobalt during the synthesis process as described in Chapter 3. The spaces between the diamond grains and bridges are filled chiefly by the binder phase (cobalt). When the compound is heated the cobalt tends to expand, due to the difference in thermal expansivity. At about 900 °C, the fracture forces apparently exceed the strength limit of diamond, i.e. 3.92 GN, and the bridges crack (201).

For the larger cracks at the PCD/WC interface a similar argument can be applied. The disparity between the linear thermal expansion of the WC substrate and the PCD is approximately 2 (Fig 5.5) and it is thought likely that at these high temperatures this effect will produce sufficient mechanical stress at the PCD/WC interface to cause subsequent cracking. Figures 4.124, 4.129 and 4.141 show an example of a crack which has propagated along the briged interface. In some cases the thermal over-loading cracks have run into the WC substrate itself.

The better performance and high resistance of the polycrystalline tools in comparison to that of carbide tools (Figs 5.7, 5.8) during machining titanium aerospace alloy could be due, in part, to their higher thermal shock resistance.

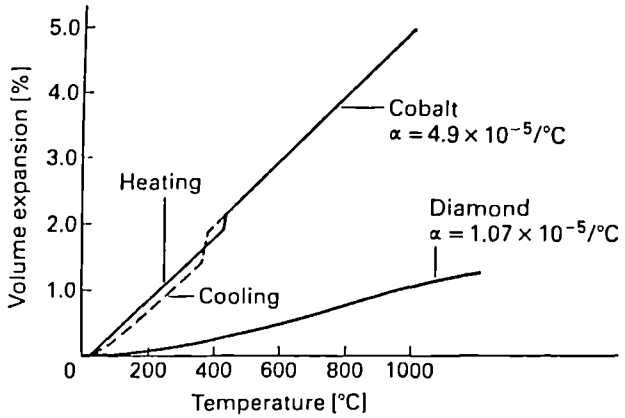

Fig 5.4 Percentage volume expansion of cobalt and diamond (199).

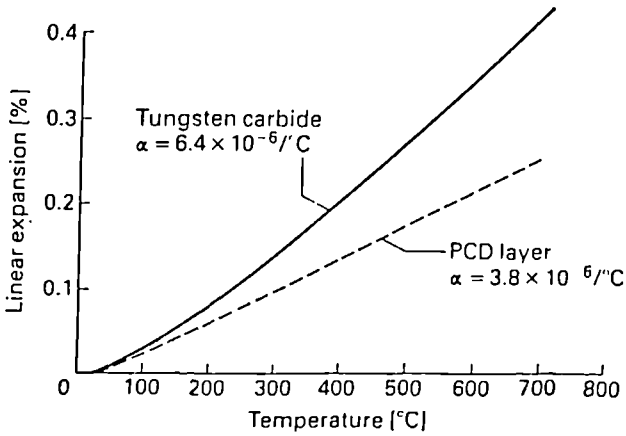

Fig 5.5 Linear thermal expansion of PCD layer and its tungsten carbide substrate (199).

10μ

Fig 5.6 Development of cracks in PCD tool as a consequence of cobalt binder phase expansion.

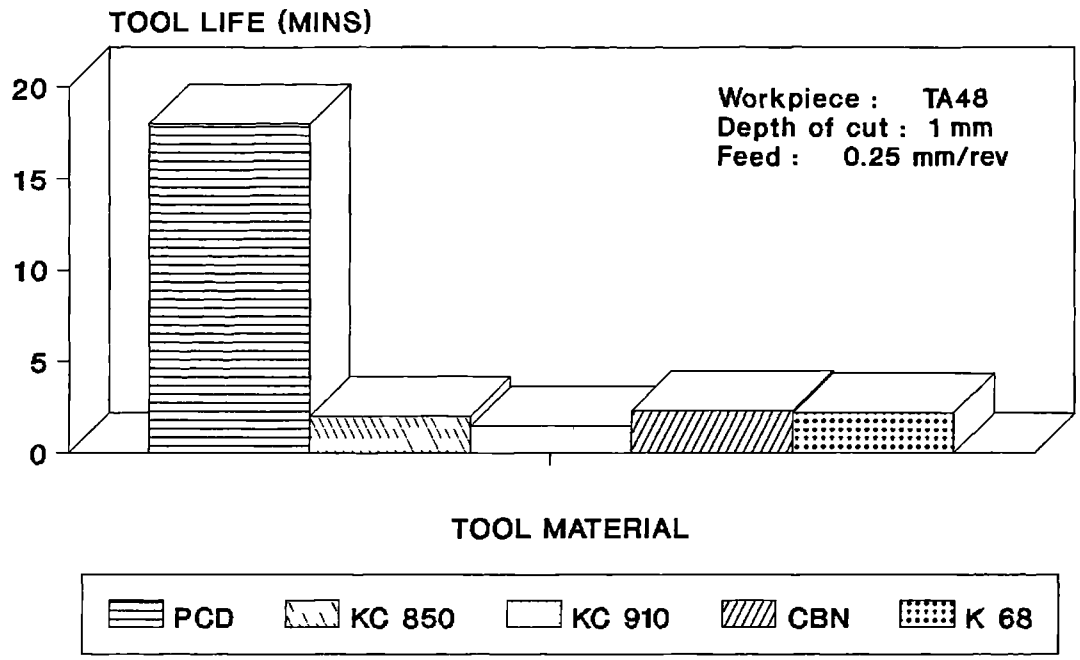

FIG 5.7 TOOL PERFORMANCE

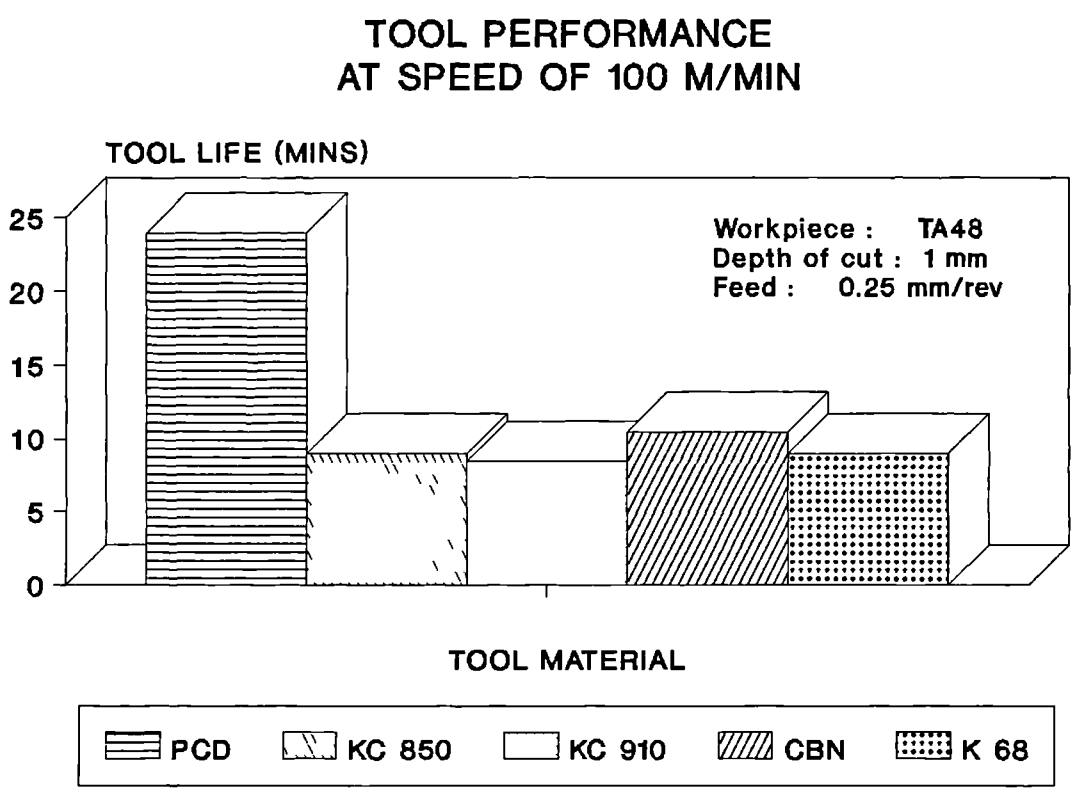

FIG 5.8 TOOL PERFORMANCE

However, it is considered most probable that the superior performance of PCD is due to the formation of a protective surface layer on the rake face, which is predominantly titanium carbide. X-ray analysis has confirmed the presence of this kind of layer on the rake face of the diamond tool (Fig 4.119, 4.121 and 4.122). This possibility has been suggested, but not previously demonstrated, by Kramer (202) and Adelsbery (203). Similarly, Kroll has found that graphite crucibles are able to withstand the attack of liquid titanium metal by forming a stable layer of titanium carbide (TiC) on the surface, which prevents direct contact between the melt and crucible. The dissolution of carbon in the liquid titanium is slow, since it can only occur by diffusion through the carbide layer (204).

Dissolution wear, occurring by diffusion of atoms from the tool material in to the swarf, is generally thought to be the reason for high rates of wear when diamond tools are used to cut ferrous materials - due to the high solubility of carbon in iron. A similar effect might have been expected when cutting titanium alloys with PCD. In fact, the presence of the titanium carbide layer on the rake face appears to serve as a diffusion barrier and restricts dissolution wear under these conditions. If this is correct, then the dissolution wear rate of tool materials will be very dependent on the formation and integrity of the protective surface layers. It should also be noted that concentration gradients will be important - ie. the composition of both tool and workpiece material will be significant.

5.2.3.2 CBN TOOLS

Within the the time scale of these cutting tests, CBN showed much higher resistance to wear (ie. less cratering and notching) than carbide tools and in term of performance was second best of diamond tools.

Figures 4.108 and 4.111 show the fracture failure modes when cutting with the CBN. Fracture or catastrophic failure occurred mainly at speeds between 50 m/min and 250 m/min. This may be due to the relatively low strength and toughness of the CBN in addition to the chemical reaction operating at these speeds. The fracture observed in many instances must have been due to the stress concentration along the cutting edge of the tools. Some workers have shown that the compressive stress is highest near the cutting edge of a tool, diminishing across the rake face to zero where the chips breaks contact with the tool and that the shear stress acting on the rake face may be less variable across the contact area (205-206).

The 'scalloped' appearance of the rake face wear observed on the diamond tools can also be seen quite clearly on the CBN tools (Figs 4.92 and 4.104). This effect is unusual and might be limited to wear of these ultra-hard solids since it has not been discussed in the metal cutting literature previously. Certainly coated and uncoated carbide tools do not show this discontinuous, scalloped form of wear, when machining titanium, but crater in a more conventional manner.

An explanation of why rapid wear can occur in one region of the crater while essentially no wear is present in an adjacent region (Fig 4.104) may be based on different interfacial conditions developing during the cut. It is possible that, under certain conditions, titanium adheres to the tool and no relative sliding occurs at the tool-chip interface (Figs 4.101 and 4.103). Therefore, an interfacial layer of workpiece forms, and the relative motion between the tool and chip is generated by shear within the titanium chip material. This 'stagnant' boundary layer might become saturated with tool constituents thereby limiting the mass transport of tool constituents from the tool surface, similar to the formation of TiC when using PCD tools. The stability of this layer is unlikely to be the same over the entire contact zone, due to local variations in presure and/or temperature, leading to dissimilar rates of wear across that region. Probably the most significant example of this uneven wear is

in Figure 4.104. In this case there has been essentially no wear in one region of its crater area and a 200 micron deep pit in another.

The fracture(s) and the type of wear observed when cutting with the CBN at high speeds suggest that there is a degree of plastic deformation taking place at these elevated temperatures. Whilst there is no direct evidence with cubic boron nitride, it has been shown that diamond is capable of extensive plastic deformation and creep, at 1000 °C, when subjected to modest contact presures - ie. 4/5 GPa. Since at that temperature diamond is about twice as hard as CBN, the relevant presure would be in the region of 2-3 GPa (207). Plastic deformation may lead to cracking on the worn flank face and the subsquent failure of the tool by fracture. The possible result of plastic deformation is shown by the nose of the CBN tool in Figure 4.108.

A hypothesis for the wear of CBN tools, when cutting steels, combines the effect of defect density (ie. dislocation) and a consequently enhanced chemical activity in what has been called "etching wear" (208-209).

It was suggested that the dislocated zones are attacked rapidly by atmospheric oxygen leading to the formation of boron oxides. This mechanism of wear is thought to be akin to that of chemical polishing resulting in the smooth grooved appearance of the tool tips.

There is a strong evidence obtained in this work to propose that the etching mechanism of wear is applicable to the cutting of titanium with CBN tools at high speeds. Thus, it is considered that there are two major components, ie:

i) 'Chemical wear' is produced by a chemical interaction of the tool with its environment, including the workpiece and the atmosphere. Then, the combination of a high dislocation density with atmospheric oxidation leads to etching wear of the CBN tool.

ii) Under these circumstance a thin protective layer of similar composition to the workpiece forms at the interface of tool/chip (Figs 4.95 and 4.101). The stability of this protective layer then becomes the controlling influence on the wear of the tool. At lower cutting speeds, and hence temperatures, the layer becomes unstable with respect to the tool and is lost, exposing the surfaces of the tool to further chemical wear. The wear of the rake face is also increased by adhesion of the layer to the base of the chips, and attrition as fragments of the tool are pulled away with the layer (210).

Tool wear is dependent upon the temperature generated by energy expenditure on both the rake and flank faces, but flank wear was the most significant failure mode when machining titanium with CBN tools. Plucking out occurred on the flank faces, mainly at the lower speeds, and the attrition type of wear mechanism appeared to be dominant under these conditions. An enlarged view of the flank face showing attrition type of wear is given in Figure 4.90. Relative movement between the plucked out particles and the flank face can cause further dislodging of grains of the tool material continuing the process of attrition.

Increased flank wear occurred as the cutting speed increased beyond 100 m/min (Figs 4.106 and 4.107), and this increase of wear was almost certainly due to higher temperatures at the chip-tool interface generated by the fast flowing chip under these high speed conditions. Work carried out by others (194-195) has shown diffusion to be the dominant wear mechanism at high temperatures (Fig 4.105), and the behaviour observed here is consistent with that view. Whilst CBN tool materials are known to be more inert than most to diffusion wear, chemical reaction - or diffusion of elements between the tool and workpiece - will occur under these conditions.

In general, cratering was low when cutting titanium with the CBN (Figs 4.99 and 4.106), but chipping occurred on the rake face of the tools. For example, Figure 4.91 shows CBN particles from the chipped area on the rake face moving down the flank face. Some of the plucked tool particles remain on the rake face and are carried away by the underside of the chip where they cause further damage to the rake face within a subsequent contact area as shown in Figures 4.98 and 4.99. Similar observations have been reported when cutting steel with CBN tools (211, 212). However, the detrimental effect of tool particles at the flank face in scoring the machined surface is probably of greater significance.

5.2.4 WEAR BY DISSOLUTION

In all cases, the process of wear leading to formation of craters is thought to involve dissolution of material from the tool by diffusion into the adjacent zones of the chip and the workpiece (213). A simple model relating the factors involved in the dissolution-diffusion process has been recently described by Dearnley (214). The most important of these factors is the solubility limit of the tool material in the workpiece which determines the magnitude of the concentration gradient in the shear zone and hence the diffusion flux. The intimate contact between the tool and the chip/workpiece at temperatures above 700 $^{\circ}$C provides an ideal environment for diffusion of tool material atoms across the tool/chip and the tool/workpiece interfaces (215). The better wear resistance of cubic boron nitride when cutting titanium at high speed may be attributable in part to the relatively low solubility of boron in titanium. From these and other cutting tests (215), it has been possible to show that, when conditions for dissolution-diffusion wear predominate, wear with polycrystalline diamond and cubic boron nitride tools is less than with carbide tools.

The estimated solubilities of tool materials in titanium at various temperatures are given in Table 5.1 (216), and these values may be taken as estimates of the maximum possible solubilities based on chemical properties alone. While estimates based on chemical properties may be quite accurate when the predicted solubilities are small, physical and geometric effects become significant when large concentrations of solute atoms must be taken into solution. If the wear of cutting tool materials in the machining of titanium proceeds by dissolution of the tool material by the titanium, then it seems reasonable that the solubility of the tool material will be limited by the solubility of the least soluble component. That is, if tungsten carbide is being employed as a tool material, it is possible to assume the solubility of WC will be no greater than the solubility of C, since the solubility of tungsten in titanium is much greater than that of carbon. Table 5.1 lists the solubilities of the tool constituents in titanium, obtained from phase diagrams (217-220). Comparison of Table 5.1 with Table 5.2 reveals that all of the tool materials (except HfN, HfO_2, La_2O_3) have predicted solubilities in titanium that are greater than that of at least one of their constituents. In all of these cases, the solubility of the tool material may be approximated by the solubility of the least soluble component divided by the number of atoms of that component per molecule of tool material. It seems that predictions based on the solubility argument agree well with the test results. In particular the analysis does explain the high wear rates and shorter tool lives (Figs 5.7, 5.8, 5.10, 5.11) of carbide tools relative to that of polycrystalline PCD and CBN tools. Furthermore, any chemical wear mechanism would be affected by changes in the cutting temperature. Since the cutting temperature for carbide tools is much higher (215) than for polycrystalline tools, an increase in wear rate of carbide tools over that of the polycrystalline might be anticipated.

Tool Materia	Solubility (mole %) 1300 ^{0}K	1400 ^{0}K	1500 ^{0}K
HfC	1.27	1.41	1.53
NbC	23.70	20.73	18.45
SiC	*	*	*
TaC	16.03	14.32	13.02
TiC	7.75	7.75	7.75
VC	*	*	*
WC	*	*	*
ZrC	4.23	4.42	4.58
BN	*	*	*
HfN	10.92	12.80	13.35
Si_3N_4	*	*	*
TiN	48.58	48.48	48.17
Al_2O_3	*	*	*
HfO_2	7.85	14.67	29.46
ZrO_2	10.47	21.58	39.50
La_2O_3	0.033	0.076	0.16
TiB_2	*	*	*

* Chemical reaction occurs

Table 5.1 Estimated Solubilities of Tool Materials in Titanium at Various Temperature

Tool Constituent	Solubility (atomic %) 1300 ^{0}K	1400 ^{0}K	1500 ^{0}K
Al	15.0	19.0	28.0
B	1.0	1.0	1.0
C	0.6	0.6	0.6
Hf	*	*	*
La	1.0	1.0	1.0
N	23.6	23.5	23.2
Nb	*	*	*
O	34.0	34.0	34.0
Si	2.2	3.0	4.0
Ta	*	*	*
Ti	100.	100.	100.
V	*	*	*
W	*	*	*
Zr	*	*	*

* These constituents are soluble over a wide range of tempratures and concentrations

Date from Ref 202.

Table 5.2 Reported Solubilities of Tool Constituents in Titanium at Various Temperature

5.2.5 CHIP-TOOL INTERACTION

A feature of the quick-stop tests, with both the carbide and the polycrystalline tools, was the fact that fracture of the inserts occurred leaving part of the cutting edge bonded to the underside of the chip (Figs 4.145-4.147), although this was less obvious with PCD (Fig 4.148). This clearly demonstrates the strength of the chip/tool interface bonding with titanium alloys, and is consistent with the failure of the corresponding welded junctions as described in Section 5.1. It also implies that the temperature of the rake face was above the critical level measured in those experiments.

The quick stop experiments also indicated that bonding across the majority of the chip/tool interface was essentially similar. Figures 4.145-4.147 show that workpiece material has been removed from the chip underside by the carbide and CBN tools. In these cases, the strong bonding across the chip/tool interface caused the tool to fracture and the cutting edge to remain dislodged in chip/workpiece root.

Metallogrophic sections of quick stop specimens made with all the cutting tools revealed a segmented chip with a well developed flow zone adjacent to the chip underside, blending into the shear zone lying adjacent to the new surface of the workpiece (Figs 4.145b, c and 4.147b, c). The thickness of the latter shear zone was less than the chip flow zone (Fig 4.146b). The sections show that a thinner chip is produced by the PCD tools, which result from the shorter chip/tool contact length. Furthermore, the stress required to shear the bond strength across the chip/tool interface is less for polycrystalline PCD tools than for the other tools tested, because it is a shorter contact length. This suggests that the interfacial movement over the PCD rake face contact area (including the cutting edge) is less than with the majority of the tools.

It is reported that (221), the lower the interfacial bond strength, the shorter is the final chip/tool contact length. Hence, PCD and CBN inserts have a shorter chip/tool contact length than carbide inserts because the inherent chip/tool bond strength is lower for these materials than for the carbide inserts, as recorded during the cutting experiments.

Examination of the quick stop specimens showed that the chip flow zone (or secondary shear zone) thickness was about the same for coated and uncoated inserts when cutting a TA48 workpiece (Figs 4.145c and 4.146b). Consequently, the reduced chip/tool contact length of the coated inserts reduces the total shear strain in the chip flow zone, resulting in a reduced heat output. Since the rake face of the inserts is in intimate contact with the chip flow zone, the rake face is heated to temperatures equivalent to those in the flow zone. Hence, the reduced rake face temperatures reported for the coated inserts (221) is probably caused by reduced shear strain in the chip flow zone, as a result of the shorter chip/tool contact length (Fig 5.3), rather than because the coating is acting as a thermal barrier as has been reported previously (222).

A tracing of Figures 4.145a and 4.146a is shown in Figure 5.9 and gives the position of the primary and secondary shear zones. The maximum chip thickness (0.31 mm) is small compared with workpiece materials such as plain carbon steel, reflecting the large shear plane angle (ø), and the small chip/tool contact length observed (215). As a result, the maximum rake face temperature occurs close to the cutting edge.

The general chip form was geometrically segmented, with narrow bands of intense shear separated by relatively undeformed regions in which the alpha grains are elongated in the direction of chip travel. Thus it would appear that the primary shear is not continuous but rather proceeds in discrete 'bursts' of catastrophic shear

a) A tool fragment of carbide seized to chip and workpiece

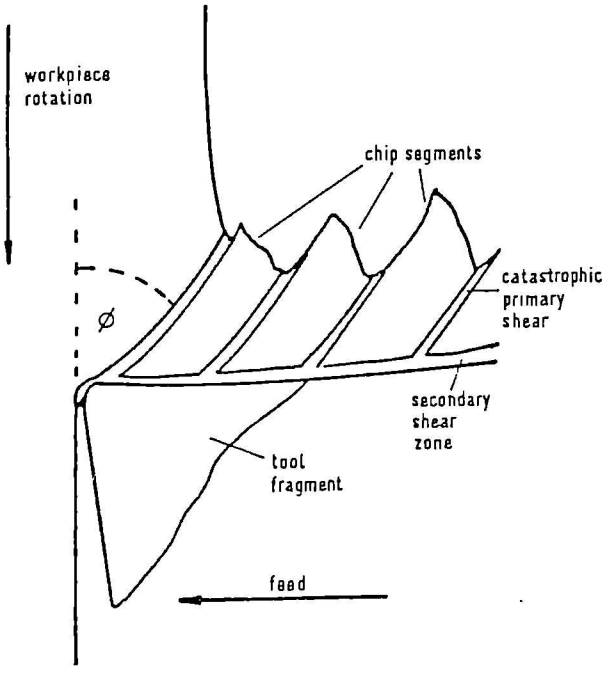

b) Tracing of a showing essential features, γ primary shear plane angle

Fig 5.9 Q.S. obtained after machining Areospace alloys.

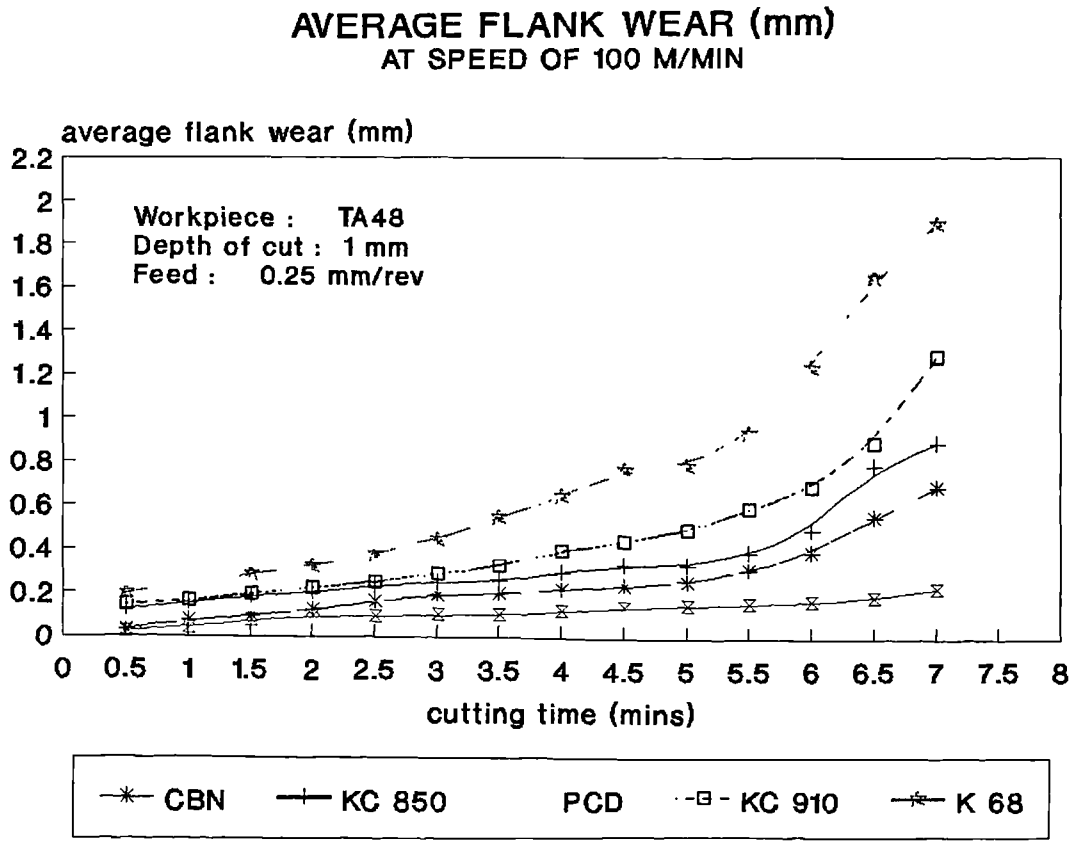

Fig 5.10 A.F.WEAR VS CUTTING TIME

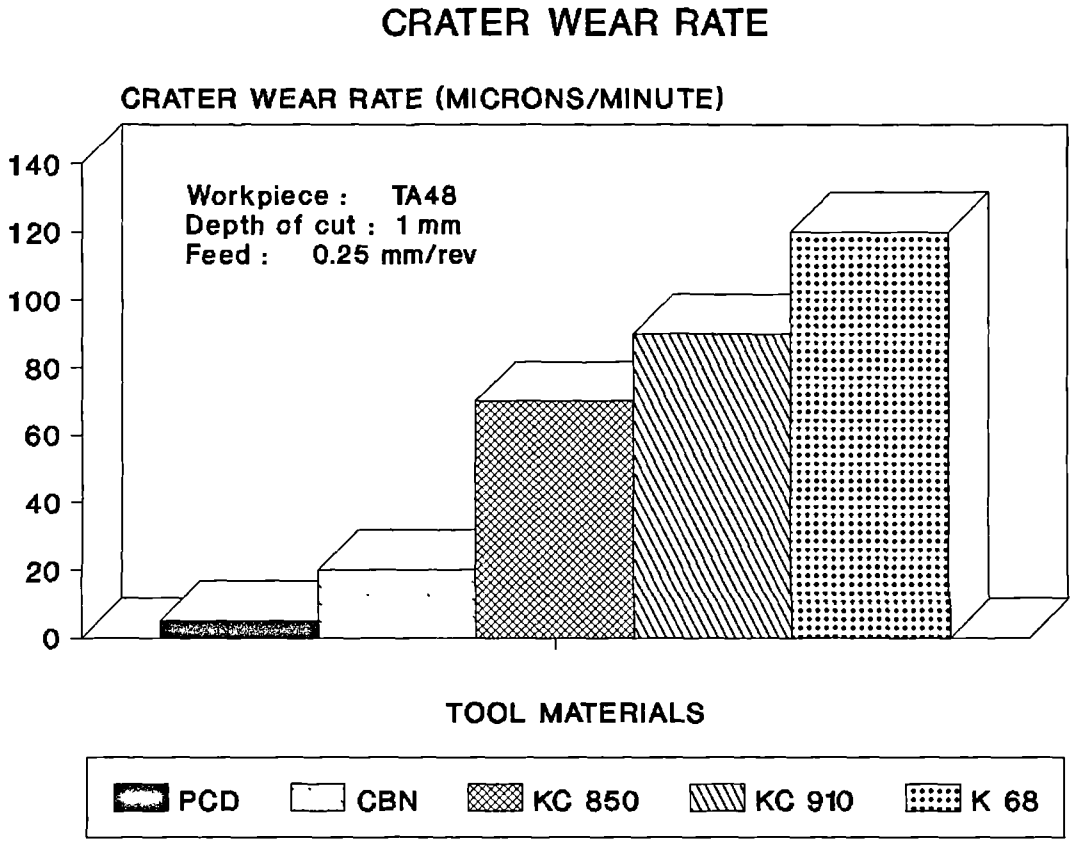

Fig 5.11 C.W.rate vs.tool materials

(223). Freeman (224) working with commercially pure titanium observed sub-micron alpha grains in the shear bands indicating that sufficient heat is generated during the intense primary shear to promote dynamic recrystallisation. During the short periods of intense catastrophic shear, the chip is displaced across the surface of the tool by plastic deformation within the flow (or secondary shear) zone. For a chip thickness of 0.31 mm at a surface speed of 100 m/min, the effective chip velocity is 64 m/min (222) and, if it is assumed that the bottom surface of the chip is welded to the upper surface of the stationary tool, the average values of strain and strain rate within the flow zone are of the order of 27 and $5.35 \times 10^{-6} s^{-1}$ respectively. These conditions are quite sufficient to raise local temperatures above 900 $^{\circ}$C and give rise to dynamic recrystallisation, as indicated by the presence of fine grains within the flow zone.

The sequence of events leading to cyclic chip formation when machining titanium has been described by Komanduri and von Turkovich (225) based on their detailed study of video tapes of low-speed machining within an SEM and high speed photography of machining under workshop conditions, and microscopic examination of sections through chips. Insofar as the actual mechanism of chip formation is concerned, cutting speed appears to have no significant effect. However, it is an important factor in determining tool temperature, tool wear, and surface finish.

5.3 CUTTING FORCES

The influence of tool material on the normal force (F_c), feed force (F_f) and radial (F_r) components of cutting force is shown in Figures 4.144-4.159, where the forces are plotted as a function of the cutting speed, at a feed 0.25 mm/rev and depth of cut of 2 mm.

Increasing the cutting speed from 25 to 50 m/min increases the forces required for chip formation with all tool materials, and the rapid increase in these forces is an indication of the changes that take place at the surface of the tool. When excessive wear occurs at the flank face, cutting edge and nose radius, an increase in the cutting force is likely to occur. When excessive wear takes place at the rake face, the feed force will rapidly increase. The radial force, which is the resultant of forces that acts against the tool, will increase as a result of excessive vibration or chatter, or as a result of nose wear or deformation. The initial increase in tool forces with carbide tools is thought to be due to the rapidly developing crater bringing about an increase in the effective rake angle. However, the crater length will also increase and it is thought that this effect causes the forces, especially the normal and feed forces, to increase also. Furthermore, the rapid fall in cutting forces with increasing speeds (beyond 50 m/min) is due to the reduction in shear strength in the flow zone, brought about by increasing temperature and by reduction in tool/chip contact length. The most rapid force drop can be seen with the CBN tool (Figs 4.154-4.156) and this is due to its relatively short 'run in' period and the rapid attainment of steady state cutting conditions.

Significant reductions in all three components of cutting force are brought about by the use of PCD tools. This reduction could be due to the formation of a protective layer (see Section 5.2.3) on the surface of the tool acting to reduce friction

forces. The effect is most apparent at higher cutting speeds, that is, in the region where PCD achieves its maximum economic advantage over the rest of the tools.

It is evident from Figures 4.154-4.159, which show variation of normal, feed and radial tool forces of all the inserts, that forces with coated carbide tools were lower than those without coatings. This observation holds even though the coating in the region of the crater is rapidly removed.

Some workers have reported that cutting forces are lower when cutting steel with coated tools than with uncoated tools (226-229) and attribute this to a lowering of friction between chip and tool. This conclusion is probably not completely correct because the present study has indicated that, although bonding across the uncoated tool/chip interface is stronger than across the coated tool/chip interface, intimate contact between chip and tool occurred for both types of tool. This resulted in the generation of chip flow zones of equivalent thickness. No evidence of sliding over the majority of the chip/tool contact area was observed, and it is likely that the reported differences in tool forces were not due to differences in interfacial friction.

Whittle (230) has recorded lower forces for coated then uncoated carbide tools when machining steel, and attributed this to an initial resistance of coated tools to crater wear. In fact, this is due to the smaller length of chip/tool contact on the coated inserts - ie. the less crater wear, the smaller the contact length. Similar results have also been presented by Snell (231) for coated and uncoated H.S.S. inserts. It was found that the presence of coating layers significantly reduces the normal, feed and radial tool forces, with the specific cutting force (i.e. vertical force divided by chip cross-section) being reduced by some 20 to 25%. It was also found that for coated inserts, the forces reached a maximum at a speed of 60 m/min, then decreased to a minimum value upon further increase in speed, before finally increasing again at higher speed. These changes in tool force were suggested to be due to coating

higher speed. These changes in tool force were suggested to be due to coating penetration and subsequent crater development, effecting an increase in the rake angle.

Schintlemeister et al (232) reported that tool forces were lower when cutting a steel (with a relatively high calcium content of 0.0033%) with (TiC/Al_2O_3 and TiC/Ti(C,N)/TiN) coated carbide tools than with uncoated carbide tools. These workers attribute this effect to the preferential deposition of calcium-aluminosilicate layers adhering to the rake faces of the coated tools. Such a layer might lower the stresses experienced by the coated tools machining steel, but these workers did not measure the rake face contact area and, since the initial cutting of titanium resulted in rapid removal of the coated layers (TiC, Al_2O_3), it is not possible to draw similar conclusions about the existence and role of the layer. However, formation of a protective layer on the face of CBN and PCD has already been observed and it is a fact that forces with these tools were lower than those with carbide tools. These layers must have brought about the reduction of the contact length and hence the tool face drag forces. According to Raw and Spick (233), a reduction in the tool face drag causes a reduction in the total cutting energy and the cutting forces. The decrease in the normal and feed forces when cutting at higher speeds is due to the reduction in the chip/tool contact length and a drop in the shear strength in the flow zone as the temperature rises with increasing speed. The small contact length and high temperature near the tool edge may result in plastic deformation of the tools at high speeds. Recorded force readings generally show that the component forces increased with prolonged cutting time under all the conditions tested. This is because the clearance angle of the cutting tools is destroyed by wear with prolonged cutting time and the area of contact on the clearance face is increased by the flank wear.

5.4 SURFACE FINISH

The surface finish generated on a workpiece during the cutting operation has been considered as the sum of two independent effects: the 'ideal' surface roughness and the 'natural' surface roughness (234). The ideal surface roughness is as a result of the geometry of the tool and the feed whereas the natural surface roughness is caused by the irregularities in the machining operation. The type of chip produced during the machining operation has a significant effect on the surface finish produced. Poor surface finish can be caused by concentrated tool wear, localized upon the boundaries of the areas of contact between the flank face and the workpiece. Poor surfaces are generally associated with one or more of the following: chatter, feedmarks, and microchips. Chatter is caused by the periodic vibration of the tool and/or workpiece. Feedmarks are produced by the impression of the tool nose radius on each revolution of the workpiece. A microchip forms at the flank face of a tool and is the counterpart of the BUE which normally forms on the rake face of a tool. Microchips occur through a process of shear with the development of a primary deformation zone similar to that normally associated with chip production at the tool rake face. High stresses and deformation do occur before microchips are formed (184). The size of the microchips are dependent on the stability of the system and, for example, a relatively small build up is expected in a rigid machine tool. Another factor which exacerbates the deterioration of surface finish is the formation of a series of notches (or grooves) on the cutting edge of worn tools. The distance between these notches being equal to the feed rate (235). Formation of the notches on the cutting edge of tool causes the surface finish produced on the workpiece to deteriorate. Pekelharing (236) has shown that these notches are funnels which channel metal in the opposite direction to the feed marks and that it was this action that resulted in the feed marks being extended.

The deterioration of surface finish can also be caused by the geometry of the cutting tool and the extent of its wear. It has been reported that the relative motion at the interface between the tool nose region and smooth areas of the freshly machined workpiece surface generates frictional and adhesive forces because of the interaction of contacting surface asperities (237). This action obviously worsens the surface finish generated. The nose radius of the carbide tools used in this project was 1.2 mm. This means that a large area of the tool nose region will be in contact with the freshly machined workpiece surface resulting in an increased tendency for the interface between the tool nose and the freshly machined workpiece to contact surface asperities - this increases the surface roughness.

Figure 4.160 and 4.161 show a general deterioration of surface finish with an increase in cutting time when machining at all speeds. This is due to an increase in the flank wear land with prolonged cutting time. An increase in the flank face wear leads to an increase in the tool-chip contact length, tending to increase the temperature and the compressive stress at the tool nose. A zone of intense shear will therefore be developed on the worn flank face. These developments might lead to the removal of tool particles at the tool nose and such particles tend to weld themselves on the freshly generated work surface resulting in the subsequent deterioration of the surface finish. It is known that carbide tools are expected to weld or adhere easily to TA48 work materials. The quasi-static studies on coated carbide tools have shown that they (KC910 and KC850) have a pronounced tendency towards welding with the work material. The poor surface finish generated when cutting with the carbide tools is therefore due, in part, to the welding of the chipped tool material from the tool nose onto the freshly machined surface (Figs 4.145b and 4.147b). Ham and Narutaki (196) have reported that round honed tools tend to produce more chipping on the cutting edge when machining titanium with ceramic tools.

The adherence of work material on the worn flank face of the tool when cutting at higher speeds can also increase the surface roughness. It has been reported by Brookes et al that the adherence of titanium to the flank face of carbide tools can take place at a temperature of about 780 °C (238). This temperature was attained when adhesion tests were carried out with carbide tools and TA48.

Notching at the tool nose can also lead to the generation of poor surface finish on the machined surface at high speed conditions. The notch observed on the tool nose and the end of depth of cut could be caused by the work-hardened workpiece material which has moved out of the flank area. Hoshi (239) has reported a significant increase in the hardness of the work hardened layer when investigating BUE during the machining of low carbon steel with carbide tool. The increase in hardness is about three times higher than that of the original workpiece material. The increased hardness could therefore lead to the notching at the tool nose, and end of depth of cut, when cutting steel at high speeds with the carbide tools. This may be true in the case of machining low carbon steel, but in machining of TA48 notching was caused by chemical reaction between the tool and the workpiece material - see Section 5.2.2.4. Notching at the tool nose, or the end of depth of cut, has a deleterious effect on the surface finish generated since the work-hardened or slow moving zone of metal tends to protect the active part of the cutting edge thereby forming an integral part of the cutting process. The notches also act as funnels which channel the metal in the opposite direction to the feedmarks resulting in extended feedmarks and an increase in the surface roughness values. Plucked out tool particles can also move down the notch at the tool nose to the tool-work piece interface, still further worsening the surface finish generated.

High surface roughness values were recorded when cutting titanium workpiece materials with the carbide tools at slower speeds. The rapid deterioration of surface finish under these conditions may be as a result of the rough cutting edge

caused by attrition wear. With the disappearance of the attrition type of wear at higher speeds, the cutting edge geometry should be better maintained. This does not happen with the coated tools at higher speeds since these tools generate a poor surface finish (Figures 4.160 and 4.161). The cause of the poor surface finish is probably due to the notch formation as mentioned previously. Another reason for the rapid deterioration of surface finish during machining operation may be due to the microstructure of the carbide tools. Carbide tools have coarse grain sizes and large pore diameters. Wear by attrition is more severe on tools with coarse grain size producing rough cutting edges and ultimately adversely affecting the surface finish generated.

CHAPTER 6

CONCLUSIONS

6.0 CONCLUSIONS

The following conclusions are based on studies of machining a titanium alloy (TA48) with a wide variety of hard cutting tools ie. carbide (coated and uncoated), polycrystalline diamond (PCD) and cubic boron nitride (CBN).

i) A simple quasi-static contact method has been developed to identify the workpiece tool interfacial temperature above which strongly adherent surface layers were formed on the rake face. These temperatures were 740, 800, 820, 760 and 900 ^{o}C for carbide grades of KC850, K68, KC910, polycrystalline Syndite and Amborite tools respectively. The method allows for a detailed study of the microstructure and composition of interfacial layers formed by reaction between the two materials. Furthermore, it can be used to study the integrity of the bulk material, and/or individual coatings on substrates, when welded junctions were subsequently separated at room temperature. Generally, fracture was initiated in the bulk of the harder tool material, rather than in the workpiece or at the welded junction interface.

ii) Quick stop tests showed that under actual cutting conditions these critical temperatures were reached or exceeded.

iii) Analysis of the contact length between the chip and tool showed that the contact length is dependent on cutting speed. Increased cutting speeds were associated with shorter contact length between the chip and the tool.

iv) The thin chips produced when machining TA48 (hence the high chip velocities), combined with the thin flow shear zone and short chip-tool contact lengths, cause higher temperatures to be produced closer to the cutting edge of the tool than when other metals. This has encouraged the use of low cutting speeds ie. <100 m/min, to obtain acceptable tool life in practice.

However, here it has been demonstrated that significantly higher cutting speeds (ie. 250 m/min) could be achieved with PCD tools.

v) Swarf characterised by the sawtooth wave form of the top of the chips is typical of that produced when machining titanium alloys over a wide range of cutting speeds. This form of chip is probably produced by catastrophic shear occurring intermittently in the primary shear zone.

vi) A mechanism of wear based on diffusion and dissolution of the tool materials predominates. The poor thermal conductivity of the titanium alloy workpiece further encourages the development of high rake face temperatures. Thus, the formation of a crater in this region undermines the integrity of the cutting edge resulting in fracture and an accelerated wear rate.

vii) Most potential tool materials either rapidly dissolve in or chemically react with titanium alloy work pieces. In this work, a coherent metallic layer is formed on the rake face by a chemical reaction. The thickness of this layer is thought to be determined by the balance between the rate of diffusion of tool material through the layer and the rate of dissolution of the reaction layer in the workpiece. Furthermore, the stability of this protective layer will become the controlling influence on the wear of the tools.

viii) Rake and flank face wear for all the tool materials tested resulted from the combination of two wear mechanisms: dissolution-diffusion and attrition. The former mechanism produced smoothly worn surfaces. Attrition, probably due to detached tool particles adhering to the swarf, causes irregularly and scarred worn surfaces.

ix) Failure of carbide tools occurred due to the plastic deformation of the tool nose caused by the high temperatures close to the cutting edge, and the

inability of the tools to support the high compressive stress in this region. Deformed carbides were often carried off in streamers attached to the back of the chip, illustrating that the bond between these carbide tools and the titanium in the region of the tool-chip contact length was intimate and strong.

x) The presence of coated layers on the carbide tools appears to have had no beneficial effect on their performance since those layers were rapidly removed leaving the tungsten carbide substrate vulnerable to cratering. However this presumes that the quality of the coated layers and their adhesion to substrate material was consistantly good.

xi) Significant numbers of the carbide and cubic boron nitride tools were unsatisfactory due to the poor surface finish generated on the workpiece. It was found that the poor surface finish was a result of chipping at the cutting edge but this effect was not observed with PCD tools.

xii) Whilst the wear mechanisms were the same for CBN and carbide tools, the wear rate of cubic boron nitride tools was less than that of the carbide (coated and uncoated) tools - and the surface finish was better. It is considered probable that the greater wear resistance is due not so much to its higher hardness and melting temperature, but rather to a slower rate of chemical reaction with the titanium alloy workpiece.

xiii) Analysis of the cutting forces showed that PCD tools had the lowest recorded values of cutting forces with CBN at intermediate level and the carbide tools had the highest.

xiv) Polycrystalline diamond is the most suitable tool material commercially available for machining titanium alloys. Out of all tools tested, the PCD tool gave the best performance and the longest tool life. It is considered that this was due to the formation of a thin protective surface layer, esentially titanium

carbide, formed between the rake face and swarf. Once formed this layer provides a barrier to further dissolution of carbon from the tool, thus reducing dissolution wear. Additionally, PCD produced the best surface finish and swarf which was better suited, in term of form and condition, for recovery.

CHAPTER 7

FUTURE WORK

7.0 FUTURE WORK

Extensive work needs to be undertaken using SEM/EDAX techniques, to accurately determine the structure of protective layers which form on the rake face of the tool, since the formation of these layers appearse to be crucial to the overall wear rate of the tool.

Although chemical effects are dominant in the wear of cubic boron nitride tools in the machining of titanium alloys, fracture in the form of chipping contributed to the early deterioration of the tools. The indentation hardness/fracture technique (ie. indentation creep and fracture measurements) should be used to investigate and assess the mechanical properties of these materials under conditions similar to those encountered in service. Furthermore, the apparent anisotropic behaviour of Amborite should be carefully examined (ie. sliding friction tests on the rake and flank face of CBN should be carried out).

Detailed studies of carbide tool test samples should be conducted, with the aid of SEM/EDAX techniques to examine the surface morphology, and metallographic sections of the coating/substrate interface to ensure a good control of the carbon level in the substrate prior to, and during deposition of the coatings.

A greater range of coated and uncoated carbide tools should be employed in machining titanium and its alloy to determine the extent which the findings of the present work are applicable to other carbide tool materials. Variations of binder content and composition should be examined, as well as variations in the composition of the carbide phase.

Further work using the transmission electron microscopy (TEM) technique should lead to a greater understanding of the saw-tooth chip formation, which appearse to be a charecteristic of titanium alloys.

REFERENCES

1. Angus H T, The Significance of Hardness, Elsevier Sequia, Wear, Vol 54, May 1979.

2. Trent E M, Metal Cutting, Butterworth, 1977.

3. Crookson J O, ISI Publication, No. 138, 83, 1971.

4. Larduner E, Powder Met., 2, 21, 1971.

5. Optiz H. & Konig W., "Materials for metal cutting", (Publ. No. 126), 1976, (London: Iron Steel Inst.), 6.

6. "Machinability of Titanium 150A," American Machinist, October 1, 1951, pp. 179.

7. Shaw M. C. et al., "Machining Titanium," A Report Prepared for the United States Air Force Wright-Patterson Air Force Base, Dayton, Ohio, Under Contract No. AF33 (600) - 22674, M.I.T., Cambridge, Massachusetts, June 1954.

8. Shaw M. C., Smith P. A., Colding B., Cook N. H., "Machining Titanium II," A Report Prepared for the United States Air Force Base, Dayton, Ohio, Under Contract No. AF33 (600) - 31636, M.I.T., Cambridge, Massachusetts, February 1954.

9. Siekmann H. J., "How to Machine Titanium," The Tool Engineer, January 1955, pp. 78-82.

10. Colwell L. V. and Quackenbush L. J., "A Study of High-Speed Milling of Titanium Alloys," ORA Project 04393, SP-316, University of Michigan, Ann Arbor, October 1961.

11. Machining Difficult Alloys, A Compendium on the Machining of High-Strength Steels and Heat Resistant Alloys, sponsored by the United States Air Force, American Society for Metals, Metals Park, Ohio, 1962, pp. 77-79.

12. Vaughn R. L., "Modern Metals Machining Technology," Trans. ASME, Journal of Engineering for Industry, February 1966, pp. 65-71.

13. Child H. C. and Dalton A. L., "Machining of Titanium Alloys, Part 1. Metallurgical Factors Affecting Machinability," Machinability, Proc. of the Conference on Machinability, October 4-6, 1965, ISI Special Report 94, Portsmouth, England, 1967, pp. 139-142.

14. Catt E. J. and Milwain D., "Machining of Titanium Alloys, Part2. General Machining Behavior of Titanium," Machinability, Proc. of the Conference on Machinability, October 4-6, 1965, ISI Special Report 94, Portsmouth, England, 1967, pp. 143-150.

15. Komaduri R., "Some Clarifications of the Mechanics of Chip Formation When Machining Titanium Alloys," Advanced Machining Research Program (AMRP), General Electric Company Annual Technical Report SRD-80-118, AFWAL/MLTM, August 16, 1980.

16. Komaduri R., "Further work on Chip Formation Characteristics When Machining Titanium Alloys," In D. G. Flom (ed), Annu, Tech. Rep. on Advanced Machining Work Program SRD-80-118, General Electric Corporate Research & Development, N.Y., USA, August 1980.

17. Lee M., "Innovative Tool Evaluation," American Metal Market/Metal Working News, August 3, 1981.

18. Jones M. G., "Pulse Laser Experiments," Advanced Machining Research Program (AMRP) General Electric Company Annual Technical Report SRD-80-118, AFWAL/MLTM August 16, 1980.

19. Schoeder T. A. and Hazra J., "Conventional To High Speed Turning of Some Aircraft Alloys," ASM Tech. Ser. 7, Oct. 1979.

20. Gorsler F. W., "Current Limits Turning Aircraft Engine Materials," American Machinist, Jan. 6, 108, 1981.

21. "Cryogenic Coolants Speed Titanium Machining," Machinery, July, 1965, pp. 98-99.

22. Konig W., Private Communication.

23. Joshi R. V., Mechanical Engineering Thesis, M.I.T., June, 1981.

24. Cook N. H., Rabinowicz E. and Vaughn R. L., "Metal Cutting Lubrication Through Continuous Electroplating," Lubrication Engineering, November, 1966, pp. 447-452.

25. Uehara K., Dambara K. and Kanda Y., "An Attempt to Improve the Cutting Performance Through Metallizing," Annual of the C.I.R.P., Vol. XVIV, 1971, pp. 439-444.

26. Kottenstette J. P. and Recht R. F., "An Ultra-High-Speed Machining Facility," Advanced Machining Research Program (AMRP) General Electric Company Annual Technical Report SRD-80-118, AFWAL/MLTM, August 16, 1980, pp. 9-1 to 9-26.

27. Lee M., "Gas Gun Machinign Experiments," Advanced Machining Research Program (AMRP) General Electric Company Annual Technical Report SRD-80-118, AFWAL/MLTM, August 16, 1980, pp. 7-1 to 7-11.

28. Wallbank J, Metal Tech 6(4) 1979.

29. Ernst H & Merchant M E, ASM 1941, Surface Treatment of Metal.

30. Merchant M E, Journal Applied Physics, Vol 16, 1945.

31. Merchant M E, Machining Theory and Practice, Oxford-Clarendon Press, 1950.

32. Chang S S & Heginbotham W B, Trans ASME 1960, 82 (B).

33. Palmer W B and Oxley P L B, Proc Inst Mechanical Engineer, Vol. 173, No. 24, 1959.

34. Hill R., The Mathematical Theory of Plasticity, Oxford-Clarendon Press, 1950.

35. Hill R Journal Mechanical Physics Solids Vol 3, 1954.

36. Lee E H & Schaffer B W, Journal Applied Mechanics Vol 18, 1951.

37. Shaw M C & Cook N H & Finnie I, Trans ASME 1953, 75.

38. Kudo H, Int Journal Mechanical Science Vol 7, 1965.

39. Childs T C H & Richings D, & Wilcox A B, Int Journal Mechanical Science Vol 14, 1972.

40. Rowe G W & Spick R T, Trans ASME 1967, 89 (B).

41. Williams J E & Smart E F & Milner D R, Metallurgia 1970, 81.

42. Trent E M, Metal Cutting, Butterworth, 1984.

43 Notter A. T. and Heath P. G., Machining of hard ferrous materials with amborite, IDR, July 1980.

44. Colwell L V, Method of Sensing the Rate of Tool Wear, Annals of CIRP, Vol XVIV, 1971.

45. Defllippi A & Ippollito R, Cutting Force & Tool Wear Relationship of Carbide, Annals of CIRP, Vol XVII (1969).

46. Defllippi A & Ippolito R, Evaluation of the Tool Wear in Frontal Milling, Ann. CIRP, 21(1), 1972.

47. Final Report on Development of Adaptive Control Techniques for Numerically Controlled Milling Machines. Report No. ML-TDR 64-279, Bendix Corpn, 1972.

48. Takegama H, Sekiguichi H & Takada K, Open Approach for Optimizing Control in Metal Cutting, Annals of CIRP, Vol XVIII, 1970.

49. Trent E. M., "New tool material and cutting techniques," Int. Conf., London, SME, 3-4 March, 1977.

50. Childs T. H. C. and Rowe G. W., Inst. Phys., "Report on Progress in Physics", 36, 225, 1973.

51. Braiden P. M., "Thermal Conditions in Metal Cutting," ISI Preprint, 1970, 126.

52. Vieregge G., Zerspannung de Elsenwerstoffe Verlage Stahleisen, Dusseldorf, 1959.

53. SECO handbook on fundamentals of metal cutting, 1982.

54. Boothroyd G., Fundamentals of Metal Machining, Arnold, 1965.

55. Nakayama K., J. Eng. Fal. Yokoma University, 5, 1956.

56. Rall D. L. and Witt G., TRANS. ASME, 78, 1956.

57. Arndt G. and Brown R. H., MTDR, 7, 1967.

58. Koch V. et al, Proc. 11th Int. MTDR Conf., 1970.

59. Wright P. K., Ph.D Thesis, University of Birmingham, 1971.

60. Trent E. M. and Wright P. K., Met. Tech, 1, 1974. Also see J.I.S.I., 211, 1973.

61. Dines B. W., Ph.D Thesis, University of Birmingham, 1975.

62. Smart E. F. and Trent E. M., Int. J. Prod. Res., 13, 1975.

63. Freeman R., Ph.D Thesis, University of Birmingham, 1975.

64. Naerheim Y., Ph.D Thesis, University of Birmingham, 1976.

65. Dearnley P. A., Surface Eng., 1, 1985.

66. Boothroyd, "Mechanics of Metal Cutting and Machine Tool", Arnold, 1965.

67. Kusters K. J., Industries Anzeiger, 89, 1956.

68. Chao B. T et al, TRANS. ASME, 83B, 1961.

69. Trent E M, Proc Inst Mechanical Engineering, Vol 166, 1952.

70. Rapier A C, British Journal Applied Physics, Vol 5, 1954.

71. Weiner J H, Trans ASME, Vol 77,, 1955.

72. Chao B T & Trigger K J, Trans ASME, Vol 80, 1958.

73. Loewen E G & Show M C, Trans ASME, Vol 76, 1954.

74. Chao B T & Trigger K J, Trans ASME, Vol 80, 1958.

75. Reichenbach G S, Trans AMSE, Vol 80, 1958.

76. Boothroyd G, British Journal Applied Physics, Vol 12, 1961.

77. Trent E M & Smart E F, Birmingham University Report on Machining Nimonic 115, 12, 1969.

78. Wright P K & Trent E M, JISI Vol 211, 1973.

79. Childs T. H. C & Rowe G. W., Inst. Phys. Rep. Prog. Phys., 1973, 36, 223.

80. Bailey J. A., Wear, 1975, 31, 243.

81. Ernst H. & Merchant M. E., A.S.M., 1941, Surface Treatment of Metals.

82. Show M. C., TRANS. ASME, 1961, Jnl. Eng. for Ind., 1961, 83.

83. Trent E. M., Jnl. Inst. Prod. Eng. 1959, 38.

84. Heginbotham W. B. & Gogia S. L., Proc. Inst. Mech. Eng., 1961, 175.

85. Optiz H. & Gappisch M., Int. Jul. MTDR, 2, 1962.

86. Optiz H. & Konig W., I.S.I. Pub, 126, 6, 1970.

87. Trent E. M., J. Iron & Steel Inst., 46, 1963.

88. Zorev N. N., "Metalcutting Mechanics", Programon 1966.

89. De Salve D. J. & Shaw M. C., MTDR, 8, 1968.

90. Dines B. W., Ph.D Thesis, University of Birmingham, 1975.

91. Shaw M. C., "Metal Cutting Principles", Clarendon Press, Oxford, 1984.

92. Zorev N N, International Production Engineering Research Conference, Pittsburgh, 1963.

93. Palmer W B & Oxely P L, Proceeding of the Institution of Mechanical Engineer's Vol 173, No. 24, 1959.

94. Chandrasekaran H & Kapoor D V, Photoelastic Analysis of Tool-Chip Interface Stresses, ASME Series B, Vol 87, No 4, 1965.

95. Andreev G S, Vestnik Mashino Stroeniya, No 5, 1958.

96. Kattwinkel W, Industrie-Anzeiger, N R 36, S29-S39, May 1957.

97. Kato S & Hamaguch K & M Yamada, Journal of Engineering for Industry, Trans AM Soc Mechanical Engineers, 94B, 1972.

98. Gordon M B, The Applicability of The Binomial Low to the Process of Friction in the Cutting of Metal Wear, Vol 10, 1967.

99. Kirk F. A. et al, I.S.I. Pub., 126, 1970.

100. Trent E. M., Met. Rev., 1969, 13.

101. Dulis E. J. & Neumeyer T. A., I.S.I. Pub., 126, 1970.

102. Brownsword R. & et al, "Materials for metal cutting", (Publ. No. 126), (London: Iron Steel Inst.), 38, 1976.

103. Wright P. K., Smart R F, ISI Report, 94, 1976.

104. Christopher J D, Cutting Tool Developments and Their Impact on Metal Removal Rate, Metal Working Production, Nov. 1981.

105. Kieffer R & Benesovsky F, Hartmetalle, 4, 1986.

106. Brooks K J, World Directory & Handbook of Hard Metals, 1979 Engineering Digest.

107. Kieffer R & Ettmayer, P, Chem-Ing Tech, 7, 1974.

108. Cookson J, Cutting Tool Material, Met. Prod, 176, Nov. 1979.

109. Exner H D, Physical & Chemical Nature of Cemented Carbides, Powder Metallurgy, 5, 13, 1970.

110. Hale T. E. & Graham D. E., Wear of Coated Carbides G E C Carbology, Sys Dept, Michigan, MIT, Report No.48232, 1981.

111. Schintlemeister W, Proc 5th Int Conf of CVD Electrochemical Society, Princeton, N J, 1975.

112. Schintlmeister W & Pacher O J , Vac Sci Tech 12(4), 1975.

113. Sadahiro T et al, Wear Resistant Coating of Cemented Carbides, Wear, 48, 1978.

114. Karapautev P, Investigations of some Wear Parameters of CVD Layers in Carbides by SEM, ANN, CIRP 27 (1), 1978.

115. Semko M F et al, SINT ALMAZY, 4, 1970.

116. Semko M F et al, SINT ALMAZY, 2, 1969.

117. Anon, Metalworking Prodn, 8, 1972.

118. Morris D F & Spanitz J F, Amer Machinist, 118 (24), 1974.

119. Bex P A & Wilson W I, IDR, 37, January 1977.

120. Bex P A, Syndite for the Machining of Titanium Alloys, Industrial Diamond Review, August 1977.

121. Diamond & Carbide Get it Together, Machinery and Production Engineering, May 2, 1979.

122. Bex P A, Syndite Cutting Tools, Preparation and use, DeBeers, Dusseldorf Conference, Section 1.9, IDR, Sept. 1979.

123. Brookes C. A. & Lambert W. A., "Ultra Hard Material Application Technology", (De Beers), Hornbeam Press LTD, 1982.

124. Oboloer M., "machining of Hard Ferrous Materials anf Grey Cast Iron with Polycrystalline CBN Cutting Tools", Advances in metal production, Conf. Proc; MPR Publication Services LTD, 1984.

125. Bridgeman P. W. & Chem J., Phys. 15, 192, 1974.

126. Suits C. G., American Scientist, 52, 395, 1964.

127. Hall H. T., U.S. Patent No. 2947610, August 2, 1960.

128. Bundy F. P. & Chem J., Phys. 38, 631, 1963.

129. Komonduri R. & Show M. C., "Surface Morphology of Synthetic Diamonds and CBN", Int. J. MTDR, Vol. 14, Pergamon Press, 1974.

130. Bhattacharyya S. K. & et al, "Aspect of Machinability Using PCD & CBN Compact Tooling", Proc. Int. Conf. Cutting Tool Materials, Kentucky, Sep. 1980.

131. Walper H., "How Manufactures are Turning to Diamond and CBN for Increased Profit", De Beers Report, Production Engineer, Feb. 1981.

132. De Beers' Handbook on PCD (Syndite) Cutting Tools Blanks, 1987.

133. Vereschagin L F et al, Almazy, 1, 1971.

134. Martirosov E B et al, Machine and Tooling 43 (6), 1972.

135. Hanneman R E and Hibbs L E, SME Tech Paper, MR73-143, 1973.

136. Bakul V N et al, Sint, Almazy, 1, 1974.

137. Karynk G G et al, International Conference "Diamond 75", Moscow, February, 1975.

138. Sandvik Coromat Report on CBN Inserts and Holder Programme HV-1000:103-ENG, 1977.

139. Wentorf R. H., "The Art and Scence of Growing Crystals", Chapter 10, Ed. J. J. Gilman, Wiley, New York, 1983.

140. Bundy F. P. & Wentorf R. H., J. Chem. Phys 38, 1144, 1963.

141. Tabuchi N. et al, Samimoto Electric Tech. Review, 1978.

142. Trent E M, The Institution of Metallurgists, Machining, November, 1979.

143. Naerheim Y & Trent E M, Met Technol, 4, 1977.

144. Trent E M & Deearnley P A, Met Technol, 9, 1982.

145. Loladze T N, Ann CIRP, 33,1, CIRP.

146. Aartung & Kramer Ann, CIRP, 31, (1), 1982.

147. Venkatesh V L & Philip P K, J Iron Steel Inst, 209, 1971.

148. Wang M Q, PhD Thesis Nanjing Aeronautical Institute, 1986.

149. Tabor D, "Some Basic Mechanics of Wear that may be Relevant to Tool Wear and Tool Failure", J. Inst. Met. 94, 369, 1967.

150. Buckley, Machining, Institute of Metallurgists, 9, 1967.

151. Loladze T N, J Inst Eng (India), 108, 1962.

152. Suh N. P., Coated Carbides - Past, Present & Future, Carbide J. 9 (1977).

153. Naik S. K. & Suh N. P., J. Eng. Ind., 97 (1975).

154. Suh N. P., Surface-treatment & Coating Technique for Cemented Carbide Tools, Proc. North American Metal Working Research Conf., 1975, SME, Dearborn, U.S.A.

155. Kramer B. M. & Suh N. P., Tool Wear by Solution: A Quantitative Understanding, J. Eng. Ind., 181, 1983.

156. Carson W. W. & et al, Metal Oxycarbides as Cutting Tool Materials, J. Eng. Ind., 98 (1975).

157. Naik S. K. & et al, The Formation of Oxycarbide during the Oxide Treatment of Cemented Carbide Tools, J. Eng. Ind., 97 (1975).

158. Carson W. W. & et al, Enhancement of Cemented Carbide Tool Properties, Natl. Sci. Found. Hard Metal Res., 2 (1973) (NTIS Publ. PB-908).

159. Tungsten Carbide Tools Treated with Group IVB and VB Metals, U.S. Patent 4,066,821 to N. H. Cook & B. M. Kramer.

160. Suh N. P. & Fillion P., Optimization of Cutting Tool Properties through the Development of Alumina Cermet, Wear 62 (1989).

161. Anon, Machinery, 84, 1954.

162. Holt J T D & Purcell J, Machinery, 85, 1954.

163. Hollis W S, Presented at Inst. Mech. Eng., Conf. on Tech. of Engineering Manufacture, London, 1958.

164. Gauthier V J, Steel 132, 1953.

165. Catt E J & Milwain D, ISI SR 94, Proc Conf Machinability 1967.

166. Boston O W, Iron Age, 173, 1954.

167. Colwell L V & Truckenmiller W C, Mech Eng, 75, 1953.

168. Merchant M E, Amer Machinist, 98, 1954.

169. Child H C & Dalton A C, ISI 94, Proc Conf Machinability, 1967.

170. Loewen E G & Shaw M C, Trans ASME, 76, 1954.

171. Loladze T N, Int Journal MTDR, 7, 1967.

172. Fersing L & Smith D N, Trans ASME, 77, 1955.

173. Kreiss W, PhD Thesis, Technischen, Hochschule Aachen, 1973.

174. Brookes C. A. & et.al, Journal of hard materials, Vol. 1, No.1, 1990.

175. Brookes. C.A. & Hooper.R.M, " Wear and hardness of new tool materials", Proceedings of the International Conference, Metal Society, NPL Teddington, 28-29 April 1981.

176. Brookes.C.A & Hooper.R.M, " Enviroment effects in the wear of Amborite Cutting gray cast iron ", Ultra hard Material Application Technology; (DeBeers),Hornbeam press LTD 1982.

177. Brookes C. A., James R. D & Nabhani F., IITT international conference, Grenoble, France, 15-19 Oct. 1990.

178. Williams.M.S.,J.APPL.Phys.,35,1965.

179. Brookes. Jill, Private Communication.

180. Brookes C. A., James R. D. & Nabhani F., "Aspect of ultra hard cutting tool wear in the machining of Aerospace alloys", IITT international conf. Feb. 1990, Paris.

181. Brookes K. J. A., "Problems in the objective assessment of hard metal as cutting tools", Int.Conf.Metal Society, London, May 1982.

182. Brookes K., "Which carbide ?", Extra report, Metal working production, July 1985, 129.

183. Brookes K. J. A., "Guide to the world's sintered carbides", Special report, Metal working production, Jan. 1987, 131.

184. Schintlmeister W., Wallgram W., Kanz J. & Gigl K., "Cutting tool materials coated by CVD", Wear, 1984,100,1.

185. Schintlmeister W. & et al, "Preparation & properties of hard metal layers for metal machining and jewellery", J. Vac. Sci. Technology, 1975, (12) 4.

186. Iredale R., (Ed) "Titanium nitride -- a new elexir for carbide tools", Feature, Metal working production, Oct. 1971, 115.

187. Trent E. M., Metal cutting, Butterworth, London, 2nd. edition, 1984.

188. Prodob M., "CVD hard coating lengthen tool life", Metal progress, ASM, May 1982.

189. Koury A. J. & et al, "Effect of solid film lubricants on tool life", ASLE Report, 78, 1978.

190. Trent E. M., Dearnley P. A., "Metal technology", Vol. 9, 1982.

191. Dearnley P. A., "Metal technology", Vol. 10, 1983.

192. Colding, Jernkontorets, Ann, 147 (1963), 1.

193. Sproul W. D. & Richman M. H., Mod. Dev. powder metal (1977), 10, 491.

194. Bex A., CIRP Annals, Vol 21, 1972.

195. Suzuki H. & Yamamoto T., Trans. J. Japan Inst. of metal, Vol. 10, 1969.

196. Ham I. & Norutaki N., Trans. ASME, Nov. 1973.

197. Ansel C. T. & Taylor J., Int. J. MTDR, 6, 1962.

198. Solaja V., Wear, Vol. 2, 1958.

199. Bex P. A. & Shafto G. R., Ultra hard material application Vol. 3, 1984.

200. Konig W. & Bomcke A., Report of the 13th Meeting of the International Group on Wear of Engineering Materials (IRG-DECD), MTM, KU Leuven (Belgium), June 1988.

201. Takagama H. & et al, Jour. of Japan Soc. of Proc. Eng., Vol. 50(7), 1984.

202. Kramer B. M. & Hartung P. D., "Cutting tool materials", F. Gorsler (ed), ASM, 1981.

203. Adelsberg L. M. & Cadoff L. H., "The reaction of liquid titanium and hafnium with carbon", AIME, Vol 239, June 1967.

204. McQuillan A. D., "Titanium", Butterworths Scientific Publication, London, 1956.

205. Rowe G. W. & Wilcox A. B., J. Iron & Steel Inst., 209, 231, 1971.

206. Amini E., J. Strain Analysis, Vol. 3, 1968.

207. Brookes.Jill.,Private Communication.

208. Brookes C. A., "Ind. Dia. Rev.", 1971, 21.

209. Poduraev V. N., Vestn Machinostr, 1979, 58, 47.

210. Brookes C. A. & Lambert W. A., "Aspect of indentation hardness of Amborite & Syndite", UMAT, Vol. 1, 1987.

211. Willson et.al. Machining Sintered Carbides with pollycrystalline Diamond Tools,ICM,Melbourne,August 1980.

212. Hodgson.T & Trendler.P.H.,International Conference on Manufacturing Engineering ,Melbourne,25-27,August 1980.

213. Larsen J. & Tanouge P. A., "Advance in hard material tool technology", Proc. of the 1976, International conference on hard material tool technology, Caregie-mellon University, U.S.A., June 1976.

214. Dearnley P. A., Wear, 101, 1, 1985.

215. Dearnley P. A., Surface Eng., 1, 1, 1985.

216. Hartung P. & Kramer B., International conference on cutting tool materials, ASME/SME/ISJ/CIRP, Cincinnati, Ohio, Sep. 1980.

217. Hartung P., S.M. Thesis, M.I.T., 1981.

218. Moffott, "The handbook of binary phase diagrams", General electric company, Schenectady, 1977.

219. Rudy E., "Ternary Phase Equilibrium in Aranstion metal-Boron-Carbide-Silicon Systems, Part V, Compendium of Phase Diagram Data", Technical report AFML-TR-65-2, Part V, May 1969.

220. Hansen M., "Constitution of the binary alloys", First supplements, McGrow-hill, New York, 1965.

221. Dearnley P. A., Metal Technology, Vol. 10, 1983.

222. Barrow G., Int. J. Mach. Tool Des. & Res., Vol. 22, 1982.

223. Komonduri R, Wear, 76, 1982.

224. Freeman R. M., Ph.D Thesis, University of Birmingham, 1974.

225. Komonduri R. & Turkovich B. F. Von, Wear, 69, 1981.

226. Snell P. O., Jerknot Ann, 154, 1970.

227. Ljingquist R., Proc. 3nd Int. Conf. on "Chemical vapour deposition", 383, 1972, Rinsdale, III, American Nuclear Society.

228. Schintlmeister W. & Pacher O., J. Vac. Sci. Tech 12, 1975.

229. Colding B., Werkstatt Betreib, 103, 1974 & Fertigungstech Betreib, 1, 1970.

230. Whittle, Carbide Tool Journal, 1982, 43.

231. Snell P. O., Jernkont Ann, 1971, 154(9).

232. Schintlmeister et al, Wear, 48, 1978.

233. Raw G. W. & Spick P. T., Trans. ASME 89B, 1967.

234. Boothroyd, Fundamentals of metal machining, Arnold, 1965.

235. Pekelharing A. J., Proc. OECD Seminar on Metal Cutting (Paris), 1986.

236. Pekelharing A. J., CIRP Annals, Vol. 20, 1972.

237. Bailey J. A. & Azargon G. A., SME Tech. Paper No. 1075-126, 1975.

238. Brookes C. A., James R. D. & Nabhani F., "Aspect of ultra hard cutting tool wear in the machining of Aerospace alloys", IITT international conf. Feb. 1990, Paris.

239. Hoshi K. & Hoshi T., Advance in MTDR, 9th. MTDR Conf., Sep. 1968.